

MECHANISM OF WEAR AND TRIBOFILM FORMATION WITH IONIC LIQUIDS  
AND ASHLESS ANTIWEAR ADDITIVES

BY

VIBHU SHARMA

Presented to the Faculty of the Graduate School of  
The University of Texas at Arlington in Partial Fulfillment  
of the Requirements for the Degree of

DOCTOR OF PHILOSOPHY

THE UNIVERSITY OF TEXAS AT ARLINGTON

AUGUST, 2016

Copyright © by Vibhu Sharma 2016

All Rights Reserved



## Acknowledgements

I would like to take this opportunity to express my gratitude to all the invaluable help, input and support I received during my graduate study to make this research possible.

First and foremost I wish to thank Dr. Pranesh B. Aswath for being my research advisor for the past 5 years. This research has been enlightened and properly guided by his enriched knowledge and expertise in the subject. His enormous experience as a research mentor provided me the right amount of structure with some level of independence to design my thesis forward. Besides having him as my research advisor, I have also had the opportunity to enjoy his pleasant personality at times in many social events. He is a delightful human being and very inspiring personality.

I also greatly appreciate the constant support and guidance from Dr. Ali Erdemir and Dr. Nicole Doerr throughout this research effort. I admire Dr. Ali Erdemir for the contribution he has made in the field of tribology and lubrication science and I was blessed to receive his counsel during my doctorate research.

In the same respect, I would also like to acknowledge the time and efforts of my graduate committee members, Dr. Ali Erdemir, Dr. Choong-Un Kim, Dr. Fuqiang Liu, Dr. Daejong Kim and Dr. Panayiotis S Shiakolas. Your valuable suggestions during my Ph.D. comprehensive exam provided me with more focused outlook towards my research work.

I would like to thank the faculty members of the materials science and engineering department at Malaviya National Institute of Technology who laid the

ground work of my knowledge in the field of materials science and metallurgical engineering. I also wish to thank all the faculty members of the department of materials science and engineering at the University of Texas at Arlington for their tutoring in my graduate studies. I would like to gracefully appreciate the MSE staff, Ms. Jennifer Standlee, Ms. Beth Robinson and Ms. Libia A. Cuauhtli, their continuous support insured the timely progress of this research work. I sincerely thank Dr. Jiechao C. Jiang, David Yan and Brian Edwards who provided me with the training on numerous equipment in the characterization lab at UTA. I am also grateful to Dr. Lucia Zuin, Dr. Yongfeng Hu and Dr. Tom Regier of the Canadian Light Source for their technical support and help with the XANES studies. My special thanks to Argonne National Laboratory, Argonne, IL and AC2T research GmbH Austria for providing the valuable resources for this research work. This work was also supported by the "Austrian COMET-Program" in the frame of K2 XTribology (project no. 849109)

I have been delighted to having worked with great team members, Mr. Sujay Bagi, Dr. Megan Maginot, Dr. Aruwajoye Olumide, Vinay Sharma, Ami Shah, Kimaya Vyavhare, Kush Shah, Sravya Josyula, Pradip Sairam Pichumani and Dr. Xin Chen in the tribology research group in the MSE department. I would like to express my gratitude to my former colleagues and mentor Dr. Giovanni Ramirez for training me on tribological experiments at Argonne National Laboratory IL.

At the end, I am honored to thank my parents, Prahlad Sharma and Jayanti Sharma, my brother Suvigya Sharma for their love and encouragement and to my good friends, Akanksha Pandey, Ajay Pareek, Varun Mehta, Sumit Uttamani, Nehal Mishra,

Manas Bapna, Rahul Jain, Arjun Modi, Hardik Shah who have supported and encouraged me throughout my graduate studies.

June 06, 2016

## Abstract

### MECHANISM OF WEAR AND TRIBOFILM FORMATION WITH IONIC LIQUIDS AND ASHLESS ANTIWEAR ADDITIVES

Vibhu Sharma, PhD

The University of Texas at Arlington, 2016

Supervisor: Pranesh B. Aswath

Increasingly stringent government regulation on emissions (EPA Emissions Standard Reference Guide and latest CAFE standards requiring an average fuel economy of 54.5 mpg (combined cars and trucks) by 2025) impose significant challenges to the automotive and lubricant industries calling for the development and implementation of lower viscosity ILSAC GF-5&6 and API-CJ4&5 oils which further limit the amount of SAPS and deposits in engines. Development of additives that result in lower ash content, volatility and anti-wear property plays a crucial role in being able to reach these standards. The current industrial additive technology i.e. zinc dialkyldithiophosphate (ZDDP) forms harmful deposits on catalytic convertor due to the volatility of Zn, S and P which, impairs its functionality and consequently results in higher emission from vehicles. In this research work, ionic liquids (IL's) that are non-volatile have been studied as new generation environment friendly antiwear additives along with other ashless anti-wear additives including boron based additives to overcome the current challenges of improving the fuel efficiency and reducing the amount of hazardous emissions. The goal of this thesis work is to study the tribological performance of selected IL's and develop a comprehensive understating of IL's chemistry and its consequences to their friction and

wear outcomes. As first approach, various P, S and F based ionic liquids are studied for their tribological properties by analyzing the friction and wear results generated using standard tribological experiments. Following this, advanced surface characterization techniques such as X-ray absorption near edge structure (XANES) spectroscopy, SEM, Nano-indentation, SPM techniques are used to investigate the chemical-mechanical properties of the antiwear films. Results indicate that the tribological properties of ionic liquids depend on their solubility in base oil (BO) as well as their chemical interaction with the rubbing surfaces. To address the solubility issue of IL's in BO, ILs with longer alkyl chain structure were carefully selected which helped enhance the van der waals interaction between strongly polar ILs and non-polar base oil. The interaction of IL's with the metal surfaces was examined by analyzing the chemical-mechanical properties of the antiwear films formed. Results indicate that ionic liquids do react with the steel surfaces and form a protective antiwear film composed of iron polyphosphates i.e. short to medium chain length which results in improved wear protection. In addition, soluble boron additive (SB) chemistries were blended with ionic liquids to study the synergism between these two ashless antiwear chemistries. Addition of soluble boron additive (SB) to phosphorous based IL (P\_DEHP) reduces the incubation time for antiwear film formation by forming boron oxide/boron phosphate film as early as the rubbing starts and subsequently a more durable iron phosphate film is formed providing long lasting wear protection. The synergistic interaction of boron chemistry with phosphorous based ionic liquids provides superior antiwear properties while eliminating volatile elements such as Zn and S from the additive technology.

## TABLE OF CONTENTS

Acknowledgements.....	3
Abstract        6	
List of Illustrations.....	13
Chapter 1. Introduction.....	22
1.1 Motivation for This Research.....	23
1.2 Objectives of This Research.....	25
1.3 Structure of This Research.....	28
Chapter 2. Background.....	31
2.1 Lubricants and Lubricant Additives.....	31
2.1.1 Zinc Dialkyldithiophosphate (ZDDP).....	32
2.1.2 Ashless antiwear additives.....	33
2.1.3 Ionic liquids.....	35
2.2 Types of Lubricated Contacts.....	41
2.2.1 Hydrodynamic lubrication regime.....	43
2.2.2 Elasto-hydrodynamic or mixed lubrication regime.....	43
2.2.3 Boundary lubrication regime.....	43
2.3 Tribofilms.....	44
2.3.1 Thermally induced tribofilms.....	47
2.3.2 Thermo-mechanically induced tribofilms.....	48
Chapter 3. Synergistic Effects of Ashless Fluorothiophosphates with Zinc Dialkyldithiophosphate (ZDDP) for Better Antiwear Properties and Tribofilm Formation	50
3.1 Introduction.....	50
3.2 Experimental Details.....	51
3.2.1 Description of Additive Chemistry.....	51



3.2.2 Tribological Test Procedure .....	52
3.2.3 Surface Characterization .....	53
3.3 Results and Discussion.....	54
3.3.1 Evaluation of Coefficient of Friction (CoF) and Wear Volume .....	54
3.3.2 Incubation Time for the Tribofilm Formation using ECR .....	57
3.3.3 Study of Surface Topography using SEM .....	59
3.3.4 Nano-mechanical Properties and 3D imaging of Tribofilms using Nano-indentation .....	60
3.3.5 Characterization of Tribofilms Chemistry using XANES .....	64
3.4 Discussion on XANES .....	79
3.4 Conclusion .....	80
 Chapter 4. Role of Cationic and Anionic Moieties of Ionic Liquids to Their Tribofilms Properties	 83
4.1 Introduction .....	83
4.2 Experimental Details .....	84
4.2.1 Structure and Chemistry of Ionic Liquids.....	84
4.2.2. Thermogravimetric (TGA) Analysis of Ionic Liquids .....	86
4.2.3. Tribological test procedure .....	86
4.2.4 Characterizations methods.....	88
4.3 Results and Discussions.....	90
4.3.1 Thermogravimetric Analysis of Ionic Liquids .....	90
4.3.2 Evaluation of Coefficient of Friction (CoF) and Wear Volume .....	91
4.3.3 Analysis of Rubbed Surfaces Using Scanning Electron Microscopy and Scanning Probe Microscopy.....	94
4.3.4 XANES Characterization of Tribofilms .....	96
4.3.4.1 Phosphorous L2,3-edge of Pure ILs.....	97

4.3.5 Nano-indentation .....	117
4.4 Conclusions.....	121
Chapter 5. Ashless chemistry of P and S based Ionic Liquids and Their tribofilm Formation Mechanism in Base oil and Fully Formulated oil (no Zinc) .....	123
5.1 Introduction.....	123
5.2 Experimental Details .....	123
5.2.1 Chemistry of Antiwear Additives.....	123
5.2.2 Tribological Test Procedure: .....	124
5.2.3 Characterization of Tribofilms.....	125
5.3 Results and Discussion.....	126
5.3.1 Thermogravimetric Analysis of Ionic Liquids.....	126
5.3.2 Coefficient of Friction.....	127
5.3.3 Topography of the Tribofilms using SEM and SPM .....	128
5.3.4 Chemical Properties of Tribofilms using XANES .....	130
5.3.5 Discussion of XANES and Development of Phenomenological Model of Tribofilms .....	142
5.4 Conclusion .....	145
Chapter 6. Advancing the tribological properties of Ionic Liquids with Synergistic Interaction of Borate Esters .....	147
6.1 Introduction .....	147
6.2 Experimental Details .....	147
6.2.1 Description of additive chemistry and Thermogravimetric analysis. ....	147
6.2.2 Tribological Test Details .....	149
6.2.3 Characterization of Tribofilms.....	151
6.3 Results and Discussion.....	152
6.3.1 Coefficient of Friction and Wear Volume.....	152

6.3.2 Incubation time for the tribofilm formation in correlation with thermogravimetric analysis (TGA) of additive chemistry .....	157
6.3.3 Topography of the Tribofilms using .....	161
6.3.4 Chemical Properties of Tribofilms using XANES .....	164
6.4 Conclusions.....	175
Chapter 7. Low phosphorous oil blends of phosphonium ionic liquids with borate esters for tribological applications in base oil.....	177
7.1 Introduction .....	177
7.2 Experimental Details .....	177
7.2.1 Chemistry of Antiwear Additives and Oil Formulation .....	177
7.2.2 Tribological Test Details .....	179
7.2.3 Characterization of Tribofilms.....	179
7.3 Results and Discussion.....	180
7.3.1 Coefficient of Friction and Wear Volume.....	180
7.3.2 Analysis of tribofilms formation using ECR .....	183
7.3.3 Chemical Properties of Tribofilms using XANES .....	186
7.3.4 Theory of tribochemical film formation .....	192
7.4 Conclusions.....	194
Chapter 8. Analysis of Tribofilms Formed using Phosphonium Ionic Liquids and Borate Esters in Fully Formulated Oil (no Zn).....	196
8.1 Introduction .....	196
8.2 Experimental Details .....	196
8.2.1 Description of additive chemistry and Thermogravimetric analysis. ....	196
8.2.2 Tribological Test Details .....	198
8.2.3 Characterization of Tribofilms.....	199
8.3 Results and Discussion.....	200

8.3.1 Coefficient of Friction and Wear Volume.....	200
8.3.2 Topography of the Tribofilms using SEM and SPM .....	203
8.3.3 Chemical Properties of Tribofilms using XANES .....	205
8.4 Conclusions.....	217
Copyrights and permission .....	219
References	220

## List of Illustrations

Figure 1: Schematic diagram of pad structure and composition [1].	27
Figure 2: The relation between the IL structure and tribological properties [2].	41
Figure 3: Tribological behavior of formulations with ZDDP and mixtures of ZDDP and ashless thiophosphates in base oil mixtures. Fig. 3(a) shows the coefficient of friction as a function of time at two different load i.e. 54N and 350N. Fig. 3(b) shows the comparison of wear volume for the different oil formulations at two different loads.	56
Figure 4: Electrical contact resistance for all the tribological tests with ZDDP and ZDDP with ashless thiophosphates conducted at 54N (a) and 350N (b).	59
Figure 5: Showing the secondary emission SEM images of the rubbed surfaces for the four different oil formulations at 54N at 350N.	60
Figure 6: Nano-mechanical properties of tribofilms obtained from nano-indentation using cyclic loading with partial unloading load function (shown in Fig. 6(a)). Fig. 6(b) & 6(c) show a comparison of nano-hardness profile of tribofilms using ZDDP and 80%ZDDP+20% PFC as a function of indentation depth at 54N and 350N respectively as well the corresponding 3-D SPM images.	64
Figure 7: (a) Phosphorous L-edge XANES TEY spectra of tribofilms generated at 54N and model compounds (b) Phosphorous L-edge XANES TEY spectra of tribofilms generated at 350 N and model compounds (c) Phosphorous L-edge XANES FY spectra of tribofilms generated at 350N and model compounds.	68

Figure 8 (a) Phosphorous K-edge XANES spectra of tribofilms generated at 54N and model compounds (b) Phosphorous K-edge XANES spectra of tribofilms generated at 350N and model compounds. ....	69
Figure 9: (a) Sulfur L-edge XANES TEY spectra of the tribofilms generated at 54 N. (b) Sulfur L-edge XANES TEY spectra for tribofilms generated at 350 N as well as the model compounds. ....	71
Figure 10: (a) Sulfur K-edge XANES spectra of the model compounds of sulfur. (b) Sulfur K-edge XANES TEY spectra of the tribofilms obtained at 54N. (c) Sulfur K-edge XANES TEY spectra of the tribofilms obtained at 350N. (d) Representative deconvolution process used to determine the contribution from the different valence states of sulfur in the tribofilm from a formulation that contains 80% ZDDP + 20%PFC18. ....	74
Figure 11: (a) Oxygen K-edge XANES spectra of model compounds containing oxygen. (b) Oxygen K-edge TEY spectra of tribofilms generated at loads of 54 and 350N. ....	77
Figure 12: (a) Zinc L-edge XANES spectra of model compounds that contain zinc (b) Zinc L-edge TEY spectra of tribofilms generated at loads of 54 and 350N. ....	79
Figure 13. Thermogravimetric analysis plot of six IL's and ZDDP showing the decomposition temperature of different additive chemistries. ....	91
Figure 14. Comparison of coefficient of friction of six IL's with ZDDP at equal phosphorous level (i.e. 0.1 wt% P) and base oil obtained under pure sliding contacts. ....	92
Figure 15. Average wear volume measured for six IL's and ZDDP blended in base oil at 0.1 wt% P and the neat base oil test. ....	93

Figure 16. Comparison of coefficient of friction and wear volume loss for six IL's and ZDDP. Data at the bottom left on the plot has the lowest wear and friction coefficient (beneficial) and the data on the top right hand corner has the higher wear and highest friction (detrimental).....	94
Figure 17. Secondary electron SEM images illustrating the morphology of worn surfaces derived from six IL's and ZDDP. ....	96
Figure 18. SPM images showing the 3D wear profile of the rubbed surfaces derived from six IL's and ZDDP. ....	96
Figure 19a. Phosphorous L <sub>2,3</sub> -edge FY spectra of pure IL's standards. ....	100
Figure 19. Phosphorous L <sub>2,3</sub> -edge spectra TEY (Fig. 19b) and FY (Fig. 19c) of tribofilms formed using ZDDP and six IL's additives. The <b>a/c</b> ratio obtained from P L edge indicating the degree of polymerization in the phosphate tribofilms is also shown in left hand side of each spectra. ....	104
Figure 20. Phosphorous K-edge FY spectra of pure IL standards (Fig. 20a) and tribofilms derived from ZDDP and six IL's as additives as well as model compounds (Fig. 20b). ....	109
Figure 21a. Sulfur K-edge spectra of sulfur containing IL standards.....	111
Figure 21. Sulfur K-edge spectra FY of model compounds (Fig. 21b) and tribofilms derived from ZDDP and six IL's (Fig. 21c). ....	113
Figure 22a. Oxygen K-edge spectra of pure IL standards. ....	115
Figure 22. Oxygen K-edge FY spectra of model compounds (Fig. 22b) and tribofilms formed from ZDDP and IL's lubrication (Fig. 22c). ....	117

Figure 23a. Showing a cyclic loading with partial unload load profile as a function of time (2s loading, 2s hold, and 2s unloading) used for nano-indentation. ....	120
Figure 23b. Nano-mechanical properties of tribofilms obtained using a cube corner (NorthStar™) probe, a typical load vs. penetration depth curve obtained (shown in top left corner) set a criteria for proper indentation. Selected hardness profiles as a function of indentation depth are displayed for ZDDP (top right) and IL N_DEHP (bottom left), and P_TFSI (bottom right) tribofilms. ....	121
Figure 24: Thermal decomposition temperature of N_DEHP and N_DBDTP IL using TGA analysis. ....	127
Fig. 25. Friction coefficient as a function of time for tribological tests conducted using a SRV tribometer for oils with N_DEHP and N_DBDTP with ZDDP in base oil and in fully formulated oil. ....	128
Figure 26. Secondary emission SEM images of the wear track derived from N_DEHP, N_DBDTP and ZDDP in base oil and fully formulated oil.....	130
Figure 27. 3-D scanning probe microscopy images of the wear track derived from N_DEHP, N_DBDTP and ZDDP in base oil and fully formulated oils. ....	130
Fig. 28. (a) Phosphorous L <sub>2,3</sub> -edge XANES TEY spectra of the tribofilms generated using N_DEHP, N_DBDTP and ZDDP in base oil and fully formulated oils. (b) Phosphorous L <sub>2,3</sub> -edge XANES TEY spectra of model compounds.....	134
Fig. 29. (a) Phosphorous K-edge XANES TEY spectra of the tribofilms generated using N_DEHP, N_DBDTP and ZDDP in base oil and fully formulated oils. (b) Phosphorous K-edge XANES TEY spectra of model compounds.....	137



Figure 30. Sulfur K-edge XANES TEY spectra of the tribofilms generated using N_DEHP, N_DBDTP and ZDDP in base oil and fully formulated oils. (b) Sulfur K-edge XANES TEY spectra of model compounds. ....	139
Figure 31: (a) Oxygen K-edge XANES TEY spectra of the tribofilms generated using N_DEHP, N_DBDTP and ZDDP in base oil and fully formulated oils. (b) Oxygen K-edge XANES TEY spectra of model compounds.....	142
Figure 32: Phenomenological model of the tribofilms generated using N_DEHP, N_DBDTP and ZDDP in base oil and fully formulated oils. ....	145
Figure 33. Coefficient of friction and wear volume obtained from test setup 1 for group1 BO, ZDDP, IL, SB and IL+SB in group 1 BO at 0.1 wt.% P and 0.02 wt.% B. ....	154
Figure 34. Coefficient of friction and wear scar diameter obtained from test setup 2 for group1 BO, ZDDP, P_DEHP and P_DEHP+SB1 in group 1 BO at 0.1 wt% P and 0.02 wt% B.....	156
Figure 35. Thermogravimetric analysis of additives of ZDDP and IL's (P_DEHP and P_DEPDT) and ECR plot of oil blends from test set up 1.....	160
Figure 36. 3D SPM images of rubbed surfaces generated under ZDDP, P_DEHP, P_DEHP+SB1 and P_DEHP+SB2 lubrication.....	163
Figure 37(a). P L-edge TEY spectra of tribofilms derived from ZDDP, ILs and IL+SB lubrication (black lines) with reference compounds (green lines).....	168
Figure 37(b). P L-edge FY spectra of tribofilms derived from ZDDP, ILs and IL+SB lubrication (black lines) with reference compounds (green lines).....	169

Figure 38. B K-edge TEY and FY of tribofilms derived from ZDDP, ILs and IL+SB lubrication (Figure 38(a)) with reference compounds (Figure 38(b)) .....	174
Figure 39: Coefficient of friction obtained for oil blends containing only SB2, P_DEHP(350P)+SB2 and P_DEHP(700P)+SB2. Showing the friction response of each oil blend for 5 mins, 15 mins and 60 mins test. ....	181
Figure 40: A plot of average CoF for the 60 mins test for each oil blend. ....	182
Figure 41: Wear volume loss obtained for oil blends containing only SB2, P_DEHP(350P)+SB2 and P_DEHP(700P)+SB2 for 60 mins test. ....	183
Figure 42: Electric contact resistance (ECR) data acquired for SB2, P_DEHP(350P)+SB2 and P_DEHP(700P)+SB2 for 5 min(black), 15 min (red) and 60 min (blue) tests. ....	185
Figure 43; Phosphorous L-edge spectra of tribofilms (black lines) derived at 5 min, 15 min and 60 min test for P_DEHP(350P)+SB2 and P_DEHP(700P)+SB2 lubrication along with model compounds (green lines). Figure 43(a) illustrates the total electron yield signal (TEY spectra) and Figure 43(b) illustrates the fluorescence yield signal (FY spectra).....	187
Figure 43c: P L-edge <b>a/c</b> ratio measured for tribofilms formed using P_DEHP(350P)+SB2 and P_DEHP(700P)+SB2 at 5 min, 15 min and 60 min test. ....	189
Figure 45: Coefficient of friction as a function of test duration obtained for low phosphorous fully formulated oil blends without AW and with AW (ZDDP, P_DEHP, P_DEHP+SB1 and P_DEHP+SB2).....	201
Figure 46: Wear volume measured for low phosphorous fully formulated oil blends without AW and with AW (ZDDP, P_DEHP, P_DEHP+SB1 and P_DEHP+SB2).....	202

Figure 47: SEM images of the wear track generated on the test flat. ....	204
Figure 48: SPM images of the wear track generated on the test flat. ....	205
Figure 49a: P L-edge TEY spectra of tribofilms derived from FFO (no Zn, no P), ZDDP FFO, P_DEHP FFO, P_DEHP+SB1 FFO and P_DEHP+SB2 FFO blends.....	208
Figure 49b: P L-edge FY spectra of tribofilms derived from FFO (no Zn, no P), ZDDP FFO, P_DEHP FFO, P_DEHP+SB1 FFO and P_DEHP+SB2 FFO blends.....	208
Figure 49c: P L-edge FY spectra of model compounds. ....	209
Figure 50a: B K-edge TEY spectra of tribofilms derived from FFO (no Zn, no P), ZDDP FFO, P_DEHP FFO, P_DEHP+SB1 FFO and P_DEHP+SB2 FFO blends (plotted in black lines) and are compared with model compounds (plotted in green lines).....	211
Figure 50b: B K-edge FY spectra of tribofilms derived from FFO (no Zn, no P), ZDDP FFO, P_DEHP FFO, P_DEHP+SB1 FFO and P_DEHP+SB2 FFO blends (plotted in black lines) and are compared with model compounds (plotted in green lines).....	211
Figure 51a: S L <sub>2,3</sub> -edge TEY spectra of tribofilms derived from FFO (no Zn, no P), ZDDP FFO, P_DEHP FFO, P_DEHP+SB1 FFO and P_DEHP+SB2 FFO blends (plotted in black lines).....	214
Figure 51b: S L <sub>2,3</sub> -edge FY spectra of tribofilms derived from FFO (no Zn, no P), ZDDP FFO, P_DEHP FFO, P_DEHP+SB1 FFO and P_DEHP+SB2 FFO blends (plotted in black lines).....	214
Figure 51c: S L <sub>2,3</sub> -edge FY spectra of model compounds. ....	215

Figure 52a: Ca K-edge TEY spectra of tribofilms derived from FFO (no Zn, no P), ZDDP FFO, P\_DEHP FFO, P\_DEHP+SB1 FFO and P\_DEHP+SB2 FFO blends (plotted in black lines)..... 216

Figure 52b: Ca K-edge FY spectra of tribofilms derived from FFO (no Zn, no P), ZDDP FFO, P\_DEHP FFO, P\_DEHP+SB1 FFO and P\_DEHP+SB2 FFO blends (plotted in black lines)..... 216

Figure 52c: Ca K-edge FY spectra of model compounds..... 217

## List of Tables

Table 1 Comparison between in-situ tribofilms and surface coatings.....	46
Table 2 Structure of the Anti-wear Additive Compounds .....	51
Table 3: Details peak fitting for the S K-edge spectra and ratio of sulfides to sulfates....	75
Table 4. Molecular structure of six IL's and ZDDP and their onset decomposition temperature. ....	85
Table 5. Schematic of the test configurations and detail of test parameters for cylinder on reciprocating flat contact under pure sliding .....	88
Table 6. P L-edge model compounds and Ionic liquids standard peak positions.....	101
Table 7. P L-edge a/c ratio of tribofilms.....	105
Table 8. P K-edge model compounds and Ionic liquids standard peak positions.....	109
Table 9. Tribological test condition employed in the SRV tests. ....	124
Table10: a/c ratio of P L <sub>2,3</sub> edge for the tribofilms derived from ZDDP, IL-P and IL-TP in TEY and FY mode .....	135
Table 11. Description of additive chemistry.....	148
Table 12. Schematic of the test configurations and detail of test parameters for test setup 1 and test setup 2.....	151
Table 13: Molecular structure of six IL's and ZDDP.....	178
Table 14: Details of low phosphorous oil formulation prepared using P_DEHP and SB2 AW additives .....	178
Table 15. Description of additive chemistry.....	197
Table 16. Schematic of the test configurations and detail of test parameters.....	199

## Chapter 1. Introduction

Increasingly stringent government regulation on emissions (EPA Emissions Standard Reference Guide [3]) and latest CAFE standards requiring an average fuel economy of 54.5 mpg (combined cars and trucks) [4] by 2025 impose significant challenges to the automotive and lubricant industries calling for the development and implementation of lower viscosity ILSAC GF-5&6 and API-CJ4&5 oils which further limit the amount of SAPS and deposits in engines [5]. Development of additives that result in lower ash content, volatility and anti-wear property plays a crucial role in being able to reach these standards. Meanwhile the automotive industry is thriving to improve the efficiency and fuel economy of the vehicles as well as their longevity and reliability. The efficiency of the automotive systems can be improved significantly by reducing the frictional losses as well as by minimizing the wear. In a recent study, Holmberg et al. [6,7] concluded that latest technological advances in the field of tribology could lead to up to 14% reduction in frictional losses in heavy duty vehicles and up to 18% friction reduction in passenger vehicles in short term (i.e. within 5-10 year). At the same time CO<sub>2</sub> emission could also be reduced by 200 million tonnes in heavy duty vehicles and 290 million tonnes in passenger vehicles. Potential technological advances in tribology include novel lubricant additives such as ionic liquids (ILs) [2,8-12], ashless fluorothiophosphates [13-16], low friction coatings [17], surface texturing [18] and low viscosity and low shear lubricant oils [19].

Of all the approaches used, additive development offers the potential for providing in-situ low friction film formation at a low cost. However, the new engine

technologies such as turbo-charged gasoline direct ignition (TGDI) and complex engine designs result in much higher combustion temperature and severe oxidative conditions, which limit the use of tradition lubricant additives. To overcome these challenges, the surge of new generation additives is undertaken. Recent studies [2,9,11,12,20,20-30] have shown that ionic liquids (ILs) that are ashless additives, offer great potential as high performance environmental friendly additives for the next generation of lubricants.

This research study focuses on oil soluble ionic liquids (ILs) that include phosphorous as one of the constituents. IL's are well known compounds and have been used in many engineering applications [31-35]. IL's in tribology is a relatively new development, with application of IL's as lubricant/lubricant additive first recognized in 2001 [36]. The advantages of ionic liquids include their negligible vapor pressure, high thermal stability, non-flammability, non-volatility and electrochemical properties that are highly desirable for tribological applications. However, their limitations have included low solubility in oils due to their highly polar structure that can be mitigated to some extent by engineering their structure [22].

### 1.1 Motivation for This Research

Recent regulatory changes have resulted in stringent limits on the amount of emissions allowed from the tailpipe of automobiles and latest CAFE standards demanding higher fuel economy i.e. 54.5 mpg in 2025 have imposed severe challenges to the automotive industries. Current lubricant additives (e.g. Zinc Dialkyldithiophosphate) used in engines are responsible for poisoning catalytic convertors resulting in increased emissions. A choice of better lubricant additives can play a major role to address these

regulation and at the same time reduces tribological losses (i.e. Frictional losses and wear) and improve fuel economy, longevity and reliability of the systems. Ionic liquids (IL's) are attractive both as a lubricant and lubricant additive. They have negligible vapor pressure, high polarity, high thermal stability, non-flammability, miscibility with water and with organic solvents and electrochemical properties which are highly desirable for tribological applications. This research work is focused on the study of ionic liquids as an environment friendly lubricant additive together with other ashless anti-wear additives and boron based additives to overcome the current challenges of improving the fuel efficiency and reducing wear and amount of hazardous emissions. This study examines the role of IL's as a lubricant additive and their influence on friction and wear behavior. The solubility of IL's also investigated in base oil as well as in fully formulated oil. In order to understand the mechanism of wear and friction this research have also included in-depth analysis of tribofilms using XANES (X-Ray Absorption Near Edge Structure. XANES analysis is very effective in understanding the chemical nature of tribofilms as it can gives very precise information of the chemical coordination of the elements present on the rubbed surfaces. The goal of this study is to reduce the amount of phosphorous, sulfur and other metallic species (such as Zinc) in the lubricant while at the same time reducing the sludge formation and deposit formation. This thesis includes tribological testing of the lubricants using the cylinder on reciprocating flat test and ball on rotating disc test set-ups. Advanced characterization techniques such as XANES will be used to understand the growth mechanism of the tribofilms. Further evaluation of the chemical and mechanical properties of the tribofilms will be done using XPS, SEM and Nano-



Indentation. Using these different techniques it is the goal of this project to develop a phenomenological model of the structure, chemistry and properties of tribofilms and relate it to the tribological properties i.e. friction and wear behavior of ionic liquids and ashless antiwear additives.

## 1.2 Objectives of This Research

The objective of this thesis is to develop an underlying mechanism of lubrication behavior of new generation antiwear additives (i.e. “Metal Free”) and at the same time transitioning from an “Ashed” antiwear additive technology (i.e. Zinc Dialkyldithiophosphate) to an “Ashless” antiwear technology with an edge on tribological properties. In pursuit of this goal, this thesis work includes in depth analysis of lubrication characteristics of carefully selected ionic liquids structures as well as ashless (i.e. “Metal Free”) antiwear additives. These specific ionic liquids structure and ashless fluorothiphosphate antiwear additive were carefully selected for the purpose of this thesis work by considering two important points, first, they should offer better antiwear properties than the existing antiwear technology (i.e. Zinc Dialkyldithiophosphate) & second and more importantly, should be environmental friendly. Hence, as first approach to this research work, antiwear behavior of new generation antiwear additives (IL’s & ashless additives) are scrutinized under mixed to boundary lubrication condition under pure sliding contact and wear results are compared with ZDDP antiwear additive at identical test conditions. In order to achieve better antiwear outcomes a synergistic mixtures of two ashless antiwear additives (ILs and/or borate esters) were prepared in optimum composition to enhance the friction and antiwear

behavior of ionic liquids. After screening out the promising ashless additives/additives mixtures in terms of their potential as antiwear additives, the second objective of this thesis is to understand the chemical and mechanical properties of the tribofilms formed under the lubrication of these additives. An in-depth characterization of the worn surface morphology as well as nano-mechanical and chemical properties of in-situ formed tribofilms shed insight into the mechanism of wear and tribofilm formation using ionic liquids by themselves and in synergistic mixtures with other ashless antiwear additive or boron based additives. In the final approach, a phenomenological model of tribofilms formed under ILs lubrication is suggested by combining the knowledge gained from the earlier approaches.

#### **Hypothesis.....**

Besides the unresolved understanding of the multidisciplinary nature of the antiwear process that includes knowledge of organic solution chemistry, surface adsorption phenomenon, inorganic chemistry, metallurgy, metrology and mechanical design and their influence on tribological system all at once. It has been widely accepted by the researchers in this field of science that the antiwear properties of a well-known additive (i.e. ZDDP) is a reflection of its capability to form fusible glassy compounds such as phosphates as well as sulfides under existing high temperature and shear forces in tribological system. These so derived additive by-product of ZDDP chemistry (i.e. phosphates and organic sulfides) nucleate on the rubbing surfaces in the form of metal polyphosphate and/or metal sulfides/sulfates where the contribution of metal cations primarily comes from either by ZDDP antiwear additive in the form of  $Zn^{+2}$  or  $Fe^{+2}$ .

cations from the oxide layer of iron from steel substrates. A schematic of ZDDP tribofilms suggested by H. Spikes [1] is shown in figure 1.

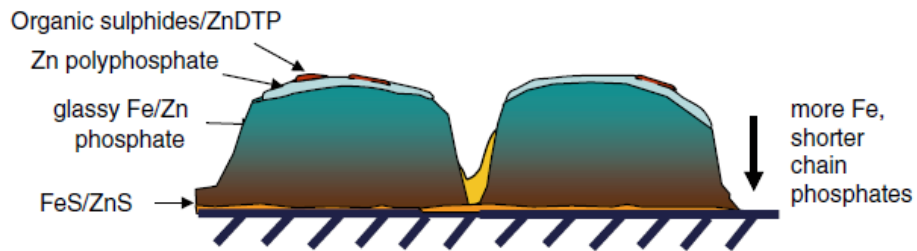


Figure 1: Schematic diagram of pad structure and composition [1].

The author postulate that the novel antiwear additive technology proposed in this thesis work containing primarily phosphorous and sulfur as well fluorine in addition under the tribological conditions (i.e. high temperature and shear forces) would also derive phosphates and sulfides compounds to form protective glassy antiwear films on the rubbing surfaces. Since the only source of metal cations to form antiwear films of metal polyphosphate/sulfides in case of “Metal Free” antiwear chemistry is  $\text{Fe}^{+2}$  from  $\text{Fe}_2\text{O}_3$  layer exists on steel substrate, the interaction of additives with the rubbing surfaces is accelerated to induce faster tribofilm formation. This would be expected to result into improved wear protection during the mechanical rubbing action at the same time minimizing the deposits formation on the After Treatment Systems that would have been resulted from the use of metal containing “Ashed” antiwear additive technology (such as ZDDP).

In order to gain the insight of this proposed hypothesis, wear surfaces will be generated using carefully selected ionic liquid chemistries and ashless

fluorothiophosphates by themselves and in synergistic mixtures in base oil (BO) as well as in fully formulated oils (FFO) with all the additives except antiwear additives (no Zn or P) at identical test condition under pure sliding contact test. The tribofilms formed under the lubricated mechanical rubbing action are analyzed using an advanced surface characterization technique such as XANES. The knowledge of chemical nature and composition of so formed tribofilms will then compliment the proposed hypothesis. In parallel to the characterization of tribofilms, a decomposition mechanism will also be studied for these proposed “Metal Free” antiwear technology using mass spectroscopy and other relevant techniques to sketch the possible pathways of tribofilms formation. Such comprehensive study will deepen the understanding of the mechanism of wear and tribofilms formation using ILs and ashless antiwear additives and will successfully explain their antiwear properties under tribological conditions.

### 1.3 Structure of This Research

This dissertation consists of eight chapters. An outline and summary of each chapter are presented here.

Chapter 1, introduction: This chapter includes an introduction to the field of interest to this research work i.e. tribology and lubrication science. It also provides the motivation and objectives behind this thesis work to the readers.

Chapter 2, background: This chapter provides a detailed background on lubricant and lubricant additives, antiwear additives such as ZDDP, ashless antiwear additives and ionic liquids, lubrication mechanism and in-situ formed tribofilms.

Chapter 3, studies the synergistic effects of ashless fluorothiophosphates with zinc dialkyldithiophosphate (ZDDP) for improved antiwear properties and tribofilm formation. Alkylphosphorofluoridithioate and Alkylthioperoxydiphosphate were added to ZDDP at 80-20 wt. % and their tribological properties were examined in base oil under pure sliding contact using cylinder on reciprocating flat tribological test setup. Tribofilms formed using only ZDDP were compared with that formed using mixtures of ZDDP and ashless fluorothiophosphates at 20 wt.% using SEM, nano-indentation and XANES.

Chapter 4, focuses on the role of cationic and anionic moieties of ionic liquids to their tribofilms properties. Six phosphorous (P) based IL's (in which P is either present in anion or in cation or in both) were chosen to examine the role of different cations and anions to their friction and wear results under pure sliding contact. XANES spectroscopy was also employed to examine the chemical interaction of ionic liquids with the steel surfaces and tribofilms formation mechanism.

Chapter 5, studies ashless chemistry of P and S based ionic liquids and their tribofilm formation mechanism in base oil and fully formulated oil (no zinc).

Chapter 6, examines the synergistic interaction of phosphonium IL's with borate ester (SB) for improvement in the antiwear properties. Binary additive mixture of IL's and SB were prepared at 0.1 wt.% P and 0.02 wt.% B and their tribological properties were evaluated under pure sliding contact using cylinder on reciprocating flat and ball on rotating disc tribological test setup. Electric contact resistance (ECR) technique was employed to study the tribofilm incubation time and XANES technique was used to study

the chemical properties of the tribofilms derived from the binary additive mixture of IL's and SB.

Chapter 7, investigates the tribological properties of low phosphorous oil blends prepared from phosphorous based IL's and borate esters. Effect of phosphorous concentration on friction and wear was studied by adding phosphorous at 350P ppm and 700P ppm. Interaction of borate esters and phosphonium IL's and evolution in the tribofilms chemistry was characterized by probing the P L-edge and B K-edge spectra acquired using XANES for 5 min, 15 min and 60 min rubbing time.

Chapter 8, examines the tribological performance of synergistic blend of phosphonium IL's and borate esters (SB) for low phosphorous oils prepared using fully formulated oil (no Zn) and compare with that of ZDDP at equal phosphorous treat rate i.e. 700P ppm. This chapter also analyzes the tribofilms formed using phosphonium ionic liquids and borate esters in fully formulated oil (no Zn) using SEM, SPM and XANES.

## Chapter 2. Background

### 2.1 Lubricants and Lubricant Additives

Lubricant is a medium that is applied between the counter surfaces in relative motion to serve two purpose, first, reduce the frictional resistance by providing relatively smoother surface and second, to promote the formation of protective tribofilms on counter surfaces to reduce materials deterioration. A lubrication system can be made available in three phase depending on the application, which are semi-solid phase as in grease, liquid phase as in oil and gaseous phase such as air, nitrogen etc. Lubrication system consists of two parts, first, lubricant matrix such as base oil, base grease and second, performance additives. The base oil serve many function such as provides thermo-oxidative stability, viscosity, density, color, heat dissipation [37]. However, there are some critical function that the base oil alone is not able to serve, for this purpose, performance additives are added to supplement the limitation and to enhance the performance of base oil [38].

Antiwear additives are among the most critical lubricant additives added in an engine oil package. Antiwear additives play a crucial role in reducing wear that can potentially enhance the efficiency and reliability of automotive engines. For this purpose, zinc dialkyldithiophosphate (ZDDP) has been used most commonly in an engine oil formulation due to its excellent antiwear and anti-oxidation properties. However, due to the volatility of Zn, S and P in ZDDP and increasing government regulation on emission, ashless antiwear additives and ionic liquids have recently been explored as possible replacement to ZDDP.

### 2.1.1 Zinc Dialkyldithiophosphate (ZDDP)

ZDDP was discovered about 80 years ago and since then it has been extensively used in the industries as an anti-wear (AW), anti-oxidant (AO) and Extreme Pressure (EP) additive [1,39-44]. Such properties of ZDDP additive were hypothesized to be gained by the formation of a thermal film or a tribofilm due to the decomposition of the ZDDP, which are well summarized by H. Spikes [1]. Jones and Coy [45] proposed the mechanism of thermal degradation of the ZDDP. In this study  $^{31}\text{P}$  and  $^1\text{H}$  NMR spectroscopy was used to identify the decomposition products of thermally heated ZDDP. It was observed that the intermolecular transfer had occurred as well as the migration of the alkyl functions from oxygen to sulfur atoms also took place (i.e. P-O-R to P-S-R). Dialkyl sulfides, alkyl mercaptan and dialkyl disulfide were found as well as soluble phosphates combined to sulfur and insoluble phosphorous bound to oxygen were confirmed. Taylor et al. [46] studied the friction behavior of ZDDP in a rolling/sliding rig type of wear test. The topographical measurement of the tribofilms was done using a space layer imaging method (SLIM). The results showed that the antiwear film formed during the rubbing was unevenly distributed and roughness was oriented in the sliding direction which, consequently result in the high friction values. Willermet et al. [40] reported that the antiwear films was formed due to the oxidative decomposition of ZDTP and was largely composed of inorganic amorphous phosphates. In a study involving the reaction of inorganic fluorides with ZDDP it was shown that replacing sulfur with fluorine in the structure resulted in a fluorinated version of ZDDP that had improved wear behavior that could be attributed to a more tenacious tribofilm formed on the



surface [47]. Additional studies on the fluorinated ZDDP indicated improved wear performance under high load conditions that could be attributed to the formation of more durable tribofilms [48]. Warren et al. [49] further explored the tribofilm surfaces and introduced two salient features “ridges and troughs” of tribofilms using an interfacial force microscopy (IFM). The nano-mechanical measurements showed that the ridges regions are harder and stiffer than the trough region thus it was concluded that ridge region carried most of the load during the wear test as they are aligned to the direction of sliding. In a recent study examining the role of contact load on wear behavior Mourhatch and Aswath have shown that increasing contract load results in tribofilms that are harder than at smaller contact loads [50] complementing the finding of Warren et al. [49].

Since, ZDDP has several advantages as a lubricant additive in term of multi-functionality as antiwear, extreme pressure, antioxidant and corrosion inhibitor, it has been used in engine oils for decades [1,40,51]. However, ZDDP has demerits as it is a main source of P, S and metallic residues of Zn in the exhaust. The presence of these elements arises to the problem of toxicity to the environment and degradation to the catalytic convertor in engines [1,52-54]. Thus a need to develop more environmental friendly additives has been recently addressed and research focus has been shifted in developing ashless i.e. metal free lubricant additives [16,53,55,56] and much recently to ionic liquids [2,2,11,30,57,58] for antiwear applications.

### *2.1.2 Ashless antiwear additives*

Metal free ashless lubricant additives have been synthesized and proposed as a promising replacement of ZDDP with better or comparable antifricition, antiwear,

antioxidant and extreme pressure properties [13,53,59-61,61,62]. Commonly recognized ashless chemistries as lubricant additive are phosphorous and sulfur based compounds i.e. phosphate esters [63], thiophosphates and dithiophosphates [16,52,64,65], alkyl/aryl mono and/or di-hydrocarbyl phosphates, amine salts of aryl/alkylaryl/ arylalkyl or aliphatic di-hydrocarbyl thiophosphates [61], diester polysulfides [62], dithiocarbamic [60], amidothiophosphates [65], Benzotriazole-thiadiazol [61] and most recently alkylthioperoxydiphosphates and alkylphosphorofluoridothioates [13,59].

Several ashless lubricant additive have been shown to possess comparable or even better AW, AO, AF and EP properties than ZDDP [13,15,16,53,55,66,67]. However, their mechanism of wear protection is still a challenge. Najman et al. [51,64] studied the mechanism of film formation and spatial distribution of chemical species in thermal and tribofilms derived from ashless antiwear chemistries using X-ray absorption near edge structure spectroscopy (XANES), Photo-emission electron microscopy (PEEM) and X-ray photoelectron spectroscopy (XPS) and concluded that the films contain short or long chain iron polyphosphates and iron sulfates. And also the topographic study using Atomic force microscopy (AFM) showed that the films were composed of elongated short and large antiwear pads oriented in the sliding direction. In a similar study, Kim et al. [16] compared the tribofilms derived from ashless dithiodiphosphates (ADDPs) and ZDDP using XANES and reported the similar kind of structure of the tribofilms with ADDPS as of ZDDP with harder crust and compliant bulk to give good antiwear performance. In addition, Kim et al. [16,52] also characterized the wear debris harvested from the wear test (i.e. ball on cylinder) ran under extreme pressure conditions of several

ashless dithiophosphates based additives and reported  $\text{Fe}_3\text{O}_4$  nanoparticles embedded in the amorphous structure of tribofilms. The wear performance was correlated to the number of nanocrystalline oxide particles with the one with smaller number of oxide particles exhibiting the best wear performance. They also compared the thickness of the films derived from the ashless dialkyl dithiophosphates and ZDDP and reported that the tribofilms formed using ashless additives were significantly thicker than the one formed by ZDDP. Nicholls et al. [54] proposed a 3 stage tribofilms formation mechanism of ashless dialkyldithiophosphate (DTP), initial physical/chemical absorption of DTP, then initial film formation on the surface when Fe are plentiful and stage3 when surface is covered with thin film of Fe phosphate and no cation is accessible from the substrate. They also characterized the tribofilms derived from the DTP using XANES and suggested that the tribofilms derived from the ashless DTP primarily contains short chain iron polyphosphates.

### *2.1.3 Ionic liquids*

The versatility of ionic liquids is not unknown in realms of science and engineering. Ionic liquids offers great flexibility of obtaining a task specific properties by designing a particular set of cation and anion, hence are available in million types for many different application. Ionic liquids have been used as electrolytes in batteries, supercritical fluids, heat transfer fluids, active pharmaceutical ingredients, solvents for chemical synthesis, engineering fluids etc. [31-35] and are still finding new application one of which is lubricants in tribology [2,30].

With the growing interest for the use of environment friendly ashless lubricant additives in engine and motor oils, ionic liquids are a possible alternative to traditional additives. Ionic liquids are synthetic salts with a melting point below 100 °C. A commonly used term in tribology is room temperature ionic liquids (RT-IL's) that have a melting point at or below room temperatures. The Ionic liquid of interest for lubrication contains a cationic and anionic species of which one or both are organic. Either cation or anion or both has/have delocalized charge, which prevents the formation of a stable crystal, resulting in a poor co-ordination of these ions. Hence these IL compounds are liquid at room temperatures [68,69].

Ionic liquids have negligible vapor pressure, high polarity, high thermal stability, non-flammability, non-volatility, miscibility with water and with organic solvents and electrochemical properties that are highly desirable for tribological applications. Minami [2] reviewed various ionic liquids for their tribological properties and proposed a relationship between the chemical structure of IL's and their lubricant properties.

Since the first article on the use of RT-IL's as a lubricant published in 2001 [36] a number of research studies have focused on finding promising ionic liquid structures to meet the required tribological properties as well as to understand the underlying mechanism of tribofilms formation [2,9,11,12,20,20-30,36,57,58,69-78]. In tribology, most commonly studied IL's include cation's such as imidazolium, ammonium/aromatic amine and phosphonium and anions those are, tetrafluoroborate, hexafluorophosphate, sulfonates and bis (fluoroalkylsulfonyl)-amides [2,23,24,26,27,72,79-86].

Jiménez et al. [83] studied 1-N-alkyl-3-methylimidazolium based ILs with tetrafluoroborate and hexafluorophosphate anions as neat lubricant and lubricant additives and reported a significant improvement in lubrication properties (friction and wear reduction) when ILs are added in base oil as an additives (1 wt. %) in comparison to when used as neat lubricants at room temperature as well at 100 °C. In another study by Jiménez et al. [87], lubrication properties of imidazolium based ILs were studied at low as well as at elevated temperatures. They reported that tetrafluoroborate 1-hexyl/octyl-3-methylimidazolium ILs show higher thermal stability and better lubricating performance than mineral and synthetic oils under extreme temperature conditions, both at low (-30 °C) and high (100 °C, 200 °C) temperatures. Tribocorrosion due to ILs was also observed in the case of more polar and shorter alkyl chain tetrafluoroborate 1-hexyl-3-methylimidazolium IL at elevated temperature. Pisarova et al. [23] studied the thermal stability and corrosion properties of ammonium based ILs with Bis (trifluoromethylsulfonyl) imide (NTF<sub>2</sub>) and methanesulfonate anions. They reported that corrosiveness of ILs depends on the choice of cation and anion, choline NTF<sub>2</sub> IL showed significantly lower corrosiveness and higher thermal stability than choline methanesulfonate IL. Pisarova et al. [82] also studied the degradation mechanism of ammonium ILs and their tribological properties using mass spectrometry. An intermolecular transmethylation in ammonium IL was identified under long term thermo-oxidative stress. They also suggested that IL altered products due to thermal degradation can negatively influence their tribological performances. Imidazolium and ammonium based ILs with halogenated anions (PF<sub>6</sub><sup>-</sup>, BF<sub>4</sub><sup>-</sup> and Bis trifluorosulfonyl imide TFSI<sup>-</sup>)

show potential improvement in friction and wear performance when used as neat lubricant or as lubricant additive in base oil. However, corrosiveness and solubility in non-polar base oil is still a limitations to their tribological application. Totolin et al. [27] studied and compared the tribological properties of halogenated and halogen free alkylborane–imidazole and phosphonium phosphate ionic liquids. They reported that phosphate tribofilms yielded from phosphonium-phosphate IL exhibit better tribological properties than fluoride based tribofilms from halogenated IL. Recently, Qu et al. [9,25,88] studied oil miscible phosphonium-phosphate ionic liquids (PP-IL) as lubricant additives in base oil as well as in fully formulated oil. They reported comparable or even superior antiwear and anti-scuffing properties of phosphonium IL in comparison with the conventional additive i.e. ZDDP in PAO base oils at 0.1% Phosphorous.

Jiménez et al. [83] studied the wear surfaces generated using 1-N-alkyl-3-methylimidazolium IL as lubricant as well as lubricant additive (1 wt.%) using scanning electron microscopy (SEM) coupled with energy dispersive spectroscopy (EDS) and x-ray photoelectron spectroscopy (XPS) in steel-aluminum contacts and reported the formation of tribolayers on steel balls containing aluminum and phosphorous. X-ray diffraction was also used to detect the formation of boron oxide over the wear track generated using 1-octyl,-3-methylimidazolium tetrafluoroborate IL on steel-titanium contact [28]. XPS has been used most commonly to investigate the chemical states of critical elements of IL derived tribofilms. Liu et al. [77] investigated wear mechanism of phosphonium based IL's using XPS and identified formation  $\text{AlF}_3$ ,  $\text{Al}_2\text{O}_3$ ,  $\text{AlO}(\text{OH})$ ,  $\text{Al}(\text{OH})_3$  as well as  $\text{AlF}_3\text{B}_2\text{O}_3$  and  $\text{AlPO}_4$  under the tribo-chemical reaction of anions

with the fresh surface. Kamimura et al. [89] used XPS and time of flight-secondary ion mass spectroscopy (TOF-SIMS) to study the chemistry of worn surfaces derived from imidazolium, pyridinium, ammonium (cation) and tetrafluoroborate ( $\text{BF}_4^-$ ) and bis(trifluoromethanesulfonyl)imide ( $\text{TFSI}^-$ ) (anion) based IL's and detected organic fluoride, iron fluoride and iron sulfates over the worn surfaces. Their study revealed that elements derived from the anion moiety of IL's are present over worn surfaces in the form of organic fluoride, iron fluoride and iron sulfates suggesting that adsorption of the anionic moiety took place followed by the tribo-chemical reaction. In another study, Minami et al. [79] studied the tribo-chemistry of phosphonium derived IL's using Auger electron spectroscopy (AES) and XPS surface analytical techniques. Boundary film composed of phosphate and fluoride structure was identified. They also suggested that formation of phosphate film inhibited the reaction of the bis(trifluoromethanesulfonyl)imide anion that yielded metal fluoride on the rubbed surfaces. Their study revealed that phosphate boundary film exhibited better tribological properties than those of fluoride boundary film. Gabler et al. [81] analyzed the tribolayer chemistry using XPS depth profiling as well as XPS imaging techniques for bis(trifluoromethanesulfonyl)imide ionic liquid with various cationic moieties. In their study, it was found that no measurable chemical modification occurred on the structure of cationic moiety during the tribotest, suggesting cation's were not involved in the formation of the tribolayer. However, it was observed that depending on the presence of cation, degradation of anionic moiety varied in the order of phosphonium > imidazolium > pyrrolidinium > sulfonium > ammonium. Similarly, in a recent study [22] influence of

cationic structure on physiochemical and lubrication properties of IL's has been studied. It was reported that larger cation's are more soluble with six carbons per alkyl chain a critical minimum for oil miscibility (found in their study). Besides it was also reported that symmetric cation's show better tribological outcomes in comparison to asymmetric cation's with identical anion. Qu et al. [90] studied the nanostructure, film thickness and compositional change of boundary film on IL lubricated metallic surfaces using cross sectional TEM coupled with EDS and compositional depth profiling by XPS. The measured mean film thickness on cast iron, steel and aluminum worn surfaces were 300, 60 and 200nm respectively. TEM analysis of boundary film on ferrous alloys revealed very fine nano crystal structure well dispersed in amorphous phase matrix while the film on aluminum comprises many larger size (tens of nm) metallic particles in less orderly manner. Recently, Qu et al. [25,88] studied oil miscible phosphonium-phosphate ionic liquids (PP-IL) as lubricant additives in base oil as well as in fully formulated oil and showed improved wear performance in the presence of ionic liquids. Qu et al. [9] also showed comparable or even superior antiwear and anti-scuffing properties of phosphonium IL in comparison with the conventional additive i.e. ZDDP in PAO base oils at 0.1% Phosphorous.



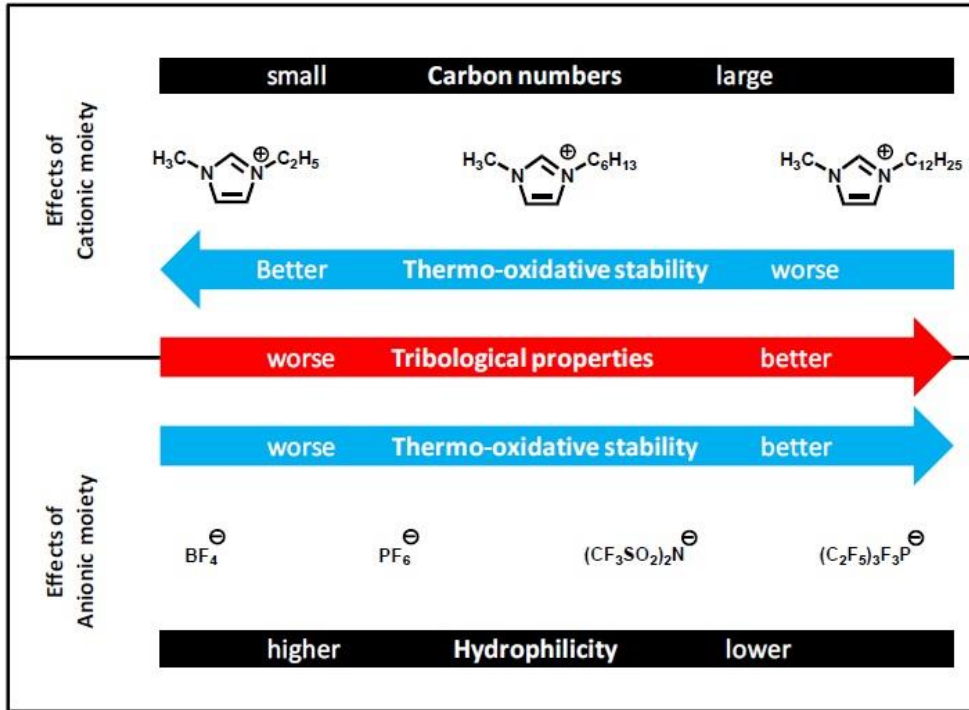


Figure 2: The relation between the IL structure and tribological properties [2].

## 2.2 Types of Lubricated Contacts

Lubricated contacts are generated via fluid film lubrication system in which a thin film of lubricant separates the interacting surfaces. The friction force and the resulting wear rate depend on the thickness of the fluid film or lubricant film. The ratio of lubricant film thickness to the surface roughness of the sliding surfaces determines the type of lubrication regime and is generally described as  $\lambda$  and shown in following equation [91];

$$\lambda = \frac{h_{min}}{\sigma^*} \quad (1)$$

$h_{min}$  = minimum thickness of the lubricant film

$\sigma^*$  = root mean square roughness of the two surfaces

Based on  $\lambda$  value, lubrication regimes can be divided into 3 types.

Hydrodynamic lubrication ( $\lambda > \sim 5$ )

Elasto-hydrodynamic lubrication or mixed lubrication ( $1 < \lambda < 5$ )

Boundary lubrication ( $\lambda < 1$ )

Ramoun et al. [92,93] has detailed the calculations for the fluid film thickness using the most commonly used elstohydrodynamic lubrication theories. The four commonly used equations for lubricant film calculation are shown below;

Grubin's equation [94]

$$H = 1.95 G^{0.73} U^{0.73} W^{0.091} \quad (2)$$

Dowson-Higginson equation [95]

$$H = 1.6 G^{0.6} U^{0.7} W^{0.13} \quad (3)$$

Archard-Cowking equation [96]

$$H = 2.04 \left( 1 + \left( \frac{2R_x}{3R_y} \right) \right)^{-0.74} G^{0.74} U^{0.74} W^{0.1} \quad (4)$$

Hamrock-Dawson equation [97]

$$H = 3.63 (1 - e^{-0.68 K}) G^{0.5} U^{0.68} W^{0.1} \quad (5)$$

Where H is the ratio of film thickness to the equivalent radius in the rolling direction. U, G and W are the speed, materials and load parameters respectively.  $R_x$  and  $R_y$  are equivalent radii in the sliding direction and transverse to it respectively.

A graphical representation of these 3 lubrication regimes can be shown in stribeck curve (figure 1 [91] ). Stribeck curve defines a relation between the coefficient of friction and lubrication parameters (absolute viscosity of oil, relative speed, component geometry and load) and plays an important role in identifying the boundary, mixed and hydrodynamic lubrication regimes [98].

### *2.2.1 Hydrodynamic lubrication regime*

At low loads and high sliding speeds two interacting surfaces are separated by a thick layer of lubricant film. Here,  $\lambda$  value can be as high as 5. A typical schematic of hydrodynamic regime is shown in figure 2(a) [91]. In hydrodynamic regime, asperity contact is negligible and the full fluid film separates the surfaces at all times. Minimum friction resistance against the motion and wear occurs in this lubrication regime. In hydrodynamic lubrication regime, physical properties of lubricant such as viscosity, load bearing capability and traction play important role on the performance of the lubrication mechanism [92].

### *2.2.2 Elasto-hydrodynamic or mixed lubrication regime*

At relatively high loads and slow speeds, a system runs into elasto-hydrodynamic regime. Due to the increasing pressure, the viscosity of the lubricant increases which when carried into the convergent zone approaching the contact area, causes elastic deformation to the interacting surfaces. Since the lubricant viscosity increases due to the hydrodynamic pressure and short time is available to carry the lubricant through the contact area, lubricant cannot escape and the surfaces remain separated. A schematic of lubricated contacts in elasto-hydrodynamic lubrication is shown in figure 2(b) [91]. Here,  $\lambda$  values is smaller than 5 and fluid film thickness is greater than  $1\mu\text{m}$  [99].

### *2.2.3 Boundary lubrication regime*

Boundary lubrication is defined as the lubrication regime where the average fluid film thickness is than root mean square roughness of the two surfaces ( $\sigma^*$ ). In boundary lubrication regime interacting surfaces move against each other under high contact loads

or pressure and very slow speeds as a result, asperities from one surface collide with the asperities of the other sliding surface and undergo both elastic as well as plastic deformations [100,101]. Ramoun et al calculated the lubricant film thickness in boundary lubrication regime and found that the oil thickness to be around 40nm-80nm [92,93]. Since, the minimum surface roughness of the moving surfaces can be as low as in sub-micron levels, still the lubricant film is no longer able to separate the two surfaces. The  $\lambda$  ratio becomes less than 1 [99]. Thus chemical properties of lubricant becomes essential for the performance of the lubrication system in boundary lubrication [100]. Here, Lubricants chemistry interact with the substrate surfaces and form atomically thin tribofilms.

### 2.3 Tribofilms

The discipline of tribology primarily deals with mechanical systems involving interactions between surfaces that are in contact or/and in relative motion to each other. Thus tribology is defined as the science and technology of interacting surfaces in relative motion and deals with force transference between surfaces moving relative to each other [102]. This force is known as friction which is a resistance to the relative motion between the interacting surfaces that results in loss of energy as well as loss of materials (i.e. wear) to the mechanical system. The losses due to friction and wear can be overcome by the application of a lubrication system which is applied between the interacting surfaces to perform primary tasks i.e. reducing friction resistance and minimizing materials deterioration from wear by promoting a protective layer or film between the contact surfaces. These protective films are commonly known as tribofilms. Tribofilms are thin

patchy films, typical thickness ranges in between 100nm-400nm [16,50,103-112], basically a byproduct of decomposition of lubricant additives which covers the surfaces of the moving parts in order to avoid the direct contact of interacting surfaces to ease the relative motion as well as minimize material removal due to wear [1,39,48,93,106,113,114]. Lubricant additives primarily an anti-wear additives (e.g. ZDDP etc.) play a significant role in the formation of tribofilms which either get physically or chemically absorbed to the surfaces of moving parts or decompose to form new ions to activate the substrate surfaces and subsequently react to form chemically active species which adhere onto the wear prone surfaces to enhance protection [1,37,110,115]. In most cases, tribofilms act like a sacrificial film which periodically form and break-down due to the shearing action during the process but it is critical that the film formation rate is higher than the film break down rate to perform the original task [37,111,116]. Also tribofilms cover the inevitable surface asperities and provide relatively smoother surfaces to move among each other with less resistance thus contribute in improving the energy efficiency of the mechanical systems. Typically, tribofilms are formed under the application of high loads and slow speed which is referred as boundary lubrication regime (discussed later). Under such conditions, points at the surface asperity contacts generate very high temperature and pressure, which induces thermo-mechanical chemical reaction that leads to the decomposition of lubricant additive chemistries and form final by-products as tribofilms [1,37,40,113-115].

Besides the application of lubricant additives and tribofilms formation mechanism various surface coating technologies have also been developed to improve the

tribological phenomenon in the mechanical systems. Surface coating technology provides a convenient way to enhance the surface properties of the part into the relative motion in order to reduce friction resistance and wear. Diamond-like coatings has shown superior wear protection behavior as well as it offer coefficient of friction as low as 0.001 in some cases [117]. However, the use of coating in real time application is still a challenge as, first coatings are expensive including both material as well as coating deposition technique cost, long time durability, synergism with lubricants oils, difficult to coat complex shapes. Advantages and disadvantages of tribofilms over surface coatings are shown in table 1.

Table 1 Comparison between in-situ tribofilms and surface coatings

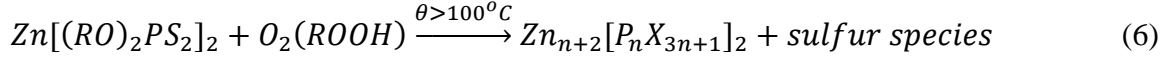
<b>Tribofilms</b>	<b>Surface coatings</b>
In-situ formed during the relative motion (rolling, sliding etc.).	Special coating techniques required on the parts prior to application.
Cost effective, additives are relatively cheaper.	Expensive. Material cost, deposition cost, power consumption.
Forms at typical areas requires protection against wear.	Cannot be applied only to typical area of surface contacts, leads to waste of coating materials.
Lubricant oil can be supplied externally at regular interval to protect the interacting surface for a long period of time.	Once the coating worn out, parts need to be removed and coat again.

The primary role of a lubricant applied into a mechanical system is to protect the parts (involved in rubbing motion) from the subsequent wear also to provide relatively smoother surface to slide against each other with less frictional resistance. To achieve these objectives, lubricant interact with the rubbing surface in the contacting zone and forms tribofilms on the surfaces by creating a nano-scale layer whose chemistry and properties are dependent on the chemistry of the additives used in the lubricant as well as the tribological conditions responsible for the formation of the tribofilms that include temperature as well as shear stress and nascent surface (i.e. surface roughness [118] ). Depending upon the type of lubricant and surface interaction, tribofilms can be classified as four types;

### *2.3.1 Thermally induced tribofilms*

Thermal film formation due to the thermo-oxidative decomposition of the lubricant additives in one of the critical mechanism leading the pathways of the tribological performance of lubricant additives. Fuller et al [119] studied the generation of thermal films using neutral and basic ZDDP without involving any friction process and detected zinc polyphosphates in these films. Several model explaining the mechanism of thermal film formation has been suggested [1]. Spedding & Watkins [42] found the evidence of thermally decomposed ZDDP by-products (Zinc polyphosphates and a mixture of alkyl sulphides) in oil solution and subsequently Watkins [41] reported that these by-products physically adsorbed on to the mating metal surfaces to give anti-wear protection. J. M. Martin [120] highlighted the thermal decomposition reactions (equation 4.3.1) taking place in ZDDP above 100°C and suggested so formed solid

poly(thio)phosphate and the native iron oxide on the substrate react and the film adhesion to surface increases.



Many studies, Yin [121,122], Suominen [108,123], Zhang [112,124], Pereira [125,126], Najman [51,64,127] Mourhatch [93,128] have proposed the thermal decomposition as a first step in film formation using lubricant additives. BoHoon [15], studied the growth mechanism of thermal film formed from using ZDDP (Zinc dialkyl dithiophosphate) and ashless DDP (dialkyl dithiophosphate) lubricant additives and proposed a model to calculate the thickness of thermal films (shown in equation 4.1);

$$d = d_0 * e^{kt} \quad (7)$$

Where, d is thickness of thermal film, d<sub>0</sub> is the constant, t is the baking time, and k is the growth rate.

### 2.3.2 Thermo-mechanically induced tribofilms

Thermo-mechanically induced tribofilms are formed under the severe lubrication conditions of boundary lubrication regime [52]. Under the boundary lubrication regime, besides the effect of temperature on the decomposition of the lubricant additive to form a protective tribofilms, various other parameters such as load, sliding speed, lubricant concentration as well as the surface roughness and rubbing time play a critical role in the formation of tribofilms. Yin et al [121] studied the effect of different physical parameters on the formation and growth of tribofilms and concluded that both increasing load and rubbing time as well as surface smoothness enhance the decomposition of the ZDDP and no unchanged ZDDP was reports at higher loads and longer rubbing time on smoother



surfaces. According to J. M. Martin [120], ZDDP tribofilms can be friction induced at a temperature well below that of thermal decomposition however the induction time for film formation is much longer. Martin [120] also suggested that tribofilms are composite materials consisting of metal sulfide crystallites embedded in a mixed Fe/Zn polyphosphate matrix. Whereas other authors [106] have suggested a nano-layered structure of tribofilms, consisting short chain polyphosphates films intergrown with the iron oxide surface layer which are then covered with a thin nano-layer of long chain polyphosphates in the case of ZDDP. Hongbing et al [129] suggested three stages of tribofilm formation by observing the change in the coefficient of friction with the film formation time where stage 1 was an induction period during which tribofilms were nucleated, where usually  $\mu$  first decreased, then increased, and finally stabilized. Stage 2 consisted of tribofilm build up characterized by a constant  $\mu$  with increasing film thickness. Stage 3 was characterized by competition between continued film formation and wear.

## Chapter 3. Synergistic Effects of Ashless Fluorothiophosphates with Zinc Dialkyldithiophosphate (ZDDP) for Better Antiwear Properties and Tribofilm Formation

### 3.1 Introduction

In this chapter, the tribological behavior of new ashless antiwear chemistries were studied in blends with ZDDP with varying ratios of ZDDP and ashless chemistries. The coefficient of friction was measured using a high frequency reciprocating cylinder on flat test set up under different load conditions i.e. 54N and 350N. The electric contact resistance (ECR) data was also collected simultaneously which indicates the incubation time for the formation of tribofilms as the test proceeded. Wear volume was calculated on the wear scar of the pin of each tests using optical microscopy and optical 3D interferometry. Wear data shows significant reduction in wear when ashless anti-wear additives were blended with ZDDP when compared to ZDDP at both at low and high load conditions. In an effort to understand the mechanism of wear morphology of the tribofilms was studied using scanning electron microscopy (SEM). High magnification images indicate a small pad like structure over the wear surface of the test samples at lower test load. These small patchy films tend to expand and merge into large patchy film at higher test loads. The film formation mechanism of these lubricant additives was further scrutinized using x-rays absorption near edge structure (XANES), and nano-indentation were performed to measure the nano-mechanical properties of the film as a function of the film depth. A comprehensive understanding of the chemistry, structure and properties of tribofilms were developed to explain the observed wear behavior.

## 3.2 Experimental Details

### 3.2.1 Description of Additive Chemistry

Neutral -100 base oil and zinc dialkyl dithiophosphate (ZDDP) were purchased from commercial vendors. The ZDDP used in this study is a secondary alcohol derived ZDDP with approximately 70% neutral and 30% basic characteristic. The Ashless additives chemistry used in this study were synthesized in the lab. For that purpose, all of the reagents were purchased from commercial suppliers and used without purification unless otherwise specified. The synthesis of the phosphorofluoridithioate and thioperoxydiphosphate is shown in the earlier publications [13,14]. Table 2 details the structure of the ZDDP and the ashless antiwear additives alkylphosphorofluoridithioates and alkylthioperoxydiphosphate.

Table 2 Structure of the Anti-wear Additive Compounds

Coded Name	Chemical Name	Chemical Structure
ZDDP	Zinc Dialkyldithiophosphate	
PFC18	Alkylphosphorofluoridithioate	
SSC18	Alkylthioperoxydiphosphate	

### 3.2.2 Tribological Test Procedure

Two different ashless antiwear additives i.e. PFC18 (octadecylphosphorofluoridothioate) & SSC18 (octadecylthioperoxydiphosphate) along with ZDDP (Zinc dialkyl dithiophosphate) were tested in boundary lubrication conditions to evaluate their tribological properties. Four different lubricant oil formulations were prepared in base oil i.e. (i) 100%ZDDP, (ii) 80%ZDDP+20%PFC18, (iii) 80%ZDDP+20%SSC18 & (iv) 80%ZDDP\_10%PFC18+10%SSC18. Phosphorous level was kept constant at 1000 ppm in all the formulations. The tribological tests were performed on a home built high frequency cylinder on flat test set-up at Argonne National Lab, Energy System division. Load was applied using a pneumatic pressure unit and friction forces were measured using a strain gauge motion sensor. The lubricant oils were run under this set up at two different loading conditions i.e. (i) 54N & (ii) 350N that results in a maximum contact pressure ( $P_{max}$ ) of 320 MPa & 800 MPa respectively. All the test were run at 300 RPM (5 Hz) reciprocation speed for the duration of an hour at 100°C temperature. Data was acquired at 5Hz rate using the DasyLab software. The stroke length was 6 mm. Tests were performed on 52100 hardened steel flat using a 52100 hardened steel bearing cylinder from RBC bearings. Both flat and pin were cleaned before each tests using standard solution followed by Isopropanol and Acetone to completely remove any oil and dust present on the initial surfaces. The rubbed surfaces after the tests were cleaned with Hexane and Isopropanol and then saved by submerging in base oil.

### *3.2.3 Surface Characterization*

After each test, the cylinders were cleaned using hexane followed by isopropanol and then they were examined under the optical microscope and 3D optical interferometry for the assessment of the wear track and calculation of the wear volume. The nature of the wear occurring at the surface was studied by examining the surface of the wear tracks. A Hitachi S-3000N Scanning Electron Microscope (SEM) was used to get secondary electron images of the wear track.

Nano-mechanical properties (i.e. hardness and elastic modulus) of the tribofilms generated on the flat were measured using a nano-indenter from Hysitron Triboscope™. The Nano-indentation were carried out using a Berkovich type tip geometry with a total included angle of 142.3 degrees and a half angle of 65.35 degrees. Nano-indentation were performed at nine different locations in a single sample. A cyclic loading profile with partial unload load was run for each indentation point to study the nano-mechanical properties of the tribofilms as a function of the film thickness. A scanning probe microscope mode in the tribo-indenter was also used to obtain topographical information as well as the 3D image of the tribofilms on the rubbed surfaces.

In order to understand the chemical nature of the tribofilms, XANES (X-Ray Absorption Near Edge Structure) spectra were obtained. XANES is a very robust technique to study the local co-ordination of the elements present on and in the tribofilms. It provides chemical information from 5nm of the surface to 400 nm in depth of the sample. XANES spectra were obtained at Canadian Light Source synchrotron facility at Saskatoon Canada. The phosphorous and sulfur L edge data were collected at

VLS-PGM (variable line spacing plane grating monochromator) beam station which operates at the energy range of 5.5 eV-250 eV with a photon resolution of more than 10,000 E/ $\Delta$ E. All the spectra were collected using a 100  $\mu$ m X 100  $\mu$ m photon beam spot size. Oxygen K edge, iron L edge and zinc L edge spectra were obtained at SGM (spherical grating monochromator) beam line which operates between 200 eV-2500 eV energy range with a photon resolution of more than 5000 E/ $\Delta$ E. Here, a spot size of 50  $\mu$ m X 50  $\mu$ m was chosen to obtain high resolution spectra. Finally, phosphorous K edge and sulfur K edge spectra were obtained a SXRMB (Soft X-ray Micro characterization Beam line) beam station which operates a high energy ranging from 1.7 – 10 keV which a photon resolution of  $3.3 \times 10^{-4}$  Insb (111). A 1 mm X 2 mm spot size was chosen to collect the spectra at the SXRMB beam line.

### 3.3 Results and Discussion

#### *3.3.1 Evaluation of Coefficient of Friction (CoF) and Wear Volume*

Coefficient of Friction (CoF) was acquired during the high frequency cylinder on flat test. Four different oil formulations were tested at two different load i.e. 54N (mixed boundary lubrication) and 350N (boundary lubrication). Figure 3a is a plot of CoF over the duration of the test. All the tests were run for an hour and the friction force data was acquired at the rate of 5Hz. The coefficient of friction at 54N is higher for all the formulations than the CoF at 350N. This is because at higher loads the surface asperities get crushed, which results in smoother surface to the rubbing motion and also stable (and perhaps thicker) tribofilm formation on the rubbing surface. Thus, the CoF curves for 350N load are lower and show good stability during the entire tests. However, the CoF

doesn't vary much with the addition of ashless fluorothiophosphates anti-wear chemistry to the ZDDP. At 54N, the friction data show high fluctuations during the test which is due to the formation of unstable tribofilms during the test that break down periodically as the test proceeds. The coefficient of friction is comparable when ZDDP is used with and without the ashless fluorothiophosphates additives.

Wear assessment was done by measuring an average wear width from the different pins (52100 steel) rubbed against the flat surfaces (flat surface) using an optical microscope and 3D optical interferometry. Figure 3b shows the comparison of wear volume loss for the different lubricant oil formulations at different loads, error bars in the figure indicate the deviation in the wear volume calculations. The addition of ashless fluorothiophosphates to ZDDP shows significant improvement in wear reduction under both 54N and 350N loads. On comparing the wear volume from the blends of ZDDP with ashless additives with oils that contain only ZDDP, a maximum wear reduction, i.e.,  $\approx 80\%$ , was observed from the blend with 80%ZDDP+20%SSC18 formulation at 54N. However, the other formulations of ashless fluorothiophosphates with ZDDP also showed significant wear volume reductions when compared to formulations that only contained ZDDP. At 350N load, the wear volume increase to much higher values than it was at 54N for all the formulations. Here also, comparing to the wear volume from formulations that only contain ZDDP, the addition of ashless fluorothiophosphates to the ZDDP improves the anti-wear properties significantly.

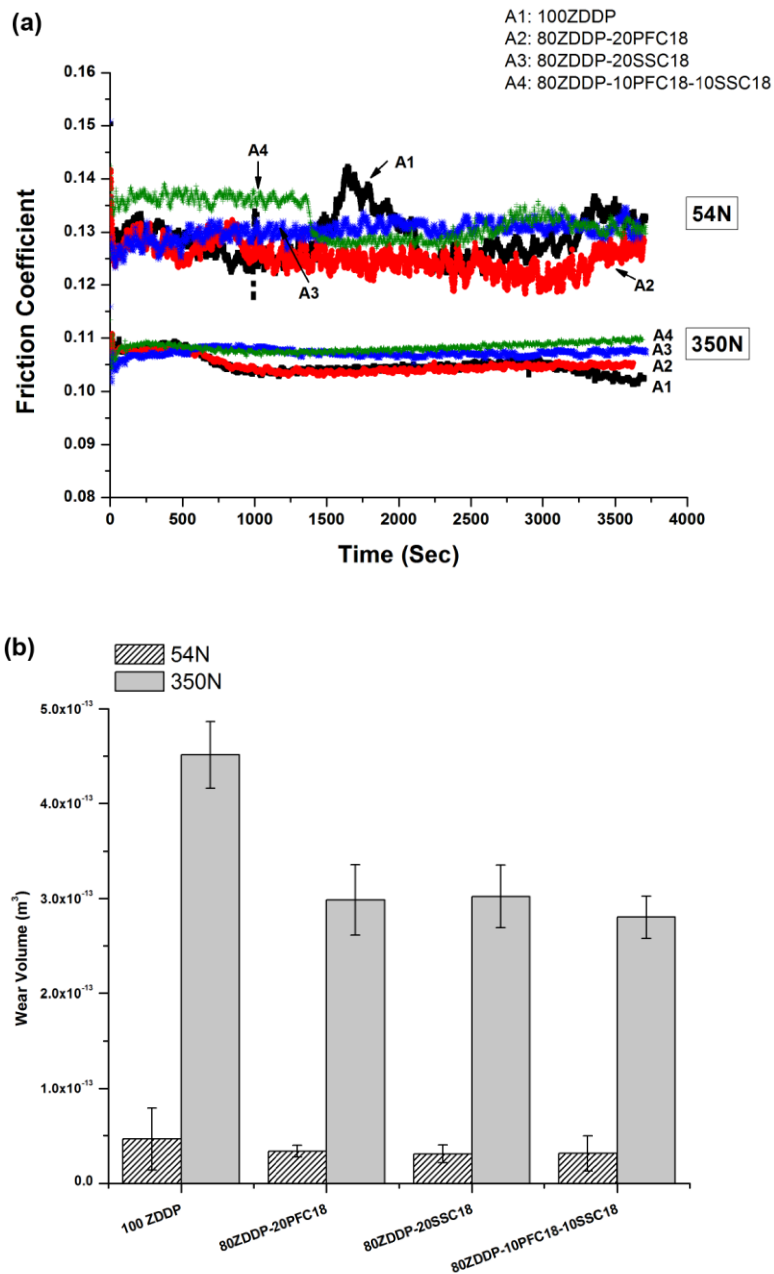


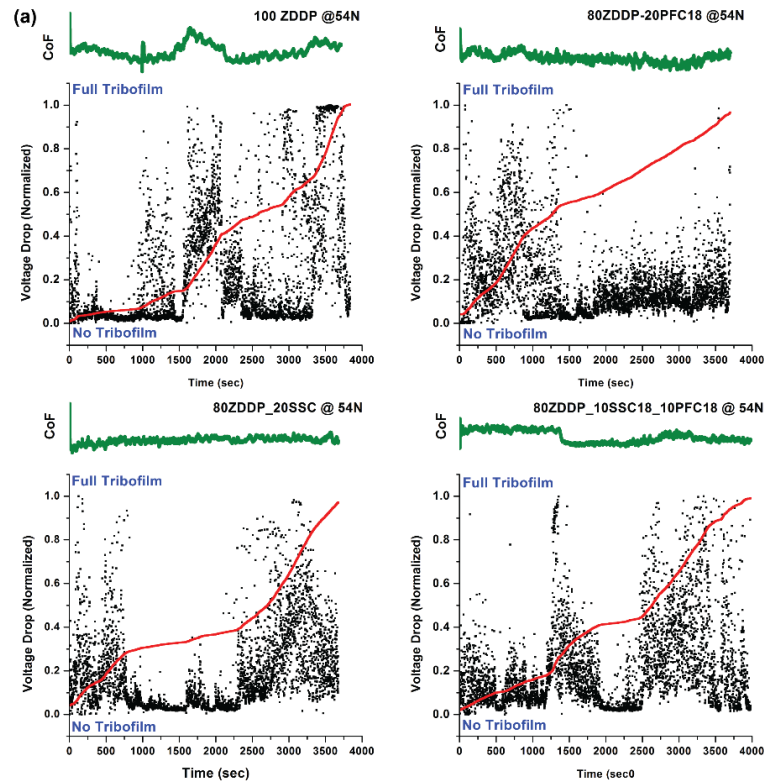
Figure 3: Tribological behavior of formulations with ZDDP and mixtures of ZDDP and ashless thiophosphates in base oil mixtures. Fig. 3(a) shows the coefficient of friction as a function of time at two different load i.e. 54N and 350N. Fig. 3(b) shows the comparison of wear volume for the different oil formulations at two different loads.



### *3.3.2 Incubation Time for the Tribofilm Formation using ECR*

Most ZDDP derived tribofilms formed at tribological contacts are generally amorphous glasses and known to have very high electrical resistivity. At the initial stage of the test when tribofilms are not formed yet, direct contact of asperities of two surfaces in tribological contact result in very low contact resistance, however, as the test progresses with the formation of protective tribofilms, the resistance between the contacting surfaces increases and can be used as a way of determining effectiveness of tribofilm formation. The voltage drop across the tribocontact ranges from 0 to 1200 mV which is normalized from 0 to 1. The 0 corresponds to no tribofilm present and 1 corresponds to when an effective tribofilm is present on the surface. The voltage drop was integrated over time to illustrate the overall effectiveness of tribofilm formation over time, larger values correspond to more net coverage of tribofilm over the duration of the test. In addition the slope of the curve indicates the effectiveness of tribofilm formation with larger slopes having better tribofilm formation. Figure 4a shows the voltage drop data for all the four formulations run under the load of 54N. The graph show potential drop between the pin and the surface as a function of time. At 54N, the incubation time for the tribofilms formation for the oil that only contains ZDDP is relatively higher than the mixes of ZDDP with ashless fluorothiophosphates, as the graphs show higher potential drop from the beginning of the test. However, the tribofilms are not stable and they break down periodically during the test as evidenced by the sharp drop in normalized voltage to 0. This also explains the large fluctuations in the friction curves at 54N load tests. Figure 4b is the plot of electrical contact resistance for the four lubricant

oil formulations used at 350N load tests. As the data indicates the tribofilms form very early in the test and stay stable for the duration of the test in the cases of ZDDP with the addition of ashless fluorothiophosphates. On the other hand in formulations that only contain ZDDP, even though the tribofilm forms in the early stages of the test they are not stable and there is constant breakdown and reformation of the tribofilms.



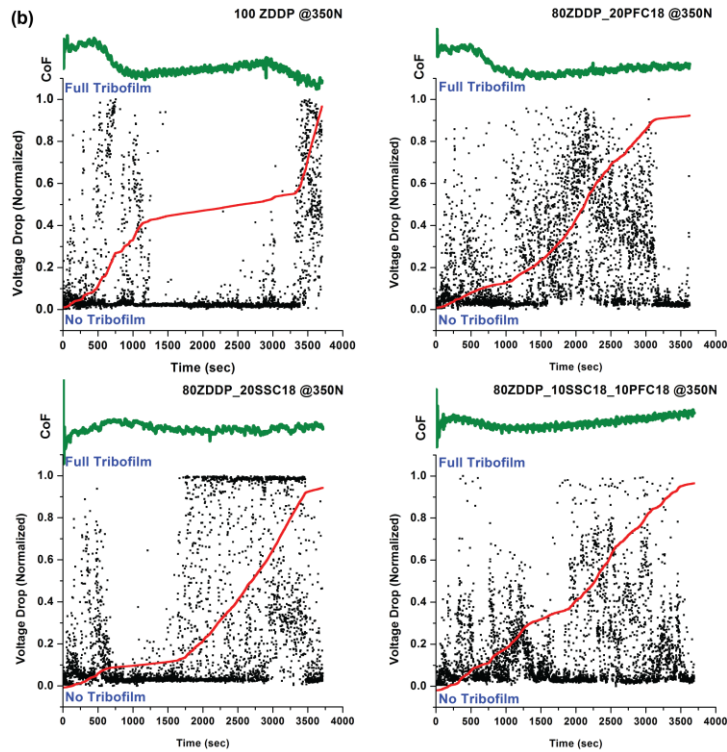


Figure 4: Electrical contact resistance for all the tribological tests with ZDDP and ZDDP with ashless thiophosphates conducted at 54N (a) and 350N (b).

### 3.3.3 Study of Surface Topography using SEM

SEM images of the tribofilms formed on the flat were imaged using S-3000N variable pressure SEM. Figure 5 is the secondary emission SEM images of the rubbed surfaces for the four different oil formulations at 54N and at 350N. At 54N load test, SEM images show less coverage of tribofilms on the wear surfaces. At higher magnification i.e. 4000X, small patches (darker contrasting areas) of tribofilms are observed. Whereas at 350N load test, the wear surfaces show features of patchy tribofilms all over the sample which also have grown larger into size than the patches of

tribofilms in 54N test. This indicates that at higher load the tribofilms tend to grow into larger pads along the sliding directions.

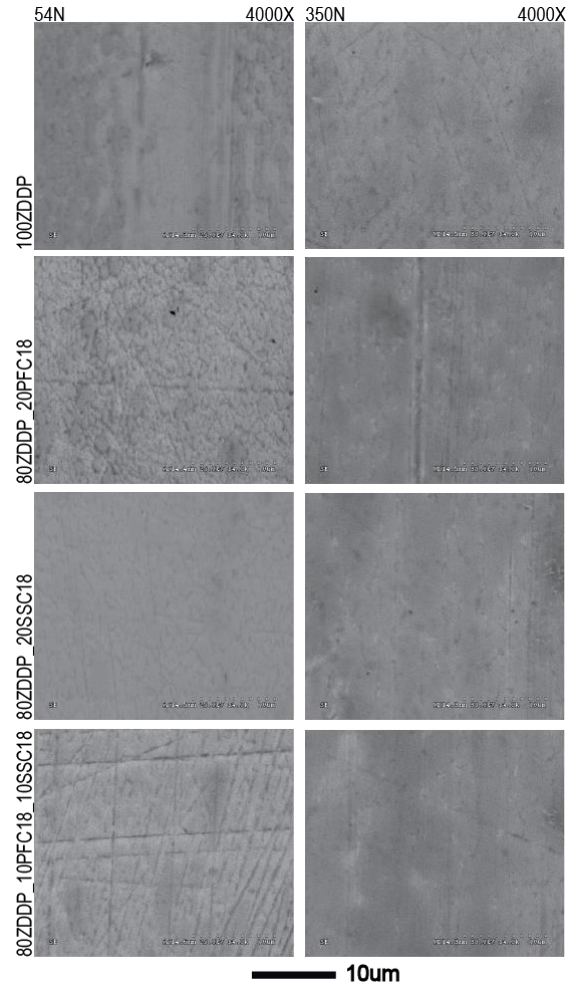


Figure 5: Showing the secondary emission SEM images of the rubbed surfaces for the four different oil formulations at 54N at 350N.

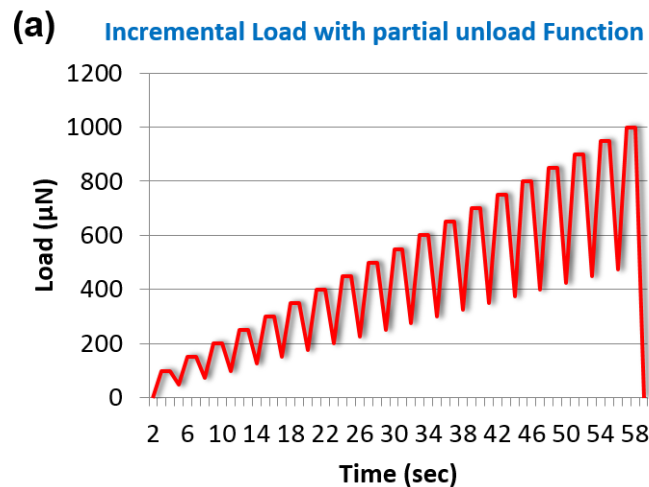
### 3.3.4 Nano-mechanical Properties and 3D imaging of Tribofilms using Nano-indentation

Nine nano-indentation tests were performed for each of the tribofilms using a cyclic loading with partial unloading load function (2 seconds for linear loading segment,

2 seconds for holding segment and 2 seconds for linear unloading segment) with a peak load ranging from 100 $\mu$ N to 1000 $\mu$ N. Figure 6a is a typical load profile as a function of time for the nano-indentation tests. Figure 6b and 6c shows the plot of hardness as a function of the indentation depth into the tribofilms generated from all the different lubricant formulations as well as the 3D images of the wear surfaces (30  $\mu$ m X 30  $\mu$ m) obtained via scanning probe microscope (SPM). SPM images were obtained before and after the nano-indentation. Images taken before the indentation were used to locate the best possible flat region in order to make sure a smoother surface is provided to the nano-indentation probe for proper indentations. However, on wear surfaces obtained at 54N load test, finding a flat region was a challenge since (as shown in fig 5 SPM images) the surfaces consist of a large number of small rounded pad like features of tribofilms with very little flat areas (caused large fluctuation in the friction data at 54N load test shown earlier). This resulted in a wider range of the nano-hardness measurements at different location of measurement. The SPM images taken on the wear surfaces generated at 350N load tests show larger pad like structure of the tribofilms. This confirms the topographical information obtained from the SEM images that at higher loads the patches of tribofilms grow larger in size resulting in a much smoother surfaces resulting in lower friction. As shown in figure 6b, hardness data obtained for the formulations containing ashless fluorothiophosphate additives with ZDDP in the mixtures of base oil show high consistency and doesn't vary much with different location of indentations whereas the hardness obtained from the formulation containing ZDDP falls into a broader range, the SPM images of the tribofilms from ZDDP formulations indicate a much smaller pad size

and uneven tribofilm formation explaining the broader range of hardness data derived from the tribofilms. This indicates that the wear surfaces generated with the blends of ashless thiophosphates with ZDDP are smoother with larger tribofilm pad sizes than the wear surface obtained using only ZDDP. It was observed that the hardness of the tribofilms generated from these tests does not vary much with penetration depth as the hardness curve drawn for the 54N load test and 350N load test gives similar outcome and also follow the same trend. In addition, the nano-mechanical properties of the tribofilms generated from the formulation using only ZDDP and formulations that contain a mixture of ZDDP with ashless fluorothiophosphate additives can be differentiated easily. As can be seen from figure 6b and 6c, the tribofilms formed from ZDDP at a load of 350N has a hardness of about ~14 GPa near the surface which eventually decreases to 6-7 GPa with film depth of 50-60 nm. Several studies in the past [16] have indicated that typical tribofilms range in thickness from 80-200 nm. Whereas, tribofilms obtained with the addition of ashless fluorothiophosphate additives with ZDDP show uniform hardness at different location of indentations and also does not vary much as a function of the film depth. The hardness near the surface of the tribofilms (< 20 nm) is about 8 GPa that decreases to 4-5 GPa as the indentation depth increases to 60 nm. Similar results were found by Kim et al. [16], where they reported the hardness of tribofilms generated using ZDDP as additive in base oils starts from higher values which eventually decreases to around 8 GPa as the indentation depth increases while the hardness of ashless DDP remains close to 5 GPa throughout the test. However, they found the tribofilms to be much thicker than the values reported in this paper, this could possibly due to the

different nature of the test used where they ran the test at very high contact pressure. In another study by Bec et al. [130], they reported the nano-hardness measurements of the tribofilms generated at 360 MPa mean contact pressure (close to the  $P_{\text{mean}}$  used in this paper). They found that the wear surfaces consists of multilayer tribofilms. The nano-indentation measurements showed that the mechanical properties of the tribofilms are heterogeneous spatially as well as with thickness also. This explains the broader hardness data obtained using ZDDP additive only (figure 6c). It can be hypnotized that the tribofilms generated from ZDDP only are non-uniform and heterogeneous in nature with varying film thickness, whereas, the tribofilms generated from ZDDP plus FTPs additives formulations are more uniform and homogeneous in nature.



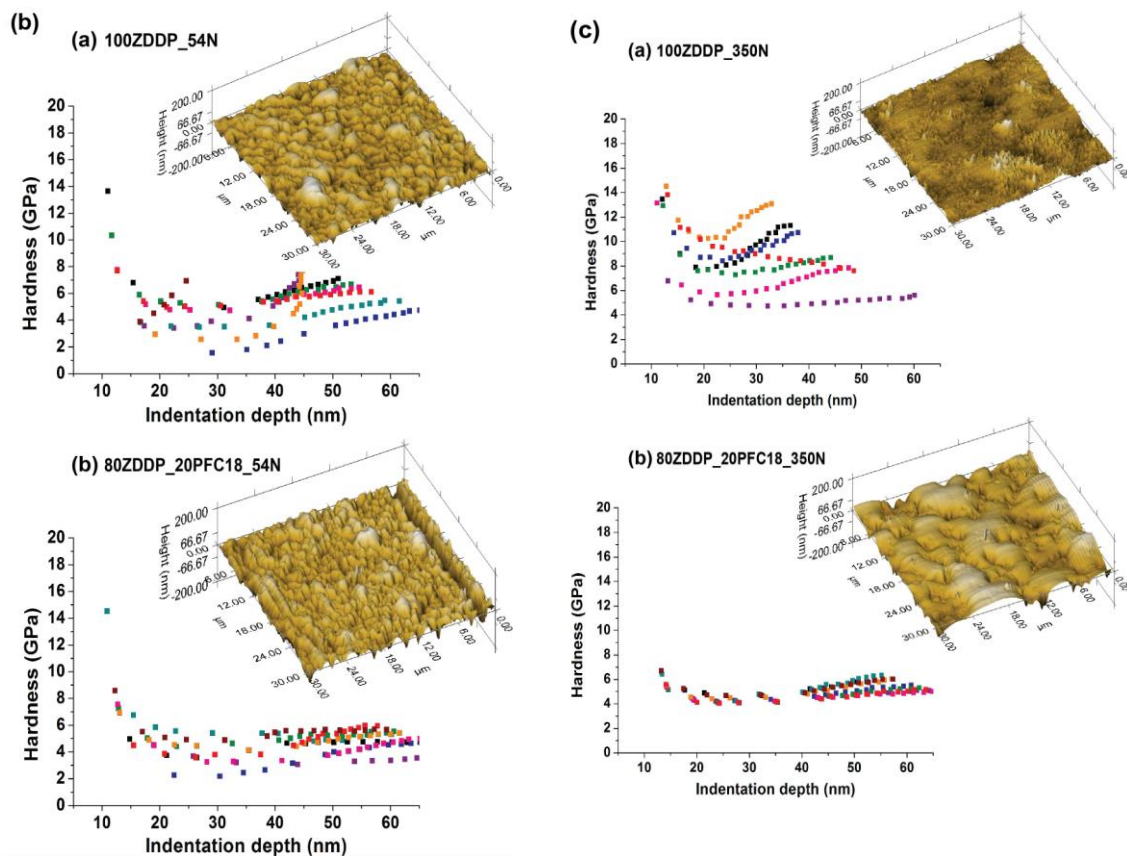


Figure 6: Nano-mechanical properties of tribofilms obtained from nano-indentation using cyclic loading with partial unloading load function (shown in Fig. 6(a)). Fig. 6(b) & 6(c) show a comparison of nano-hardness profile of tribofilms using ZDDP and 80%ZDDP+20% PFC as a function of indentation depth at 54N and 350N respectively as well the corresponding 3-D SPM images.

### 3.3.5 Characterization of Tribofilms Chemistry using XANES

XANES analysis has been used extensively in tribology to examine the chemical nature of the tribofilms derived using various anti-wear additives [13,14,16,51,54,64,126,127,131-133]. It provides chemical information for total electron



yield (TEY) and fluorescence yield (FY) for the P L-edge of 5 and 60 nm respectively and sampling depths for TEY and FY at the P K-edge are 50 nm and >800 nm, respectively [108,134]. Both TEY and FY spectra were acquired from the tribofilms formed using the four different formulations studied here.

#### 3.3.5.1 Phosphorous Characterization (P L<sub>2,3</sub>-edge and P K-edge)

Phosphorous L edge XANES spectra provides a wealth of chemical information as the depth of sampling is close to the average thickness of the anti-wear tribofilms which is 50-100 nm in most cases. The phosphorous L edge TEY and FY spectra of the tribofilms generated from ZDDP and combinations of ZDDP with ashless PFC18 & SSC18 compounds along with the model compounds Zn<sub>3</sub>(PO<sub>4</sub>)<sub>2</sub> and FePO<sub>4</sub> are shown in the Figure 7a, 7b and 7c. Here, different peak positions of the model compounds are assigned as **a**, **c**, **c'** and **d**. Peak labelled as **a** corresponds to the spin orbital splitting of the phosphorous 2p electrons present in Zn<sub>3</sub>(PO<sub>4</sub>)<sub>2</sub> whereas peaks labelled as **c** and **c'** are attributed to the transition of the phosphorous 2p electrons to the t\*<sub>2</sub> molecular orbital in Zn<sub>3</sub>(PO<sub>4</sub>)<sub>2</sub> and FePO<sub>4</sub> compounds respectively, and peak **d**, located ~146.0 eV is a shape resonance peak, is characteristic of all phosphates regardless of the structure, whether crystalline or glassy [121,132,135]. From the graphs, it can be deduced that for the tribofilms generated at 350N, phosphorous is primarily present in the form of zinc phosphate rather than iron phosphate as the peak position **c** is well aligned to the tribofilms spectra both in TEY and FY modes. Moreover, the pre-peak shoulder for the tribofilms also matches with peak position **a**, corresponding to the zinc phosphate. However, clear differences between the chemistry of the tribofilms formed from different

formulations cannot be observed here. In case of tribofilms derived from 54N load tests, a mere presence of  $\text{FePO}_4$  can be observed in the case of 100ZDDP and 80ZDDP\_20SSC18 additives formulations. This can be explained as at lower loads there is a competition between the  $\text{Zn}^{+2}$  cation and  $\text{Fe}^{+2}$  cation to form an anti-wear films but at higher loads decomposition of ZDDP increases and thicker pads of anti-wear films formed that reduces the availability of  $\text{Fe}^{+2}$  cation and leads to the formation of zinc phosphate on the rubbing surfaces.

Phosphorous L edge spectra also used for the determination of the chain length of the polyphosphates present in the tribofilms using peak intensity ratio of peaks **a** and **c**. Chain lengths of polyphosphates are characterized on the basis of peak height of **a** relative to peak **c** where ratio **a/c** up to 0.3-0.4 represents short-chain polyphosphates and **a/c** > 0.6 indicates long-chain polyphosphates [51,132,136]. Tribofilms studied in this work show very small pre-peak intensity of **a** in TEY mode which becomes less evident or starts to disappear in FY mode, suggesting presence of short-chain polyphosphates and mono phosphates at the surface ( $\approx 5$  nm) of the tribofilms whereas the bulk ( $\approx 30$ -40 nm) is largely made up of mono phosphates.

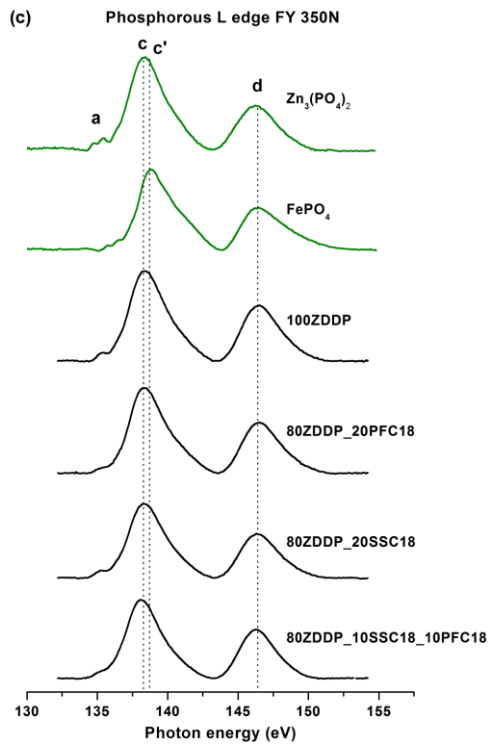
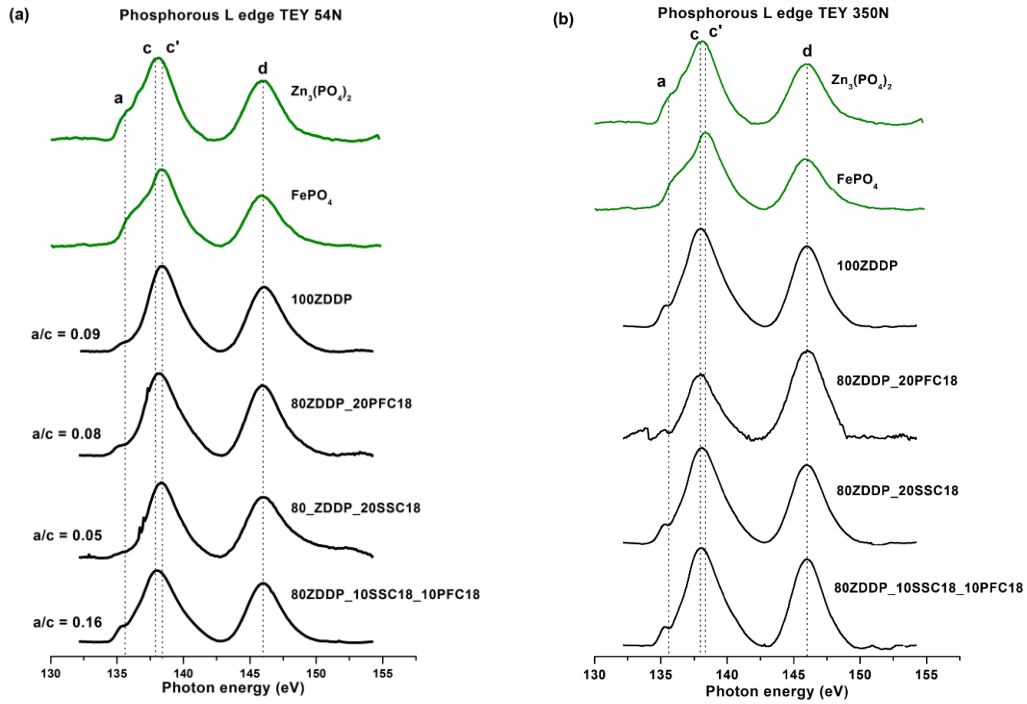


Figure 7: (a) Phosphorous L-edge XANES TEY spectra of tribofilms generated at 54N and model compounds (b) Phosphorous L-edge XANES TEY spectra of tribofilms generated at 350 N and model compounds (c) Phosphorous L-edge XANES FY spectra of tribofilms generated at 350N and model compounds.

Phosphorous K edge spectra are shown in Figure 8a, 8b. Only TEY spectra of phosphorous K edge are considered as the depth of sampling for P K-edge at FY mode (1-2  $\mu\text{m}$ ) is much higher than the thickness of the tribofilms thus can be disregarded for the purpose of this study. On the other hand, the TEY spectra provides cumulative chemical information in the tribofilms from 50-75 nm. P K-edge spectra from the tribofilms are plotted with the model compounds for the comparison. Two peak position are shown in the graphs labelled as **c** and **c'** which corresponds to the transition of the core phosphorous 1s electron to unoccupied p-like valence state [16] for  $\text{Zn}_3(\text{PO}_4)_2$  and  $\text{FePO}_4$  respectively. Two main difference between the model compounds, zinc phosphate and iron phosphate are first, main peak position for  $\text{FePO}_4$ , **c'** (2153.2 eV), has slightly higher energy than the main peak position, **c** (2152.3 eV), for  $\text{Zn}_3(\text{PO}_4)_2$  and second, P K-edge spectra for iron phosphate show small pre-edge that is more evident in FY graph. The spectra for ZDDP and the mix between ZDDP and ashless chemistries indicates that in the bulk of the tribofilms, phosphorous is primarily present in the form on  $\text{Zn}_3(\text{PO}_4)_2$  which is similar to the findings in P L-edge FY.

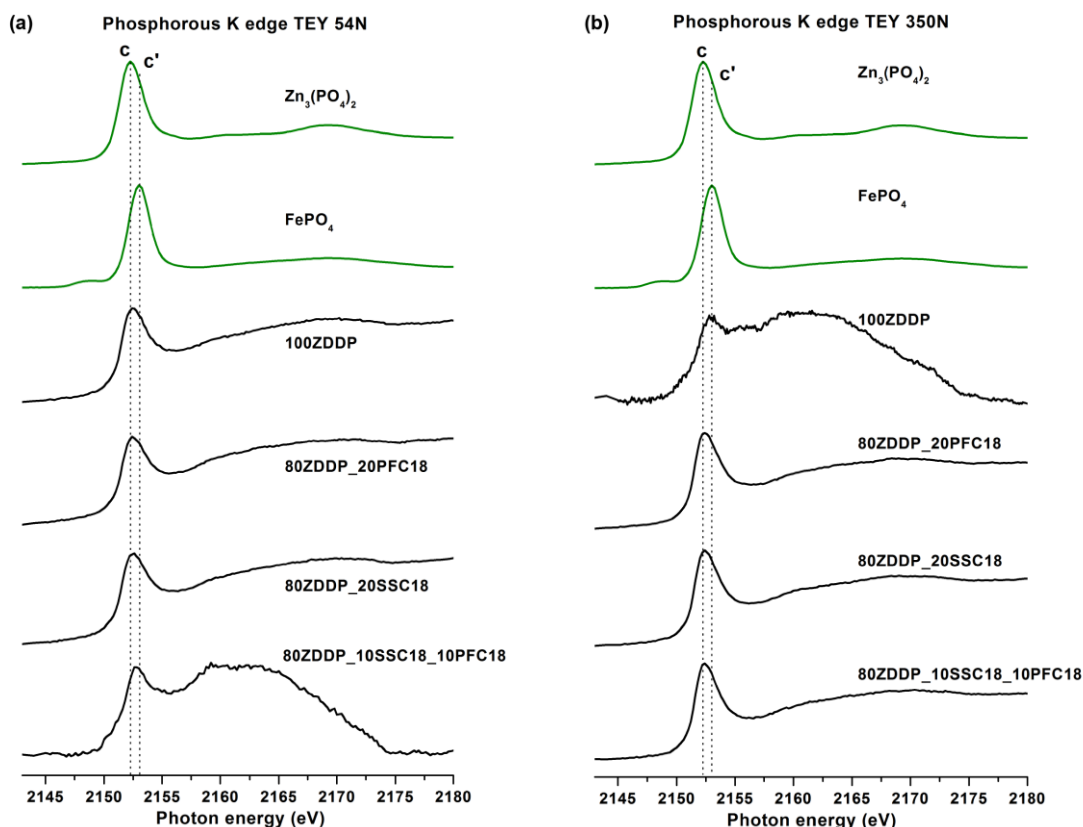


Figure 8 (a) Phosphorous K-edge XANES spectra of tribofilms generated at 54N and model compounds (b) Phosphorous K-edge XANES spectra of tribofilms generated at 350N and model compounds.

### 3.3.5.2 Sulfur Characterization (S L-edge and S K-edge)

Sulfur L-edge spectra provides a useful information regarding the local coordination/oxidation state of sulfur near the surface of the tribofilms [48,127,137-139]. The S L-edge spectra are plotted for the tribofilms derived from ZDDP and combinations of ZDDP with ashless PFC18 & SSC18 compounds and compared with the spectra of several model compounds in figure 9 a and 9b. Differences in the spectra of the model

compounds and their relative peak energies are detailed by Kim et al. in an earlier study [16]. At the outset it is important to note that the S L-edge spectra are much weaker than the spectra for the P L-edge indicating a preponderance of phosphates species near the surface of the tribofilm. The TEY spectra of the S L-edge suggests that the sulfur is present primarily in the form of sulfides rather than sulfates in the tribofilms. Presence of sulfates is more noticeable in the case of tribofilms generated at 54N load tests. A broad peak at position **f** indicates that sulfur is present in a mixture of different sulfate (Zn and Fe) species and is the primary species of sulfur present near the surface, the presence of small amounts of ZnS and FeS cannot be ruled out. On the other hand, TEY spectra of the tribofilms generated at 350N tests resemble the ZnS and to a lesser extent the presence of FeS. Figure 9b is showing the FY data of the tribofilms formed at 350N and model compounds. The sampling depth at S L-edge FLY is about 40-50 nm while the sampling depth at S L-edge TEY spectra is about 4-5nm. Here, interestingly, the spectra of the tribofilms resemble closely to the spectra of the ZnS as the peak positions **a**, **b**, **c**, **d** and **e** from ZnS aligns to the tribofilms spectra for the 350N load tests but still the broad shoulder after peak position **b** and also broadened peak **c** suggest that more than one type of sulfide species are present i.e. ZnS as well as FeS in the bulk of the tribofilms. Nicholls et al. [54] explained the mechanism for the sulfide formation in the tribofilms using the principle of hard acids and soft bases which suggests that soft bases as  $S^{2-}$  prefers to react with the borderline soft acid  $Zn^{+2}$  over the harder acid  $Fe^{+2}$  and  $Fe^{+3}$ . They also expressed thermodynamically that the free energy of the ZnS formation is more negative than FeS. However, thermodynamically zinc prefer to form zinc polyphosphates

instead of zinc sulfides thus most zinc gets consumed in the form of polyphosphates and becomes less available to form zinc sulfide while available iron can react with sulfur to form iron sulfides.

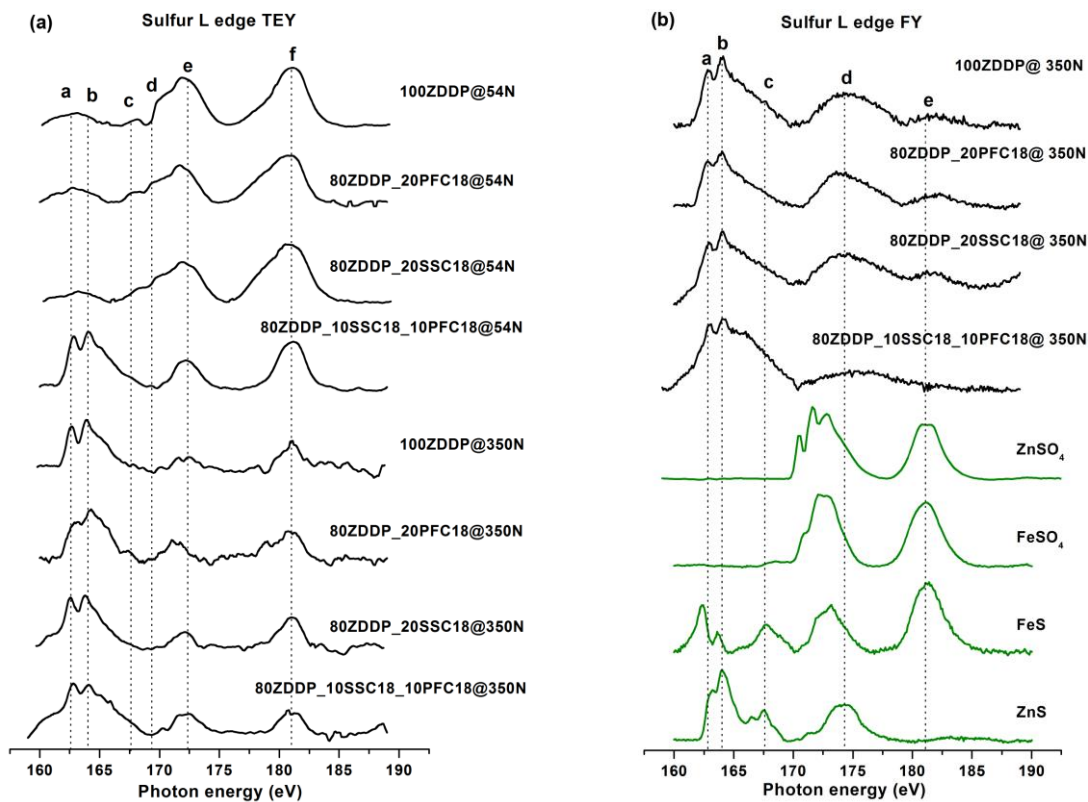


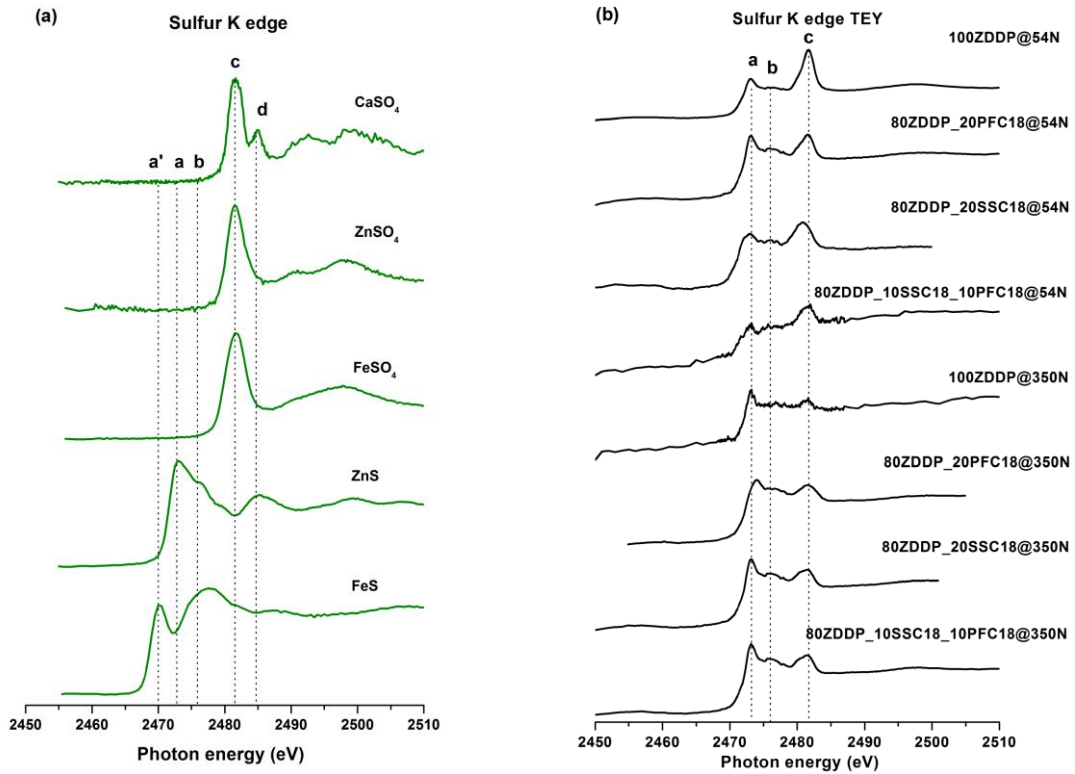
Figure 9: (a) Sulfur L-edge XANES TEY spectra of the tribofilms generated at 54 N. (b) Sulfur L-edge XANES TEY spectra for tribofilms generated at 350 N as well as the model compounds.

Figure 10a, 10b and 10c are plots of sulfur K edge spectra in TEY and FY mode for model compounds and tribofilms respectively. Figure 10d is the deconvoluted plot of S K-edge of 80ZDDP+20PFC18 detailing the contribution of the different sulfur species in the overall spectra from the tribofilm. Only TEY spectra for the model compounds are

shown for the comparison as there is no significant difference in the spectra for the two modes, since the chemistry of the model compounds does not change with the sampling depth in XANES. Sulfur can exist in different valence states ranging from -2 to +6 with -2 being the reduced states and the +6 being the oxidized states. The absorption edge of the different valence states can be easily distinguished by XANES spectra. In addition, the spectra from the model compounds indicate that the K-edge is ideally suited to distinguish between the different sulfides of Fe and Zn and between sulfides and sulfates. The peak identified as **a'** is unique to FeS while the peak labeled **a** is present in ZnS. On the other hand peak **c** is primarily present in sulfates and is common to both FeSO<sub>4</sub> and ZnSO<sub>4</sub>. From the plots, S K-edge TEY spectra of the tribofilms indicate that a mixture of sulfide and sulfate species are present in the tribofilms, interestingly, the intensity of the sulfate peaks are less pronounced in the case of the tribofilms formed under 350N load tests than the tribofilms formed under 54N load tests. Moreover, sulfate peaks tend to diminish in FY mode in all the cases as plenty of oxygen is available in the surface region rather than in bulk thus sulfur gets oxidized to form sulfates on the surfaces but not in the bulk of the tribofilms. S K-edge spectra of the tribofilms both in TEY (Figure 10b) and FY (Figure 10c) mode indicate that besides sulfate, sulfur is also present in the form of ZnS as the peak position **a** (i.e. 2473 eV) from the ZnS model compound spectra aligns to the spectra of the tribofilms. This confirms the earlier information from the S L-edge FY data that in the bulk of the tribofilms sulfur is dominantly present in the form of ZnS with a small presence of FeS. A ratio of peak area ratio (**a/c**) under peaks **a** and **c** provide additional insight into the relative proportion of ZnS and sulfates are measured by



deconvoluting the spectra as detailed in Figure 10d and provided in detailed in Table 3. It is evident from the data using both measures that in comparison to ZDDP by itself, formulations that contain a mix of ZDDP with ashless additives PFC18 and SSC18 have higher ratio of ZnS in the tribofilms that are generally more beneficial from a tribological point of view.



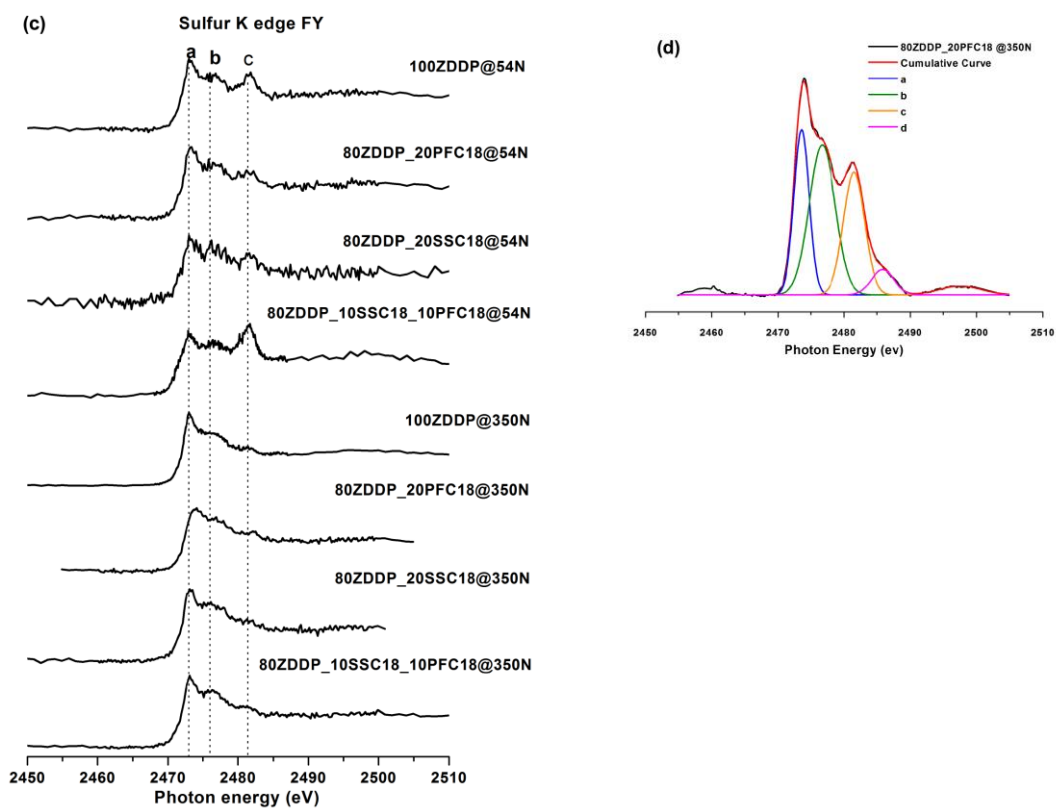


Figure 10: (a) Sulfur K-edge XANES spectra of the model compounds of sulfur. (b) Sulfur K-edge XANES TEY spectra of the tribofilms obtained at 54N. (c) Sulfur K-edge XANES TEY spectra of the tribofilms obtained at 350N. (d) Representative deconvolution process used to determine the contribution from the different valence states of sulfur in the tribofilm from a formulation that contains 80% ZDDP + 20%PFC18.

Table 3: Details peak fitting for the S K-edge spectra and ratio of sulfides to sulfates.

Sample	S K-edge TEY photon energy (eV)					a/c ratio Height
	a'	a	b	c	d	
FeS	2470.03	x	2475.82	2481.39	x	
ZnS	x	2472.72	2475.93	x	2484.70	
100% ZDDP @ 54N	x	2472.85	2476.32	2481.60	2484.79	0.48
80% ZDDP + 20% PFC18 @54N	x	2472.87	2476.03	2481.36	2485.07	1.05
80% ZDDP + 20% SSC18 @54N	x	2472.37	2475.98	2480.67	2484.91	0.94
80% ZDDP + 10% SSC18 + 10% PFC18 @54N	x	2472.78	2476.15	2481.3	X	0.79
100% ZDDP @350N	x	2473.1	2476.04	2481	X	1.58
80% ZDDP + 20% PFC18 @350N	x	2473.50	2476.67	2481.51	2485.86	1.34
80% ZDDP + 20% SSC18 @350N	x	2472.90	2475.83	2481.10	2485.11	1.35
80% ZDDP + 10% SSC18 + 10% PFC18 @350N	x	2472.93	2475.78	2481.15	2485.33	1.26

### 3.3.5.3 Oxygen Characterization (O K-edge)

Even though oxygen is present in only one valence state, it can be bound directly with different cation's such as Zn and Fe as well present in different anions such as sulfate and phosphates that can subsequently be bound with cation's such as Fe and Zn. The resulting O K-edge XANES absorption spectra of such compounds are distinctively different when viewed as pure model compounds as shown in Figure 11a. It is clearly evident that Fe<sub>2</sub>O<sub>3</sub> can be distinguished from ZnSO<sub>4</sub>, Zn<sub>3</sub>(PO<sub>4</sub>)<sub>2</sub>, ZnO, FeSO<sub>4</sub> and FePO<sub>4</sub> by the nature of the pre-edge peaks present at 530-532 eV. However, in a tribofilm O is

present in multiple anions and is bound to different cation's making it difficult to uniquely identify the local environment for oxygen. However, some distinctive differences can be ascertained by an examination of the spectra. Oxygen K-edge spectra were recorded in both TEY and FY mode for the tribofilms generated from all the four formulation ran at 54N and 350N load tests, the TEY and FY spectra being very similar, only the TEY spectra are shown for reference while the discussion pertains to both TEY and FY spectra. O K-edge TEY spectra of the tribofilms shown in Figure 11b. We can eliminate the possibility of the oxidation of zinc and iron as the spectra of the tribofilms do not show the presence of these compounds. Other than that, results are quite complicated and hard to distinguish as the earlier companion P, S, Zn and Fe spectra showed more or less the presence of all the  $ZnSO_4$ ,  $Zn_3(PO_4)_2$ ,  $FeSO_4$  and  $FePO_4$  model compounds in the tribofilms. However, for the tribofilms generated under 350N load tests presence of peak at 538.6 eV is matching with the primary peak of  $Zn_3(PO_4)_2$  model compound and also the pre-peak bump at 531.9 eV is less pronounced, therefore, we can say that  $Zn_3(PO_4)_2$  is present as the major constituent of tribofilms formed at 350N load tests. Whereas, at 54N load tests, pre-peak bump at 531.9 eV becomes more noticeable in the spectra suggesting some sulfates ( $ZnSO_4$ ) is present. In two of the compositions that contain SSC18. This may arise from the fact that the compositions with SSC18 have loosely bound sulfur that is readily available under tribological conditions to form sulfates of Zn.

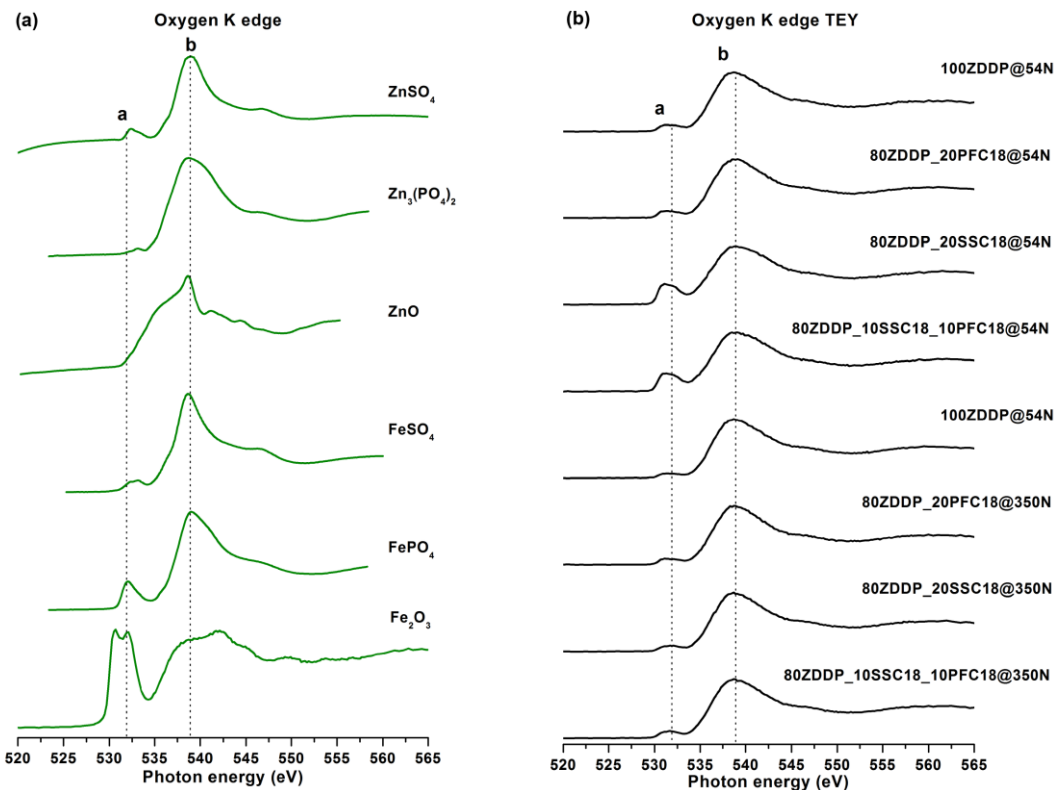


Figure 11: (a) Oxygen K-edge XANES spectra of model compounds containing oxygen. (b) Oxygen K-edge TEY spectra of tribofilms generated at loads of 54 and 350N.

#### 3.3.5.4 Zinc Characterization (Zn L-edge)

The Zn L-edge may be used to characterize the coordination of Zn with other elements such as O, S, F as well as anions such as phosphates and sulfates. The model compounds shown in Figure 12a indicate that the absorption spectra of Zn L-edge for the different compounds are distinctively different and may be used to distinguish between the different species. The spectra were acquired for all the tribofilms tested at 54N and 350N in both TEY and FY mode and the spectra in TEY and FY are very similar and

only the TEY spectra (Figure 12b) are shown for discussion. It is evident from a comparison of the spectra of the tribofilms with that of the model compounds that the preferred compound present is  $Zn_3(PO_4)_2$  in all cases. The S K-edge spectra has indicated the presence of ZnS as the primary S containing compound in the tribofilm, however the Zn L edge clearly indicates that the primary Zn containing compound is  $Zn_3(PO_4)_2$ . This suggests that while ZnS is present in the tribofilm the phosphates of Zn are the predominant species. This is also self-evident from the P and S L edge spectra that indicated that the relative intensity of the P L-edge spectra was much stronger than the S L-edge indicating a preponderance to the formation of phosphates. This can be correlated to the study by Nicholls et al. [54], where they reported that zinc phosphate is the thermodynamically more stable form of zinc.

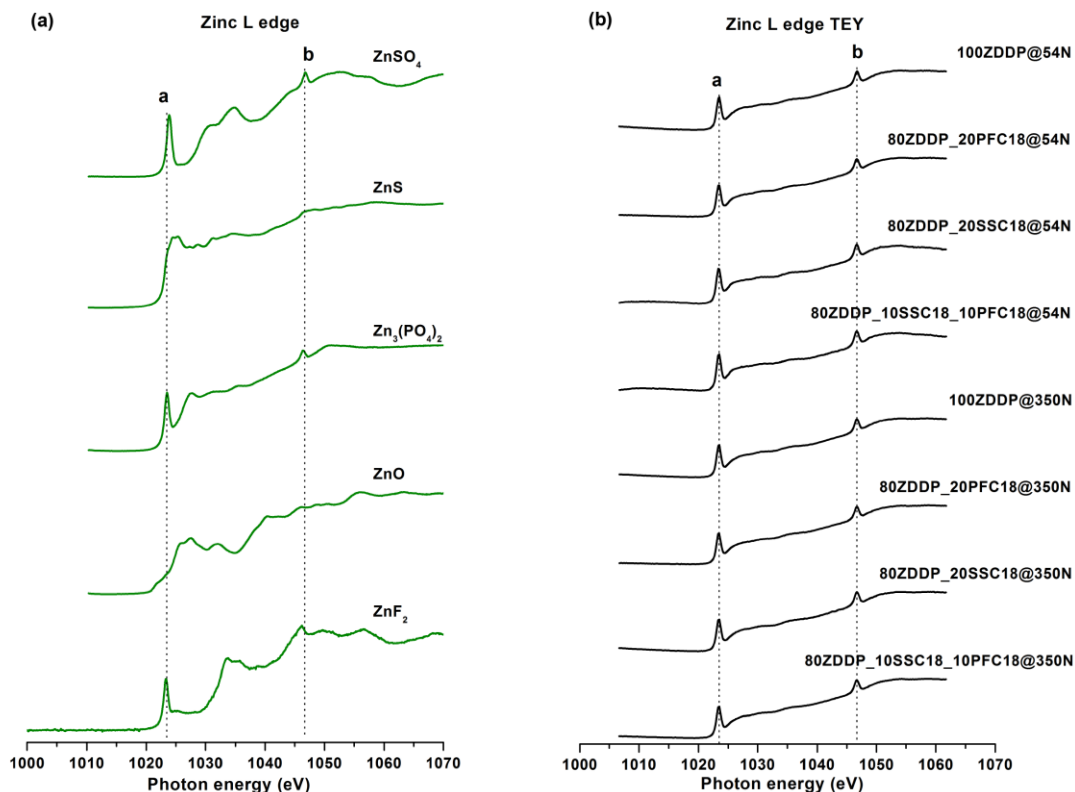


Figure 12: (a) Zinc L-edge XANES spectra of model compounds that contain zinc (b) Zinc L-edge TEY spectra of tribofilms generated at loads of 54 and 350N.

### 3.4 Discussion on XANES

The complementary XANES spectra at different edges and different elements provide a detailed way by which chemistry of tribofilms may be analyzed. A comparison of the P and S L-edge spectra of the tribofilms indicate that phosphorous spectra are much stronger than the sulfur spectra suggesting that phosphates of Zn are the dominant species in the tribofilms. The sulfur present in the tribofilms is largely sulfates at lower loads and transition to ZnS at higher loads. When tribofilms from ZDDP are compared to those formed from mixtures of ZDDP and ashless fluorothiophosphates and ashless

thiophosphates it is evident that sulfide species are more dominant in the mixtures when compared to when ZDDP is used by itself. The O K-edge clearly indicates that oxides of Fe are not present in any significant quantity in the tribofilm and the most likely candidates are phosphates of zinc and some sulfates of Zn and Fe. The P K-edge spectra indicate the presence of phosphates of Zn and when the S K-edge spectra is considered it is evident that from the TEY spectra that at lower loads (54N) there is a larger proportion of sulfates when compared to the higher loads (350N). It is also evident from the S K-edge spectra that tribofilms from ZDDP have a higher proportion of sulfates relative to sulfides when compared to blends that contain ZDDP and ashless PFC18 and SSC18 that have a larger proportion of sulfides of Zn. The presence of the ashless fluorothiophosphates and/or ashless thiophosphates appears to assist in the formation of Zn phosphates and ZnS in the tribofilm. This is also confirmed by the Zn L-edge spectra that indicate the primary presence of Zn phosphate in the tribofilm. Fluorine K edge analysis (not shown here) indicated very little presence of any fluorine at the surface of the tribofilm indicating that while the presence of fluorine certainly helps in the formation of the tribofilm and its stability very little of it is left behind on the wear surfaces.

### 3.4 Conclusion

The frictional behavior of lubricant formulation with ZDDP and ZDDP blended with ashless fluorothiophosphate and/or ashless thiophosphates are essentially identical indicating no mechanistic change tribologically with the addition of the ashless antiwear additives to the mix.



The wear behavior both at low (54N) and high (350N) loads indicate that mixtures with ZDDP and ashless antiwear additives have significantly superior wear behavior when compared to ZDDP by itself. The incubation time to form tribofilms is shorter when mixtures of ZDDP and ashless antiwear additives are used in comparison to ZDDP by itself.

Morphology of the wear surface using scanning electron microscopy indicates that at lower loads (54N) tribofilms are not well developed and largely heterogeneous while at higher loads (350 N) the tribofilms develop a larger pad like structure that is interconnected and aligned in the direction of rubbing. Formulations with a mixture of ZDDP and ashless additives yielded stable pad like tribofilms while the ones from ZDDP alone were more heterogeneous.

Scanning probe microscopy and nano-mechanical testing of the tribofilms indicate that properties at 54N in all cases have a large degree of scatter due to the heterogeneous nature of the tribofilms while at 350N the hardness data in the formulation with ZDDP and ashless additives is uniform and independent of depth while those from ZDDP alone exhibit a large amount of scatter, a consequence of their heterogeneous nature.

The P and S Ledge XANES Data indicate the preponderance of phosphates (short chain or monophosphates) of Zn in the tribofilm while the S that is present is largely in the form of ZnS. When only ZDDP is present the surface of the tribofilms contains sulfates of Zn while in the case of ZDDP with ashless antiwear additives a mixture of sulfates and sulfides of Zn are present.

The O K-edge XANES spectra indicates very little presence of oxides of Fe or Zn in the tribofilm and complement the P L-edge spectra that indicate the primary presence of phosphates of Zn.

The P and S L edge XANES spectra indicate the presence of Zn Phosphates and in the case of S, primarily the presence of ZnS. The S K-edge spectra complement the L-edge spectra wherein the S is present more as a sulfate when only ZDDP is used whereas when mix of ZDDP and ashless antiwear additives are used the reduced form of S is more likely to be present.

The Zn L-edge spectra complements all the other XANES data confirming that the coordination of Zn is largely in the form of Zn phosphates.

## Chapter 4. Role of Cationic and Anionic Moieties of Ionic Liquids to Their Tribofilms Properties

### 4.1 Introduction

In this chapter, the relationship between the ionic liquid (IL) chemistry to its tribological properties such as coefficient of friction, wear and chemical-mechanical properties of tribofilms is examined. Six phosphorous (P) based ILs (in which P is either present in anion or in cation or in both) were chosen to examine the role of different cations and anions. The six IL's used as additives were blended in group I base oil at 0.1 wt. % P treat rate and their tribological performance was evaluated using a line contact cylinder on reciprocating flat test configuration under pure sliding. ZDDP at 0.1 wt. % P and base oil tests were also conducted for baseline comparison. All ILs showed comparable or lower coefficient of friction compared to ZDDP which exhibited a higher but consistent coefficient of friction for the duration of the test. IL N\_DEHP and P\_TFSI showed comparable or slightly better wear protection than ZDDP whereas N\_DBDTP, P\_TMPP, P\_DMP and P\_DEDTP exhibited worse wear outcomes than ZDDP. XANES analysis of pure IL standards and their tribofilms indicate that the tribofilms from IL are the result of decomposition of the IL chemistry and reaction of these decomposition products with underlying steel substrate. No residues of the original IL chemistry was found on the wear tracks. Nano-indentation results indicated that tribofilm hardness increases from the surface towards the bulk of the films, which when combined with P L-edge spectra indicate that short chain phosphates formed at the surface result into lower hardness than medium chain phosphate formed in the bulk.

## 4.2 Experimental Details

### 4.2.1 Structure and Chemistry of Ionic Liquids

Group I base oil (mixture of 60 wt. % solvent neutral 150W and 40 wt. % bright stock 90W) and zinc dialkyl dithiophosphate (ZDDP) were purchased from commercial vendors. The ZDDP used in this study is a secondary alcohol derived ZDDP with approximately 70% neutral and 30% basic characteristic. Six different ionic liquids studied were provided from AC2T Research GmbH Austria. Table 4 details the chemical structure of the antiwear additives used including ZDDP and the six ionic liquids. The six IL's were chosen carefully to provide not just a diversity of chemistries but also an opportunity to examine the role of different cations and anions. Choline bis(2-ethylhexyl)-phosphate (N\_DEHP) and choline dibutyl-dithiophosphate (N\_DBDTP) have the same cation while one anion has phosphate structure and the other one has a thiophosphate structure. Tetradecyl-trihexyl-phosphonium bis(2,3,4-trimethylpentyl)-phosphinate (P\_TMPP) and tetradecyl-trihexyl-phosphonium bis(trifluoroethylsulfonyl)-imide (P\_TFSI) have the same cation while one anion is a phosphinate the other one is a fluoro-sulfonyl amide. Lastly methyl-tributyl-phosphonium dimethyl-phosphate (P\_DMP) and tetrabutyl-phosphonium O,O-diethyl-diphosphate (P\_DEDTP) have similar (not same) cations while the anions have either a phosphate or thiophosphate moiety.

Table 4. Molecular structure of six IL's and ZDDP and their onset decomposition temperature.

Coded name	Chemical name	Chemical structure	Onset decomposition temperature (°C)
ZDDP	Zinc dialkyl-dithiophosphate (R = C4, C6 and C8)		206
N_DEHP	Choline bis(2-ethylhexyl)-phosphate		258
N_DBDTP	Choline dibutyl-dithiophosphate		172
P_TMPP	Tetradecyl-trihexyl-phosphonium bis(2,4,4-trimethylpentyl)-phosphinate		362

P_TFSI	Tetradecyl-trihexyl-phosphonium bis(trifluoromethylsulfonyl)-imide		413
P_DMP	Methyl-tributyl-phosphonium dimethyl-phosphate		326
P_DEDTP	Tetrabutyl-phosphonium O,O-diethyl-dithiophosphate		261

#### 4.2.2. Thermogravimetric (TGA) Analysis of Ionic Liquids


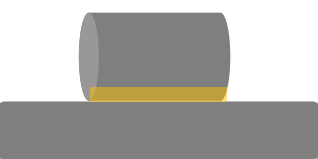
Thermogravimetric analysis (TGA) of the ionic liquids was performed using Shimadzu TGA-51 Thermogravimetric analyzer. TGA was performed in nitrogen (N<sub>2</sub>) atmosphere at a heating rate of 10 °C/min from RT to 600 °C with a N<sub>2</sub> flow rate of 20 mL/min. Each test was repeated twice for the consistency of the data.

#### 4.2.3. Tribological test procedure

Oils containing ionic liquids were formulated in group 1 mineral base oil at 1000 ppm phosphorous level. Ionic liquids were mixed in base oil by pulse ultrasonication for 15 minutes in DI water bath. Tribological test were carried out for each oil formulation immediately after the mixing. The tribological performance of these IL formulated oils were tested using a cylinder on reciprocating flat tribometer at Argonne National

Laboratory [56]. Schematic of the test configurations and detail of test parameters for cylinder on reciprocating flat contact under pure sliding are shown in Table 5. Friction and wear performance of ILs are compared with ZDDP at equal phosphorous level (i.e. 0.1 wt. % P). Load was applied using a pneumatic pressure unit and friction forces were measured using a strain gauge motion sensor. Oil formulations containing ILs in base oil were tested under this set-up at 134 N applied load that generates a 500 MPa initial Hertzian contact pressure. All the test were run at 300 RPM (5 Hz) in pure sliding contact for the duration of an hour at 100 °C. Data was acquired at 5 Hz using the DasyLab software. Tests were performed on 52100 hardened steel flat using a 52100 hardened steel bearing cylinder from RBC bearings. Both flat and cylinder pin were cleaned before each tests using Stoddard solution followed by isopropanol and acetone to completely remove any oil and dust present on the initial surfaces. The rubbed surfaces after the tests were cleaned with heptane and isopropanol and then saved by submerging in sulfur free base oil.

Table 5. Schematic of the test configurations and detail of test parameters for cylinder on reciprocating flat contact under pure sliding

Tribological test	Cylinder on reciprocating flat contact
	<div style="display: flex; justify-content: space-around; align-items: center;"> <div style="text-align: center;"> <p>Front View</p>  </div> <div style="text-align: center;"> <p>Side View</p>  </div> </div>
Base oil	Group I mineral oil (60 wt.% SN 150W + 40 wt.% BS 90W)
Viscosity	10.068 mm <sup>2</sup> /sec at 100°C
Treat rate	Phosphorous: 1000ppm
Applied load	82 N
Initial Hertzian contact pressure	500 MPa
Temperature	100 °C
Speed	0.06 m/sec, 5 Hz
Stroke length	6 mm
Cylinder/Ball	Φ 4 mm x 6 mm, 52100 steel (60-61 HRC)

#### 4.2.4 Characterizations methods

In order to make a precise measurement of average wear width, cylinders after each test were gently cleaned using heptane followed by isopropanol shower. Wear width were measured at nine locations on each cylinders using optical images obtained from an Olympus metallographic microscopy. The nature of the wear occurring at the surface was studied by examining the surface of the wear tracks using a Hitachi S-3000N SEM to obtain secondary electron images of the wear track and high resolution 3D images of the



wear track were acquired using a nano-indentation from Hysitron Triboscope<sup>TM</sup> in SPM mode.

Tribochemistry of the films generated on the rubbing surfaces using IL's and ZDDP were characterized using XANES spectroscopy. It provides chemical information including local coordination of elements at different depths of penetration, for example in the case of phosphorous, surface can be probed from 5 nm to 60 nm in the case of P L-edge and from 50 nm of the surface to >800 nm in the case of P K-edge [108,134]. XANES spectra were obtained at The Canadian Light Source synchrotron facility at Saskatoon Canada. The phosphorous L-edge (P L-edge) data were collected at VLS-PGM (variable line spacing plane grating monochromator) beam station that operates at the energy range of 5.5 – 250 eV with a photon resolution of more than 10,000 E/ $\Delta$ E. All the spectra were collected using a 100  $\mu$ m x 100  $\mu$ m photon beam spot size. Oxygen K-edge (O K -edge) spectra were obtained at SGM (spherical grating monochromator) beam line that operates between 200 – 2500 eV energy range with a photon resolution of more than 5000 E/ $\Delta$ E. Here, a spot size of 50  $\mu$ m x 50  $\mu$ m was chosen to obtain high resolution spectra. Finally, phosphorous K-edge (P K-edge) and sulfur K-edge (S K-edge) spectra were obtained at SXRMB (Soft X-ray Microcharacterization Beamline) beam station which operates at higher energy from 1.7 – 10 keV with a photon resolution of  $3.3 \times 10^{-4}$  eV. A 1 mm x 2 mm spot size was chosen to collect the spectra at the SXRMB beam line.

Nano-mechanical properties i.e. hardness of the tribofilms generated on the flat were measured using a Hysitron Triboscope<sup>TM</sup>. Nano-indentation tests were carried out

using a NorthStar™ Cube Corner probe with a total included angle of 90° and <40 nm tip radius. Nano-indentation were performed at nine different locations in a single sample. A cyclic loading profile with partial unload load was run for each indentation point to study the nano-mechanical properties of the tribofilms as a function of film thickness.

## 4.3 Results and Discussions

### 4.3.1 Thermogravimetric Analysis of Ionic Liquids

Figure 13 is a plot of weight loss as a function of temperature for six IL's and ZDDP antiwear additive. The onset of decomposition temperature for ILs and ZDDP additive was approximated using tangent analysis and is shown in Table 4. ZDDP additive showed onset decomposition temperature i.e. about 206 °C that is lower than ILs except N\_DBDTP (i.e. 172 °C). N\_DEHP was approximated to be about 258 °C whereas onset decomposition temperature of N\_DBDTP was recorded to be about 172 °C. The P=O bond has a dissociation energy of 544 kJ/mole while P=S has a dissociation energy of 335 kJ/mole, hence it is easier for the P=S linkage to be the point of initial thermal decomposition in N\_DBDTP leading to a lower decomposition temperature in comparison to N\_DEHP. Similarly, N\_DEDTP (P=S linkage) has lower onset decomposition temperature than P\_DMP (P=O linkage). Choline based ILs exhibit lower thermal stability than phosphonium based IL structures with similar anions (N\_DEHP vs. P\_DMP and N\_DBDTP vs. P\_DEDTP). P\_TFSI exhibited the highest thermal stability of all with onset decomposition temperature of about 413 °C.

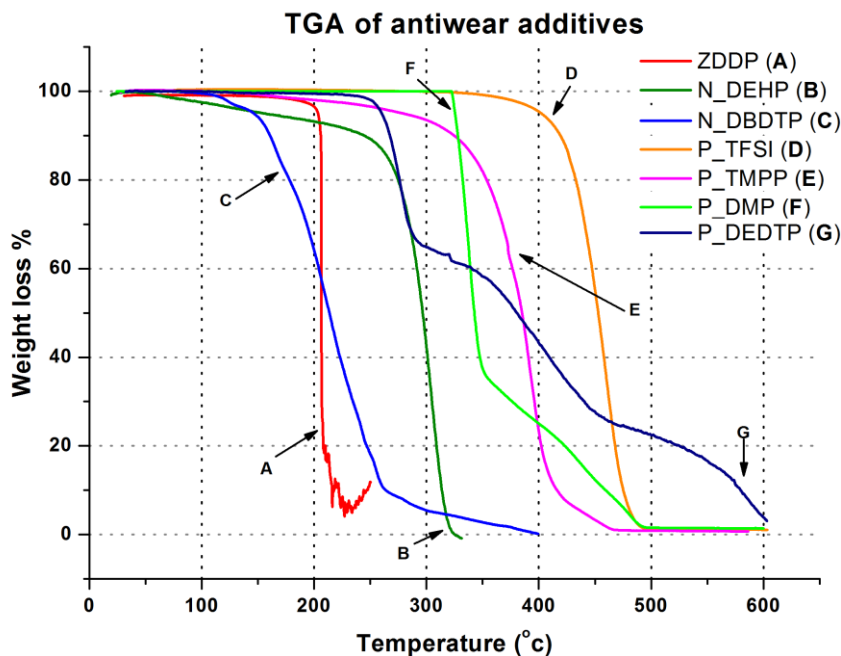


Figure 13. Thermogravimetric analysis plot of six IL's and ZDDP showing the decomposition temperature of different additive chemistries.

#### 4.3.2 Evaluation of Coefficient of Friction (CoF) and Wear Volume

Figure 14 is a graph of friction coefficient as a function of the test duration for six ionic liquids and comparing their friction characteristic with ZDDP at equal phosphorous level as well as with group I base oil that has no additives. All six IL's and ZDDP show improvement in friction response compared to base oil when added at 0.1 wt% P treat rate. IL N\_DEHP has the lowest friction coefficient however the CoF tends to increase at the end of the test. IL's N\_DBDTP, P\_DMP and P\_TFSI also display lower friction coefficient in comparison to ZDDP for the duration of the test. On the other hand, ZDDP

exhibits stable friction behavior throughout the test whereas all six IL's exhibit some level of variance in the friction with the progression of the test.

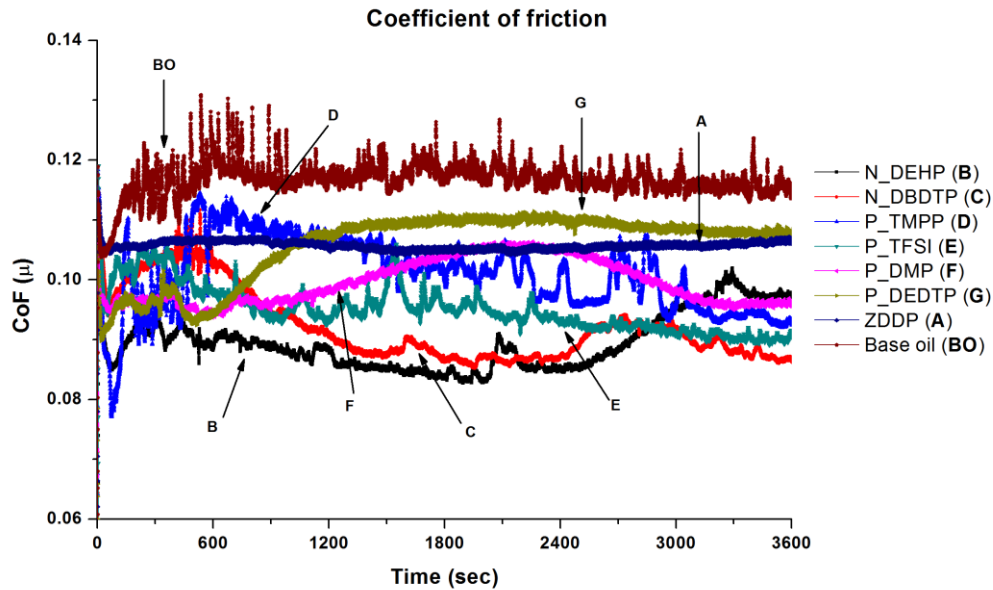


Figure 14. Comparison of coefficient of friction of six IL's with ZDDP at equal phosphorous level (i.e. 0.1 wt% P) and base oil obtained under pure sliding contacts.

Wear was calculated by measuring the average wear width on the cylinder after each test using optical microscopy. Figure 15 is a plot of an average wear volume loss for six IL's along with ZDDP and base oil. In comparison with base oil, all IL's showed significant improvement in wear protection in base oil formulations. When compared with ZDDP, N\_DEHP exhibited comparable antiwear performance whereas P\_TFSI had slightly lower wear volume loss. On the other hand P\_DBDTP, P\_TMPP, P\_DMP and P\_DEDTP exhibited significantly higher wear volume losses. Figure 16 summarizes tribological performances (i.e. CoF and wear volume loss) of six IL's along with ZDDP

and base oil. Data at the bottom left on the plot has the lowest combination of wear and coefficient of friction (beneficial) and the data on the top right hand corner would have the higher wear and highest friction (detrimental). Hence, N\_DEHP and P\_TFSI have better tribological performance compared to ZDDP while P\_DMP and P\_DEDTTP have significantly worse wear but comparable frictional outcomes in comparison to ZDDP.

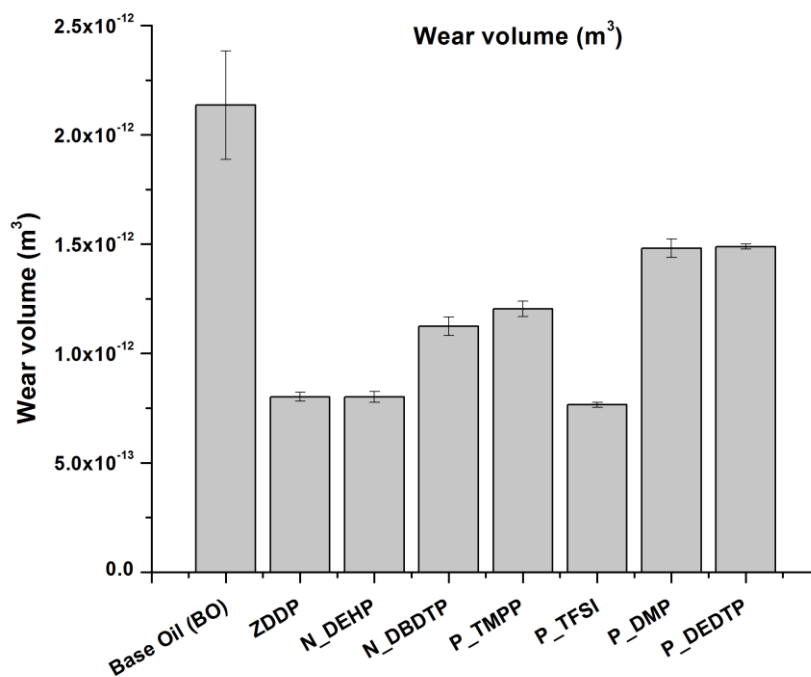


Figure 15. Average wear volume measured for six IL's and ZDDP blended in base oil at 0.1 wt% P and the neat base oil test.

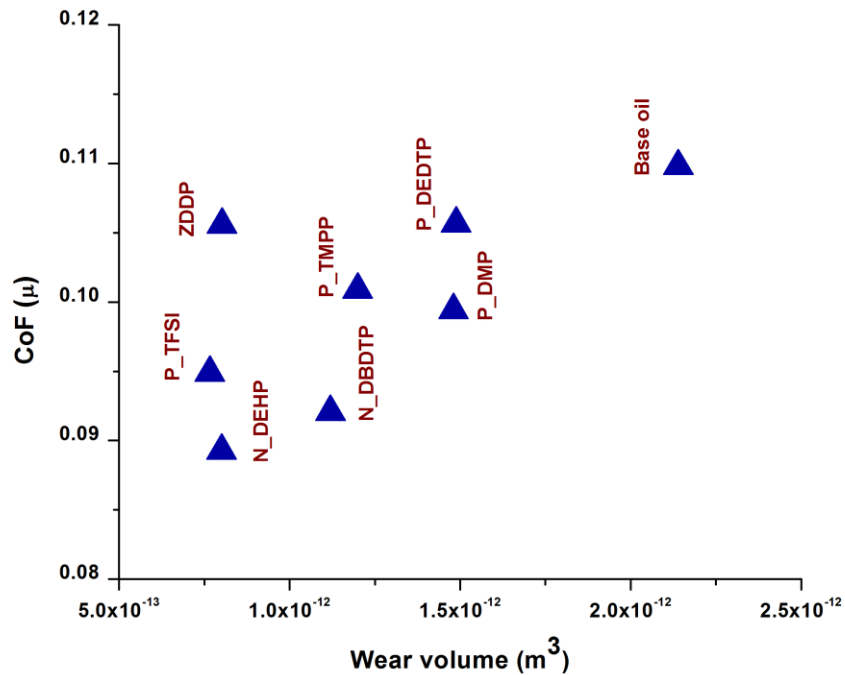


Figure 16. Comparison of coefficient of friction and wear volume loss for six IL's and ZDDP. Data at the bottom left on the plot has the lowest wear and friction coefficient (beneficial) and the data on the top right hand corner has the higher wear and highest friction (detrimental).

#### 4.3.3 Analysis of Rubbed Surfaces Using Scanning Electron Microscopy and Scanning Probe Microscopy.

Figure 17 is the secondary electron SEM images of the worn flat surfaces. SEM image of ZDDP lubricated surface exhibits regions of abrasive wear with scratches aligned to the sliding direction together with the formation of protective patchy tribofilms whereas worn surfaces lubricated under N\_DEHP and P\_TFSI show smoother wear surfaces. N\_DEHP exhibits better coverage of tribofilms (as evidenced by the dark

patches on the surface that are less conductive regions corresponding to patchy tribofilms) over the wear track with mild scratches aligned in the sliding direction. The SEM image obtained for P\_TFSI lubricated wear track indicates mild polishing wear. The SEM image of N\_DBDTP worn surface shows patchy tribofilm formation, with patch sizes that are larger than what is seen in N\_DEHP. On the other hand the wear surfaces observed in the case of P\_TMPP, P\_DMP and P\_DEDTP exhibit deeper scratches compared to N\_DEHP, N\_DBDTP and P\_TFSI with P\_DMP and P\_DEDTP exhibiting the highest surface roughness. The analysis of the morphology of worn surfaces thus correlates to the wear volume discussed earlier as IL's P\_TMPP, P\_DMP and P\_DEDTP had significantly higher wear volume whereas IL's N\_DEHP and P\_TFSI exhibited comparable or even better wear protection than ZDDP. In order to further compliment the findings of SEM results, SPM images were obtained using a nano-indentation technique in SPM imaging mode. SPM images of rubbed surfaces are obtained for 60  $\mu\text{m}$  x 60  $\mu\text{m}$  area on the wear track while keeping the Z-axis ( $\pm 200$  nm) same. SPM images of IL's and ZDDP lubricated surfaces are shown in Figure 18. The arrow in Figure 18 represents the direction of rubbing. 3D wear profile of ZDDP lubricated surface exhibits slightly higher surface roughness with a number of small islands type features typical of patchy tribofilms covering the asperities whereas 3D profiles of N\_DEHP and P\_TFSI lubricated surfaces show smoother features on the wear track with smaller patches representative of tribofilms. SPM images of P\_DEDTP, P\_TMPP and P\_DMP lubricated surfaces show scratches with larger peak to valley heights in the direction of rubbing that compliments the SEM results discussed earlier.

The SPM images of N\_DBDTP are slightly rougher than N\_DEHP but smoother than P\_DEDTTP, P\_TMPP and P\_DMP.

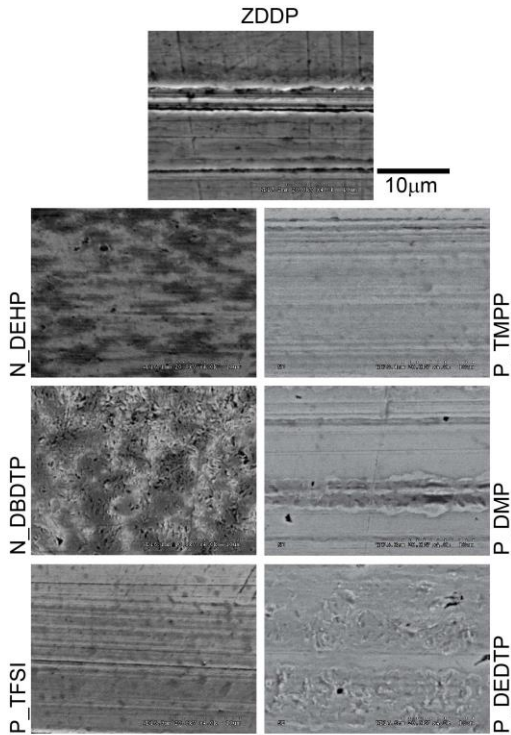


Figure 17. Secondary electron SEM images illustrating the morphology of worn surfaces derived from six IL's and ZDDP.

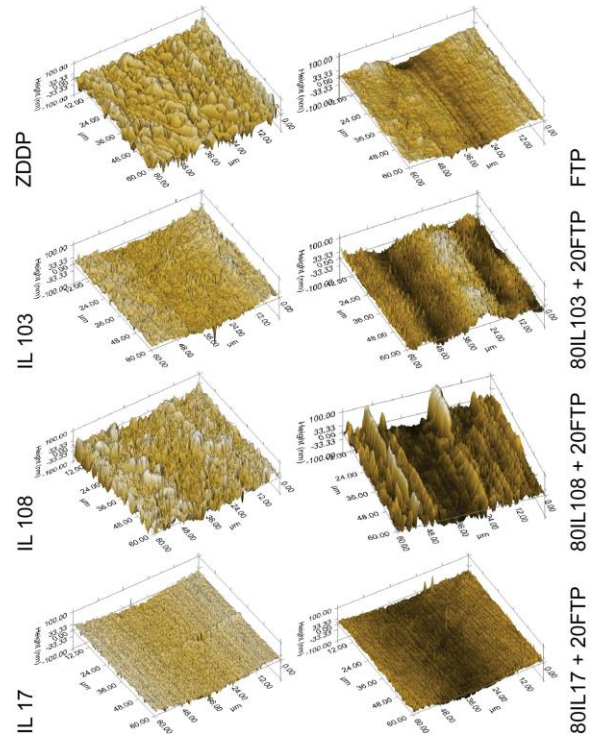


Figure 18. SPM images showing the 3D wear profile of the rubbed surfaces derived from six IL's and ZDDP.

#### 4.3.4 XANES Characterization of Tribofilms

X-ray absorption near edge structure (XANES) spectroscopy is a non-destructive technique to characterize the chemical nature of tribosurfaces. XANES technique has a unique capability to provide information about the local coordination of elements present on the surface (5-50 nm) as well in the bulk of the sample (up to several hundred nm) [134]. It utilizes a high flux of high-energy soft/hard x-ray photons from a synchrotron



radiation source. If the flux of photons directed to the sample has sufficient energy to excite a core level electron of an atom, a photoelectron is created and it occupies unoccupied energy states. As a result, a hole is created in either K or L levels which subsequently gets filled up by electron from high energy shell followed by emission of a fluorescent photon which is detected by fluorescence detector inside the main chamber and plotted as fluorescence yield spectra (FY). Total electron yield spectra are collected by measuring a neutralization current that is applied to the sample to balance the positive charge created on the sample as X-ray photon absorption lead to the excitation of core level electrons to continuum. XANES spectra provide details about the electronic and geometric structure of the absorbing atom [140-143]. In tribology, XANES analysis has been used extensively to examine the chemical make-up of the tribofilms derived using various additives [11,13,14,16,51,54,56,64,126,127,131-133]. In this study, XANES spectra are acquired in total electron yield (TEY) and fluorescence yield (FY) mode. TEY spectra is more surface sensitive whereas FY spectra give information from the bulk of the samples, in case of Si L-edge the sampling depth of TEY and FY mode is 5 nm and up to 60 nm respectively [134].

#### 4.3.4.1 Phosphorous L<sub>2,3</sub>-edge of Pure ILs

P L-edge spectra of pure ionic liquid standards were also acquired in order to characterize the absorption edge of these novel compounds. To the author's best knowledge, this is a first the study to characterize the spectra features of a class of phosphorous based ionic liquids using P L<sub>2,3</sub>-edge and P K-edge. Previously, Kruse et al. [144] have studied the P L-edge spectral features of a number of phosphorous compounds

such as mineral P, organic P and P-bearing minerals. Similarly, Kasrai et al. [51,132,136,145,146] studied the P L-edge and P K-edge spectral features of various sodium, iron and zinc polyphosphate glasses and proposed a relationship between the phosphate chain length and a peak ratio of pre-edge shoulder and main absorption edge. P L-edge spectra of pure IL standards is used to differentiate the chemical nature of the tribofilms formed using these novel additives from their respective original structures. P L-edge spectra of pure IL standards are shown in Figure 19a. The absorption peaks observed are labeled as **A**, **B**, **C**, **C'**, **C''**, **D** and **D'**. Where peak **D** is a shape resonance peak, which is a characteristic peak of phosphate coordination irrespective of the cation it is associated with. Peak **D** is commonly present in IL's N\_DEHP, P\_TMPP and P\_DMP, which have phosphate anion in their respective structures. The photon energy for peak **D** in Figure 19a is equivalent to the photon energy for peak **d** in Figure 19b, which is present in both FePO<sub>4</sub> and Zn<sub>3</sub>(PO<sub>4</sub>)<sub>2</sub> as well as in all the tribofilms composed of phosphate antiwear films. Main absorption edge for N\_DEHP was observed at 138.09eV (peak **C**), which is attributed to diethyl-hexyl-phosphate anionic moiety since here the only source of phosphorous is the cation. The absorption edge of N\_DEHP IL is approximately 0.4 eV lower than the absorption edge for FePO<sub>4</sub> (138.06 eV for N\_DEHP vs. 138.47 eV for FePO<sub>4</sub>) as shown in Table 6. P L-edge spectra of N\_DBDTP IL is similar to N\_DEHP as their chemical make is similar with the only difference being two of the four O atoms are replaced with S atoms in the phosphate. This is reflected in the P L-edge spectra where the shape resonance peak **D'** for N\_DBDTP is slightly shifted to a lower energy compared to N\_DEHP (peak **D**). P\_TFSI spectra exhibits a main absorption

edge (peak **C'**) at lower energy 135.79 eV compared to N\_DEHP that is at 138.09 eV. This is attributed to the tetradecyl-trihexyl-phosphonium cation that is the only source of phosphorous in the P\_TFSI structure, the shift to lower energy is likely due to the lower binding energy of the  $2p$  electrons in organic moiety in the cation in comparison to the binding energy when P is bound to O in the anion. P L-edge spectra of P\_TMPP and P\_DMP ILs are quite rich as both ILs contain phosphorous in their respective cation and anion moieties. In the case of P\_TMPP, peak **D'** originates from the trimethyl-pentyl-phosphinate anion whereas IL P\_DMP show peak position **D** originating from dimethyl-phosphate. Besides that, multiple peaks are observed in the energy range 135 eV-140 eV. Presence of peak **C'** in both P\_TMPP and P\_DMP is attributed to the phosphonium cation (P-C coordination) in their respective spectra, which is also seen in the P\_TFSI (peak **C'**) that only has phosphonium cation as a source of phosphorous in the structure. As seen earlier from N\_DEHP, absorption edge peak **C** corresponds to the phosphate (P-O coordination) anion structure that is also present in P\_TMPP and P\_DMP ILs. Peak **C''** is speculated to originate from the proximity of phosphonium cation and phosphate anion in P\_TMPP and P\_DMP, which is also present in P\_DEDTP.

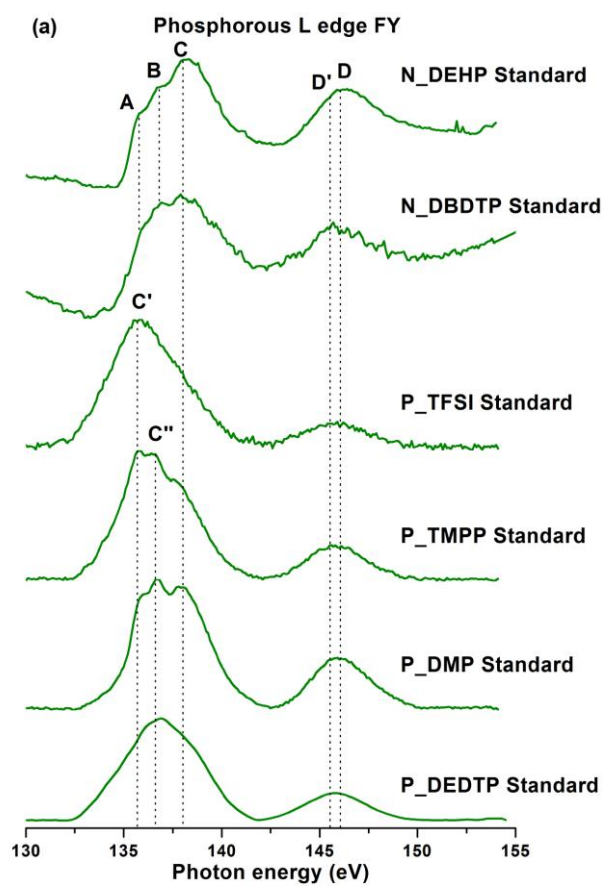


Figure 19a. Phosphorous L<sub>2,3</sub>-edge FY spectra of pure IL's standards.

Table 6. P L-edge model compounds and Ionic liquids standard peak positions.

Chemical compounds	Peak energy (eV)								
	A	B	C	D	E	a/a'	b/b'	c/c'	d
N_DEHP Standard	135.6	136.4	138.0		146				
N_DBDTP Standard		136.8	138.0	145.5					
P_TFSI Standard	135.7								
P_TMPP Standard	135.7	136.8			146				
P_DMP Standard	135.7	136.8	138.0		146				
P_DEDTP Standard		136.8		145.5					
Iron phosphate						135.8	136.7	138.4	146
Zinc Phosphate						136	137.9	138	146

#### 4.3.4.2 Phosphorous L<sub>2,3</sub> -edge of Tribofilms

P L-edge TEY and FY spectra of the tribofilms generated under IL and ZDDP lubrication are plotted in Figure 19b and 19c respectively along with the model compounds. In Figure 19b and 19c, pre-edge shoulder and absorption edge for Zn<sub>3</sub>(PO<sub>4</sub>)<sub>2</sub> and FePO<sub>4</sub> are designated as **a'**, **b'** and **c'** and **a**, **b** and **c** respectively. Peaks labelled as **a'**, **a** and **b'**, **b** correspond to transition from spin-orbit split of phosphorous 2*p* electrons (into the 2*p*<sub>3/2</sub> and 2*p*<sub>1/2</sub> levels, which are usually referred to as the L<sub>3</sub>- and L<sub>2</sub>-edges, respectively) into the first unoccupied 3*s*- like antibonding state [147]. In Zn<sub>3</sub>(PO<sub>4</sub>)<sub>2</sub> and FePO<sub>4</sub> peaks labelled as **c'** and **c** are attributed to the transition of the phosphorous 2*p*

electrons to the *3p-like* antibonding state [147] in  $\text{Zn}_3(\text{PO}_4)_2$  and  $\text{FePO}_4$  respectively. Peak **d** in Figure 19b and 19c is commonly present in both  $\text{Zn}_3(\text{PO}_4)_2$  and  $\text{FePO}_4$  as well as in tribofilms spectra, is a shape resonance peak owing to *2p* to *3d* transition [148], which is a characteristic of all phosphates regardless of the structure. When comparing the tribofilms spectra with the model compound, P L-edge TEY and FY spectra from ZDDP tribofilm indicate the formation of zinc polyphosphates as the peaks **a'**, **b'** and **c'** from  $\text{Zn}_3(\text{PO}_4)_2$  model compounds overlaps with the pre-edge shoulder and absorption edge of ZDDP tribofilms. However the possibility of formation of  $\text{FePO}_4$  cannot be ruled out completely as iron cations are also available during the wear process. P L-edge spectra of ILs tribofilms show the presence of peak **d** suggesting that these novel antiwear additives undergo tribochemical reaction by decomposition of their original structure and form phosphate tribofilms during the rubbing action by reacting with counter surfaces. Since only iron cations are available from the substrate, these IL lubricated tribofilms are composed of iron polyphosphates, which can also be confirmed by matching the pre-edge shoulder (peaks **a** & **b**) and main absorption edge (peak **c**) of  $\text{FePO}_4$  model compound with P L-edge spectra of ILs derived tribofilms in Figure 19b and 19c. XANES spectra can also be used to estimate relative thickness of antiwear films formed by considering the signal strength of their respective spectra. In case of P L-edge TEY spectra, all tribofilms spectra show good signal strength suggesting that tribosurfaces are enriched with phosphates films. Whereas P L-edge FY spectra which provide information relatively deeper into the tribofilm (up to 50 nm), a poorer signal to noise ratio can be

seen in the case of P\_TFSI and P\_TMPP lubricated tribofilms suggesting thinner tribofilms.

P L-edge spectra can also be used to determine the chain length of the polyphosphates present in the tribofilms using peak intensity ratio of pre-edge shoulder (**a**) to main absorption edge (**c**). Chain lengths of polyphosphates are characterized on the basis of peak height of peak **a** relative to peak **c** where ratio **a/c** up to 0.3-0.4 represents short-chain polyphosphates and **a/c** > 0.6 indicates long-chain polyphosphates [51,132,136]. The **a/c** ratio of tribofilms derived from ILs and ZDDP is shown in Table 7. From Table 7, it is apparent that tribofilms in this study are primarily made up of short chain polyphosphates at the surface whereas the bulk of the tribofilms are composed of more medium chain polyphosphate films except N\_DBDTP, P\_DMP and P\_DEDTP. Hence, a layered structure of tribofilms is observed with shorter chain at the top of the film and medium chain polyphosphate films in the bulk and close to the tribofilms substrate interface. Highest **a/c** or in other words longer chain polyphosphate films were observed in the case of N\_DEHP, which earlier showed wear behavior comparable or better than ZDDP in Figure 15 & 16. P\_TFSI that showed comparable or better antiwear outcome in comparison to ZDDP also have similar **a/c** ratio as of ZDDP tribofilms. In addition, N\_DBDTP, P\_DMP and P\_DEDTP have lower **a/c** ratio and higher wear volume loss (Figure 15). Thus, it can be hypothesized that antiwear performance of these novel additive is a function of chain length of polyphosphate films formed under their respective lubrication. An exception to this rule, P\_TMPP tribofilms exhibited medium chain polyphosphate tribofilm, however the signal to noise ratio is very poor. Here, it can

be deduced that even though P\_TMPP forms medium chain polyphosphates of iron on the rubbing surfaces, their film formation rate is a less competitive than film removal rate, which results in thinner protective phosphate films on the counter surfaces and consequently larger wear volume losses as seen in Figure 15.

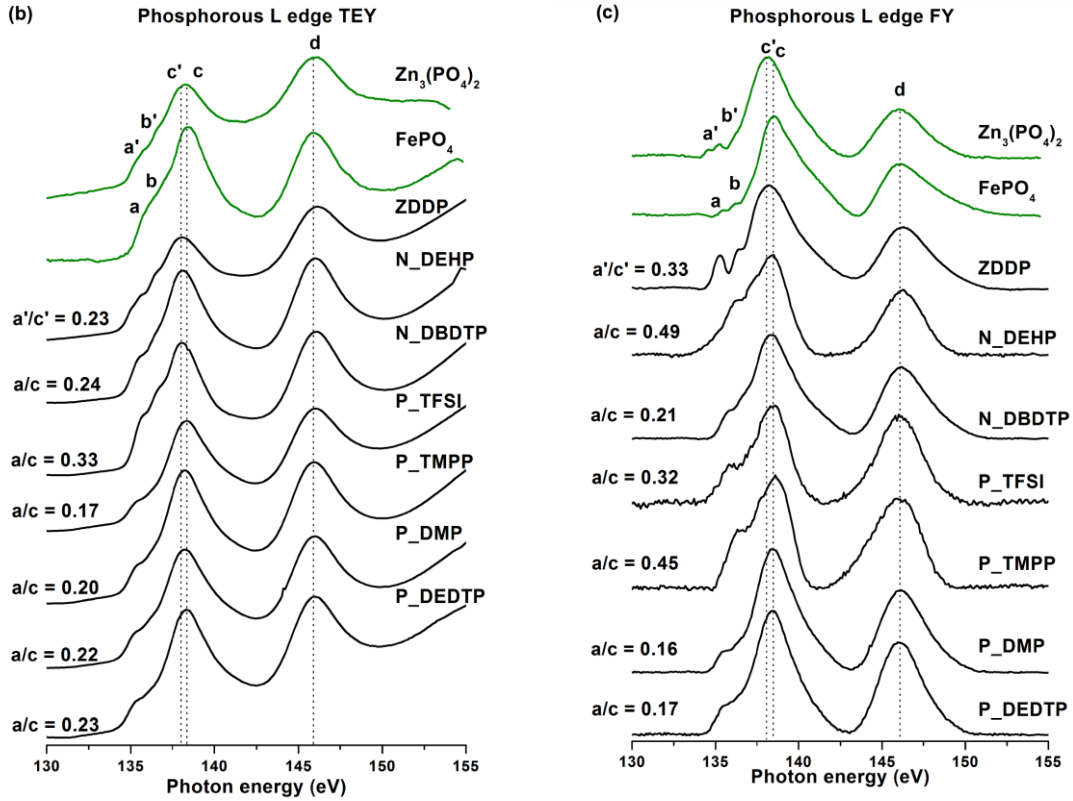


Figure 19. Phosphorous L<sub>2,3</sub>-edge spectra TEY (Fig. 19b) and FY (Fig. 19c) of tribofilms formed using ZDDP and six IL's additives. The a/c ratio obtained from P L edge indicating the degree of polymerization in the phosphate tribofilms is also shown in left hand side of each spectra.



Table 7. P L-edge a/c ratio of tribofilms.

Additive chemistry	TEY	FY
ZDDP	0.23	0.33
N_DEHP	0.24	0.49
N_DBDTP	0.33	0.21
P_TFSI	0.17	0.32
P_TMPP	0.2	0.45
P_DMP	0.22	0.16
P_DEDTP	0.23	0.17

#### 4.3.4.3 Phosphorous K-edge of Pure ILs

In order to further consolidate the earlier findings that ILs do undergo a tribochemical reaction during the rubbing action, decompose and form tribofilms, P K-edge spectra of original ILs structures are plotted in Figure 20a and compared with the P K-edge spectra of their respective tribofilms in Figure 20b. From Figure 20a and 20b, it can be seen that the main absorption edge of all six IL standards are at lower energy than the absorption edge of their respective tribofilms. Table 8 highlights the energy of the main absorption edge obtained for six IL standards as well as model compounds  $Zn_3(PO_4)_2$  and  $FePO_4$ . From Figure 20a, a correlation between the chemical structure of IL's and their respective P K-edge spectra can be deduced. P K-edge spectra of N\_DEHP exhibit main absorption edge at photon energy 2151.8 eV that is identified as peak **C**. Peak **C** arises from the phosphate anion, since the only source of phosphorous in N\_DEHP is (2-ethylhexyl)-phosphate anion. The absorption edge (peak **C**) for N\_DEHP phosphate structure was found to be at slightly lower energy than the absorption edge energy of  $Zn_3(PO_4)_2$  (peak **b'** in Figure 20b) as well as  $FePO_4$  (peak **b** in Figure 20b) and N\_DEHP derived tribofilms (peak **b** in Figure 20b) as the source of cation is different in

all cases. Thus, the main absorption edge energy for these different phosphate structures can be ordered as  $N\_DEHP < Zn_3(PO_4)_2 < FePO_4 = N\_DEHP$  tribofilm (Table 8). In the case of P\_TFSI, phosphorous is only present in phosphonium cation (i.e. organo-phosphorous), and a respective absorption edge (peak  $C''$ ) for P-C coordination was observed at 2148.2 eV. N\_DBDTP has the same cation as in N\_DEHP but a different anion (i.e. dithiophosphate) where two O atoms are being replaced by two S atoms. The P K-edge FY spectra of N\_DBDTP standard show two main absorption edges at energies of 2149.08 eV and 2150.05 eV and are identified as peaks  $C'_1$  and  $C'_2$  respectively. Peaks  $C'_1$  and  $C'_2$  are possibly originating from P-S & P-O coordination in dibutyl-dithiophosphate structure. We can further consolidate our findings by analyzing the P K-edge spectra of P\_TMPP and P\_DEDTP. P K-edge spectra of P\_TMPP exhibit two main absorption edges since both cation and anion have phosphorous in their respective structure. The first absorption edge at energy 2148.25 eV aligns with the peak  $C''$ , which is originating from P-C coordination in tetradecyl-trihexyl-phosphonium cation. The second absorption edge in the P K-edge spectra of P\_TMPP was found at energy 2150.1 eV matching with peak  $C'_2$ , which is believed to be originating from the phosphinate anion where phosphorous is bound with two O atoms as in the case of dithiophosphate anion in N\_DBDTP. N\_DEDTP has phosphorous both in cation and anion structure and its P K-edge spectra is more complicated as the absorption edge is influenced by three different phosphorous coordination i.e. P-C, P-S and P-O. Peak analysis using Origin pro identified three peaks in the main absorption edge of P\_DEDTP P K-edge FY spectra. The main absorption edge obtained at peak energy 2150.1 eV aligns with the peak  $C'_2$  and

is commonly found in N\_DBDTP and P\_TMPP with P-O coordination where one P atom is bound with two O atoms. The second absorption edge located at energy 2149.1 eV is found to match with the peak  $C'_1$  that is also observed in N\_DEDTP with P-S coordination where one P atoms is bound with two S atoms. And finally, a third peak identified at energy 2148.2 eV aligns with peak  $C''$  is considered to be originating from P-C coordination in tetrabutyl-phosphonium. In the case of P\_DMP, the first absorption edge (peak  $C'$ ) was observed at 2148.2 eV originating from phosphonium cation and the second absorption edge was observed at 2151.86 eV (i.e. peak  $C$ ) originating from phosphate anion which is similar to the absorption edge observed in the case of N\_DEHP with the similar phosphate anion structure. The main absorption edge (peak  $C'_2$ ) observed in N\_DEDTP for the P-O bond is found to be  $\sim 2.2$  eV lower than peak  $C$  for the N\_DEHP P K-edge. It is speculated that the partial replacement of O atoms by S atoms in dithiophosphate structure results in the change in the molecular symmetry and the local chemical environment of phosphate structure, leading to main absorption edge to be shifted at lower energy in N\_DBDTP than N\_DEHP for P-O binding.

#### 4.3.4.4 Phosphorous K -edge of Tribofilms

Figure 20b is a plot of P K-edge FY spectra of tribofilms derived from ZDDP and six IL's used in this study. The P K-edge spectra of tribofilms are compared with model compounds  $Zn_3(PO_4)_2$  and  $FePO_4$  in Figure 20b. Primary absorption edge of  $Zn_3(PO_4)_2$  is labelled as peak  $b'$  and a pre-edge shoulder and main absorption edge for  $FePO_4$  are labeled as peak  $a$  and peak  $b$ . When spectra for  $Zn_3(PO_4)_2$  and  $FePO_4$  model compounds are compared, two main differences were evident, first the absorption edge for  $Zn_3(PO_4)_2$

at peak **b'** (i.e. 2152.19 eV) is lower than the absorption edge for FePO<sub>4</sub> at peak **b** (i.e. 2153.22 eV), second, FePO<sub>4</sub> P K-edge spectra has a pre-edge shoulder at peak **a** (i.e. 2148.48 eV) that is absent in Zn<sub>3</sub>(PO<sub>4</sub>)<sub>2</sub>. The information obtained from the P K-edge FY spectra of phosphate model compounds now can be used to do fingerprint match analysis of ZDDP and IL's tribofilms. P K-edge FY of ZDDP tribofilms show a main absorption edge matching with absorption edge of Zn<sub>3</sub>(PO<sub>4</sub>)<sub>2</sub> at peak **b'** suggesting that phosphorous in ZDDP tribofilms is mainly present in the form of zinc phosphate. P K-edge FY spectra of tribofilms derived from six IL's used as lubricant additives show two main features, a pre-edge shoulder at peak **a** and an absorption edge at peak **b** confirming that phosphorous from the P containing ILs contributes to the formation antiwear films composed of iron polyphosphate by interacting with the iron surfaces during the rubbing action. The spectra also clearly indicate that the tribofilms from IL are the result of decomposition of the IL and reaction of these decomposition products with the underlying Fe substrate. No evidence of physically adsorbed IL on the surface of the tribofilm is present.

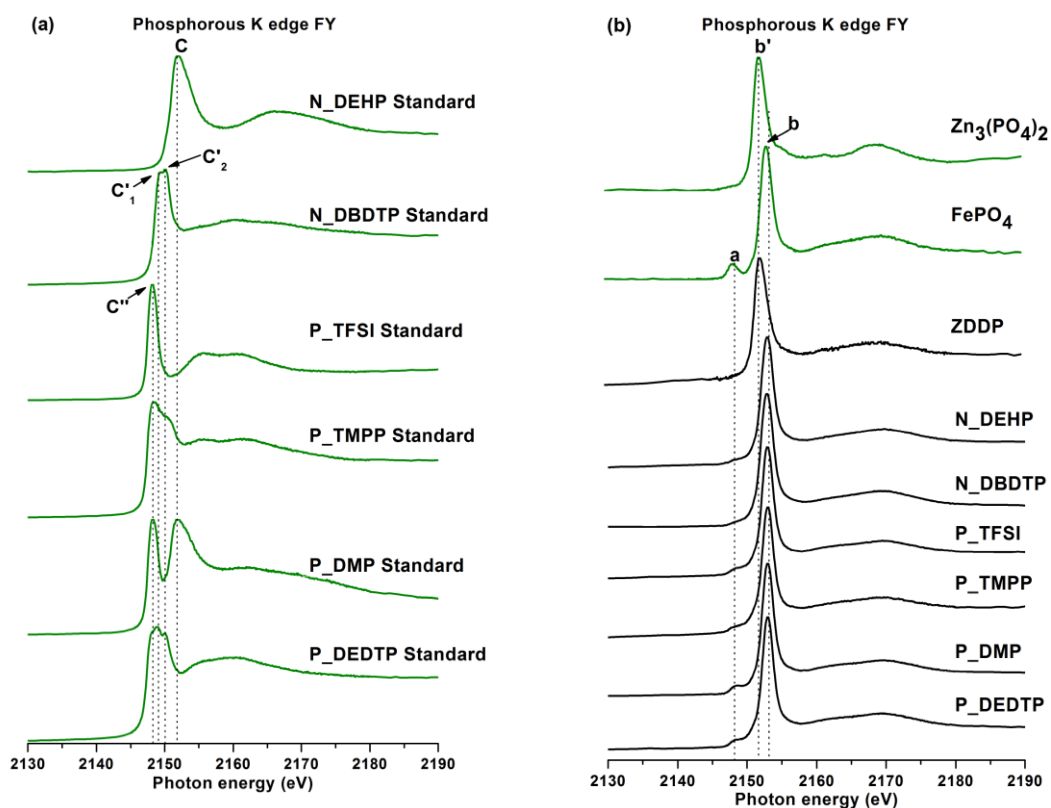


Figure 20. Phosphorous K-edge FY spectra of pure IL standards (Fig. 20a) and tribofilms derived from ZDDP and six IL's as additives as well as model compounds (Fig. 20b).

Table 8. P K-edge model compounds and Ionic liquids standard peak positions.

Model compounds	Peak energy (eV) (Figure 20a)				Peak energy (eV) Figure 20b)		
	C	C' <sub>1</sub>	C' <sub>2</sub>	C''	a	b	b'
N_DEHP Standard	2151.83						
N_DBDTP Standard		2149.08	2150.05				

P_TFSI Standard				2148.26			
P_TMPP Standard			2150.1	2148.25			
P_DMP Standard	2151.83			2148.25			
P_DEDTP Standard		2149.08	2150.05	2148.25			
Iron phosphate					2148.31	2153.22	
Zinc Phosphate							2152.2

#### 4.3.4.5 Sulfur K-edge of IL Standards and Tribofilms

Sulfur K-edge FY spectra of S containing IL standards (i.e. N\_DBDTP, P\_DEDTP and P\_TFSI) are shown in Figure 21a. The main absorption edge and post edge shoulders identified from S containing ILs are labelled as **A**, **B**, **C**, **D** and **E** (in Figure 21a). Both N\_DBDTP and P\_DEDTP have S containing dithiophosphate anionic moiety with the only difference is in their respective alkyl group that is dibutyl in N\_DBDTP and diethyl in P\_DEDTP, therefore exhibit main absorption edge ( peak **A** and peak **B**) and post edge shoulder (peak **C**) at the same photon energy. However, a fine difference can be seen as the relative intensity of peak **A** which is higher than peak **B** in

the case of P\_DEDTP whereas relative intensity of peak **A** and peak **B** is almost same in N\_DBDTP. On the other hand, S K-edge spectra of P\_TFSI standard with fluorosulfonylimide anionic moiety has a main absorption edge (peak **D**) and post edge shoulder (peak **E**) at higher energy than dithiophosphate containing ILs (N\_DBDTP and P\_DEDTP).

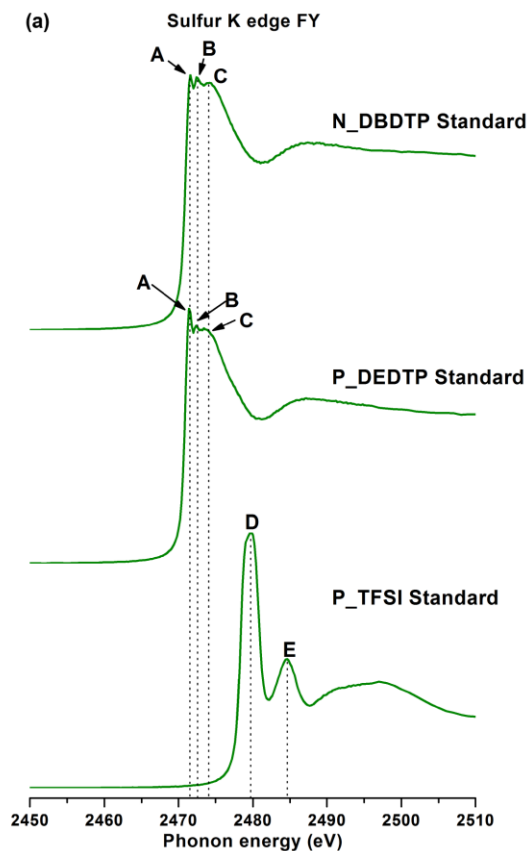


Figure 21a. Sulfur K-edge spectra of sulfur containing IL standards.

S K-edge spectra of tribofilms are plotted in Figure 21c and are compared with the model compounds in Figure 21b. Since sulfur exists in different valence states ranging from -2 to +6 with -2 being the reduced states and the +6 being the oxidized states various peaks have been identified in S K-edge model compounds spectra. The

absorption edge identified from sulfur model compounds are labeled as **a**, **b**, **c**, **d** and **e** in Figure 21b. Where peak **a** and **c** corresponds to iron sulfide, peak **b** and **e** corresponds to zinc sulfide and peak **d** corresponds to sulfates and is characteristic of sulfate regardless of structures. Peak **e** also distinguishes calcium sulfate from zinc sulfate and iron sulfates. In Figure 21c, S K-edge FY spectra of ZDDP tribofilms primarily show two main absorption edge at peak **b** and peak **d** suggesting that sulfur in ZDDP tribofilms is primarily present in the form of ZnS (peak **b**) and sulfates (peak **d**) mainly ZnSO<sub>4</sub> as well as FeSO<sub>4</sub> to some extent. It can also be deduced from the spectra that sulfide to sulfate ratio is higher in ZDDP tribofilms. N\_DEHP, P\_TMPP and P\_DMP do not have sulfur in the pristine structures yet their respective S K-edge tribofilm spectra exhibit a weak sulfur signal. The mineral base oil used in this study has sulfur impurity of about 300 ppm, which may provide a small amount of sulfur thus S K-edge spectra of N\_DEHP, P\_TMPP and P\_DMP show weak sulfur signal confirming that there is not much sulfur present in their respective tribofilms. S K-edge FY spectra of N\_DBDTP tribofilms feature peak **a**, **c** and **d** confirming the formation of FeS and FeSO<sub>4</sub> in the tribofilms. Relative intensity of sulfide peak to sulfate peak is higher in the case of N\_DBDTP than the other sulfur containing IL's. P\_TFSI and P\_DEDTP also show strong signal for sulfates rather than sulfides in their respective S K-edge spectra.

S K-edge spectra can also be used to distinguish the state of sulfur in pristine IL standards and IL derived tribofilms. N\_DBDTP and P\_DEDTP derived tribofilms have main absorption edge at peak position **d** (2481.5 eV) in Figure 21c whereas the main absorption edge for pure N\_DBDTP and P\_DEDTP was found to be at lower energy i.e.



peak **A** and peak **B** (2471.5 eV and 2472.5 eV) in Figure 21a suggesting that sulfur in the tribofilms is primarily present in the form of  $\text{FeSO}_4$  instead of as in pure IL standard. In the case of P\_TFSI, the main absorption edge of tribofilm was found at peak **d** (2481.5 eV) in Figure 21c whereas the main absorption edge of pure P\_TFSI standard observed at peak **D** (2479.7 eV) and post-edge shoulder at peak **E** (2484.6 eV) in Figure 21a which suggest a change in the sulfur environment from the P\_TFSI derived tribofilms to its respective chemistry in pure IL.

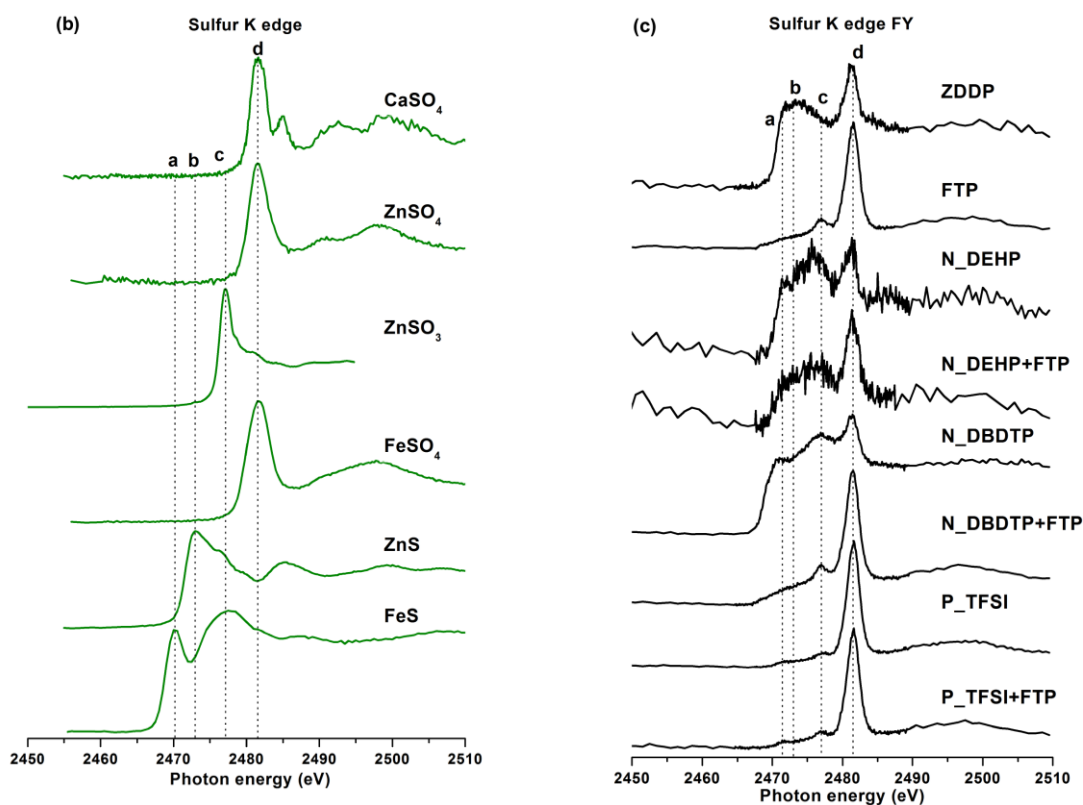


Figure 21. Sulfur K-edge spectra FY of model compounds (Fig. 21b) and tribofilms derived from ZDDP and six IL's (Fig. 21c).

#### 4.3.4.6 Oxygen K-edge of IL Standards and Tribofilms

Figure 22a illustrates the O K-edge spectra of six IL standards. The main absorption edge and the pre-edge and post-edge peaks are identified and labelled as peak **A**, **B**, **C**, **D**, and **E**. In all ILs except P\_TFSI, oxygen has two linkage i.e. O bound with alkyl group (O-R linkage) and O bound with P atom (P-O linkage) while in the case of P\_TFSI, O is only bound with S atoms. The oxygen K-edge spectra is more complex to resolve due to the superposition of multiple contributions at the main edge. However, all the model compounds except P\_TFSI have P-O linkages that give rise to the pre-edge peak identified as **A**. This peak in the P\_TFSI is accentuated, however, the likely origin of that large pre-edge is due to the O=S linkage. The main peaks located between 537 eV and 539 eV (**B**, **C**, and **D**) has contribution from multiple sources. Two absorption edge are observed for N\_DEHP at energy 537.8 eV i.e. peak **C** and 539 eV i.e. peak **D**. These two absorption edge are believed to originate from O-R and P-O linkage. Similar peaks are also observed in the case of P\_DMP that has similar anion as in N\_DEHP where four O atoms are bound with one P atom. When N\_DEHP and N\_DBDTP spectra are examined, peak **D** is diminished relative to peak **B** in N\_DBDTP compared to N\_DEHP. This possibly is because the four oxygen atoms in N\_DEHP that are in P=O and P-O-C configuration and in N\_DBDTP they are configured as P-O-C only.

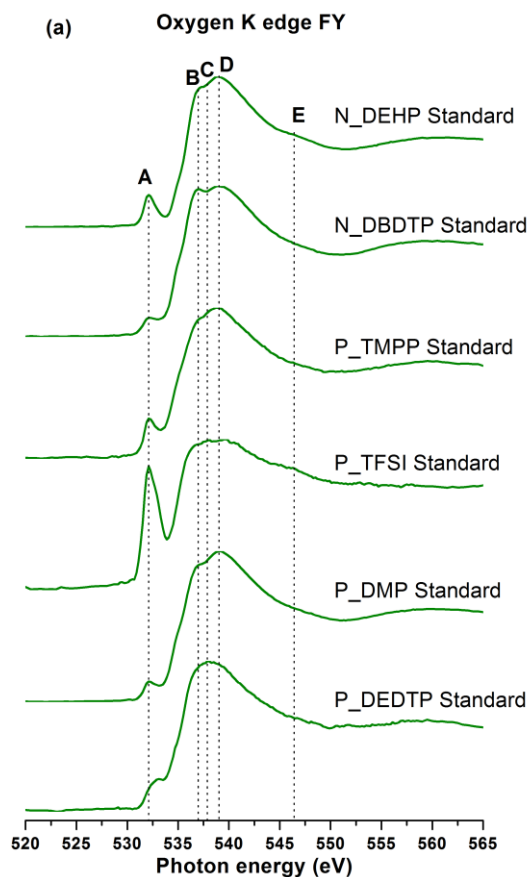


Figure 22a. Oxygen K-edge spectra of pure IL standards.

O K-edge spectra of tribofilms are plotted in Figure 22c and compared with model compounds in Figure 22b. O K-edge spectra were acquired in both TEY and FY mode for the tribofilms and the model compounds as well as pure IL standards, TEY and FY spectra being very similar, only the FY spectra are shown for reference while the discussion pertains to both TEY and FY spectra. Figure 22c is a plot for the O K-edge FY spectra of tribofilms derived from ZDDP and IL lubrication. Three peaks are identified and labeled as peak **a**, **b** & **c**. By fingerprint matching of these peaks with model compounds in spectra Figure 22b, it can be deduced that peak **a** is uniquely present in all

the model compounds where oxygen is associated with Fe cation such as  $\text{FePO}_4$ ,  $\text{FeSO}_4$  and  $\text{Fe}_2\text{O}_3$ , peak **b** is a main absorption edge that is originating from either  $(\text{PO}_4)^{-2}$  or  $(\text{SO}_4)^{-2}$  structure whereas peak **c** is a main absorption edge for  $\text{Fe}_2\text{O}_3$  model compound. O K-edge spectra of tribofilms generated using N\_DEHP, N\_DBDTP and P\_TFSI show main absorption edge at peak **b** (538.9 eV) with a pre-edge peak at peak **a** (531.9 eV) whereas ZDDP tribofilms only show main absorption edge at peak **b**, suggesting the ZDDP tribofilms are primarily composed of  $\text{Zn}_3(\text{PO}_4)_2$  and  $\text{ZnSO}_4$  while the tribofilms derived from N\_DEHP, N\_DBDTP and P\_TFSI are composed of  $\text{FePO}_4$  in the case of N\_DEHP and  $\text{FePO}_4$  and  $\text{FeSO}_4$  in the case of N\_DBDTP and P\_TFSI. A dominant presence of peak **c** (542.18 eV) in the case of tribofilms derived from P\_TMPP, P\_DMP and P\_DEDTTP indicate oxidation of the surfaces since peak **c** is characteristic absorption edge for  $\text{Fe}_2\text{O}_3$ . This results from O K-edge spectra complements the wear results (seen in Figure 15) as ILs P\_TMPP, P\_DMP and P\_DEDTTP showed higher wear losses since the surface chemistry obtained using these ILs is being dominated by oxidation of the surfaces rather than formation of phosphate antiwear films. Whereas O K-edge spectra of additives with lower wear losses such as ZDDP, N\_DEHP, P\_TFSI show more phosphate formation on the rubbed surfaces rather than oxide formation.

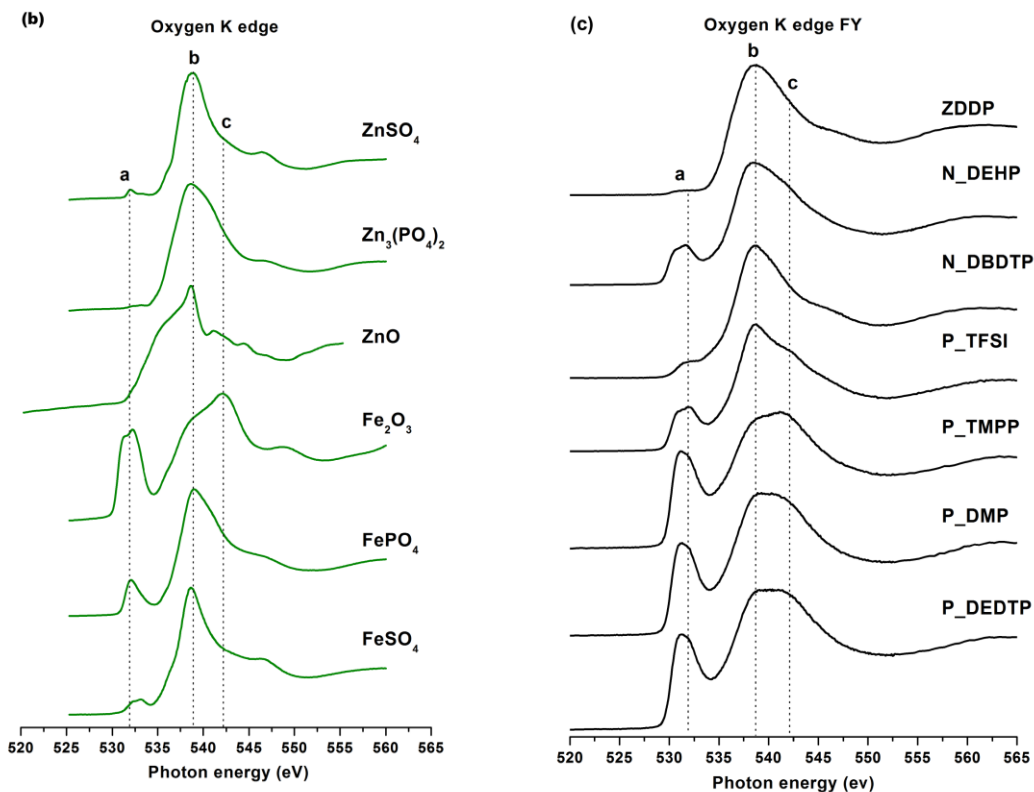


Figure 22. Oxygen K-edge FY spectra of model compounds (Fig. 22b) and tribofilms formed from ZDDP and IL's lubrication (Fig. 22c).

#### 4.3.5 Nano-indentation

Since, XANES analysis revealed that the tribofilms derived from different additives such as ZDDP or IL's have different chemical make-up, it is important to understand the resultant mechanical properties of these different tribochemical films to evaluate their respective antiwear behavior. Nano-mechanical properties of tribofilms derived from IL lubricated surfaces were measured using nano-indentation technique. Hardness of IL derived tribofilms were compared with ZDDP lubricated tribofilms. Nano-indentation were performed on each tribofilms sample using a cyclic loading with

partial unload function as shown in Figure 23a. Figure 23b shows a plot of tribofilm hardness as a function of film depth for ZDDP and IL's. Nano-mechanical properties of best antiwear performing IL's are compared with ZDDP in Figure 23b. In Figure 23b, top left graph shows a plot of applied vertical load against penetration depth that is generated after each indentation test. Such typical load v/s depth plots were set as a criteria for the selection of proper indentation and hardness profile plotted for a particular indent location in the other three hardness plots. In the case of ZDDP, hardness profile varies with the indentation location, however, a general trend can be observed where ZDDP tribofilm hardness increases with the indentation depth up to 100nm and then remains constant. ZDDP tribofilms show large variation in hardness, where minimum hardness observed is ~3 GPa and maximum hardness is ~10GPa. Compared with ZDDP tribofilm hardness profile, both N\_DEHP and P\_TFSI show more consistent hardness profiles at different indentation locations suggesting that IL derived tribofilms have more uniform properties. N\_DEHP tribofilms show low hardness at near surface and then hardness increases to peak value ~12 GPa at 40-50 nm indentation depth and then starts to decrease with further depth as measurement gets influenced by substrate hardness (alloy steel) that has hardness ~8-10 GPa [50]. P\_TFSI show variation in hardness profiles at different locations but more than one location show similar hardness profiles suggesting that there are region of low hardness and high hardness. This could be explained as, in the case of peak to peak contact due to much higher contact pressure high hardness film forms whereas at regions of valley to valley contact remains relatively soft. Similarly,

Bec et al. [149] also reported that pad regions (4 to 8 GPa) are harder than the valley region (1-3 GPa).

In all cases, surface of the tribofilms is softer than the bulk of the tribofilms with hardness increasing with indentation depth. This results are consistent with previous studies where similar hardness profile has been reported for the tribofilms. Nehme et al. [111] studied the effect of contact load on tribofilms properties and reported that ZDDP tribofilms hardness increase with indenter depth as well as with increasing contact pressure during the wear test. Furthermore, films hardness can also be correlated with the surface chemistry. P L--edge TEY spectra from XANES offer information up to 10-15 nm from the surface whereas FY gives information up to 50-60 nm. P L -edge a/c ratio calculated earlier in XANES analysis indicate that in the case of ZDDP P L--edge a/c ratio increase from 0.23 (TEY) to 0.33 (FY) that subsequently results in increase in the ZDDP tribofilms hardness from 3 GPa to 8-9 GPa respectively (as seen in Figure 23a). Similarly, N\_DEHP and P\_TFSI have higher a/c ratio in FY spectra than TEY, which is an indicative of longer chain phosphates formation in the bulk of the films than the tribofilms at surface. From their respective hardness profile, it can be deduced that at the surface tribofilms with shorter chain phosphate have lower hardness (~3-4 GPa) and as the phosphate chain length increase the hardness of the films also increases (up to ~12 GPa). Highest hardness observed in the case of N\_DEHP ~12 GPa that has highest a/c ratio of 0.49. This result is consistent with theoretical model developed by Mosey et al. [150] where they showed that longer chain lengths and crosslinking of zinc phosphate films resulted in higher stiffness tribofilms.

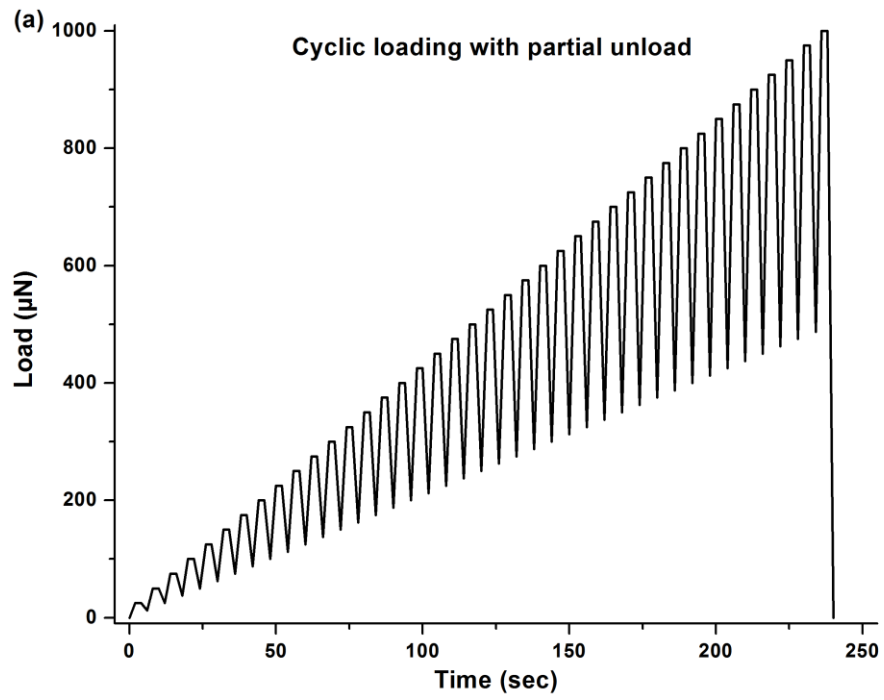


Figure 23a. Showing a cyclic loading with partial unload load profile as a function of time (2s loading, 2s hold, and 2s unloading) used for nano-indentation.



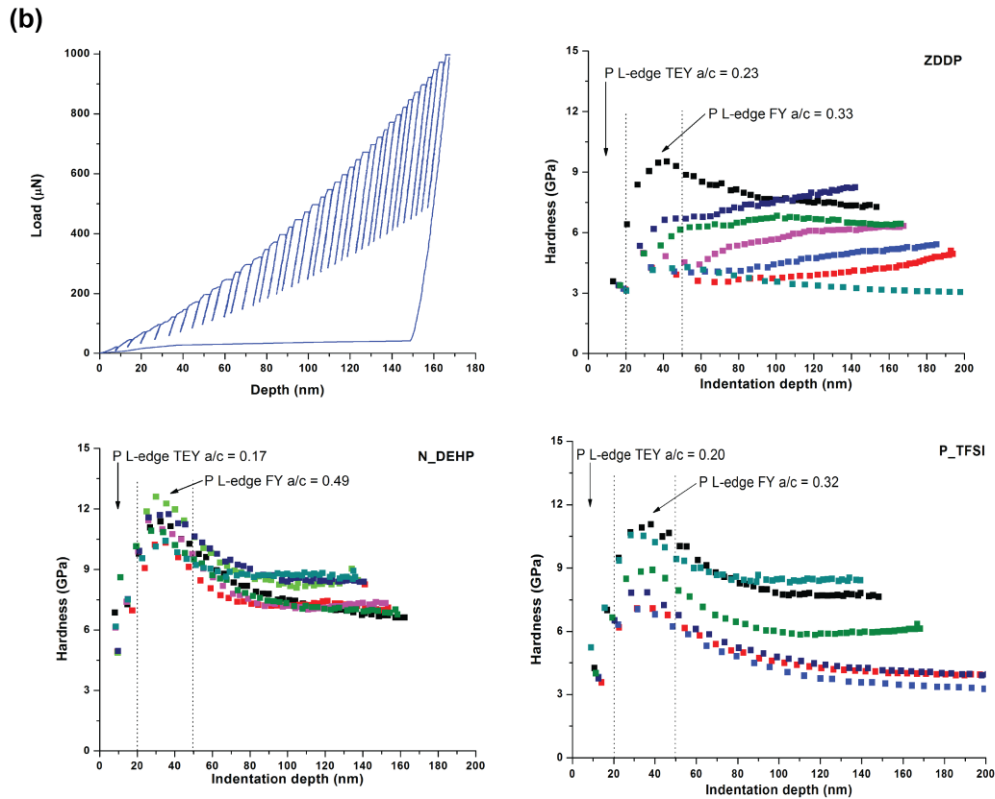


Figure 23b. Nano-mechanical properties of tribofilms obtained using a cube corner (NorthStar<sup>TM</sup>) probe, a typical load vs. penetration depth curve obtained (shown in top left corner) set a criteria for proper indentation. Selected hardness profiles as a function of indentation depth are displayed for ZDDP (top right) and IL N\_DEHP (bottom left), and P\_TFSI (bottom right) tribofilms.

#### 4.4 Conclusions

Tribological properties of six ILs are studied and compared with ZDDP additive at equal phosphorous treat rate (i.e. 0.1 wt. % P) in group I BO. All ILs showed variance in their friction curve while ZDDP showed relatively consistent friction coefficient. Lowest CoF was recorded for IL N\_DEHP. Both IL N\_DEHP and P\_TFSI showed

comparable or even better wear protection than ZDDP whereas N\_DBDTP, P\_TMPP, P\_DMP and P\_DEDTP showed worse wear outcomes than ZDDP.

XANES analysis (P L<sub>2,3</sub> & K-edge and S K-edge) indicate that tribofilms derived from IL lubricated surfaces have different chemical make-up than the original IL chemistry as the original structure of ILs are not found on the worn surface. Thus, it can be hypothesized that phosphorous containing ILs do participate in the tribochemical reaction during the rubbing action and form antiwear phosphate films on tribosurfaces under mixed to boundary lubrication conditions by interacting with Fe substrate. XANES analysis also showed that. These findings further lay out a strong understanding on the ability of ILs to interact with the rubbing surface and form glassy antiwear films composed of phosphates of Fe.

P L-edge spectra of tribofilms showed that the surface of the tribofilms are composed of short chain polyphosphate and medium chain phosphates formed in the bulk except N\_DBDTP, P\_DMP and P\_DEDTP.

## Chapter 5. Ashless chemistry of P and S based Ionic Liquids and Their tribofilm

### Formation Mechanism in Base oil and Fully Formulated oil (no Zinc)

#### 5.1 Introduction

In this chapter, two ionic liquids, choline bis(2-ethylhexyl) phosphate (N\_DEHP) and choline dibutyl dithiophosphate (N\_DBDTP) are studied as lubricant additives in group1 mineral base oil (BO) and fully formulated oils with no zinc and no phosphorous (FFO). Tribological behavior of these IL's was evaluated using a cylinder on reciprocating flat Schwing-Reib-Verschleiss (SRV®) tribotester (Optimol Instruments Prüftechnik GmbH, Munich, Germany). Tribological behavior of IL's as lubricant additives is compared with zinc dialkyl dithiophosphate (ZDDP) at equal phosphorus level (0.1% P) in BO and FFO. Surface morphology of the worn surfaces were studied using scanning electron microscopy (SEM) and 3D profile of wear track was acquired using scanning probe microscopy (SPM). Chemical nature of the tribofilms was characterized using X-ray absorption near edge structure spectroscopy (XANES). A simple phenomenological model was developed to explain the formation of tribofilms from ionic liquids in comparison to how they form with ZDDP.

#### 5.2 Experimental Details

##### *5.2.1 Chemistry of Antiwear Additives*

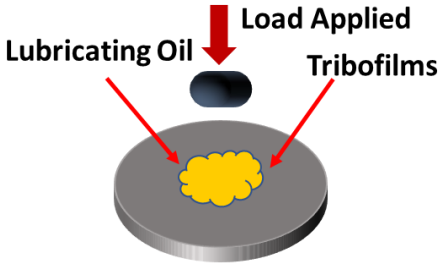
Table 9 shows the details of the chemical structure of N\_DEHP and N\_DBDTP along with ZDDP used in this study. Neutral -100 base oil and zinc dialkyl dithiophosphate (ZDDP) were purchased from commercial vendors. The ZDDP used in

this study is a secondary alcohol derived ZDDP with approximately 70% neutral and 30% basic characteristics. Ionic liquids are provided by AC2T Research GmbH.

*5.2.2 Tribological Test Procedure:*

The tribological behavior of the IL's was evaluated using a cylinder-on-flat oscillating reciprocating motion SRV tribometer. Oil formulation containing N\_DEHP, N\_DBDTP and ZDDP were prepared at 0.1% Phosphorous treat rare in group1 base oil. Ionic liquids were dispersed in base oil by pulse ultrasonication in bath (using 2 seconds pulse on time, 4 seconds pulse off time) for 80 seconds at 26% amplitude. Tests were performed on 100Cr6 (hardness 800 HV) steel flat using a 52100 hardened steel bearing cylinder. Fresh specimens were used for each lubricant sample. The specimens were subsequently washed in three different solvents (toluene, isopropanol and petroleum ether) for ten minutes each, using an ultrasound bath, before and after the tribological experiments. The SRV rig parameters are listed in Table 9.

Table 9. Tribological test condition employed in the SRV tests.

Tribological Test: SRV (Cylinder on Disc Configuration)	
Applied Load	56 N
Temperature	100 °C
Stroke Length	4 mm
Speed	30 Hz
Lubricant Amount	2-3 drops ( $\approx$ 0.1 ml)
Duration of Test	1 hour

### 5.2.3 Characterization of Tribofilms

The mechanism of wear was studied by microscopic examination of the wear tracks generated on discs. A Hitachi S-3000N Scanning Electron Microscope (SEM) was used to get secondary electron images of the wear track. 3D profile of the wear track was obtained using a nano-indenter from Hysitron Triboscope<sup>TM</sup> in SPM imaging mode. SPM images were acquired using a Berkovich tip with a total included angle of 142.3 degrees and a half angle of 65.35 degrees.

XANES spectra were obtained to elucidate the tribo-chemistry of the rubbed surfaces. It provides chemical information including local coordination of elements at different depths of penetration, for example in the case of phosphorous, surface can be probed from 5 nm to 60 nm in the case of P L edge and from 50 nm of the surface to >800 nm in the case of P K edge [54,134]. XANES spectra were obtained at Canadian Light Source synchrotron facility at Saskatoon Canada. The phosphorous L edge (P L edge) data were collected at VLS-PGM (variable line spacing plane grating monochromator) beam station that operates at the energy range of 5.5 eV-250 eV with a photon resolution of more than 10,000 E/ $\Delta$ E. All the spectra were collected using a 100  $\mu$ m X 100  $\mu$ m photon beam spot size. Oxygen K edge (O K edge) spectra were obtained at SGM (spherical grating monochromator) beam line which operates between 200 eV-2500 eV energy range with a photon resolution of more than 5000 E/ $\Delta$ E. Here, a spot size of 50  $\mu$ m X 50  $\mu$ m was chosen to obtain high-resolution spectra. Finally, phosphorous K edge (P K edge) and sulfur K edge (S K edge) spectra were obtained at SXRMB (Soft X-ray Micro characterization Beam line) beam station which operates at energy ranging

from 1.7 – 10 keV with a photon resolution of  $3.3 \times 10^{-4}$  InSb (111). A 1 mm X 2 mm spot size was chosen to collect the spectra at the SXRMB beam line.

### 5.3 Results and Discussion

#### 5.3.1 Thermogravimetric Analysis of Ionic Liquids

Figure 24 is a plot showing weight loss as a function of temperature for N\_DEHP and N\_DBDTP IL. The onset of decomposition for N\_DEHP was approximated to be about 258 °C whereas onset decomposition temperature of N\_DBDTP was recorded to be about 172 °C. The P=O bond has a dissociation energy of 544 kJ/mol while P=S has a dissociation energy of 335 kJ/mol., hence it is easier for the P=S linkage to be the point of initial thermal decomposition in N\_DBDTP leading to a lower decomposition temperature in comparison to N\_DEHP. A lower decomposition temperature of N\_DBDTP explains relatively poor tribological performance observed later as the additive was decomposing too early resulting in loss of IL during the test.

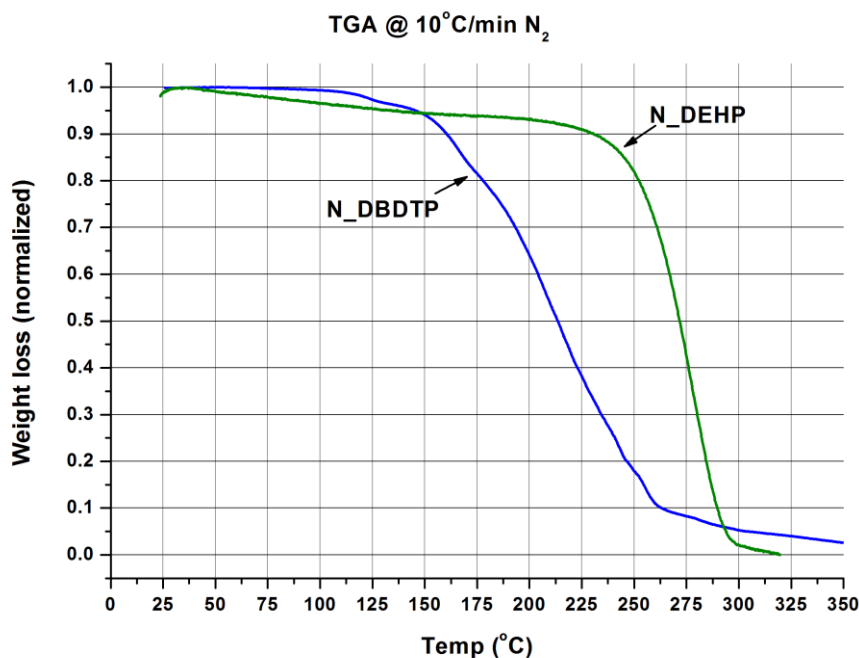


Figure 24: Thermal decomposition temperature of N\_DEHP and N\_DBDTP IL using TGA analysis.

### 5.3.2 Coefficient of Friction

Coefficient of friction was recorded for six different oil formulations for the duration of the SRV tribological test (i.e. 1 hour). Figure 25 shows a comparison of friction behavior of N\_DEHP and N\_DBDTP with ZDDP in BO and FFO formulations. It can be deduced from the CoF plot that both ionic liquids and ZDDP show similar friction profiles in base oil formulation. Similar frictional response was also observed for the FFO formulations containing N\_DEHP, N\_DBDTP and ZDDP. However, N\_DBDTP in FFO showed higher CoF throughout the test in comparison to N\_DEHP and ZDDP in FFO. Nevertheless, it is worth noticing that both N\_DEHP and N\_DBDTP show stable frictional response during the SRV tribotesting. In addition, it is also evident that under

the test conditions in this study there is very little difference in frictional response between oils with ZDDP and oils with ionic liquids.

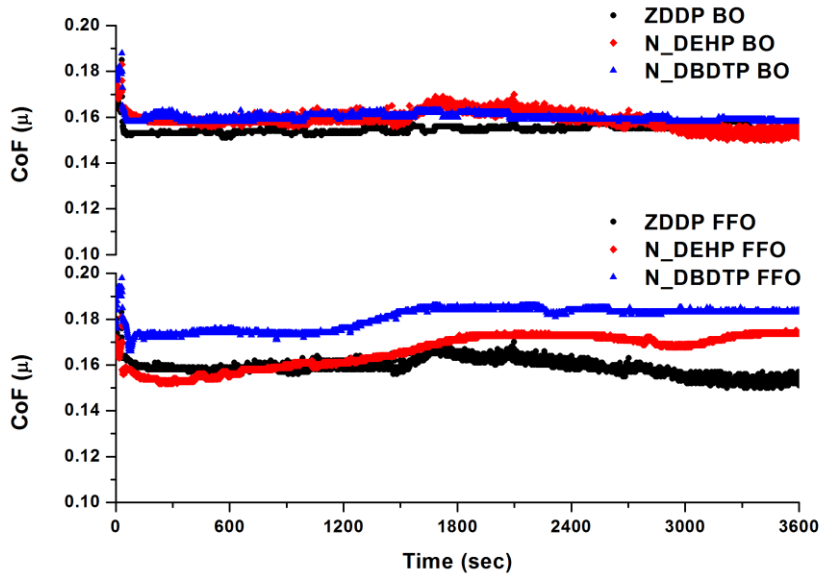


Fig. 25. Friction coefficient as a function of time for tribological tests conducted using a SRV tribometer for oils with N\_DEHP and N\_DBDTP with ZDDP in base oil and in fully formulated oil.

### 5.3.3 Topography of the Tribofilms using SEM and SPM

Figure 26 is the secondary electron SEM images of the rubbed surfaces for six different oil formulations. In case of base oil formulations, SEM images of N\_DEHP show smoother surfaces than the wear surfaces generated under ZDDP lubrication. SEM images of N\_DEHP do show features of initial scratches that occurred at the beginning of the test however, at higher magnification it is evident that initial scratches are covered with tribofilms. On the other hand, ZDDP derived worn surfaces show deeper scratches



on the wear track which are evident at high magnification. The darker region in the SEM images pertains to formations of patchy tribofilms (i.e. nonconductive phosphates films). SEM images indicate worn surfaces generated under N\_DBDTP lubrication have wider coverage of tribofilms than ZDDP in base oil. In case of fully formulated oil (no Zinc), both ZDDP and N\_DEHP lubricated worn surfaces show similar small pad like features as well as minimum scratches over the wear tracks while N\_DBDTP lubricated worn surfaces show non-uniform wear profile. It can also be deduced that wear surfaces derived using the same antiwear additives in base oil and fully formulated oil mixes are very different. In case of FFO, wear profiles are dominated by the influence of other additives than ZDDP or IL's. SPM images were acquired in 30  $\mu\text{m}$  X 30  $\mu\text{m}$  area of the wear track and are compared by keeping the Z-axis same. SPM images (shown in figure 27) compliment the SEM results as the 3D profile of N\_DEHP lubricated surface show smoother surface profile than ZDDP in base oil mixes. Deep scratches can also be observed in the 3D image of N\_DBDTP BO lubricated surfaces as was observed in SEM images. Similarly, in case of FFO, SPM images confirm the small pad like features over the wear tracks.

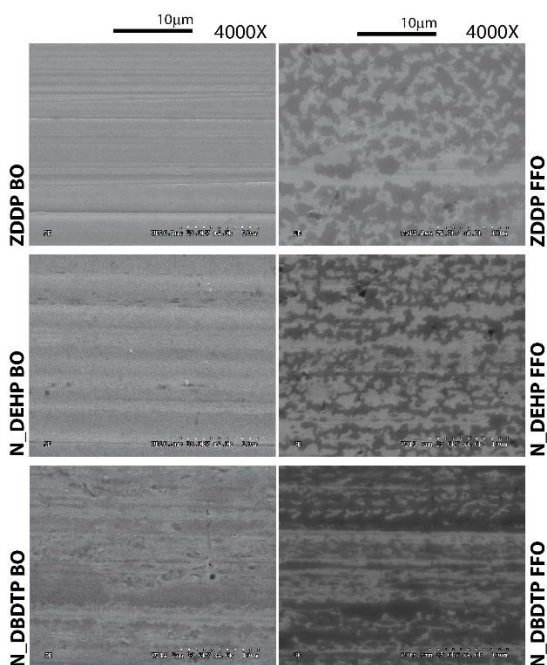


Figure 26. Secondary emission SEM images of the wear track derived from N\_DEHP, N\_DBDTP and ZDDP in base oil and fully formulated oil.

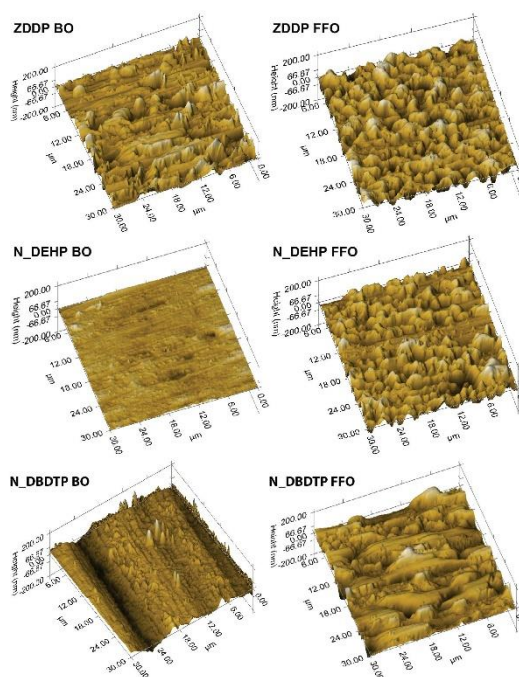


Figure 27. 3-D scanning probe microscopy images of the wear track derived from N\_DEHP, N\_DBDTP and ZDDP in base oil and fully formulated oils.

#### 5.3.4 Chemical Properties of Tribofilms using XANES

The principle of X-ray absorption spectroscopy involves excitation of core level electrons i.e. transition to un-occupied states, ionization threshold and shape resonance by the absorption of x-ray photons. Fine structures resulting from the absorption spectra are known as XANES and EXAFS (extended X-ray absorption fine structure). Though the basic principle of XANES and EXAFS is the same, their analysis results in different set of information regarding the chemical structure of the absorbing atom. The fine structure of EXAFS contains information related to the interatomic distance, coordination number,

and the degree of order whereas XANES spectra provide details about the electronic and geometric structure of the absorbing atom [140-143]. In tribology, XANES analysis has been considered more useful and used extensively to examine the chemical make-up of the tribofilms derived using various anti-wear additives [13,14,16,51,54,56,64,126,127,131-133]. XANES spectra are acquired in total electron yield (TEY) and fluorescence yield (FY) mode. TEY spectra is more surface sensitive whereas FY spectra give information from the bulk of the samples, in case of phosphorous L edge the sampling depth of TEY and FY mode is 5 nm and up to 60nm respectively [108,134]. Both TEY and FY spectra were acquired from the tribofilms formed under the IL lubrication in BO and FFO.

#### 5.3.4.1 Phosphorous Characterization (P L<sub>2,3</sub>-edge and P K-edge)

Both phosphorous L<sub>2,3</sub> and K edge XANES have been used extensively to study the structure and chemistry of phosphorous in tribofilms in the past [16,48,125,131,151]. The L<sub>2,3</sub> absorption edge is particularly suited to determine the chain length of the phosphates while the K-edge finds application in delineating the different cationic species in the polyphosphate network. Figure 28a is the P L edge TEY spectra of tribofilms derived from ZDDP, N\_DEHP and N\_DBDTP in group1 base oil and FFO. P L edge tribofilms spectra are compared with model compounds (plotted in figure 28b). Signature peaks of model compounds are designated as **a**, **a**<sup>1</sup>, **b**, **c**<sup>1</sup>, **c**<sup>2</sup>, **c**<sup>3</sup>, **c**<sup>4</sup> and **d** where peaks **a** and **c**<sup>2</sup> are characteristic peaks for P in zinc phosphate coordination and **a**<sup>1</sup> and **c**<sup>3</sup> are of iron phosphate coordination. Peak **d** is a shape resonance peak, is characteristic of all phosphates regardless of the structure. Peaks labeled as **a**, **a**<sup>1</sup> and **b** corresponds to spin

orbital splitting of phosphorous 2p electrons present in phosphates of zinc, iron and calcium whereas peaks labeled as  $c^1, c^2$  and  $c^3$  are attributed to the transition of the phosphorous 2p electrons to the  $t_2^*$  molecular orbital in tri-calcium phosphate, zinc phosphate and iron phosphate compounds respectively. From figure 28a, it can be seen that all tribofilms spectra show peak **d**, suggesting the formation of phosphate tribofilms using either ZDDP or IL's in base oil mixes. When compared with model compounds spectra, ZDDP BO tribofilms spectra show peaks matching peak **a** and  $c^2$  from zinc phosphate model compounds while N\_DEHP BO and N\_DBDTP BO derived tribofilms show peaks matching with  $a^1$  and  $c^3$  from iron phosphate model compounds. Both IL tribofilms in BO mixes show different P L-edge signature than their respective model compound spectra (i.e. N\_DEHP standard and N\_DBDTP standard), suggesting that IL's participated in tribo-chemical reaction to form antiwear films composed of iron polyphosphates. Further characterization of P L-edge using peak **a** ( $a^1$ ) to peak  $c^2$  ( $c^3$ ) ratio reveal information on the chain length of polyphosphates formed. Chain lengths of polyphosphates are characterized on the basis of peak height of **a** relative to peak **c** where the **a/c** ratio up to 0.3-0.4 represents short-chain polyphosphates and **a/c**>0.6 indicates long-chain polyphosphates [51,132,136]. Tribofilms derived from base oil formulations containing either ZDDP or N\_DEHP/ N\_DBDTP show **a/c** ratio of less than 0.4, suggesting short chain polyphosphates formation over the rubbed surfaces. However, it's worth noticing that compared to ZDDP BO (**a/c** maximum of 0.11), both N\_DEHP BO and N\_DBDTP BO tribofilms show higher **a/c** ratio (0.24 and 0.34 maximum respectively), suggesting relatively longer chain polyphosphate formation. Table 10

highlights the **a/c** ratio obtained from the P L edge spectra in TEY and FY mode for tribofilms generated from base oil formulations. It was found that **a/c** ratio for ZDDP BO tribofilms remains consistent through the depth of the tribofilms and suggest tribofilms are composed of short chain polyphosphates of Zn and Fe. The **a/c** ratio obtained for N\_DEHP BO and N\_DBDTP BO tribofilms suggests layered structure and in the case of N\_DEHP BO, **a/c** ratio of P L edge increases from surface (TEY spectra) to the bulk (FY spectra) of the tribofilms (from 0.19 to 0.24). This is due to the fact that near the interface of the substrate and tribofilms the availability of iron cation is higher hence polymerization of iron polyphosphates takes place at relatively higher rate than the surface of the tribofilms which may be iron deficient. On the other hand, **a/c** ratio of N\_DBDTP BO tribofilms decreased from surface (TEY spectra) to the bulk (FY spectra) of tribofilms (from 0.34 to 0.19), suggesting that at the interface of tribofilms and iron substrate, sulfur from N\_DBDTP structure dominates the reaction with iron cation's to form iron sulfides (will be discussed in S K edge section) thus results in shorter chain phosphate formation at the interface with the metal substrate when compared to the surface of the tribofilms. This may account for the poorer wear performance of N\_DBDTP compared to N\_DEHP.

Similarly, P L-edge spectra of tribofilms derived from ZDDP, N\_DEHP and N\_DBDTP in fully formulated oils ( no zinc) are plotted in figure 28a (bottom) and are compared with model compounds in figure 28b. Here, peak **d** is a characteristic peak of phosphate coordination. Peak **a<sup>1</sup>**, **b**, **c<sup>1</sup>** and **c<sup>4</sup>** are typical of  $\beta$ -tri calcium phosphate. All tribofilms spectra show peak energy matching with  $\beta$ -tri calcium phosphate independent

of antiwear chemistry. It's also worth noticing that IL's tribofilms spectra in case of FFO does not match with IL standard spectra suggesting a tribo-chemical reaction of ionic liquids under the rubbing action resulting in new chemical species formation.

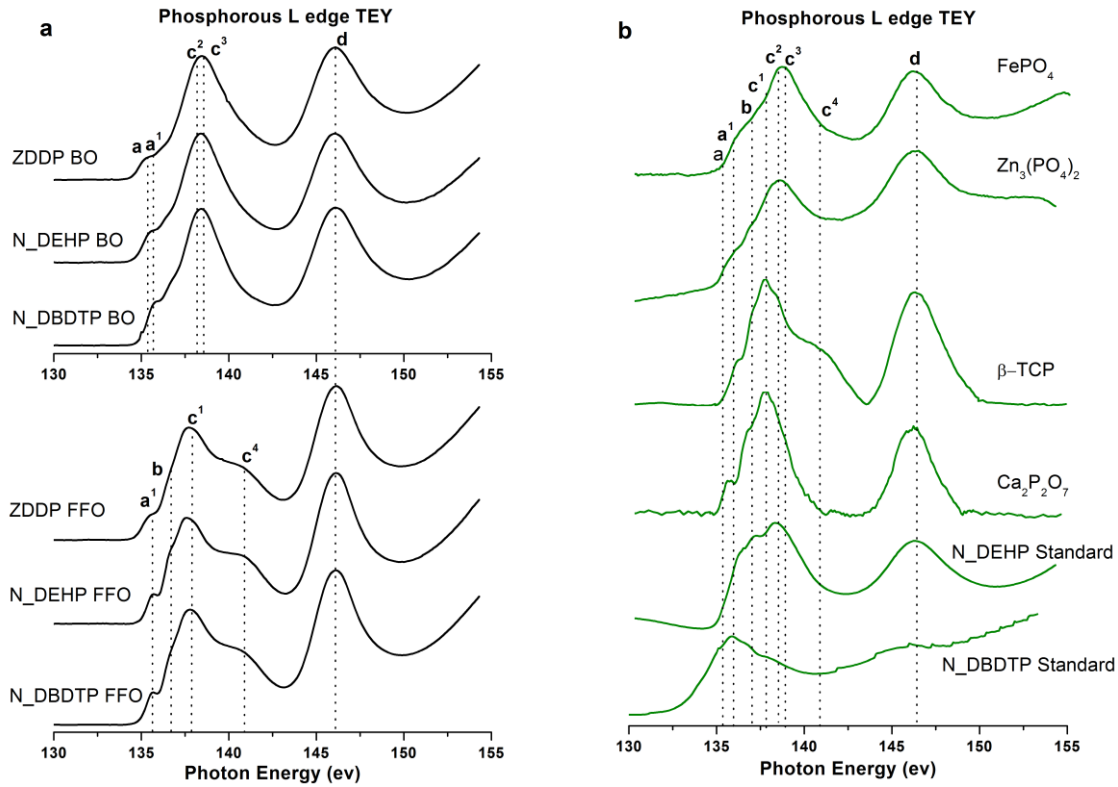


Fig. 28. (a) Phosphorous L<sub>2,3</sub>-edge XANES TEY spectra of the tribofilms generated using N\_DEHP, N\_DBDTP and ZDDP in base oil and fully formulated oils. (b) Phosphorous L<sub>2,3</sub>-edge XANES TEY spectra of model compounds.

Table10: a/c ratio of P L<sub>2,3</sub> edge for the tribofilms derived from ZDDP, IL-P and IL-TP  
in TEY and FY mode

Oil formulation	a/c (P L-edge TEY)	a/c (P L-edge FY)
ZDDP BO	0.1	0.09
IL-P BO	0.19	0.24
IL-TP BO	0.34	0.2

Phosphorous K edge spectra of tribofilms derived from BO and FFO formulations are shown in Figure 29a (top and bottom respectively). P K edge TEY spectra provide cumulative chemical information in the tribofilms from 50-75 nm. P K-edge spectra from the tribofilms are compared with respective model compounds (plotted in figure 29b). In figure 29b, peak positions are labelled in the graph as **a<sup>1</sup>**, **a<sup>2</sup>** and **a<sup>3</sup>** which correspond to the transition of the core phosphorous 1s electron to unoccupied p-like valence state [16] for  $\beta$ -tri calcium phosphate, zinc phosphate and iron phosphate respectively. Two main difference between the model compounds, zinc phosphate and iron phosphate are first, main peak position for iron phosphate, **a<sup>3</sup>** (2153.2 eV), has slightly higher energy than the main peak position, **a<sup>2</sup>** (2152.2 eV), for zinc phosphate and second, P K-edge spectra for iron phosphate shows a small pre-edge. P K edge spectra of ZDDP BO tribofilms show main peak between peaks **a<sup>2</sup>** and **a<sup>3</sup>** suggesting that in the bulk of ZDDP BO tribofilms, phosphorous is present as a mixture of iron phosphate and zinc phosphate. A slight pre-edge is also evident in ZDDP BO P K edge TEY spectra which further confirm the presence of iron phosphate in the bulk of ZDDP

BO tribofilms. This can be explained as follows, in the tribofilm close to the Fe substrate easy availability of iron cation resulting in formation of iron phosphates. In an earlier study of tribofilms using XANES, Kim et al. [16] also showed that ZDDP tribofilms are composed of a mixture of iron phosphate and zinc phosphate in the bulk of the tribofilms whereas zinc phosphate dominates the surfaces. P K edge TEY spectra of N\_DEHP BO and N\_DBDTP BO tribofilms show the presence of peak  $\mathbf{a}^3$  that is associated with the formation of iron phosphates. Signal strength of P K edge spectra for N\_DEHP BO tribofilms is relatively weak suggesting that the film thickness in this case is smaller than the tribofilms derived from ZDDP BO and N\_DBDTP BO. The broadening of the N\_DEHP P K-edge TEY spectra after the primary edge shows the influence of metallic iron from the bulk of the substrate.

In case of FFO formulation, P K edge TEY spectra of the tribofilms are plotted in figure 29a (bottom). From figure 29a (bottom) it is again evident that the role of other additives from FFO formulations such as over-based detergent play a dominant role in the formation of tribofilms as P K edge TEY of tribofilms show a main edge at  $\mathbf{a}^1$  and post-edge shoulder at  $\mathbf{b}$  that matches with  $\beta$ -tri calcium phosphate P K edge spectra in all cases irrespective of antiwear additive chemistry. It is also worth noticing that P K edge TEY spectra of both N\_DEHP and N\_DBDTP standard (figure 29b) show a main edge at slightly lower absorption energy than their respective tribofilms spectra in BO and FFO confirming that IL's in BO and FFO (no zinc) formulations undergo a tribo-chemical reaction to form phosphate tribofilms on the rubbed surfaces.



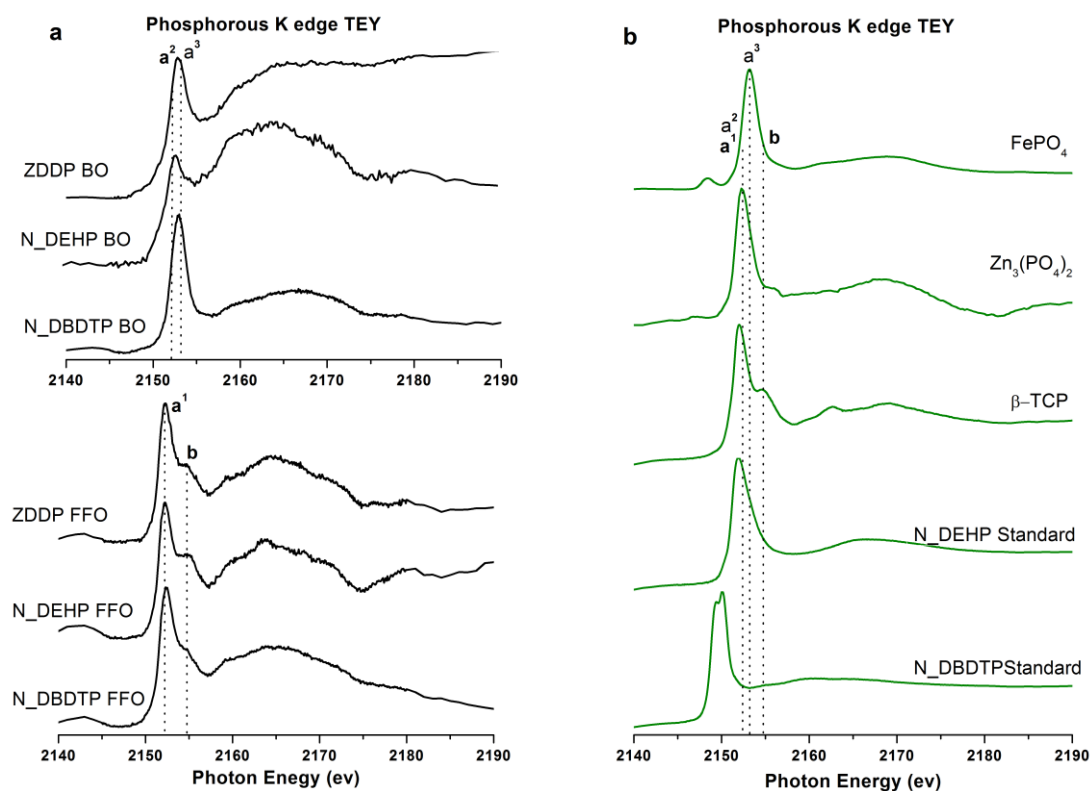


Fig. 29. (a) Phosphorous K-edge XANES TEY spectra of the tribofilms generated using N\_DEHP, N\_DBDTP and ZDDP in base oil and fully formulated oils. (b)

Phosphorous K-edge XANES TEY spectra of model compounds.

#### 5.3.4.2 Sulfur Characterization (S K-edge)

Sulfur K-edge XANES has been used extensively in the past to study the valence state and local coordination of sulfur in the tribofilm [16,48,125,131,151,152]. Sulfur can exist in different valence states ranging from -2 to +6 with -2 being the reduced states and the +6 being the oxidized states. The absorption edge of the different valence states can be easily distinguished by XANES spectra. Sulfur K edge spectra of tribofilms generated in BO and FFO formulations are plotted in TEY mode, as shown in figure 30a. In

addition, the S K edge spectra from the model compounds indicate that the S K-edge is ideally suited to distinguish between the different sulfides of Fe and Zn and between sulfides and sulfates. Figure 30b is a plot of S K edge spectra of model compounds, here primary peaks of each model compounds are labeled as **a**, **b**, **c**, **d**, **e**. Where peaks **a** and **c** corresponds to iron sulfide, peaks **b** and **e** corresponds to zinc sulfide and peak **d** corresponds to sulfates and is characteristic of sulfate regardless of the cation. Peak **e** also distinguishes calcium sulfate from zinc sulfate and iron sulfates. From figure 30a, S K edge of ZDDP BO show multiple peaks suggesting that sulfur is present in different species. Presence of peaks **a** and **c** indicate the presence of iron sulfide as well peak **b** suggests the formation of zinc sulfide. Peak **d** corresponds to sulfate formations which would most likely be zinc sulfate and to some extent iron sulfate. On the other hand, S K edge spectra of N\_DEHP BO and N\_DBDTP BO indicate that sulfur is primarily present in the form of sulfates rather than sulfides of Fe. Since N\_DEHP itself does not have any sulfur in the original structure, the presence of sulfur peaks in S K edge of N\_DEHP BO can be related to the sulfur coming from group1 mineral base oil. Since S K edge spectra are plotted after normalizing each spectra to 0 to 1, the peak intensity of S K edge of N\_DEHP looks similar to ZDDP BO and N\_DBDTP BO spectra, however, the low concentration of sulfur in N\_DEHP BO tribofilms can be seen as signal to noise ratio is high in comparison with S K edge spectra of ZDDP BO and N\_DBDTP BO. In the case of S K edge spectra of tribofilms derived from FFO mixes (no zinc), peaks **d** and **e** is commonly present in all cases suggesting that sulfur is primarily present in the form of calcium sulfates however presence of iron sulfate and zinc sulfate cannot be ruled out

completely. Interestingly, S K-edge spectra of ZDDP FFO also show peaks **b** and **c** indicating the presence of zinc sulfide and iron sulfide respectively. On the other hand, S K-edge of N\_DEHP and N\_DBDTP in FFO show peak **c** in addition to peaks **d** and **e**, indicating the sulfur is also present in the form of iron sulfides.

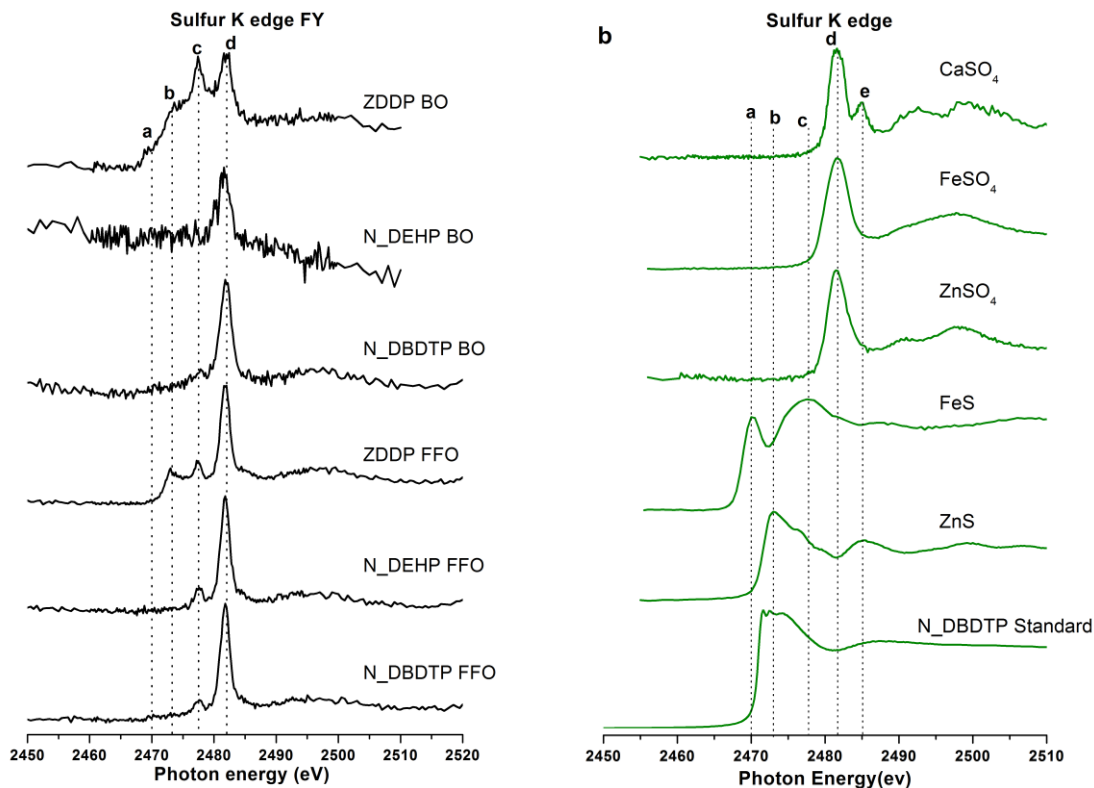


Figure 30. Sulfur K-edge XANES TEY spectra of the tribofilms generated using N\_DEHP, N\_DBDTP and ZDDP in base oil and fully formulated oils. (b) Sulfur K-edge XANES TEY spectra of model compounds.

#### 5.3.4.3 Oxygen Characterization (O K-edge)

Oxygen K edge TEY spectra of tribofilms generated using ZDDP and IL's in BO and FFO are plotted in figure 31a and are compared with model compounds in figure

31b. Figure 31b illustrates the distinctive feature of O K edge spectra for each model compounds. Oxygen can only exist in one valence state, however its absorption edge show distinctive features depending upon the cation such as iron, zinc or calcium it either directly bound with or its presence in different anions such as sulfate and phosphates that can subsequently be bound with cation's such as iron, zinc and calcium. However, in a tribofilm O is coupled with to different cation's making it difficult to uniquely identify the local environment for oxygen. However, some distinctive differences can be ascertained by examination of the O K edge spectra. O K-edge spectra were recorded in both TEY and FY mode for the tribofilms, TEY and FY spectra being very similar, only the TEY spectra are shown for reference while the discussion pertains to both TEY and FY spectra. In case of BO formulations, O K edge TEY spectra of the tribofilms generated using ZDDP, N\_DEHP and N\_DBDTP show similar features where two peaks are identified and labeled as **a** and **d**. Peak **a** is a distinctive peak for oxygen species associated with iron such as iron phosphate, iron sulfate and iron oxide. However, the possibility of formation of iron oxide can be eliminated as O K edge spectra of tribofilms in BO formulation does not show main absorption edge of iron oxide (peak **f**). Thus, we can conclude that N\_DEHP BO and N\_DBDTP BO tribofilms are primarily composed of iron phosphate as well iron sulfate to some extend in case of N\_DBDTP BO. A pre-edge peak **b** present in ZDDP BO tribofilms might suggest some oxidation of zinc, resulting in the formation of zinc oxide. Other than that, O K edge TEY of ZDDP BO is quite complicated and hard to distinguish as the earlier companion P and S showed more or

less the presence of all the  $\text{ZnSO}_4$ ,  $\text{Zn}_3(\text{PO}_4)_2$ ,  $\text{FeSO}_4$  and  $\text{FePO}_4$  model compounds in the tribofilms.

On the other hand, O K edge spectra of tribofilms derived from FFO formulations are very different than the tribofilms formed in BO formulation with similar antiwear chemistries. Here, both ZDDP FFO and N\_DEHP FFO show similar peaks that are identified using peak fitting and matched with model compounds. Peak matching suggests oxygen is primarily present in the form of  $\beta$ -tri calcium phosphate, however, formation of other phosphates and sulfates cannot be eliminated completely. N\_DBBDTP FFO O K edge TEY spectra on the other hand show the presence of iron oxide as peak **f** can be clearly identified. O K edge TEY spectra of the tribofilms clearly suggest different tribo-chemical reaction in BO and FFO formulation while using the same antiwear chemistries. Calcium from over-based detergent participates in the tribo-chemical reaction to form calcium species over the rubbed surfaces. On the other hand in the case of BO formulations, XANES spectra suggest the interaction of antiwear chemistries with the rubbing surface and film formation due to the reaction of antiwear additives with iron substrate.

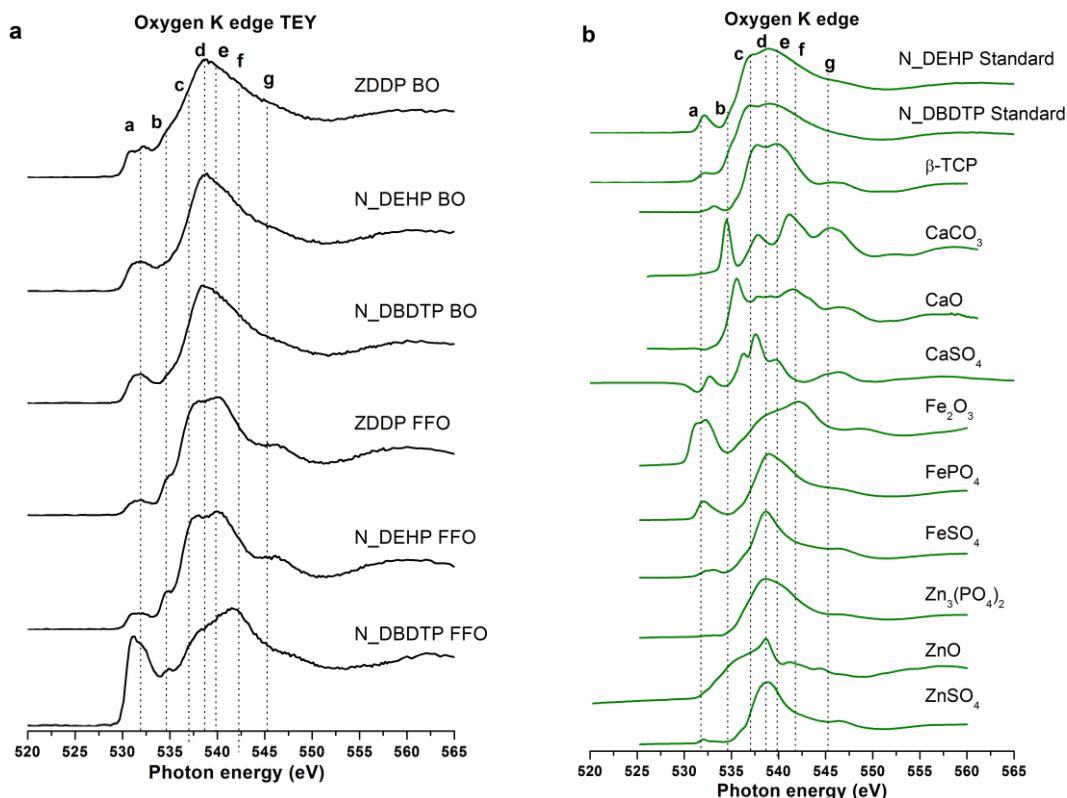


Figure 31: (a) Oxygen K-edge XANES TEY spectra of the tribofilms generated using N\_DEHP, N\_DBDTP and ZDDP in base oil and fully formulated oils. (b) Oxygen K-edge XANES TEY spectra of model compounds.

### 5.3.5 Discussion of XANES and Development of Phenomenological Model of Tribofilms

In depth characterization of IL & ZDDP lubricated rubbed surfaces using XANES at different edges for the critical elements such as P, S and O provides a comprehensive understanding of the chemical nature of the tribofilms. A possible phenomenological model of tribofilms thus can be drawn for all six formulations as shown in Figure 32. Based on the information obtained from P L edge and P K edge, it can be deduced that both N\_DEHP BO and N\_DBDTP BO tribofilms consist of a layered structure of

phosphate films as a change in **a/c** ratio (representative of phosphate chain length) has been observed from the surface to the bulk of the tribofilms. On contrary, ZDDP tribofilms in this study showed more or less similar chain length of phosphate films through the depth of ZDDP tribofilms and they are significantly shorter in length compared to ones formed when IL are used. Earlier studies have shown that longer chain polyphosphates yield better tribological properties and are generally considered to be more beneficial [150,153-155] Since N\_DEHP does not have sulfur in the original structure, the presence of sulfate peak in S K edge TEY of N\_DEHP base oil tribofilms might be considered to be influenced by the sulfur coming from the mineral base oil used in this study (Group 1 base oils typically have more than 300 ppm of sulfur in them and there are some unsaturated hydrocarbons that are prone to easy breakdown under tribological conditions releasing the sulfur for reaction with the tribofilm). On the other hand, N\_DBDTP has dithiophosphate anion in its chemical make-up also does not show a clear peak at **b** confirming a contribution of sulfur coming from N\_DBDTP to the tribochemical reaction in the form films of iron sulfates near the surface of the tribofilm. On the other hand in the case of ZDDP BO tribofilms, S K edge TEY spectra clearly indicate the formation of both zinc sulfides as well as iron sulfide (peaks **a**, **b** & **c**). O K edge spectra further compliments the finding of P L edge, P K edge and S K edge results and confirm that the tribofilms are primarily consist of phosphate and sulfate species and eliminates the possibility of formation of oxides species in the tribofilms when only base oil is used. It can be postulated that in the case of N\_DEHP and N\_DBDTP the formation of polyphosphates of Fe dominate the tribofilm formation while in the case of ZDDP a

mixture of polyphosphates of Zn/Fe and sulfates and sulfides of Zn/Fe form in the tribofilm. The presence of sulfides of Fe and Zn have been shown when ZDDP is used in the past in several studies [1,16,48,119] however, in this study we illustrate the formation of primarily phosphates of Fe when both P containing and P and S containing IL's are used in base oil chemistry.

When fully formulated oils are used, in addition to antiwear additives a number of other additives are present that include detergents, dispersants, antioxidants etc. Of these the detergents are one of the most active chemical species and are made up of over-based calcium sulfonates. The P L edge and P K edge spectra of N\_DEHP FFO, N\_DBDTP FFO and ZDDP FFO tribofilms primarily indicate that phosphorous is primarily present in the form of  $\beta$ -tri calcium phosphate however a possibility of iron phosphate in the case of IL's FFO and zinc phosphate and iron phosphate in the case of ZDDP FFO tribofilms cannot be completely eliminated. The formation of phosphates of calcium in tribofilms has been shown in the past when calcium based detergent have been used in the oil [25,137]. S K edge TEY spectra of tribofilms derived from FFO formulation indicates the sulfur is primarily present in the form of sulfates mainly calcium sulfate as post edge shoulder peak **e** is present in all tribofilms spectra that matches with the post edge shoulder peak in calcium sulfate model compound S K edge spectra. In addition, both N\_DEHP FFO and N\_DBDTP FFO show presence of iron sulfide as peak **a** and peak **c** are evident in their respective S K edge TEY spectra. In the case of ZDDP FFO tribofilms, in addition to the sulfates (peak **d** and peak **e**) formation of zinc sulfides (peak **b**) and iron sulfides (peaks **a** and peak **c**) is also well evident. O K edge spectra of



tribofilms from FFO mixes suggest the phosphate anion containing oxygen is primarily associated with calcium cation. In addition, peak **b** in the O K-edge is associated with the  $\text{CaCO}_3$  that is present in all the fully formulated oils and is likely to be coming from the detergent chemistry that is incorporated into the tribofilm. A small amount of  $\text{Fe}_2\text{O}_3$  in the tribofilm cannot be ruled out. However, it must be noted that the primary chemical make-up of the tribofilms in fully formulated oil are the phosphates of Ca ( $\beta$ -TCP) and to some extent the formation of sulfides and sulfates of Fe in N\_DEHP and N\_DBDTP and those of Fe and Zn when ZDDP is used.

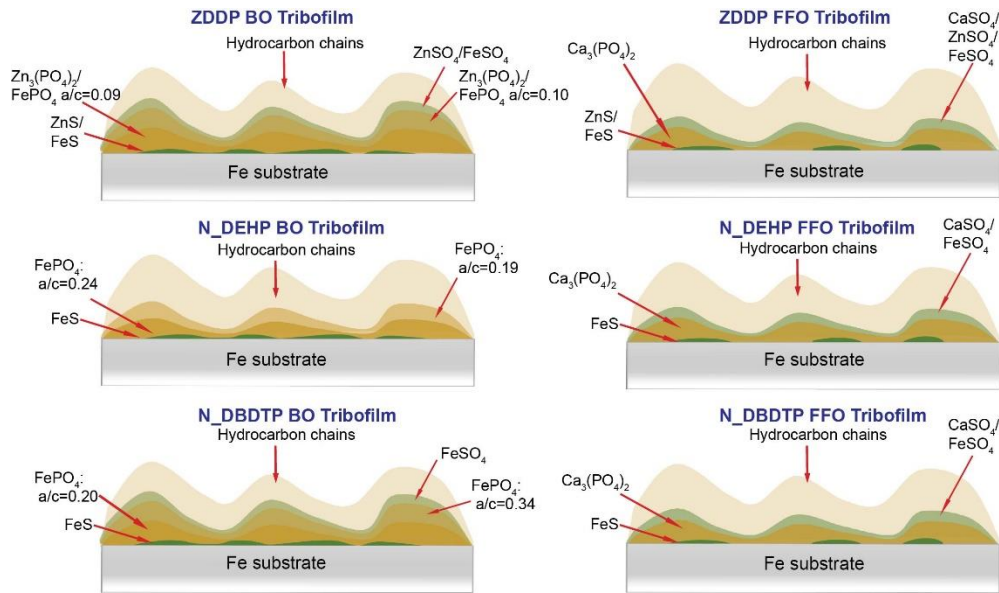


Figure 32: Phenomenological model of the tribofilms generated using N\_DEHP, N\_DBDTP and ZDDP in base oil and fully formulated oils.

#### 5.4 Conclusion

The tribofilms formed using phosphorous and sulfur containing IL's are very similar to those formed when ZDDP antiwear additives are used. Zn polyphosphates

formed when ZDDP is used are replaced with iron polyphosphates when IL's are used indicating that the underlying substrate reacts with the degradation products of the ionic liquids to form protective tribofilms in base oils. Pad like tribofilms are formed on the wear surface in fully formulated oils where as in the case of base oil chemistries the tribofilms are more continuous in nature both in the case of ZDDP and IL's. When fully formulated oils are used, the detergent chemistry plays an important role in reacting with the degradation products of the antiwear additives and forming tribofilms that are constituted of phosphates of calcium. When comparing phosphorous (N\_DEHP) and phosphorous and sulfur (N\_DBDTP) containing ionic liquids, the sulfur in these ionic liquids is actually detrimental to the wear and friction performance. It is also evident from this study that soluble IL's offer the possibility of equivalent wear performance to ZDDP when examined under bench top tribological examination. This study provides a framework to understand the mechanism of wear protection when ionic liquids are used in the place of ZDDP. However, before they find application in engine oil, further more rigorous compatibility studies and stability studies have to be conducted.

## Chapter 6. Advancing the tribological properties of Ionic Liquids with Synergistic Interaction of Borate Esters

### 6.1 Introduction

In this chapter, a synergistic interaction of phosphonium IL's with borate esters (SB) has been studied in base oil blends. Phosphonium IL's were mixed with borate ester at 0.1 wt. % phosphorous and 0.02 wt. % boron in group1 mineral base oil. A cylinder on reciprocating flat and ball on rotating disc tribometer were employed to evaluate the friction and wear performance in pure sliding contacts. Tribological performance of these novel ashless additive blends were compared with ZDDP in base oil. An electric contact resistance setup was used to study the incubation time and progression of tribofilm formation. Topography of the lubricated surfaces were analyzed by obtaining 3D images of the wear track using scanning probe microscope (SPM) and local coordination of phosphorous and boron on and in the bulk of the tribofilms were characterized using X-ray absorption near edge structure (XANES) spectroscopy. Synergistic interaction of IL with SB showed significant reduction in wear compared to ZDDP and IL and SB alone.

### 6.2 Experimental Details

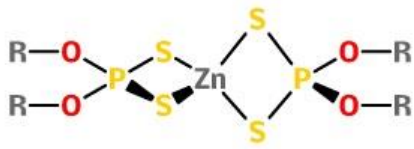
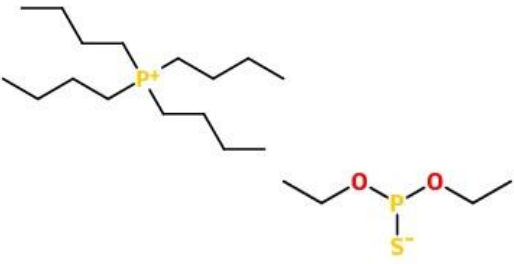
#### *6.2.1 Description of additive chemistry and Thermogravimetric analysis.*

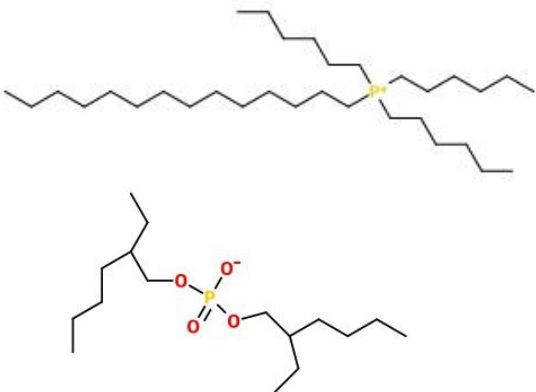
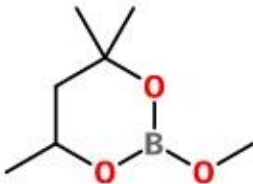
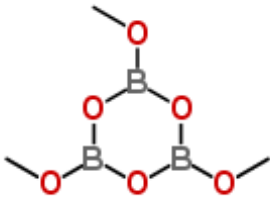
Table 11 details the chemistry of the additives used. ZDDP purchased from a commercial vendor, is a secondary alcohol derived ZDDP with approximately 70% neutral and 30% basic characteristics, details of which are available in Parekh et. al. [47]. Phosphonium ionic liquids, Tetrabutylphosphonium O,O-diethyl-phosphoro-dithionate (P\_DEPDT) and Trihexyltetradecylphosphonium bis(2-ethylhexyl) phosphate (P\_DEHP)

and borate ester 2-Methoxy-4,4,6-trimethyl-1,3,2-dioxaborinane (SB1) were provided from AC2T research GmbH Austria. Trimethoxyboroxine (SB2) was provided from Argonne National Laboratory. Base oil blends were prepared in a group 1 base oil (mixture of 60 wt.% solvent neutral 150W and 40 wt.% bright stock 90W) purchased from a commercial vendor.

Thermogravimetric analysis (TGA) of ZDDP and ionic liquids was performed using Shimadzu TGA-51 Thermogravimetric analyzer. TGA was performed in nitrogen (N<sub>2</sub>) atmosphere at a heating rate of 10 °C/min from room temperature to 600 °C with a N<sub>2</sub> flow rate of 20 mL/min. Each test was repeated twice for the consistency of the data.

Table 11. Description of additive chemistry.

Coded Name	Chemical Name	Chemical Structure
<b>ZDDP</b>	Zinc dialkyl-dithiophosphate	 <p>R = 1°, 2°, 3° alkyl or aryl group</p>
<b>P_DEPDT</b>	Tetrabutylphosphonium O,O-diethyl-phosphoro-dithionate	

<p><b>P_DEHP</b></p>	<p>Trihexyltetradecylphosphonium bis(2-ethylhexyl)phosphate</p>	
<p><b>SB 1</b></p>	<p>2-Methoxy-4,4,6-trimethyl- 1,3,2-dioxaborinane</p>	
<p><b>SB 2</b></p>	<p>Trimethoxyboroxine</p>	

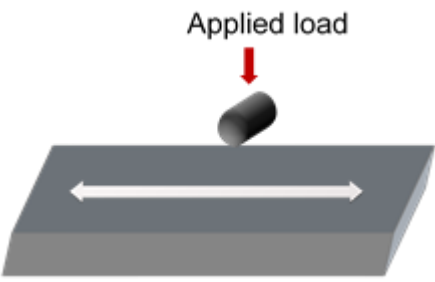
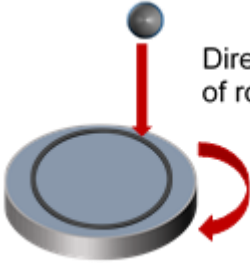
### 6.2.2 Tribological Test Details

Oil samples were formulated by blending ZDDP, IL's and borate ester individually or as mixtures of IL and SB in base oil. All blends were prepared by keeping the phosphorous (P) and boron (B) concentration at 1000 ppm and 200 ppm respectively

as applicable. Tribological test were conducted at Argonne National Laboratory, Energy Systems Division. The first group of tribological experiments employed a cylinder on reciprocating flat contact testing machine [56] (test setup 1) to determine the performance characteristics of the additives. The best performing blends were further examined using a ball on rotating disc contact test configuration using a Nanovea tribometer (test setup 2). Table 12 provides schematic of the test configurations and highlights the test parameters. Test setup 1 was also equipped with electric contact resistance (ECR) measurement setup. ECR data was collected in-situ during the test in order to gain insight into the incubation time for film formation at the tribological contacts. Test specimens were cleaned before each test using Stoddard solution followed by isopropanol and acetone to completely remove any oil and dust present on the surfaces. The rubbed surfaces after the tests were cleaned with heptane and isopropanol and then saved by submerging them in sulfur free base oil.

Table 12. Schematic of the test configurations and detail of test parameters for test setup

1 and test setup 2.

Tribological test	Cylinder on reciprocating flat contact	Ball on rotating disc contact
		
Base oil	Group I mineral oil (60 wt.% SN 150W + 40 wt.% BS 90W)	Group I mineral oil (60 wt.% SN 150W + 40 wt.% BS 90W)
Viscosity	10.068 mm <sup>2</sup> /sec at 100 °C	10.068 mm <sup>2</sup> /sec at 100 °C
Treat rate	Phosphorous: 1000ppm and Boron: 200 ppm	Phosphorous: 1000ppm and Boron: 200 ppm
Applied load	82 N	2 N
Initial Hertzian contact pressure	500 MPa	510 MPa
Temperature	100 °C	100 °C
Speed	0.06 m/sec, 5 Hz	0.06 m/sec
Stroke length	6 mm	
Cylinder/Ball	Φ 4 mm x 6 mm, 52100 steel (60-61 HRc)	Φ 12.7 mm, 52100 alloy steel (58-60 HRc)
Flat/Disc	12 mm x 12 mm x 8 mm, 52100 alloy steel (60-61 HRc)	Φ 20 mm, 52100 alloy steel (60-61 HRc)
Duration	1 hour	1 hour

### 6.2.3 Characterization of Tribofilms

Wear scar width generated on cylinder (from test setup 1) and wear scar diameter (WSD) generated on ball (from test setup 2) after rubbing were measured using optical

images obtained from an Olympus brand metallographic microscope. Wear width was measured at nine locations on each cylinder (from test setup 1) and each oil samples was tested twice. Thus, wear width for each oil sample is an average of 18 measurements. WSD on the ball ((from test setup 2) is an average of two measurements from two repeated tests for each oil sample. The surface topography of the wear track and wear mechanism was examined by obtaining 3-dimensional (3D) images of the rubbed surfaces using Hysitron Triboscope<sup>TM</sup> in scanning probe microscopy (SPM) imaging mode.

Chemical nature of the tribofilms formed in-situ during tribological tests was characterized using XANES spectroscopy. XANES spectra were obtained at The Canadian Light Source synchrotron facility at Saskatoon Canada. The phosphorous L-edge (P L-edge) and Boron K edge (B K-edge) spectra were collected at VLS-PGM (variable line spacing plane grating monochromator) beam station that operates at the energy range of 5.5 eV-250 eV with a photon resolution of more than 10,000 E/ $\Delta$ E. All the spectra were collected using a 100  $\mu$ m X 100  $\mu$ m photon beam spot size.

## 6.3 Results and Discussion

### 6.3.1 Coefficient of Friction and Wear Volume

Figure 33 is the coefficient of friction (CoF) and wear volume obtained from test setup 1 for all the blends. CoF curve acquired from each oil blend is plotted in figure 33(a) and the average coefficient of friction for the last 15 minutes of the test is shown in the bar chart embedded in figure 33(a). Friction curve for group 1 BO without additives (labeled as **A**) exhibits large variance and high CoF value for the duration of the test in



comparison with oil blends containing ZDDP (**B**), ILs and binary mixtures of IL+SB. Oil blends containing only SB1 (**C**) and SB2 (**D**) show similar frictional characteristic as of group 1 BO consisting large variance and spikes in the friction curve with high CoF value. This result indicates that boron concentration (i.e. 200 ppm) was too small for any improvement in friction characteristic when using only boron based additives in base oil (i.e. SB1 and SB2). However, the 200 ppm B concentration was chosen to meet the current industrial standard of boron in engine oils [156]. Comparing the oil with ZDDP alone with blends containing ILs and binary mixture of IL+SB, ZDDP exhibits a stable friction curve with consistent CoF value while P\_DEHP (**H**) and P\_DEHP+SB2 (**J**) exhibit higher CoF at the beginning of the test and the CoF decreases as the test progresses and the test ends with a CoF smaller than that of ZDDP. In the case of P\_DEHP+SB1 (**I**), large fluctuations were observed at the beginning and higher CoF value than P\_DEHP and P\_DEHP+SB2. On the other hand, oils with P\_DEPDT (**E**) exhibit a significantly lower CoF for the first 500 seconds of the test and then friction increases and remains consistent for the remainder of the test. Similar behavior was seen for P\_DEPDT+SB1 (**F**) and P\_DEPDT+SB2 (**G**), where CoF is lower in the initial stage of the test and then friction increases and reaches a plateau, however, the duration of the lower friction was reduced from 500 seconds for P\_DEPDT to 100 seconds with P\_DEPDT+SB2 and almost negligible for P-DEPDT+SB1. These results indicate that addition of borate esters to phosphonium ILs (P\_DEHP and P\_DEPDT) does not result in significant improvement in their stable friction behavior at the end of test but plays a significant role in determining the frictional performance at the early stages of the test.

The lowest average CoF at the end of the test was achieved with a binary mixture of P\_DEHP+SB2 as shown in the bar chart in Figure 33(a).

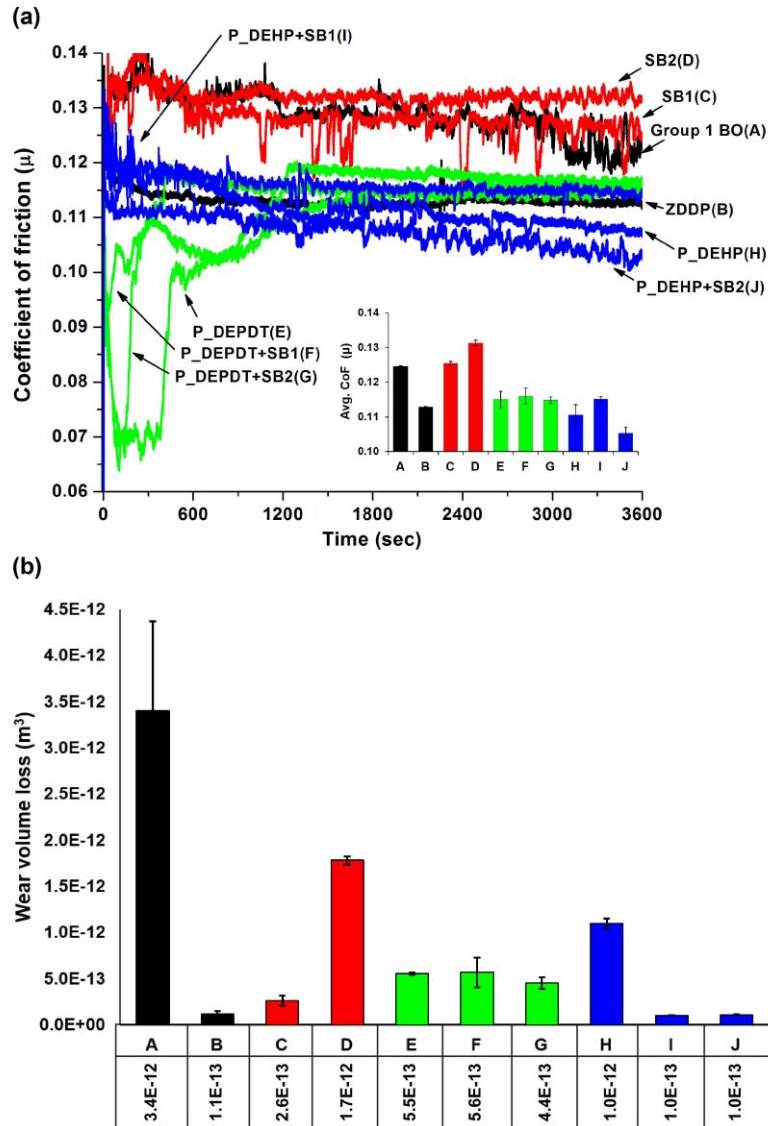


Figure 33. Coefficient of friction and wear volume obtained from test setup 1 for group1 BO, ZDDP, IL, SB and IL+SB in group 1 BO at 0.1 wt.% P and 0.02 wt.% B.

Wear volume calculated from the cylinders (from test setup 1) are plotted in Figure 33(b). Group 1 BO (**A**) shows the largest wear on the cylinder while the addition of additive chemistry results in significant reduction in wear. Comparing the wear volume of ZDDP (**B**) with ashless blends containing only IL's, SB and IL+SB, both SB1 (**C**) and SB2 (**D**) as well as P\_DEHP (**H**) and P\_DEPDT (**E**) show higher wear volume. Moreover, oil blends containing P\_DEPDT+SB1 (**F**) and P\_DEPDT+SB2 (**G**) show poorer wear protection than ZDDP. On the other hand, P\_DEHP+SB1 (**I**) and P\_DEHP+SB2 (**J**) show comparable or better antiwear performance than ZDDP at equal phosphorous levels (i.e. 1000 ppm). The error bar on the bar chart denotes the consistency of the test results.

Figure 34 illustrates the coefficient of friction and WSD obtained from test setup 2 for the selected additive chemistries that exhibited better antiwear results from test setup 1. An average CoF for the different oil blends obtained are plotted in Figure 34(a). None of the blends exhibited a significant improvement in friction compared to ZDDP with the lowest friction recorded for the oil with P\_DEHP+SB1. The WSD measured for the different blends are plotted in Figure 34(b) and their respective optical images of wear scar on ball are also presented. Error bar on the friction and WSD bar diagram denotes the consistency and reproducibility of the data. Tribological tests from Group 1 BO results in the highest WSD. Addition of antiwear additives to the base oil significantly improves the wear protection. Moreover, in comparison to ZDDP additive, both P\_DEHP and binary mixture of P\_DEHP+SB1 exhibited smaller WSD. The new ashless additive

chemistry of P\_DEHP and P\_DEHP+SB1 showed remarkable improvement in wear protection by 18.7% and 35.6% respectively compared to ZDDP at 0.1 wt. % P treat rate.

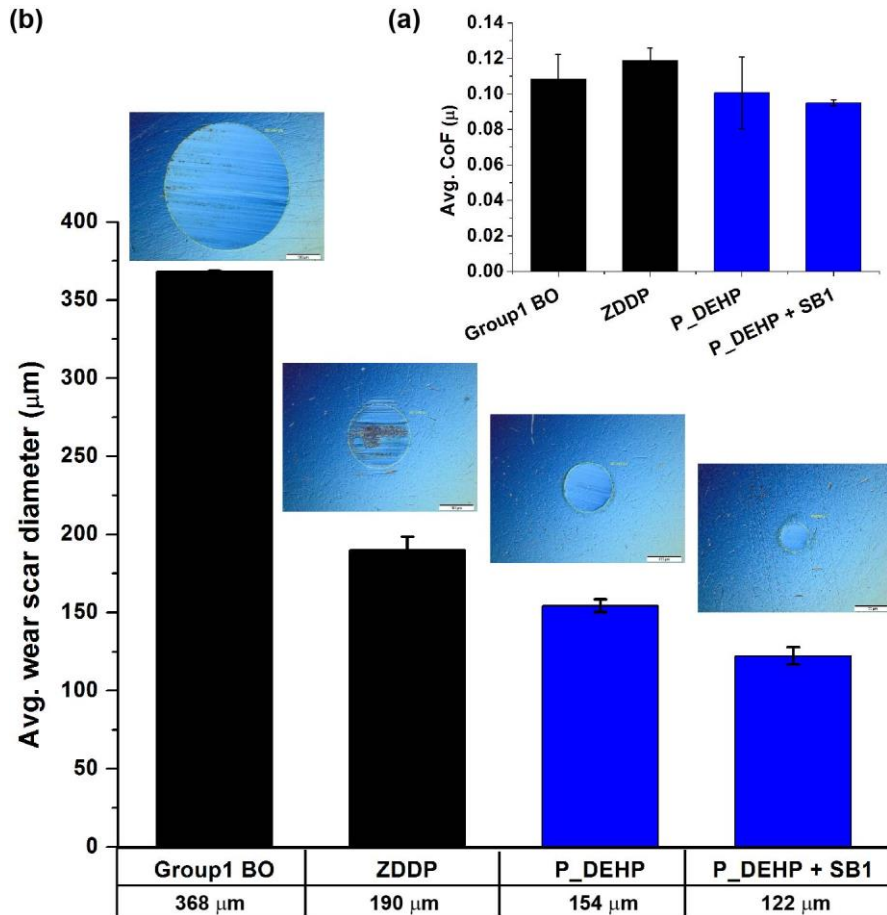


Figure 34. Coefficient of friction and wear scar diameter obtained from test setup 2 for group1 BO, ZDDP, P\_DEHP and P\_DEHP+SB1 in group 1 BO at 0.1 wt% P and 0.02 wt% B.

### *6.3.2 Incubation time for the tribofilm formation in correlation with thermogravimetric analysis (TGA) of additive chemistry*

The glassy phosphate films formed on the tribological surfaces are known to have very low electric conductivity [56]. Hence, an ECR measurement can be used as a way of determining the effectiveness of tribofilm formation by applying an electric circuit between counter surfaces. As the protective tribofilm starts to form, the resistance increases and voltage drop builds up between the counter surfaces. Figure 35 summarizes the ECR data (i.e. voltage drop) collected from test setup 1 for the selected additive chemistries and a TGA plot acquired for ZDDP and ILs (P\_DEHP and P\_DEPDT). TGA graph is positioned on the bottom right corner in Figure 35 and remaining graphs are the ECR data plotted together with CoF (top) as a function of test duration. The voltage applied between the counter surfaces is 100 mV. The voltage drop readings at the interface are shown as black dots in ECR plot obtained from each test and values of each voltage drop reading were integrated and plotted as the red curve superimposed on the voltage drop data. The integrated values of voltage drop has been normalized to the maximum value obtained in the case of P\_DEHP+SB2 to the remaining plots to illustrate the overall effectiveness of tribofilm formation over time. Voltage drop close to 100 mV correspond to more net coverage of tribofilm while values closer to 0 mV correspond to no tribofilm coverage. In addition, the slope of the red curve indicates the effectiveness of tribofilm formation with larger slopes having progressively larger tribofilm formation. From Figure 35, the ECR plot of the test with ZDDP indicates that voltage drop reaches maximum in the very early stages of the test, indicating very short incubation time for the

tribofilms formation using ZDDP. The ECR plot exhibits low voltage drop for about 1500 seconds in the case of P\_DEHP and 600 seconds for P\_DEPDT at the start of the test, suggesting a prolonged incubation time for the tribofilm formation. On the other hand, the addition of SB to P\_DEHP reduced the incubation time significantly and the tribofilm begins to form as early as the start of the tests. ECR data indicates that the binary mixtures of P\_DEHP and SB result in a quick and stable film formation that exhibit better wear protection as seen in figure 33(b) and 34(b). These results indicate a synergistic interaction of P\_DEHP with soluble boron additives.

The friction response of each additive blend can also be correlated with the tribofilm formation. In the case of ZDDP, tribofilms form at an early stages of the test its friction response remains relatively consistent, however, the ECR data does indicate partial removal of the tribofilm periodically followed by new film formation. In the case of P\_DEPDT, a clear correlation of friction and tribofilm formation can be seen. P\_DEPDT shows poor film formation at earlier stages of the test till about 600 seconds and then voltages drop starts to gain to an intermediate level (60-70 mV) for the test duration from 600-1200 seconds and finally the voltage drops reaches maximum. In the case of P\_DEPDT there is a correlation between the frictional response and the observed ECR data indicating that the lower friction probably results with the formation of easily removable tribofilms that are not very protective of the surfaces. However, once stable tribofilms are formed after the initial incubation period, the ECR and frictional data indicate more stability. One of the striking benefits of the addition of SB additives to

DEHP can be deduced from the ECR graphs where we can see that in the presence of SB2, DEHP exhibits the best tribofilm formation

When analyzing the thermal stability of these additive chemistries along with the time scale formation of the tribofilms during the test, a correlation can be deduced between the thermal stability of the additive chemistry and their incubation time for tribofilms formation. In figure 35, TGA graph of the additives shows that ZDDP starts to decompose at a lower temperature (about 200°C) compared to both P\_DEHP (about 325°C) and P\_DEPDT (about 300°C) IL's. The ECR plots show that ZDDP results in the shortest incubation time for the tribofilms formation (about at 100 seconds) than P\_DEPDT (about 600 seconds) and P\_DEHP (about 1200 seconds). Hence it can be hypothesized that higher thermal stability of the additive chemistry results in delayed decomposition of the additives to form by-products and react with the rubbing surfaces to form protective tribofilms. This is significantly mitigated by the addition of SB into the mix where the incubation time is significantly reduced.

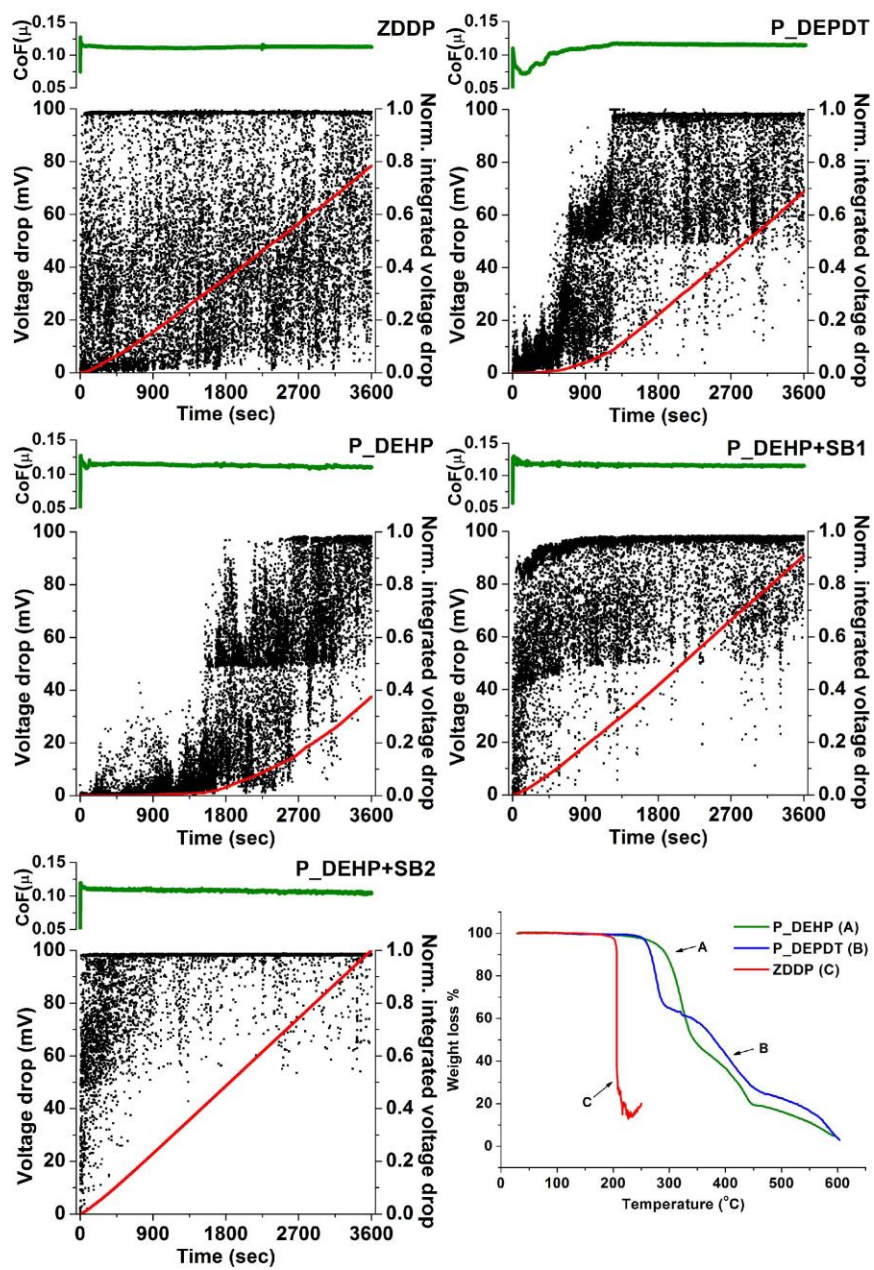


Figure 35. Thermogravimetric analysis of additives of ZDDP and IL's (P\_DEHP and P\_DEPDT) and ECR plot of oil blends from test set up 1.



### 6.3.3 Topography of the Tribofilms using

Topography of the wear track generated under ZDDP, IL and IL+SB lubrication was studied by obtaining 3D images using SPM imaging technique. Figure 36 illustrates the SPM images of the wear track for the flat samples (test setup 1). The arrow next to the images delineates the sliding direction. SPM images are produced for  $60\ \mu\text{m} \times 60\ \mu\text{m}$  area of the wear track while keeping the z-axis same i.e.  $\pm 200\ \text{nm}$ . SPM image of ZDDP lubricated wear track demonstrates island type features that are typical of ZDDP tribofilms [49,56]. These island of patchy tribofilms are unevenly distributed on the wear track. Deep scratches are also observed on the wear track, which are oriented in the sliding direction. SEM image (provided in the supplement data) covering a larger region also illustrates non-uniform patches of films along with the deep scratches on ZDDP wear track. In an earlier study Taylor et al. [46] suggested that uneven distribution of ZDDP antiwear films and the roughness oriented in the direction of rubbing results in high friction under ZDDP lubrication. Recently, Gosvami et al. [157] studied the mechanism of ZDDP antiwear film growth under single-asperity sliding contact on Fe-coated Si wafer using AFM. They reported patchy tribofilms formation is a result of heterogeneous nucleation dependent on the atomic-scale surface roughness. The surface roughness leads to varying contact stress, which essentially means the energy barrier for tribochemical reaction is lower where contact stress is higher and vice-versa. 3D image of P\_DEPDT reveals similar topography as seen for ZDDP consisting non-uniform distribution of patchy tribofilms. However, in P\_DEPDT patch size varies more significantly than that in ZDDP. Furthermore, P\_DEPDT show CoF values very close to

ZDDP for the last half hour of the test. ECR data from figure 35 indicates that P\_DEPDT films starts to form and remain intact for the later half of the test, combining these results indicates a correlation between friction and tribofilm topography as P\_DEPDT tribofilms with topographical features similar to ZDDP once formed show similar frictional behavior. The first half of the P\_DEPDT test exhibit much smaller CoF (in Figure 33(a)). Since, there was no protective film on the surface for that duration as learnt from ECR data (Figure 35), the lower CoF arises from large polishing wear (abrasive type) leading to increase in the contact area (from line contact to area contact), which consequently reduces maximum contact pressure. Wear track of P\_DEHP also consists of many island type feature along with few scratches. The features on the wear tracks are much smaller than ZDDP and P\_DEPDT and the surface looks smoother and more uniform. It can be speculated that a polishing type wear had occurred resulting in a smooth surface during the prolonged incubation time of P\_DEHP films (as evident in Figure 35). The polishing mechanism produces uniform asperities on the surface, which consequently results in a more uniform nucleation and growth of the patchy tribofilms. The wear surfaces derived from the lubrication of P\_DEHP +SB1 and P\_DEHP+SB2 exhibit a significantly different topography. The wear tracks are much smoother and no island type features are observed. The SPM images reveals few minor scratches on the surface, which are believed to be present from the sample preparation process. It is evident that with the presence of SB1 or SB2 in addition to P\_DEHP, there is minimal wear that occurs and the larger island like patchy tribofilms are not formed. Moreover, the ECR data indicates

that larger areas are covered with tribofilms and this is matched by the SPM images that indicate that the whole region of interest is covered by a uniform tribofilm.

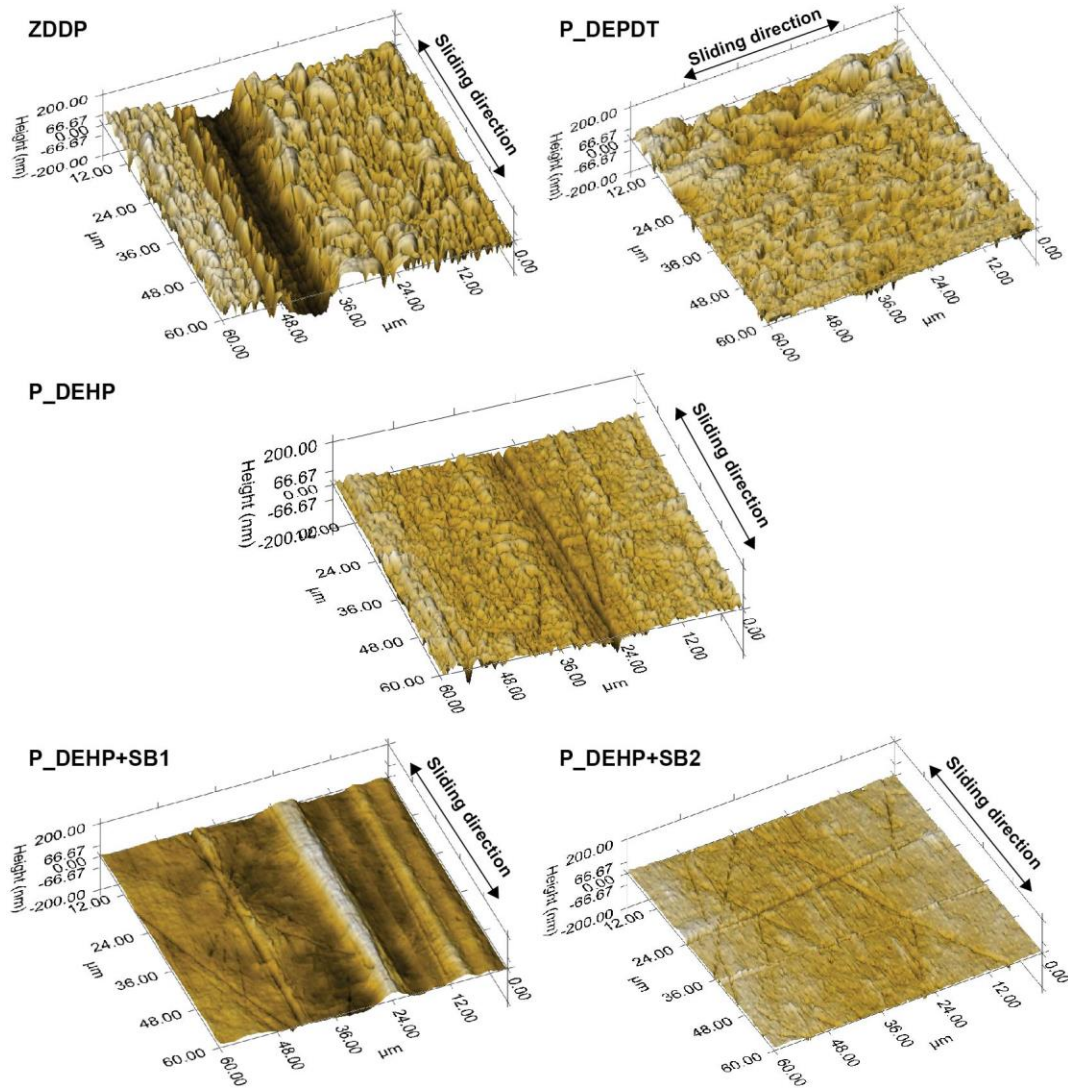


Figure 36. 3D SPM images of rubbed surfaces generated under ZDDP, P\_DEHP, P\_DEHP+SB1 and P\_DEHP+SB2 lubrication.

### 6.3.4 Chemical Properties of Tribofilms using XANES

The antiwear properties of additives are derived from their ability to form protective film on the rubbing surfaces under high contact temperature and shear forces in a tribological system. The knowledge of the type of chemical film formed and the local coordination of the elements present on the surface and in the bulk of the film is critical to advance the mechanistic understanding of surface protection with tribofilm formation. For this purpose, XANES technique has been extensively used to examine the chemical nature of the tribofilms formed using various antiwear additives [11,13,14,16,48,51,54,56,64,126,127,131-133,137,138,151]. In this study, P L-edge and B K-edge spectra are analyzed in both total electron yield (TEY) and fluorescent yield (FY) mode. TEY spectra offer more surface sensitive information whereas FY spectra give information from the bulk of the sample, in the case of Si L-edge the sampling depth of TEY and FY mode is about 5 nm and 70 nm respectively [134].

#### 6.3.4.1 Phosphorous Characterization (P L<sub>2,3</sub>-edge)

P L-edge TEY and FY spectra of tribofilms are plotted and compared with model compounds ( $Zn_3(PO_4)_2$ ,  $FePO_4$  and  $BPO_4$ ) and IL standards (P\_DEPDT std and P\_DEHP std) in figure 37(a) and 37(b). P L-edge spectra of the tribofilms were acquired from three different locations on the wear scar to examine the variance in the chemical composition on the wear track. The pre-edge shoulders and primary absorption edge from model compounds  $Zn_3(PO_4)_2$  and  $FePO_4$  are identified as **a'**, **b'**, **c'** and **a**, **b**, **c** respectively. Peaks labeled as **a'**, **a** and **b'**, **b** correspond to transition from spin-orbit split of phosphorus 2p electrons ( $2p_{3/2}$  and  $2p_{1/2}$  levels, which are usually referred to as the L<sub>3</sub>-

and L<sub>2</sub>-edges, respectively) into the first unoccupied *3s-like* antibonding state [147] in Zn<sub>3</sub>(PO<sub>4</sub>)<sub>2</sub> and FePO<sub>4</sub>. Peaks labeled as **c'** and **c** are attributed to the transition of the phosphorus *2p* electrons to the *3p-like* antibonding state [147] in Zn<sub>3</sub>(PO<sub>4</sub>)<sub>2</sub> and FePO<sub>4</sub> respectively. Peak **d** in figure 37(a) and 37(b) is commonly present in both Zn<sub>3</sub>(PO<sub>4</sub>)<sub>2</sub> and FePO<sub>4</sub> as well as in tribofilms spectra, and is a shape resonance peak owing to *2p* to *3d* transition [148]. Comparing the P L-edge TEY and FY spectra of tribofilms with model compounds based on fingerprint match analysis, peak **d** is commonly found in all tribofilms spectra as well as in model compounds and IL standards. This indicates that all the tribofilms derived from either ZDDP or IL's and IL+SB form phosphate antiwear films. ZDDP tribofilms showed main absorption edge at peak position **c'** which corresponds to the main absorption edge of Zn<sub>3</sub>(PO<sub>4</sub>)<sub>2</sub>, which suggests that ZDDP tribofilms are primarily compounds of phosphate of zinc. However, since Fe cations were also available from the substrate during the test, possibility of FePO<sub>4</sub> formation cannot be ruled out completely. Both P L-edge TEY and FY spectra of the tribofilms derived from P\_DEPDT, P\_DEHP and mixture of P\_DEHP+SB exhibit main absorption edge at peak position **c** which aligns with the main absorption edge of FePO<sub>4</sub> that strongly suggests that tribofilms in these cases are composed of phosphates of iron. In addition, both P\_DEHP+SB1 and P\_DEHP+SB2 tribofilms exhibited the main absorption edge at relatively higher energy (at peak **c**) than the main absorption edge from BPO<sub>4</sub>. This indicates no significant contribution of BPO<sub>4</sub> in the P L-edge spectra of the P\_DEHP+SB1 and P\_DEHP+SB2 tribofilms. However, in the next section using the B K-edge spectra, presence of absorption edge peak for BPO<sub>4</sub> model compound is found in

the P\_DEHP+SB1 and P\_DEHP+SB2 tribofilms. Here, it can be speculated that, since availability of iron is more redundant at the actual contact than boron, phosphate chemistry is dominated by FePO<sub>4</sub> formation than BPO<sub>4</sub>. All tribofilms exhibited similar peak intensity for spectra collected at multiple locations on each wear scar except ZDDP tribofilms. In the case of P L-edge FY spectra of ZDDP tribofilms, one spectra exhibited significantly higher counts than the other two, indicating a chemical variance in the film.

P L-edge spectra can be further characterized to determine the chain length of polyphosphates formed on the wear track. The degree of polymerization of the phosphate films is determined by analyzing the peak intensity ratio of pre-edge peak **a** or **a'** to main absorption edge **c** or **c'**, which is called as *a/c* ratio. The *a/c* ratio below 0.3 represents short-chain polyphosphates and *a/c* above 0.6 represents long-chain polyphosphate [51,132,136]. The *a/c* ratio of P L-edge TEY and FY spectra of tribofilms were calculated and shown in figure 37(a) and 37(b). The *a/c* ratio of TEY and FY spectra for all the tribofilms is less than 0.3, which suggest that the surface of the all the tribofilms are composed of short-chain polyphosphates of zinc (in the case of ZDDP) and iron (in the case of both ILs and binary mixture of IL+SB). The *a/c* ratio of P L-edge FY spectra which represents more bulk chemistry of tribofilms also showed formation of short-chain polyphosphates for P\_DEPDT, P\_DEHP, P\_DEHP+SB1 and P\_DEHP+SB2 while ZDDP films exhibited region where medium chain phosphates are found. Tribofilms derived from IL's and IL+SB showed similar *a/c* ratio irrespective of the location where spectra were acquired. On the other hand, in the case of P L-edge FY spectra of ZDDP films, a significant variance in the *a/c* ratio was observed depending on location of

measurement. This again confirms the inhomogeneity in the chemical make-up of ZDDP tribofilms. IL P\_DEPDT exhibited shorter chain polyphosphate formation in the bulk of the film in comparison to the surface as the a/c ratio becomes smaller from TEY to FY spectra. On the other hand, P\_DEHP showed higher degree of polymerization of phosphate films in the bulk than the surface. Similar results were observed in the previous study [11,57], where the sulfur containing ionic liquid (N\_DBDTP) exhibited longer chain polyphosphates formation at the surface than the bulk and only phosphorus containing ionic liquid (N\_DEHP) yielded an increase in phosphate chain length from the surface towards the bulk of the tribofilms. It can be hypothesized that sulfur from sulfur containing IL i.e. P\_DEPDT dominates the reaction with the metal substrate first to form sulfates/sulfides of iron thus hinders the polymerization of phosphate films near the film-substrate interface, while in the case of P\_DEHP, more iron cations are available near the interface than the surface of the films, higher polymerization occurs near the interface than surface. However, in the case of ZDDP, since the availability of zinc cation is similar at the surface of the tribofilm and at the interface of the tribofilm and the metal surface, similar a/c ratio observed in TEY and FY spectra except one location where a high a/c ratio observed.

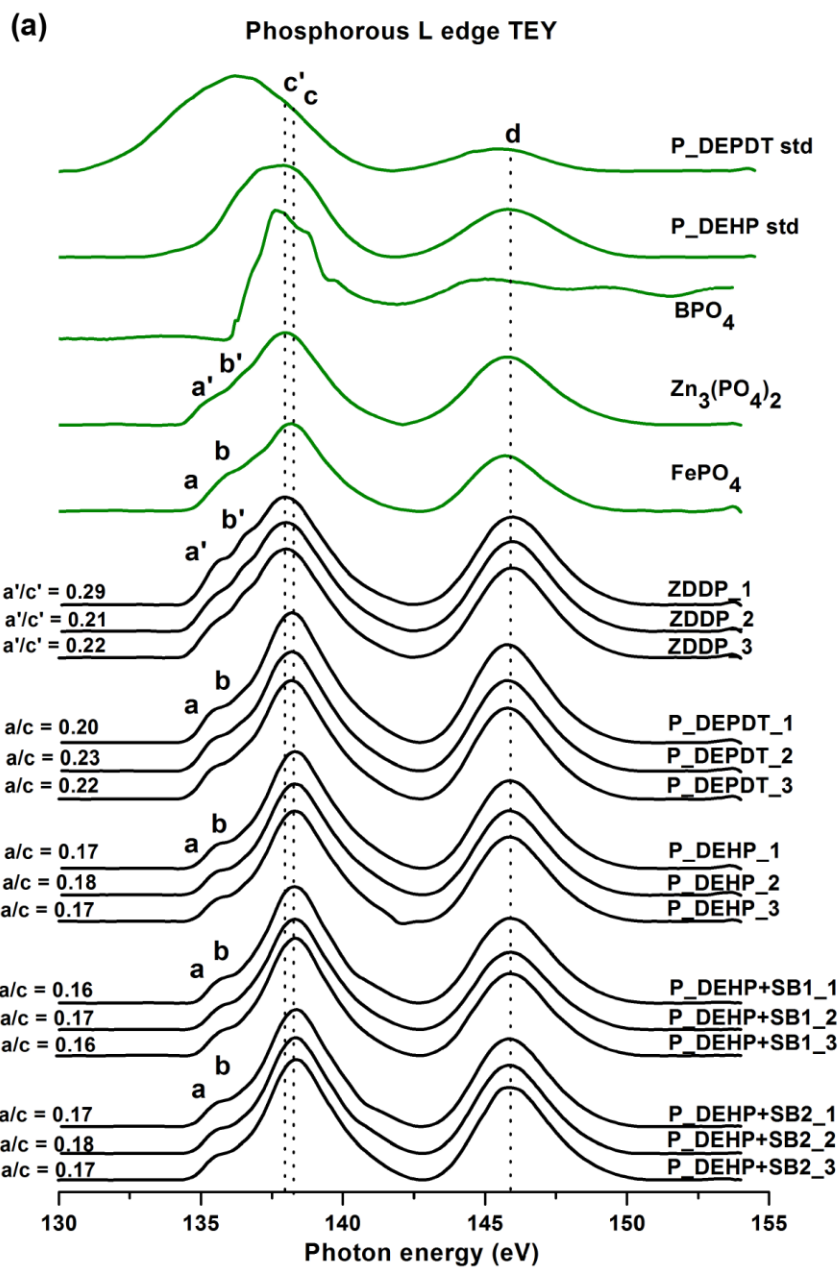


Figure 37(a). P L-edge TEY spectra of tribofilms derived from ZDDP, ILs and IL+SB lubrication (black lines) with reference compounds (green lines)



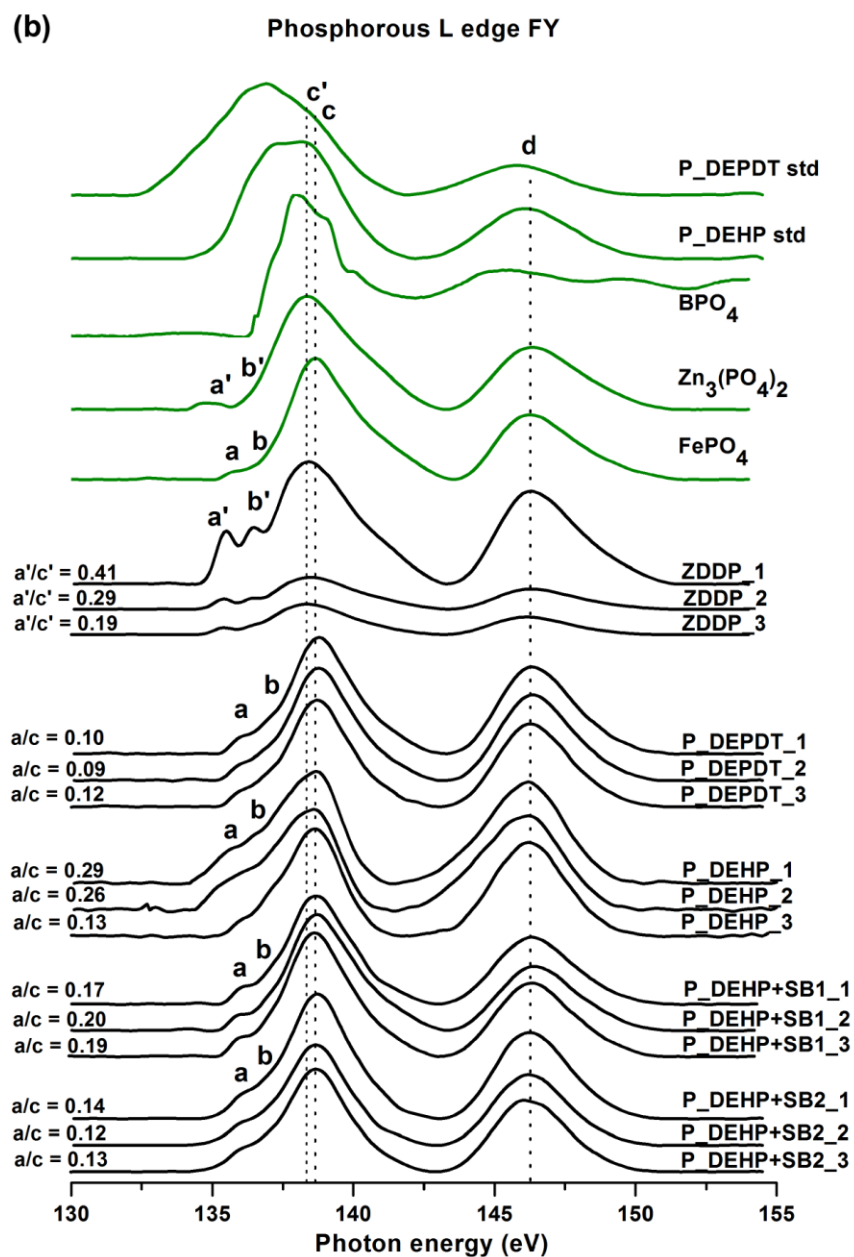


Figure 37(b). P L-edge FY spectra of tribofilms derived from ZDDP, ILs and IL+SB lubrication (black lines) with reference compounds (green lines)

#### 6.3.4.2 Boron Characterization (B K-edge)

This study is focused on the synergistic interaction of borate esters with phosphonium ionic liquids. Thus, boron chemistry in the tribofilms have also been investigated using XANES spectroscopy. Figure 38(a) is a plot of B K-edge TEY (bottom) and FY (top) spectra of tribofilms. For the purpose of the fingerprint match type analysis of tribofilms spectra, B K-edge spectra of several model compounds were also acquired and presented in figure 38(b). As reported by Kasrai et al. [158], B K-edge TEY probes at near the surface (~6 nm) and FY obtain information from the bulk (~100 nm). Kasrai et al. [158] also reported that TEY spectra get influenced by the surface modification as TEY measurement only probes up to 6 nm from the surface. In order to present a clean spectral feature of the model compounds, only B K-edge FY spectra (bulk) are shown in figure 38(b). From figure 38(b), three peaks are identified for B K-edge spectra of model compounds and are labelled as peak **a** (194.0 eV), **b** (198.4 eV) and **c** (202.9 eV, broad). Peaks **a** and **c** are attributed to the boron in trigonal coordination and peak **b** is assigned to tetrahedral coordination [158]. Peaks **a** and **c** are commonly present in B<sub>2</sub>O<sub>3</sub> and H<sub>3</sub>BO<sub>3</sub>. BPO<sub>4</sub> exhibits all three peaks, where peak **b** originates from tetrahedral B and is a dominant peak, since the compound in its pure form has boron in tetrahedral coordination. Relatively weak peaks **a** and **c** in BPO<sub>4</sub> spectra are believed to originate from surface modification [158]. The main absorption edge for FeB is located at 191.9 eV. FeB spectra also exhibit peak **a**, which could originate due to surface modification. The peak **a** for h-BN is shifted to 192.4 eV, which is about 1.6 eV lower energy than that of B<sub>2</sub>O<sub>3</sub>. The borate esters SB1 standard and SB2 standard spectra also

exhibits peak **a** owing to the trigonal coordination of boron, in addition SB2 standard spectra exhibits a post edge peak at 194.7 eV. The model compounds spectra can now be used to characterize the tribofilms spectra in figure 38(a). The B K-edge TEY and FY spectra of SB1 and SB2 tribofilms look very similar and exhibits a dominant peak **a** indicating that boron is primarily present as trigonal B. In addition, the width of peak **a** in SB1 tribofilms TEY and FY spectra (FWHM is ~1.2 eV) further suggests a greater likelihood of the formation of B<sub>2</sub>O<sub>3</sub>/H<sub>3</sub>BO<sub>3</sub> (FWHM 0.9 eV/1 eV) on the surfaces since the width of peak **a** for SB1 standard spectra is too sharp (FWHM ~0.5 eV). In the case of SB2 tribofilms TEY and FY spectra, a post edge peak after peak **a** from SB2 standard is missing, which also eliminates the possibility of residual SB2 standard chemistry within the SB2 tribofilms. A mere presence of peak **b** suggests that a partial transformation had occurred to produce tetrahedral boron species in SB1 and SB2 tribofilms under the thermo-mechanical action. Zhang et al. [159] also reported transformation of trigonal coordination to tetrahedral coordination in boron in the tribofilms upon rubbing. Interestingly, the blending of IL's P\_DEHP and P\_DEPDT with the borate esters SB1 and SB2 show a noticeable effect in the spectra. B K-edge FY spectra of P\_DEHP+SB1 tribofilms exhibit dominant presence of peak **a**, which is again attributed to the formation of B<sub>2</sub>O<sub>3</sub>/H<sub>3</sub>BO<sub>3</sub>. In addition, a resolved peak **b** can be seen that also suggests the formation of BPO<sub>4</sub> in the tribofilms due to the interaction of borate esters with P\_DEHP. Furthermore, P\_DEHP+SB1 FY spectrum exhibits a weak peak at peak **a'** (195.4 eV). In an earlier study, Zhang et al. [159] reported that peak **a'** originates from the p2s from phosphate structure. Hence, the presence of peak **a'** in P\_DEHP+SB1

can be assigned to the FePO<sub>4</sub>. P L-edge (in earlier section) also showed FePO<sub>4</sub> in P\_DEHP+SB1 tribofilms. On the other hand, P\_DEHP+SB1 TEY spectra exhibit a broad peak at peak **a'**, suggesting that surface of P\_DEHP+SB1 tribofilms is dominated by the FePO<sub>4</sub>. However, a pre-edge shoulder at peak **a** is seen, indicating that to some extent boron is also present on the surface in the form of B<sub>2</sub>O<sub>3</sub>/H<sub>3</sub>BO<sub>3</sub>. This indicates that the chemistry of P\_DEHP+SB1 tribofilm changes from the surface towards the bulk as boron was mainly found in the bulk (FY spectra) as both trigonal B (B<sub>2</sub>O<sub>3</sub>/H<sub>3</sub>BO<sub>3</sub>) and tetrahedral B (BPO<sub>4</sub>) and a small proportion of boron found at the surface (TEY spectra) as trigonal B only. Similar results were observed when SB1 added to P\_DEPDT. Here again, boron is mostly present in the bulk (FY) both as trigonal B (B<sub>2</sub>O<sub>3</sub>/H<sub>3</sub>BO<sub>3</sub>) and tetrahedral B (BPO<sub>4</sub>) and in less extent on the surface (TEY) as trigonal B (B<sub>2</sub>O<sub>3</sub>/H<sub>3</sub>BO<sub>3</sub>). In cases of P\_DEHP+SB1, the chemistry of the tribofilms at the surface is largely dominated by the phosphorus in the form of FePO<sub>4</sub>. B K-edge TEY and FY spectra of P\_DEHP+SB2 tribofilms exhibit peak **a** and peak **b** where the intensity of peak **a** is stronger than peak **b** indicating that both in bulk and at surface, boron is primarily present as trigonal B (B<sub>2</sub>O<sub>3</sub>/H<sub>3</sub>BO<sub>3</sub>) while the presence of tetrahedral B (BPO<sub>4</sub>) can be also noticed clearly. Peak **a'** is not observed in FY spectra whereas merely noticed in TEY spectra attributing to FePO<sub>4</sub> at the surface.

B K-edge FY spectra of P\_DEPDT+SB2 again indicates that boron is present in the bulk as trigonal B (B<sub>2</sub>O<sub>3</sub>/H<sub>3</sub>BO<sub>3</sub>) and tetrahedral B (BPO<sub>4</sub>) however, in this case, intensity of peak **b** is stronger than peak **a**. This result suggests that SB2 largely interacts with P\_DEPDT to form BPO<sub>4</sub> film. B K-edge TEY spectra of P\_DEPDT+SB2 also

exhibit similar chemistry as in FY, in addition, peak  $a'$  is also observed. This indicates that the boron chemistry in P\_DEPDT+SB2 is similar in bulk and at surface however, FePO<sub>4</sub> exhibits a noticeable presence at the surface (TEY). In a summary, all tribofilms derived from borate ester indicate that boron is primarily present as trigonal B. The addition of phosphonium ILs (P\_DEHP and P\_DEPDT) results in addition BPO<sub>4</sub> films in the tribofilms. In the case of SB1 mixture (i.e. P\_DEHP+SB1 and P\_DEPDT+SB1) boron chemistry changes significantly from surface towards the bulk, borates and boron phosphates are mainly found in the bulk (FY) while the surface (TEY) of the tribofilms are dominated by phosphate of iron (peak  $a'$ ). On the other hand, mixtures of SB2 (i.e. P\_DEHP+SB2 and P\_DEPDT+SB2) exhibit borates and boron phosphates in bulk as well as at the surface. However, the peak  $a'$  becomes noticeable in TEY spectra attributing to the FePO<sub>4</sub> at surface. In a similar study using XANES, Zhang [159] reported that when borated dispersant are mixed with the ZDDP, composition of boron changes in the surface and the bulk as the film grows. From B K-edge spectra, we can also eliminate the possibility of the formation of FeB in the P\_DEHP+SB and P\_DEPDT+SB tribofilms, as the B K-edge spectra of the tribofilms do not show features matching with the B K-edge spectra of FeB model compound.

These results suggests borate chemistry mostly present in the bulk whereas iron phosphate film dominates boron chemistry at the surface of the tribofilms as the spectra for P L-edge and B K-edge are acquired at the same time at the same location of tribofilms and from similar depths as the energy range of acquisition are very similar. Combining these findings with ECR results, we can speculate that when boron additive is

mixed with phosphorus ILs, borate films start to deposit on the surface in the earliest stages of the test leading to very short incubation time (figure 35 for P\_DEHP+SB1 and P\_DEHP+SB2) but are subsequently consumed during the wear process thus less boron is found at the surface which is then compensated by the formation of phosphate films which start to form after relatively longer incubation time (figure 35 for P\_DEHP and P\_DEPDT). Hence, the binary additive mixture of IL with SB showed improvement in the wear protection when compared with only ILs blends as seen in figure 33(b).

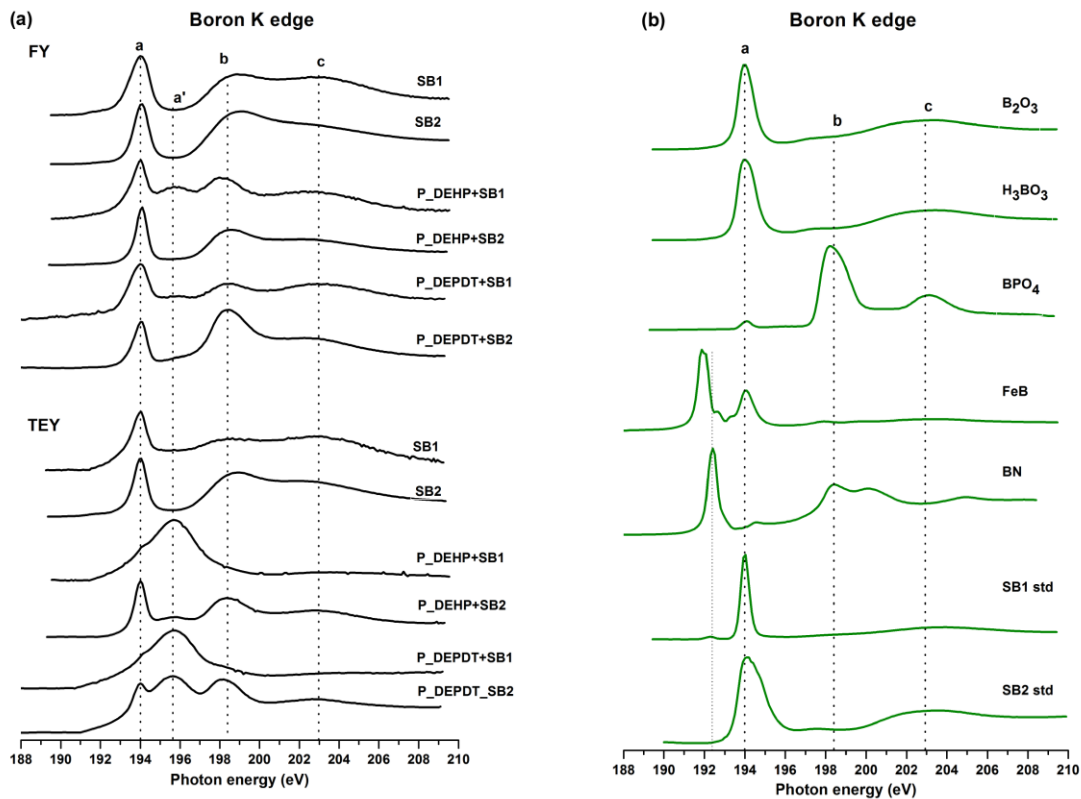


Figure 38. B K-edge TEY and FY of tribofilms derived from ZDDP, ILs and IL+SB lubrication (Figure 38(a)) with reference compounds (Figure 38(b))

## 6.4 Conclusions

The synergistic effect of borate esters with phosphonium ILs was studied for antiwear application. Results indicate that addition of borate ester to phosphonium IL results in significant improvement in wear protection compared to ZDDP as well as ILs and SBs alone at 0.1 wt.% P and 0.02 wt.% B treat rate both in cylinder on reciprocating flat contact and ball on rotating contact disc tribotest setup.

ECR and TGA of additive chemistry indicate that incubation time for tribofilms formation depends on the thermal stability of the additives, ZDDP with lowest decomposition temperature results in shorter incubation time compared to P\_DEPDT and P\_DEHP. However, addition of boron chemistry to P\_DEHP and P\_DEHP results in significantly shorter incubation time for tribofilm formation which subsequently resulted in lower wear.

XANES analysis of P L-edge indicated that ZDDP tribofilms are primarily composed of zinc polyphosphate films that are inhomogeneous in nature with variation in phosphate chain length at different locations and shorter chain phosphates at the surface compared to the bulk. On the other hand, tribofilms derived from P\_DEHP and P\_DEPDT lubrication are composed of short chain iron phosphate films and exhibited similar phosphate chain length at different locations. P containing IL (P\_DEHP) exhibited relatively longer phosphate chain length in the bulk compared to the surface while both P and S containing IL (P\_DEPDT) had shorter phosphate chain length in the bulk compared to the surface. Tribofilms formed from P\_DEHP+SB blends had short chain iron polyphosphates both at surface and in the bulk.

Boron in SB1 and SB2 derived tribofilms is primarily found as trigonal B mainly as  $B_2O_3/H_3BO_3$  and to some extent tetrahedral B both at surface and in the bulk. Tribofilms derived from IL+SB blends showed the interaction of borate ester with phosphonium IL as  $BPO_4$  is formed in the bulk tribofilms along with  $B_2O_3/H_3BO_3$ .



## Chapter 7. Low phosphorous oil blends of phosphonium ionic liquids with borate esters for tribological applications in base oil

### 7.1 Introduction

In this chapter, Trihexyltetradecylphosphonium bis(2-ethylhexyl)phosphate (P\_DEHP) ionic liquid was mixed with borate ester (SB) in group I base oil. Low phosphorous (P) oil blends were prepared by keeping the phosphorous concentration at 700 ppm and 350 ppm. Borate ester was added at 500 ppm boron treat rate. Tribological properties of these oil blends in a cylinder-on-flat contact under pure sliding revealed noticeable improvement in friction and wear protection, especially in the case of P\_DEHP (700 ppm P) + SB blend. Time-scale tribofilm formation was achieved by running the experiments for 5, 15 and 60 min. Thereby, synergistic interaction between P\_DEHP and SB could be connected with the formation of  $B_2O_3/H_3BO_3$  and  $BPO_4$  in addition to  $FePO_4$  tribofilms. Blends containing only SB resulted in tribofilms composed of trigonal boron as  $B_2O_3/H_3BO_3$ .

### 7.2 Experimental Details

#### 7.2.1 Chemistry of Antiwear Additives and Oil Formulation

Table 13 details the chemistry of the additives used. Trihexyltetradecylphosphonium bis(2-ethylhexyl) phosphate (P\_DEHP) was purchased from a IOLITEC Ionic Liquids Technologies Inc. and borate ester Trimethoxyboroxine (SB2) was provided from Argonne National Laboratory. Base oil blends were prepared in a group 1 base oil (mixture of 60 wt.% solvent neutral 150W and 40 wt.% bright stock 90W) purchased from a commercial vendor. Table 13 shows the details of AW chemistry

used and Table 14 highlights the low phosphorous oil blends prepared using P\_DEHP and SB2 additives in group 1 mineral base oil.

Table 13: Molecular structure of six IL's and ZDDP

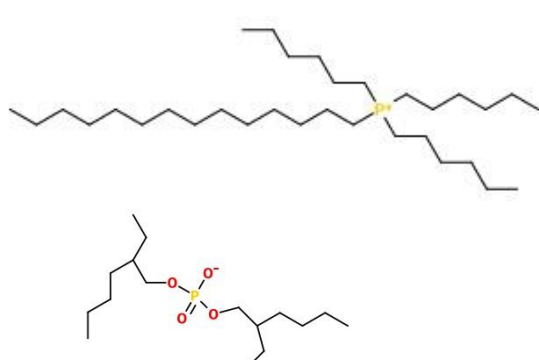
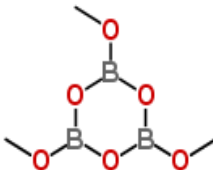
Coded Name	Chemical Name	Chemical Structure
<b>P_DEHP</b>	Trihexyltetradecylphosphonium bis(2-ethylhexyl)phosphate	
<b>SB 2</b>	Trimethoxyboroxine	

Table 14: Details of low phosphorous oil formulation prepared using P\_DEHP and SB2

AW additives

S. No.	Additives (ppm)	Formulations	Oil matrix
1	500 B	SB	Group1 mineral base oil
2	350 P + 500 B	P_DEHP1+SB	Group1 mineral base oil
3	700 P + 500 B	P_DEHP2+SB	Group1 mineral base oil

### *7.2.2 Tribological Test Details*

Tribological test were conducted at Argonne National Laboratory, Energy Systems Division. The tribological experiments employed a cylinder on reciprocating flat contact testing machine [56] to study the tribological performance of the oil blends with different phosphorous concentration. Test setup was also equipped with electric contact resistance (ECR) measurement setup. ECR data was collected in-situ during the test in order to gain insight into the incubation time for film formation at the tribological contacts. For this purpose, a 100 mV of potential is applied between the test cylinder and flat and the voltage drop across the counter surfaces were recorded as the test progress. Test specimens were cleaned before each test using Stoddard solution followed by isopropanol and acetone to completely remove any oil and dust present on the surfaces. The rubbed surfaces after the tests were cleaned with heptane and isopropanol and then saved by submerging them in sulfur free base oil.

### *7.2.3 Characterization of Tribofilms*

Wear scar width generated on cylinder from test specimen was measured using optical images obtained from an Olympus brand metallographic microscope. Wear width was measured at nine locations on each cylinder and each oil samples was tested twice. Thus, wear width for each oil sample is an average of 18 measurements. The surface topography of the wear track and wear mechanism was examined by obtaining 3-dimensional (3D) images of the rubbed surfaces using Hysitron Triboscope<sup>TM</sup> in scanning probe microscopy (SPM) imaging mode.

Chemical nature of the tribofilms formed in-situ during tribological tests was characterized using XANES spectroscopy. XANES spectra were obtained at The Canadian Light Source synchrotron facility at Saskatoon Canada. The phosphorous L-edge (P L-edge) and Boron K edge (B K-edge) spectra were collected at VLS-PGM (variable line spacing plane grating monochromator) beam station that operates at the energy range of 5.5 eV-250 eV with a photon resolution of more than 10,000 E/ $\Delta$ E. All the spectra were collected using a 100  $\mu$ m x 100  $\mu$ m photon beam spot size.

### 7.3 Results and Discussion

#### 7.3.1 *Coefficient of Friction and Wear Volume*

Coefficient of friction obtained for different oil blends at 5 mins (black line), 15 mins (red line) and 60 mins (blue line) tests are plotted in Figure 39. All three oil blends show stable frictional behavior. A small variance is observed in CoF value for 5 mins tests compared to 60 mins tests for each oil blend. This could be attributed to the original surface roughness of the test specimen. In the initial stages of the test, frictional resistance between the counter surfaces is dominated by the original surface roughness which could vary a little while preparing the sample. Once the initial surface asperities are removed and stable tribofilms form on the counter surface, a stable friction response is observed. Moreover, after 5 mins of 15 mins tests, similar CoF observed as in 60 mins at same period of the test which indicates the consistency in the additive performance. An average of coefficient of friction was calculated for 60 mins tests and are plotted in Figure 40. Oil blend containing only SB2 exhibits highest CoF value while binary additive blends containing P\_DEHP and SB2 results in lower CoF. In addition,

P\_DEHP(700P)+SB2 exhibits lower CoF compared to P\_DEHP(350P)+SB2. This suggests that higher phosphorous content in the oil blend results in improvement in CoF values.

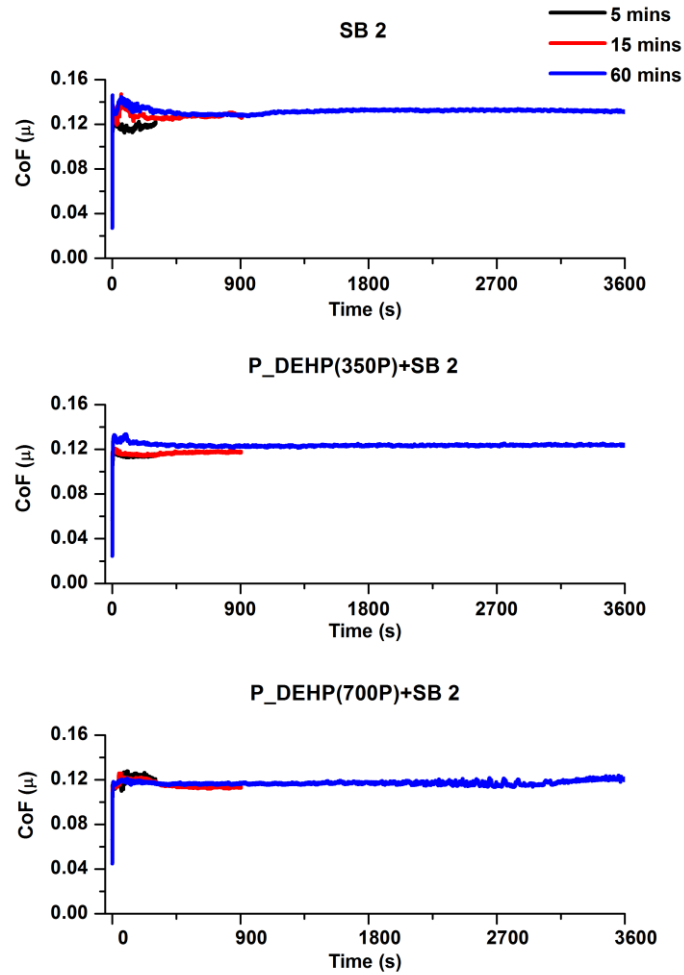


Figure 39: Coefficient of friction obtained for oil blends containing only SB2, P\_DEHP(350P)+SB2 and P\_DEHP(700P)+SB2. Showing the friction response of each oil blend for 5 mins, 15 mins and 60 mins test.

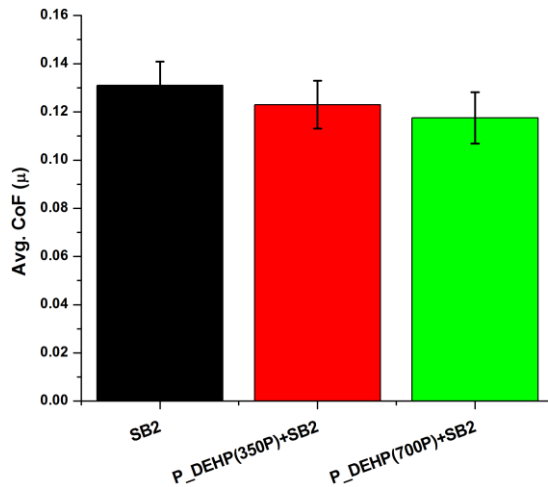


Figure 40: A plot of average CoF for the 60 mins test for each oil blend.

Wear volume on cylinder after each test was calculated by measuring the wear scar width using an optical microscopy images for 60 min tests. The wear scar width was measured at nine location on each test cylinder and each test was repeated twice hence wear scar width value used for the calculations is an average of eighteen measurements. Wear volume chart for 60 min tests are presented in Figure 41. Wear scar width for 5 mins and 15 mins test was minimal for precise measurements hence not presented in this chapter. Borate ester (SB2) exhibits relatively higher wear losses compared to blends containing P\_DEHP and SB2. Moreover, effect of phosphorous content in the oil blend can also be seen in Figure 41. The addition of phosphorous from P\_DEHP to the SB2 at 350P ppm shows improvement in the wear protection which is further increased by adding P\_DEHP at 700P ppm to SB2.

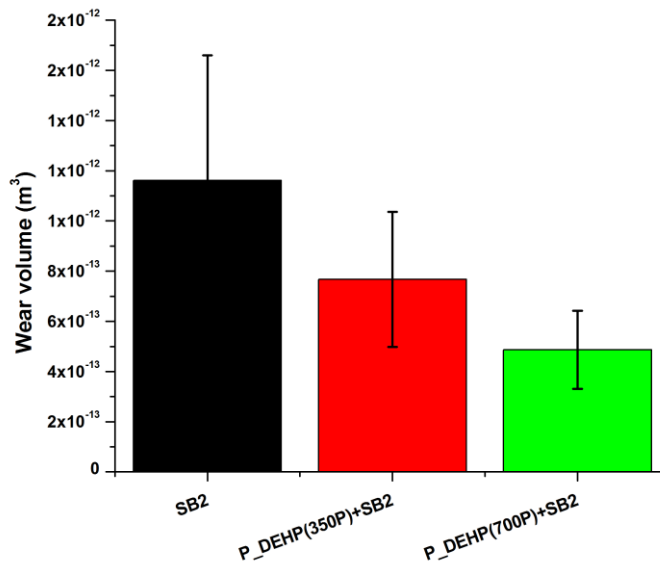


Figure 41: Wear volume loss obtained for oil blends containing only SB2, P\_DEHP(350P)+SB2 and P\_DEHP(700P)+SB2 for 60 mins test.

### 7.3.2 Analysis of tribofilms formation using ECR

ECR data acquired from each oil blend is plotted as voltage drop as a function of test time in Figure 42 for 5 min (black)), 15 min (red) and 60 min (blue) tests. Non-zero voltage drop value is an indicative of formation of non-conductive glassy tribofilms and voltage drop close to zero mV suggest no film formation between the counter surfaces [56]. In the case of only SB2, 5 min test does not show potential build up except the first point which could originate due to separation of counter surfaces from oil. Once the test started voltage drop value becomes near zero for the 5 min test which is also observed in the case of 15 min and 60 min test where voltage drop reaches to 100 mV around 300 sec after the test started. This results indicates that incubation time for tribofilm formation for

SB2 is ~300 sec. After ~300 sec, both 15 min and 60 min test show voltage drop value which periodically vary between 0-100 mV till ~900 sec test time. This corresponds to the film formation which is sacrificial in nature. In this test duration (~300sec - ~900sec), the film formation rate is similar to film removal rate under constant shearing. After ~900 sec, more stable voltage drop is observed and the voltage drop value vary between ~50mV – 100 mV till ~2700 sec test time. In this test duration, most voltage drop value remained close to 100 mV indicating stable and effective film formation. After ~2700 sec maximum acquired voltage drop value starts to decrease till the end of the test i.e. 3600 sec. ECR data acquired for test run under P\_DEHP(350P)+SB2 lubrication shows relatively small incubation time for film formation. Voltage drop starts to form as early as ~ 100 sec from the beginning of the test in 5 min, 15 min and 60 min tests. After ~100 sec, voltage drop value vary in between 50 mV – 100 mV. This results indicate that addition of phosphorous from P\_DEHP at 350 P ppm to SB2 results in shorter incubation time for tribofilm formation and once the films are formed film formation rate is higher than film removal under shearing thus the voltage drop does not go back to 0 mV and stay between 50 mV – 100 mV. In the case of P\_DEHP(700P)+SB2, voltage drop starts to build up as early as the test starts however, till ~300 sec of the test, the film removal rate is higher than film formation hence the voltage drop varies between 0 mV – 50 mV. After ~300 sec, voltage drop value reached to 100 mV indicate full film formation. Voltage drop value remains close to 100 mV for the rest of the duration of the test except few point where voltage drop falls to 50 mV. This results indicate that synergistic interaction of P\_DEHP with SB2 reduces the incubation time for tribofilm formation as



well as results in more stable and effective film formation. Amount of phosphorous also determine the effectiveness of the tribofilms. Addition of P\_DEHP at 700P ppm to SB2 results in more effective tribofilm formation than P\_DEHP(350P)+SB2.

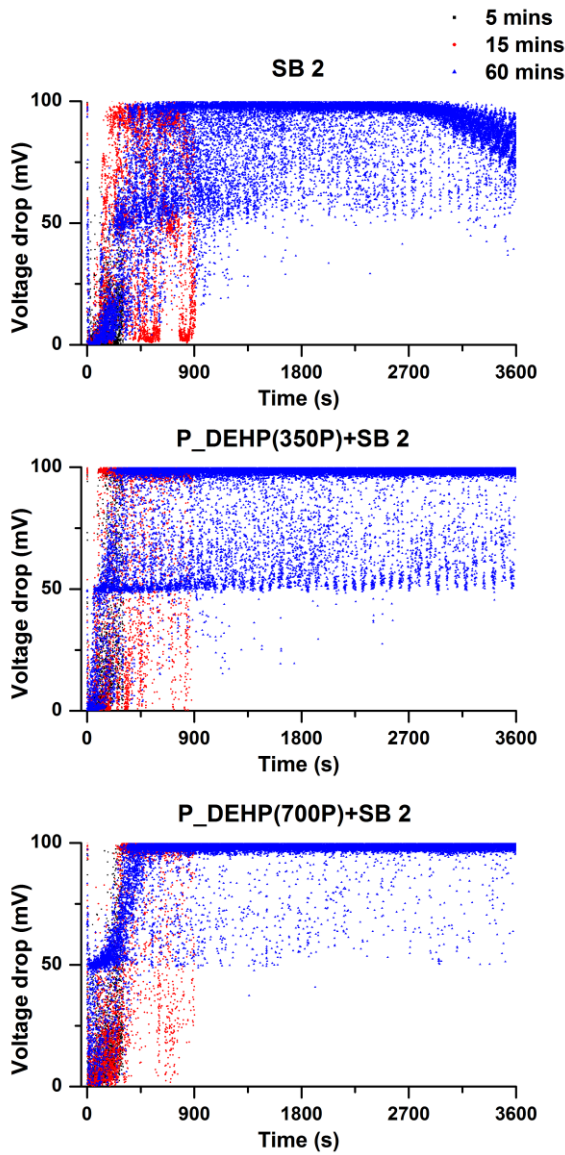


Figure 42: Electric contact resistance (ECR) data acquired for SB2, P\_DEHP(350P)+SB2 and P\_DEHP(700P)+SB2 for 5 min(black), 15 min (red) and 60 min (blue) tests.

### 7.3.3 Chemical Properties of Tribofilms using XANES

#### 7.3.3.1 Phosphorous Characterization (P L<sub>2,3</sub>-edge)

Phosphorous L-edge TEY and FY spectra of tribofilms derived from low phosphorous oil blends containing P\_DEHP at 350P ppm/700P ppm and SB2 at 500B ppm for 5 min, 15 min and 60 min test are illustrated in Figure 43a and 43b respectively. Phosphorous L-edge spectra of the tribofilms are plotted in black lines and are compared with model compounds plotted in green lines. Figure 43a presents the P L-edge TEY spectra which offers chemical information of local coordination of phosphorous from near surface region i.e. ~5-10 nm [108,134]. Surface of the tribofilms derived from 5 min, 15 min and 60 min test and different phosphorous treat rate (350P ppm and 700P ppm) were probed using P L-edge TEY signal which exhibited four peaks that are labeled as peak **a**, **b**, **c** and **d**. As discussed in the earlier chapter, peak **d** is a shape resonance peak and is commonly present in both FePO<sub>4</sub> and BPO<sub>4</sub> model compounds along with all the tribofilms spectra. Presence of peak **d** in tribofilms spectra indicates that phosphorous is primarily present as phosphate species in the tribofilms. In addition, the photon energy of pre-edge shoulders peaks **a** and **b** and a main absorption edge peak **c** from the tribofilms spectra closely matches with FePO<sub>4</sub> model compound spectra. Similarly, the tribofilms P L-edge FY spectra which offer chemical information from the bulk of the sample up to 50-60 nm [108,134] also exhibited spectral features matching with the FePO<sub>4</sub> model compound. This confirms that tribofilms derived from P\_DEHP (350P/700P)+SB2 lubrication are primarily composed of FePO<sub>4</sub> chemistry. The main absorption edge from P L-edge spectra of BPO<sub>4</sub> model compound was not clearly

resolved in the P L-edge spectra of tribofilms. Here, we can speculate that since availability of Fe cation (from substrate) is much higher than B (added at 500 ppm) at the tribological contacts, the likelihood for  $\text{FePO}_4$  formation is much higher than  $\text{BPO}_4$  in the tribofilms. Hence when probing the P L-edge, the tribofilms spectra get influenced by the more dominantly present species i.e.  $\text{FePO}_4$  chemistry which might results in the suppression of spectral features of  $\text{BPO}_4$  chemistry. In order to probe the  $\text{BPO}_4$  chemistry in the tribofilms, B K-edge spectra was acquired and discussed in the next section (7.3.3.2).

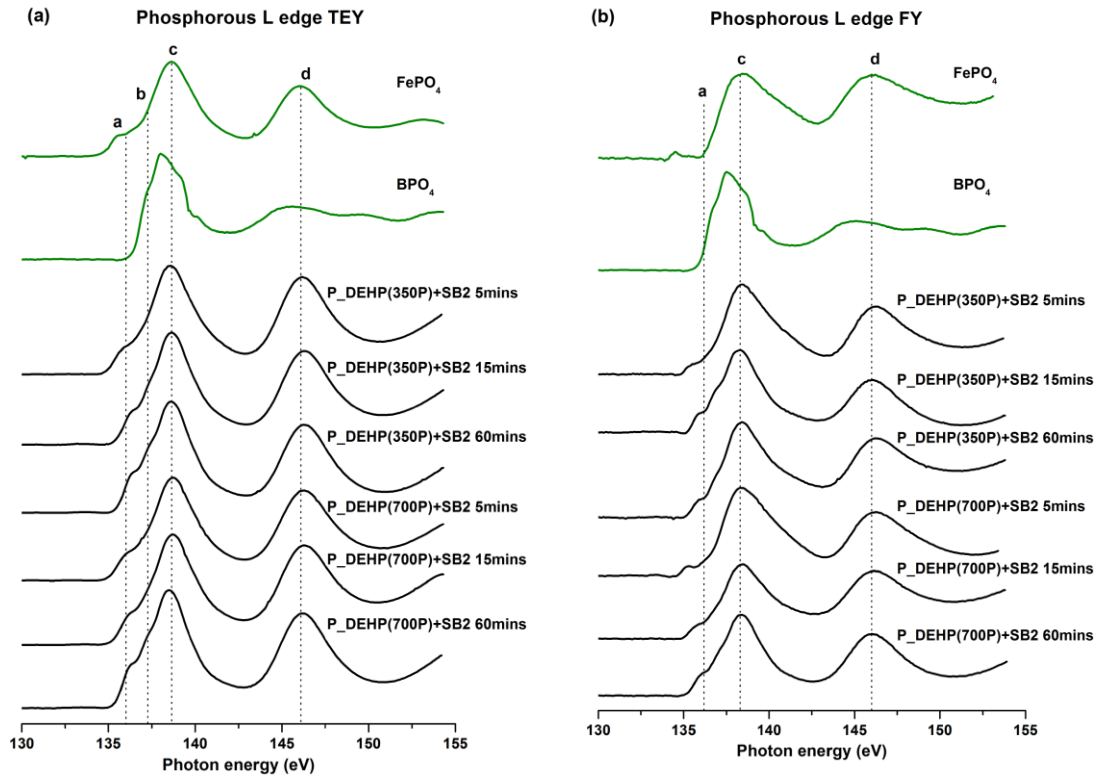


Figure 43; Phosphorous L-edge spectra of tribofilms (black lines) derived at 5 min, 15 min and 60 min test for  $\text{P\_DEHP(350P)+SB2}$  and  $\text{P\_DEHP(700P)+SB2}$  lubrication along with model compounds (green lines). Figure 43(a) illustrates the total electron

yield signal (TEY spectra) and Figure 43(b) illustrates the fluorescence yield signal (FY spectra)

In order to gain insight into the effect of rubbing time and phosphorous concentration to the formation and composition of tribofilms, extent of phosphate films polymerization was analyzed using the peak **a** to peak **c** ratio from P L-edge TEY and FY spectra of tribofilms (from Figure 43a and 43b). Previous studies have suggested that **a/c** ratio below 0.3 corresponds to short-chain phosphate polymerization and **a/c** ratio above 0.6 indicate long-chain phosphate formations [51,132,136]. The **a/c** ratio of tribofilms formed at 5 min, 15 min and 60 min test for oils containing P\_DEHP(350P)+SB2 and P\_DEHP(700P)+SB2 is measured and plotted in Figure 43c. P L-edge TEY **a/c** ratio is presented as green bar and P L-edge FY **a/c** ratio in blue bars. The **a/c** ratio acquired from TEY spectra exhibits relatively higher value in comparison with FY for each test suggesting that at near surface region, relatively higher degree of polymerization had occurred than in the bulk of the tribofilms in all cases. In all cases, short-chain phosphate film formation has observed since the maximum **a/c** ratio measured is 0.3 (P\_DEHP(350P)+SB2 60 min test and P\_DEHP(700P)+SB2 60 min test). The **a/c** ratio in each cases is found to be increasing with increasing rubbing time. In the case of P\_DEHP(350P)+SB2 TEY/FY, the **a/c** ratio increases from 0.2/0.09 to 0.25/0.14 and 0.3/0.19 for 5 min, 15 min and 60 min test respectively. Similarly, P\_DEHP(700P)+SB2 TEY/FY also shows increase in the **a/c** ratio with rubbing time both at near surface (TEY) and in the bulk (FY). This results indicates that the tribofilms derived from

P\_DEHP(350P/700P)+SB2 results in layered phosphate films where the surface of the films is composed of relatively higher degree of polymerization of phosphate film than the bulk of the tribofilms.

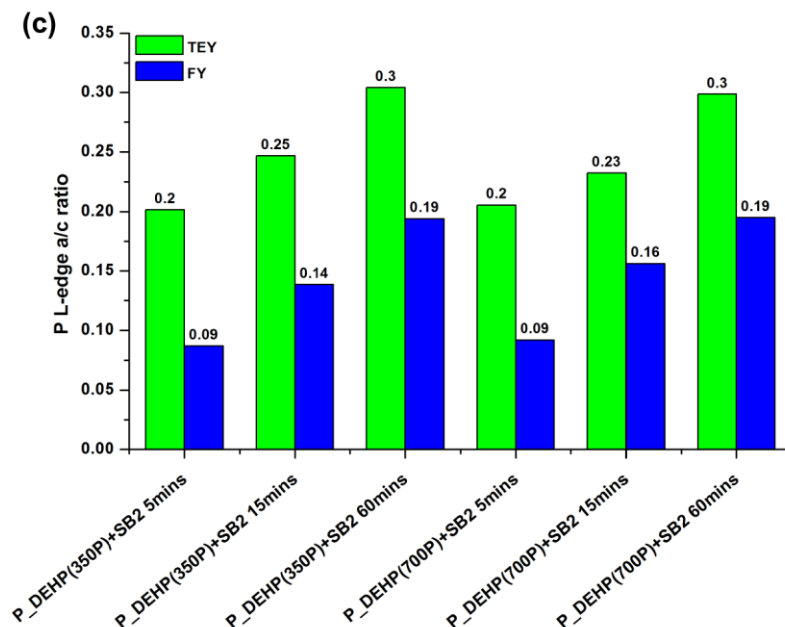


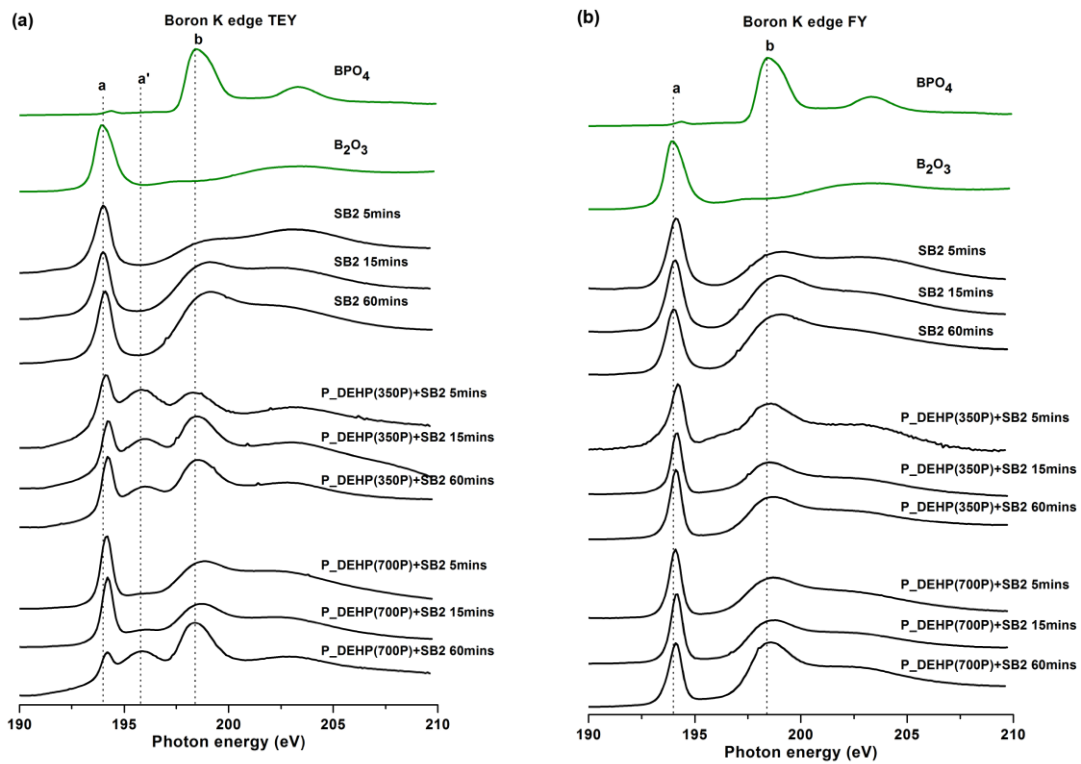
Figure 43c: P L-edge a/c ratio measured for tribofilms formed using P\_DEHP(350P)+SB2 and P\_DEHP(700P)+SB2 at 5 min, 15 min and 60 min test.

### 7.3.3.2 Boron Characterization (B K-edge)

B K-edge TEY and FY spectra of tribofilms derived from SB2, P\_DEHP(350P)+SB2 and P\_DEHP(700P)+SB2 for 5 min, 15 min and 60 min test are plotted in Figure 44a and 44b. The local coordination of boron in the tribofilm is probed by comparing the B K-edge tribofilm spectra with model compounds i.e. trigonal boron ( $B_2O_3$ ) and tetrahedral boron ( $BPO_4$ ). In Figure 44a and 44b, the trigonal boron peak for  $B_2O_3$  is labeled as peak **a** and tetrahedral boron peak for  $BPO_4$  is identified as peak **b**.

Zhang et al. [159] reported that peak **a** originates from the  $p_{2s}$  from phosphate structure. Here, the presence of peak **a** in P\_DEHP(350P/700P)+SB2 can be assigned to the  $FePO_4$  chemistry. Since P L-edge (in earlier section 7.3.3.1) also showed  $FePO_4$  in P\_DEHP(350P/700P)+SB2 tribofilms. B K-edge TEY and FY spectra of SB2 exhibit a presence of peak **a** while peak **b** is merely present. The presence of peak **a** in SB2 derived tribofilms for 5 min, 15 min and 60 min tests indicates that boron is primarily present as trigonal boron as  $B_2O_3$ . A mere presence of peak **b** indicates that under thermo-mechanical shearing partial transformation of trigonal boron to tetrahedral boron had occurred. In an earlier study, Zhang et al. [159] also reported transformation of trigonal coordination to tetrahedral coordination in boron in the tribofilms upon rubbing. B K-edge TEY and FY spectra for P\_DEHP(350P/700P)+SB2 derived tribofilms exhibit two absorption edge labeled as peak **a** and peak **b**. Again, comparing with the model compound spectra, presence of peak **a** at a photon energy of 194.1 eV suggests that boron in these tribofilms is trigonal boron species i.e.  $B_2O_3$ . In addition, presence of much resolved peak **b** at 198.4 eV suggests that to some extent boron is also present at boron phosphate in the tribofilms derived from the binary additive mixture of phosphonium IL (P\_DEHP) and borate ester (SB2). These results clearly indicate the synergism between these two ashless antiwear additives. Moreover, it can also be seen that the contribution of trigonal boron to tetrahedral boron coordination changes with the rubbing time as shown in Figure 44c. The peak intensity for peak **b** increases from 5 min rubbing test to 60 min rubbing. B K-edge TEY and FY spectra of P\_DEHP and SB2 at 700P ppm for 60 min test exhibit highest ratio of  $BPO_4$  to  $B_2O_3$ . The ratio of  $BPO_4$  to

$B_2O_3$  is relatively higher in TEY signal than FY, suggesting the boron in the bulk of the tribofilms is dominantly present as  $B_2O_3$  while  $BPO_4$  contribution increases at near surface region. We can hypothesize that, during the rubbing test boron from borate ester first get to the counter surfaces and forms  $B_2O_3$  tribofilms which later interact with phosphorous from P\_DEHH IL and form  $BPO_4$  which enhances the crosslinking between phosphate film networks.



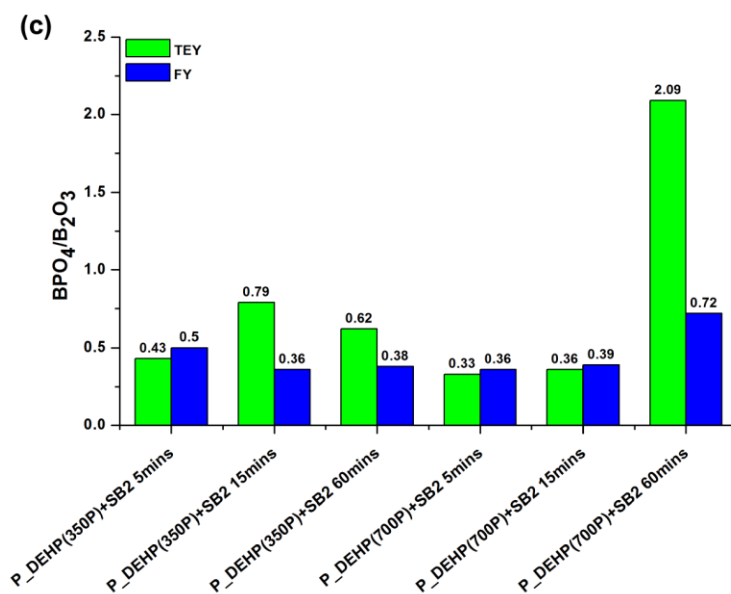


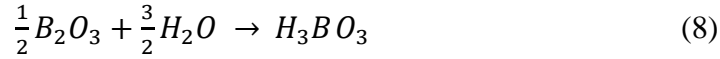
Figure 44; Boron K-edge spectra of tribofilms (black lines) derived at 5 min, 15 min and 60 min test for SB2, P\_DEHP(350P)+SB2 and P\_DEHP(700P)+SB2 lubrication along with model compounds (green lines). Figure 44(a) illustrates the total electron yield signal (TEY spectra) and Figure 44(b) illustrates the fluorescence yield signal (FY spectra). Figure 44(c) BPO<sub>4</sub>/B<sub>2</sub>O<sub>3</sub> ratio measured for tribofilms formed using P\_DEHP(350P)+SB2 and P\_DEHP(700P)+SB2 at 5 min, 15 min and 60 min test.

#### 7.3.4 Theory of tribochemical film formation

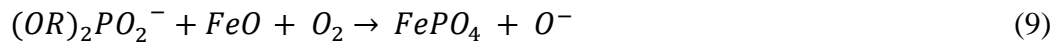
As seen in section 7.3.3 as well as in 6.3.4, synergistic interaction between phosphonium phosphate IL and borate esters resulted in the formation of FePO<sub>4</sub>, B<sub>2</sub>O<sub>3</sub>/H<sub>3</sub>BO<sub>3</sub> and BPO<sub>4</sub> tribochemical films on the rubbed surfaces. XANES analysis also indicated no residual P\_DEHP compound on the rubbed surfaces (section 6.3.4.1). The P L-edge spectra primarily exhibited FePO<sub>4</sub> formation suggesting that P\_DEHP IL reacts with the Fe surfaces to form FePO<sub>4</sub>. The B K-edge spectra showed no interaction of



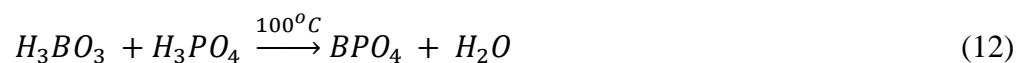
boron chemistry with the Fe surfaces (no absorption edge for FeB) and boron was only found either as  $B_2O_3/H_3BO_3$  and  $BPO_4$ . The author hypothesizes that under the thermo-mechanical shearing, borate esters (SB) form decomposition by-products of  $B_2O_3$  which get adsorbed on the counter surfaces in the initial stages of the test. However, since the tribological experiments were run in ambient air (relative humidity  $\approx 50\%$ ),  $B_2O_3$  can also hydrolyses to form boric acid ( $H_3BO_3$ ). Erdemir et al. [160] studied the lubrication mechanism of boron chemistry and reported that  $B_2O_3$  transforms into  $H_3BO_3$  at the tribological contacts following the reaction (8).



On the other hand, formation of  $FePO_4$  from the interaction of P\_DEHP with Fe surface can be speculated to follow a chemical reaction between native iron oxide layers exist on the Fe surfaces and phosphonium and phosphate ions. Najman et al. [64] proposed the chemical pathway for the formation of iron polyphosphates tribofilms on the rubbing surfaces using ashless thiophosphate additives. In this study, the author speculates that under thermo-mechanical shearing, nascent Fe surfaces (Fe ions) are generated from the breakdown of iron oxide layers, which are positively charged. Alkyl phosphate (DEHP cation) in P\_DEHP will have higher affinity to get adsorbed at Fe ions surface to form iron phosphate tribofilms following the possible chemical pathway given as;



Reactions (8), (9) and (11) provide possible pathway for the formation of B<sub>2</sub>O<sub>3</sub>/H<sub>3</sub>BO<sub>3</sub> and FePO<sub>4</sub> compounds in the tribofilms, which are observed from XANES analysis of the wear track. Besides these compounds, the B K-edge spectra of the synergistic blends of P\_DEHP and SB also exhibited the formation of BPO<sub>4</sub> compound. From Figure 44c is also noticed that with rubbing time, BPO<sub>4</sub> formation increases in the tribofilms relative to B<sub>2</sub>O<sub>3</sub>/H<sub>3</sub>BO<sub>3</sub>. Thus, it can be believed that under the thermo-mechanical shearing, BPO<sub>4</sub> forms at the expense of B<sub>2</sub>O<sub>3</sub>/H<sub>3</sub>BO<sub>3</sub> at the availability of phosphoric acid from the original P\_DEHP IL under ambient condition (relative humidity ≈50%). Possible chemical reactions for the formation of BPO<sub>4</sub> is given in reaction 12. The free enthalpy of formation at 100°C  $\Delta H_{373}^0$  for H<sub>3</sub>BO<sub>3</sub> is -1089.48 kJ/mol<sup>-1</sup> and  $\Delta H_{373}^0$  for H<sub>3</sub>PO<sub>4</sub> is -1275.57 kJ/mol<sup>-1</sup> and  $\Delta H_{373}^0$  for H<sub>2</sub>O is -271.282 kJ/mol<sup>-1</sup> [161]. By balancing the reaction, the free enthalpy of formation  $\Delta H_{373}^0$  for BPO<sub>4</sub> is found to be -2093.77 kJ/mol<sup>-1</sup>.



#### 7.4 Conclusions

Antiwear properties of the synergistic mixtures of borate esters with phosphonium IL was studied for low phosphorous oil blends (at 350P ppm and 700P ppm) in order to comply with the current engine oil specifications (ILSAC GF5: 800P ppm).

Antiwear properties measured for these oil blends on a cylinder-on-flat contact under pure sliding revealed noticeable improvement in wear protection due the synergism of borate ester (SB2) with P\_DEHP IL than borate esters alone. Phosphorous treat rate

can also be combined with the wear outcomes since P\_DEHP(700 ppm P) + SB blend resulted in lowest wear volume losses than P\_DEHP(350P)+SB2 while oil blend with no P in the case of SB2 exhibited highest wear volume losses.

ECR data indicated that shorter incubation time is achieved from the synergistic interaction of SB2 with P\_DEHP and shortest incubation time was obtained from the oil blend containing P\_DEHP(700P)+SB2.

Time-scale tribofilm formation was achieved by running the experiments for 5, 15 and 60 min. XANES analysis using P L-edge revealed that phosphorous is primarily present as  $\text{FePO}_4$  and phosphate chain polymerization increases with rubbing time (increase in P L-edge  $a/c$  ratio from 5 min to 60 min rubbing time). B K-edge spectra revealed the formation of  $\text{BPO}_4$  enhanced  $\text{B}_2\text{O}_3/\text{H}_3\text{BO}_3$  tribofilms for P\_DEHP+SB2 blends while SB2 alone forms  $\text{B}_2\text{O}_3/\text{H}_3\text{BO}_3$  tribofilms. B K-edge revealed that  $\text{BPO}_4$  to  $\text{B}_2\text{O}_3/\text{H}_3\text{BO}_3$  ratio increase with rubbing suggesting that during the thermos-mechanical shearing action, initial  $\text{B}_2\text{O}_3/\text{H}_3\text{BO}_3$  tribofilms formed from SB2 chemical interact with P\_DEHP IL to form  $\text{BPO}_4$ .

## Chapter 8. Analysis of Tribofilms Formed using Phosphonium Ionic Liquids and Borate Esters in Fully Formulated Oil (no Zn)

### 8.1 Introduction

In this chapter, antiwear properties of synergistic blend of phosphonium IL (P\_DEHP) and borate ester is studied in fully formulated oil (no Zn, no P). Low phosphorous oil blends were prepared by blending the P\_DEHP in FFO at 700 ppm P treat rate. Borate ester was blended at 200 ppm B treat rate. Antiwear performance of the mixtures obtained was evaluated using a cylinder on reciprocating flat tribological testing under pure sliding. Friction and wear properties were compared with those of a reference oil containing ZDDP at 700 ppm P. Surface topography and 3D profiling of the rubbed surfaces were analyzed using scanning electron microscopy (SEM) & scanning probe microscopy (SPM), respectively. X-ray absorption near edge structure spectroscopy (XANES) was used to describe the chemical nature of the tribofilms.

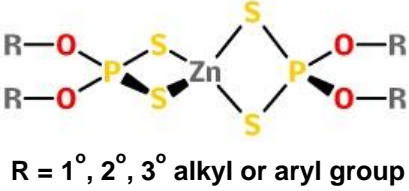
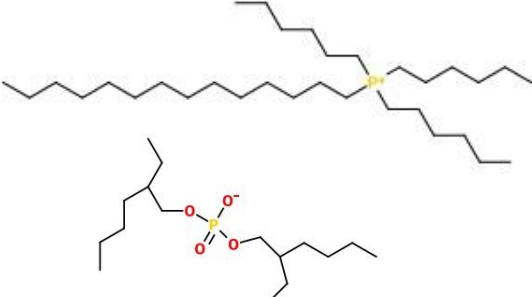
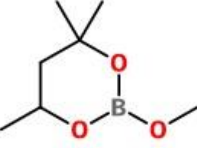
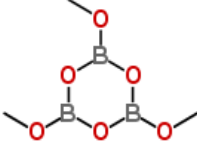
### 8.2 Experimental Details

#### *8.2.1 Description of additive chemistry and Thermogravimetric analysis.*

Table 15 details the chemistry of the additives used. ZDDP purchased from a commercial vendor, is a secondary alcohol derived ZDDP with approximately 70% neutral and 30% basic characteristics, details of which are available in Parekh et. al. [47]. Phosphonium ionic liquid Trihexyltetradecylphosphonium bis(2-ethylhexyl) phosphate (P\_DEHP) and borate ester 2-Methoxy-4,4,6-trimethyl-1,3,2-dioxaborinane (SB1) were provided from AC2T research GmbH Austria. Trimethoxyboroxine (SB2) was provided from Argonne National Laboratory. Base oil blends were prepared in a group 1 base oil

(mixture of 60 wt.% solvent neutral 150W and 40 wt.% bright stock 90W) purchased from a commercial vendor.



Table 15. Description of additive chemistry.

Coded Name	Chemical Name	Chemical Structure
<b>ZDDP</b>	Zinc dialkyl-dithiophosphate	 <p>R = 1°, 2°, 3° alkyl or aryl group</p>
<b>P_DEHP</b>	Trihexyltetradecylphosphonium bis(2-ethylhexyl)phosphate	
<b>SB 1</b>	2-Methoxy-4,4,6-trimethyl-1,3,2-dioxaborinane	
<b>SB 2</b>	Trimethoxyboroxine	

### *8.2.2 Tribological Test Details*

Oil samples were formulated by blending ZDDP, IL's and borate ester individually or as mixtures of IL and SB in base oil. All blends were prepared by keeping the phosphorous (P) and boron (B) concentration at 700 ppm and 200 ppm respectively as applicable. Tribological test were conducted at Argonne National Laboratory, Energy Systems Division. Tribological experiments were performed using a cylinder on reciprocating flat contact testing machine [56]. Table 16 provides schematic of the test configuration and highlights the test parameters. Test setup was also equipped with electric contact resistance (ECR) measurement setup. ECR data was collected in-situ during the test in order to gain insight into the incubation time for film formation at the tribological contacts. Test specimens were cleaned before each test using Stoddard solution followed by isopropanol and acetone to completely remove any oil and dust present on the surfaces. The rubbed surfaces after the tests were cleaned with heptane and isopropanol and then saved by submerging them in sulfur free base oil.

Table 16. Schematic of the test configurations and detail of test parameters.

Tribological test	Cylinder on reciprocating flat contact	
		<div style="display: flex; justify-content: space-around; align-items: center;"> <div style="text-align: center;"> <p>Front View</p>  </div> <div style="text-align: center;"> <p>Side View</p>  </div> </div>
Matrix	Fully formulated oil (no Zn, no P)	
Viscosity	10.02 mm <sup>2</sup> /sec at 100 °C	
Treat rate	Phosphorous: 700 ppm and Boron: 200 ppm	
Applied load	82 N	
Initial Hertzian contact pressure	500 MPa	
Temperature	100 °C	
Speed	0.06 m/sec, 5 Hz	
Stroke length	6 mm	
Cylinder/Ball	Φ 4 mm x 6 mm, 52100 steel (60-61 HRc)	
Flat/Disc	12 mm x 12 mm x 8 mm, 52100 alloy steel (60-61 HRc)	
Duration	1 hour	

### 8.2.3 Characterization of Tribofilms

Wear scar width generated on cylinder after rubbing was measured using optical images obtained from an Olympus brand metallographic microscope. Wear width was measured at nine locations on each cylinder and each oil samples was tested twice. Thus, wear width for each oil sample is an average of 18 measurements. The surface topography of the wear track and wear mechanism was examined by obtaining 3-

dimensional (3D) images of the rubbed surfaces using Hysitron Triboscope™ in scanning probe microscopy (SPM) imaging mode.

Chemical nature of the tribofilms formed in-situ during tribological tests was characterized using XANES spectroscopy. XANES spectra were obtained at The Canadian Light Source synchrotron facility at Saskatoon Canada. The phosphorous L-edge (P L-edge) and Boron K edge (B K-edge) spectra were collected at VLS-PGM (variable line spacing plane grating monochromator) beam station that operates at the energy range of 5.5 eV-250 eV with a photon resolution of more than 10,000 E/ΔE. All the spectra were collected using a 100 μm x 100 μm photon beam spot size. The phosphorous K-edge, sulfur K-edge and calcium K-edge spectra were obtained from SXRMB (Soft X-ray Micro characterization Beam line) beam station which operates a high energy ranging from 1.7 – 10 keV which a photon resolution of  $3.3 \times 10^{-4}$  Insb (111). A 1 mm X 2 mm spot size was chosen to collect the spectra at the SXRMB beam line.

### 8.3 Results and Discussion

#### 8.3.1 *Coefficient of Friction and Wear Volume*

The coefficient of friction obtained from different oil blends are plotted in Figure 45. The FFO blends without AW additive and with AW additives i.e. P\_DEHP, P\_DEHP+SB1 and P\_DEHP+SB2 exhibit similar frictional response as a function of rubbing time. CoF decreases in the initial stages of the test (up to ~300 sec) and then slightly increases (~300-900 sec)) and then remains consistent (CoF ~0.12) for the rest of the test duration. On the other hand, ZDDP FFO oil blend shows an increase in the CoF



in the initial state of the test (up to ~300 sec) and then remains consistent (CoF ~ 0.14) for the remaining duration of the test. This results indicates that IL's and borate ester AW chemistry does not influence the friction behavior of the FFO (without AW) and the coefficient of friction is mainly determined by the FFO (no Zn, no P) lubrication properties. However, the addition of ZDDP to FFO (no Zn, no P) shows an increase in the CoF value suggesting that the tribofilms formed using ZDDP AW additive results in higher CoF.

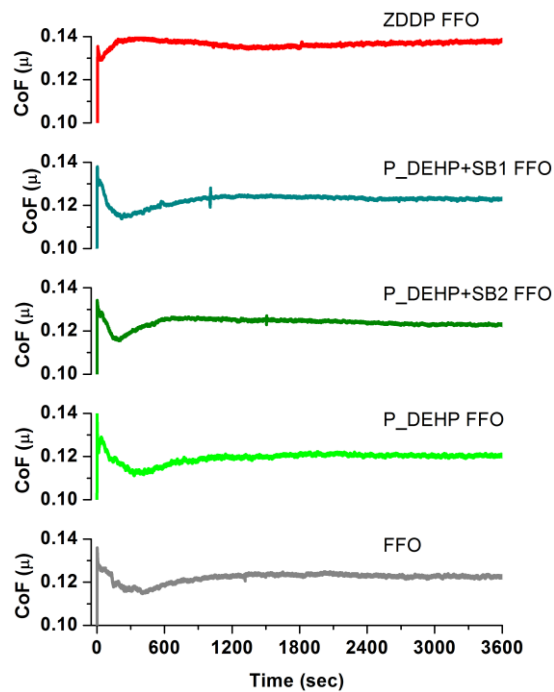


Figure 45: Coefficient of friction as a function of test duration obtained for low phosphorous fully formulated oil blends without AW and with AW (ZDDP, P\_DEHP, P\_DEHP+SB1 and P\_DEHP+SB2).

The antiwear performance of phosphonium IL and binary additive mixture of phosphonium IL and borate esters in low phosphorous FFO blends is measured and compared with that of FFO without AW and ZDDP FFO blends. Wear volume measured on test cylinders is presented as bar diagram in the Figure 46. The error bar on each bar denotes the standard deviation in the data for two repeated tests. FFO without AW exhibits the highest wear volume and the addition of AW additives to FFO (no Zn, no P) results in lower wear volume. ZDDP FFO blends exhibits better antiwear outcomes compared to FFO only blends. However the antiwear performance of ZDDP FFO blends is poorer than the FFO blends containing P\_DEHP only and binary mixtures of P\_DEHP+SB1 and P\_DEHP+SB2. P\_DEHP FFO blends offers the lowest wear volume and addition of borate esters (SB1 and SB2) to P\_DEHP results in slightly higher wear volume than P\_DEHP only but much lower than ZDDP and FFO without AW.

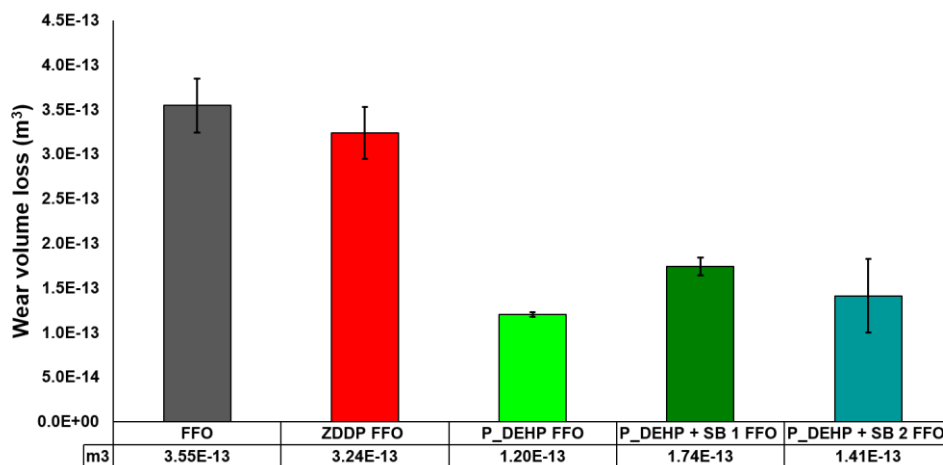


Figure 46: Wear volume measured for low phosphorous fully formulated oil blends without AW and with AW (ZDDP, P\_DEHP, P\_DEHP+SB1 and P\_DEHP+SB2).

### *8.3.2 Topography of the Tribofilms using SEM and SPM*

Wear features, in-situ tribofilms derived on the mating surfaces after the rubbing tests were examined using SEM and SPM imaging techniques. SEM images of the wear track generated on the test flat are presented in Figure 47. SEM images of the wear surfaces typically exhibit three features i.e. bright region, darker region and region of material removal such as scratches and metal pull-out. Bright regions were acquired from the conductive metal surfaces (Fe surfaces) and darker region are derived from the formation of non-conductive tribofilms. Test flat lubricated under FFO without AW (no Zn, no P) exhibit bright spots and dark spot, suggesting that wear surfaces are covered with tribofilms to some extent. In addition, regions of metal pull-out are also evident, indicating abrasive type wear condition. ZDDP FFO derived wear surface shows few mild scratches in addition to the bright and dark spots. ZDDP FFO lubricated surface exhibits larger coverage of tribofilms (dark spot) than FFO without AW. Similarly, P\_DEHP, P\_DEHP+SB1 and P\_DEHP+SB2 lubricated surfaces illustrates few mild scratches along with region of tribofilm coverage (dark spots). On comparison with ZDDP FFO, P\_DEHP FFO exhibits large patch size of tribofilms and spots are relatively darker suggesting the tribofilms are relatively thicker.

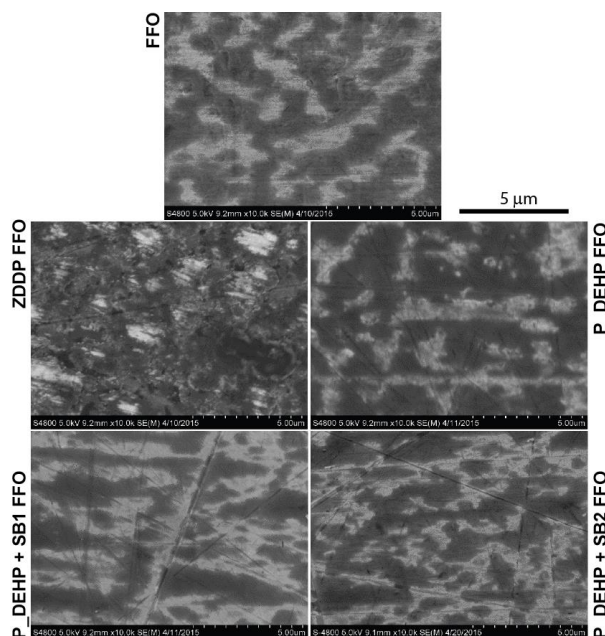


Figure 47: SEM images of the wear track generated on the test flat.

3D profile of the wear track was acquired by using nano-indentation in SPM imaging mode. Figure 48 shows the SPM images obtained from test flat after rubbing and arrow next to the image denotes the sliding direction. SPM images are produced for  $60\ \mu\text{m} \times 60\ \mu\text{m}$  area of the wear track while keeping the z-axis same i.e.  $\pm 200\ \text{nm}$ . FFO SPM image exhibits small pad like features consistently observed on the wear track. SPM image of ZDDP lubricated wear track demonstrates island type features that are typical of ZDDP tribofilms [49,56]. Comparing with FFO only, surface feature (island pads) are more pronounced in the case of ZDDP FFO. This may explain the relatively higher coefficient of friction observed in the case of ZDDP FFO in Figure 45. In the case of P\_DEHP FFO, surface topography looks similar to FFO without AW. Wear track is consistently covered with patches of island type featured tribofilms. In the case of

P\_DEHP+SB1 and P\_DEHP+SB2, island type features are observed however, the pad size are relatively large.

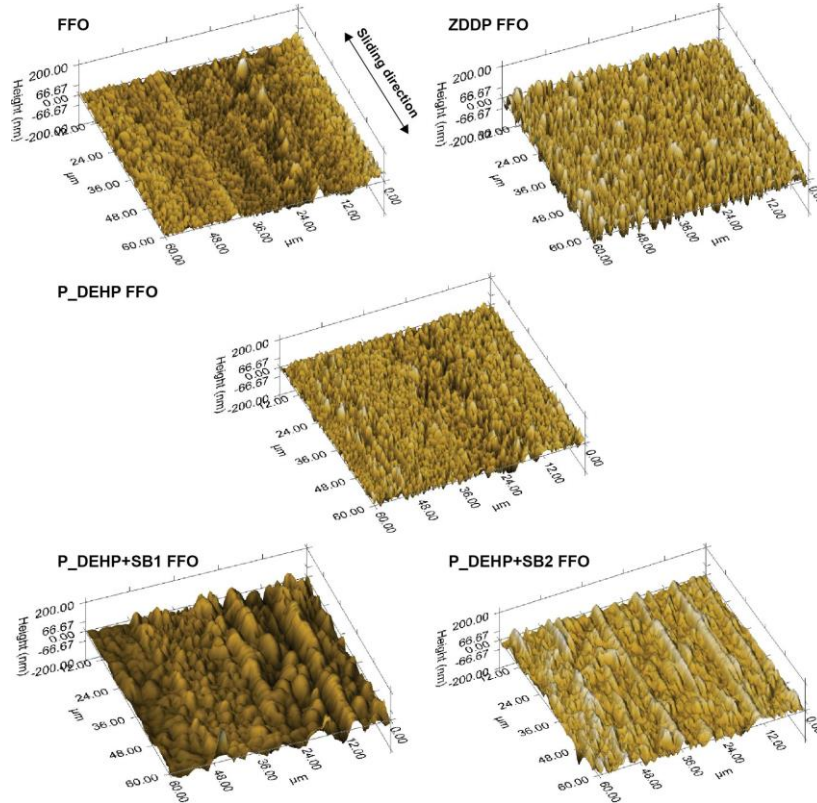


Figure 48: SPM images of the wear track generated on the test flat.

### 8.3.3 Chemical Properties of Tribofilms using XANES

#### 8.3.3.1 Phosphorous Characterization (P L<sub>2,3</sub>-edge)

Phosphorous species formed in the tribofilms are determined by probing the P L-edge using synchrotron source. P L-edge spectra are acquired in both TEY and FY detection modes to obtain the local coordination of phosphorous at near surface and in the bulk of tribofilms respectively. Figure 49a and 49b represents the P L-edge TEY and FY spectra respectively for tribofilms derived from different FFO blends with and without

AW chemistry. P L-edge spectra of model compounds are plotted in Figure 49c for fingerprint match analysis. P L-edge TEY and FY spectra of FFO (no Zn, no P) derived tribofilms exhibited no absorption edge since the FFO blend didn't contain phosphorous in the original chemistry. P L-edge TEY and FY spectra of tribofilms derived from FFO blends containing AW chemistry ZDDP, P\_DEHP, P\_DEHP+SB1 and P\_DEHP+SB2 exhibited a main absorption edge at peak **c**, pre-edge shoulder at peaks **a** and **b**, post-edge at peak **c'** and a shape resonance at peak **d**. Upon comparing with the model compounds spectra (Figure 49c), peak **d** is commonly present in all the phosphate structures while the main absorption edge peak **c** aligns well with calcium phosphates ( $\beta$ -TCP and  $\text{Ca}_2\text{P}_2\text{O}_7$ ). The main absorption edge energy for  $\text{BPO}_4$  is also closely matches with peak **c** while the main absorption edge energy for  $\text{FePO}_4$  and  $\text{Zn}_3(\text{PO}_4)_2$  were observed at higher photon energy than peak **c**. Furthermore, the presence of a post edge peak **c'** in the tribofilms spectra is found to be a characteristic peak for calcium phosphate species and is commonly observed in both  $\beta$ -TCP and  $\text{Ca}_2\text{P}_2\text{O}_7$ . These results indicate that in tribofilms derived from FFO blends containing ZDDP, P\_DEHP, P\_DEHP+SB1 and P\_DEHP+SB2, phosphorous is primarily present as calcium phosphate species ( $\beta$ -TCP and  $\text{Ca}_2\text{P}_2\text{O}_7$ ).  $\beta$ -TCP (Ortho-phosphate structure) exhibits relatively higher peak intensity for peak **c'** than  $\text{Ca}_2\text{P}_2\text{O}_7$  (Pyro-phosphate structure). P L-edge FY spectra of P\_DEHP, P\_DEHP+SB1 and P\_DEHP+SB2 show relatively higher intensity for peak **c'** than ZDDP suggesting that in the P\_DEHP and P\_DEHP+SB blends  $\beta$ -TCP contribution is relatively higher. In chapter 6, same AW chemistry ZDDP, P\_DEHP and mixture of P\_DEHP and SB1/SB2 showed the formation of zinc phosphate (ZDDP) and iron

phosphate for (P\_DEHP and P\_DEHP+SB1/SB2) in base oil blends. Fully formulated oil (no Zn, no P) used in this study contains detergent chemistry. Detergents are nanoparticles of CaCO<sub>3</sub> that are overbased with calcium sulfonate which is a part of the micelle structure around the calcium carbonate. This clearly indicates that the addition of calcium based detergents from FFO (no Zn, no P) influences the phosphorous chemistry of tribofilms formed using same AW additives. Sharma et al. [11] in previous study also reported the formation of calcium phosphate in the tribofilms for FFO blends containing ZDDP and other IL's structures while in base oil blends ZDDP forms zinc phosphates films and IL's forms iron phosphates. Similarly, Najman et al. [127] reported that antiwear films chemistry formed with ashless antiwear changed from iron phosphate to calcium phosphate with the addition of calcium based detergents in the base oil blends. They proposed that an exchange of Fe for Ca occurred in the AW films since  $-\Delta H^\circ$  values for FePO<sub>4</sub> (1297 kJ) is lower than  $-\Delta H^\circ$  values for Ca<sub>3</sub>(PO<sub>4</sub>)<sub>2</sub> (4120 kJ). Similarly, replacement of Zn for Ca in the tribofilms has been reported for ZDDP tribofilms formed with the interaction of calcium based detergent chemistry since  $-\Delta H^\circ$  for zinc phosphate is much lower than that of calcium phosphate [162-164].

P L-edge TEY spectra was further analyzed to obtained the phosphate chain polymerization in the tribofilms. The phosphate chain polymerization was estimated by taking a peak intensity ratio of peak **a** to peak **c**. Literature review [51,132,136] suggest that **a/c** ratio below 0.3 corresponds to short chain phosphates and above 0.6 corresponds to long chain phosphate formation. The **a/c** ratio calculated from P L-edge TEY spectra is shown in Figure 49a for FFO blends containing ZDDP, P\_DEHP, P\_DEHP+SB1 and

P\_DEHP+SB2. P L-edge TEY spectra of ZDDP FFO lubricated surface show an **a/c** ratio of 0.25 which corresponds to the short chain phosphate at near surface of the tribofilms. Similarly, P\_DEHP, P\_DEHP+SB1 and P\_DEHP+SB2 derived tribofilms results in an **a/c** ratio of 0.23, 0.26 and 0.26 respectively which again corresponds to short chain phosphates. Kasrai et al. [164] reported that addition of calcium based detergents inhibits that long chain poly-phosphate formation in ZDDP tribofilms. However, in our study, same AW additives in base oil blends without detergents chemistry (chapter 6) also showed short-chain phosphates formation. Hence the effect of calcium on phosphate chain polymerization cannot be determined.

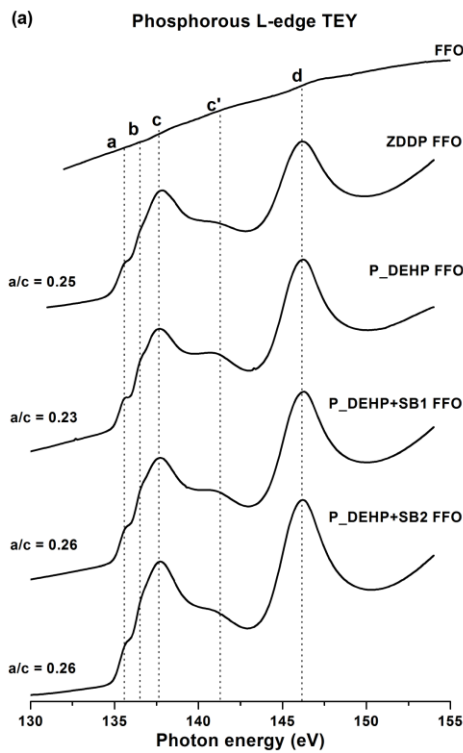


Figure 49a: P L-edge TEY spectra of tribofilms derived from FFO (no Zn, no

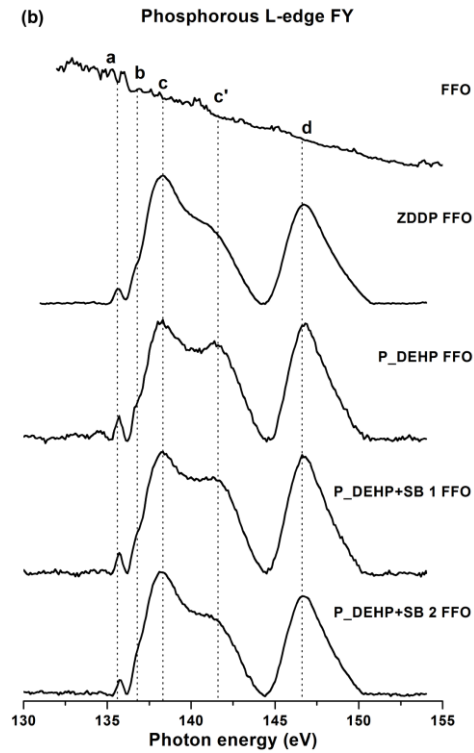


Figure 49b: P L-edge FY spectra of tribofilms derived from FFO (no Zn, no



P), ZDDP FFO, P\_DEHP FFO, P), ZDDP FFO, P\_DEHP FFO,  
P\_DEHP+SB1 FFO and P\_DEHP+SB2 P\_DEHP+SB1 FFO and P\_DEHP+SB2  
FFO blends. FFO blends.

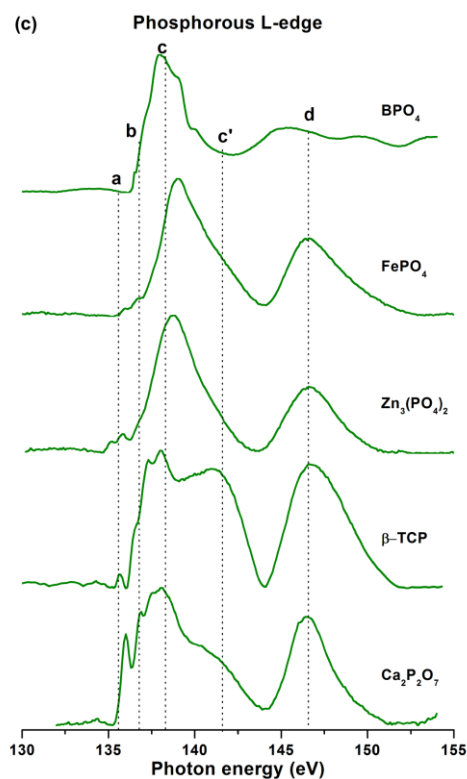


Figure 49c: P L-edge FY spectra of model compounds.

### 8.3.3.2 Boron Characterization (B K-edge)

The interaction of borate esters with P\_DEHP in FFO (n Zn, no P) blends is examined by probing the B K-edge spectra of tribofilms. B K-edge TEY and FY spectra of tribofilms formed using P\_DEHP+SB1 and P\_DEHP+SB2 (plotted in black line) are shown in Figure 50a and 50b and are compared with model compounds (plotted in green

lines). B K-edge TEY probes at near the surface (~6 nm) and FY obtain information from the bulk (~100 nm) [158]. Different boron species can be easily distinguished by examining their characteristic absorption edge (discussed in section 6.3.4.2). In Figure 50a and 50b three peaks are assigned as peak **a**, peak **b** and peak **c**. Peak **a** and peak **c** arise at photon energy of 194.0 eV and 202.9 eV respectively which are attributed to trigonal coordination of boron species and peak **b** originates at photon energy of 198.4 eV corresponds to the tetrahedral coordination [158]. Peaks **a** and **c** are commonly present in B<sub>2</sub>O<sub>3</sub> and H<sub>3</sub>BO<sub>3</sub> while BPO<sub>4</sub> exhibits peak **a**, peak **c** and peak **b** where peak **c** is slightly shifted to higher photon energy. Peak **b** originates from tetrahedral B is a dominant peak, since the compound in its pure form has boron in tetrahedral coordination. Relatively weak peaks **a** and **c** in BPO<sub>4</sub> spectra are believed to originate from surface modification [158]. The B K-edge TEY and FY spectra of tribofilms exhibit a strong absorption edge at peak **a** and mild peak intensity around 198.4 eV and 204 eV which is slightly shifted to higher photon energy than peak **c**. It is clear from the B K-edge TEY spectra of tribofilms that boron at near surface (TEY) and in the bulk (FY) of the tribofilms is dominantly present as trigonal B (B<sub>2</sub>O<sub>3</sub>/H<sub>3</sub>BO<sub>3</sub>). In addition to that, presence of weak intensities at photon energy of 198.4 eV and ~204 eV suggest two possibilities, first the likelihood for the formation of BPO<sub>4</sub> in the tribofilms due to the interaction of borate esters and P\_DEHP and second, a thermo-mechanical shearing induced partial transformation of boron from trigonal coordination to tetrahedral coordination in the tribofilms upon rubbing [159]. In base oil study (discussed in chapter 6 and 7), synergism between borate esters and P\_DEHP have shown a clear absorption

edge at 198.4 eV which can be attributed to the formation of  $BPO_4$ . Here, it can be speculated that calcium and phosphorus interaction due to the addition of calcium based detergent in FFO blends dominates the phosphates formation in the tribofilms which essentially inhibits the formation of both  $FePO_4$  and  $BPO_4$  which is evident in tribofilms formed in base oil blends.

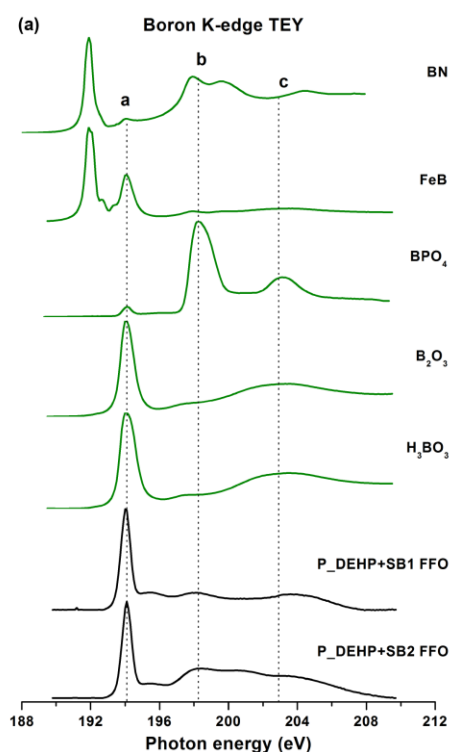


Figure 50a: B K-edge TEY spectra of tribofilms derived from FFO (no Zn, no P), ZDDP FFO, P\_DEHP FFO, P\_DEHP+SB1 FFO and P\_DEHP+SB2 FFO blends (plotted in black lines) and are compared with model compounds

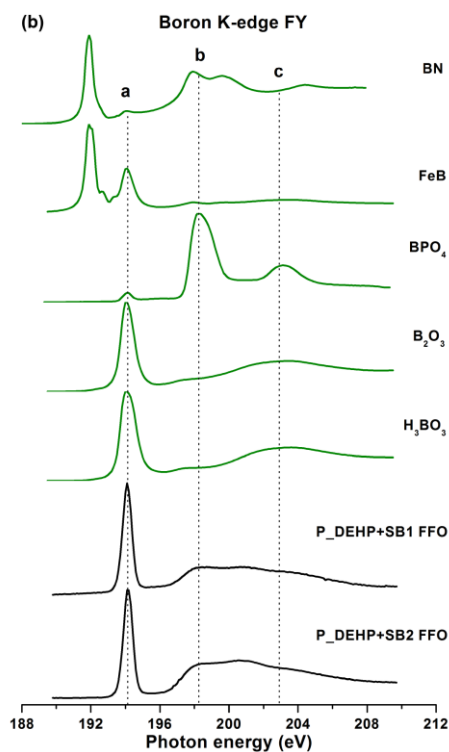


Figure 50b: B K-edge FY spectra of tribofilms derived from FFO (no Zn, no P), ZDDP FFO, P\_DEHP FFO, P\_DEHP+SB1 FFO and P\_DEHP+SB2 FFO blends (plotted in black lines) and are compared with model compounds

(plotted in green lines).

(plotted in green lines).

### 8.3.3.3 Sulfur Characterization (S L<sub>2,3</sub>-edge)

Sulfur species formed in the tribofilms using FFO blends with or without AW were probed by acquiring the S L-edge spectra. The S L-edge spectra were acquired in both TEY and FY modes to examine the sulfur chemistry in the tribofilms as a function of film thickness [134]. The primary source of sulfur in the tribofilms originate from the fully formulated oil used in the study as base matrix that contains detergent chemistry. Detergents commonly are nanoparticles of calcium carbonate that are overbased with calcium sulfonate which is a part of the micelle structure around the calcium carbonate. Besides that, ZDDP AW additive also contains sulfur in its original structure however, both phosphonium IL (P\_DEHP) and borate ester (SB1 and SB2) do not contain sulfur in their original structure. S L-edge spectra TEY and FY of tribofilms (black lines) are presented in Figure 51a and 51b and are compared with the model compounds spectra (green lines) in Figure 51c. Differences in the spectra of the model compounds and their relative peak energies are detailed by Kim et al. [16]. S L-edge TEY (Figure 51a) and FY (Figure 51b) spectra of the tribofilms exhibits similar absorption signature for each FFO blend however the signal to noise ratio is reduced in FY spectra. No significant changes were observed in the sulfur chemistry from the near surface region towards the bulk of the tribofilms for individual blend besides the observation that overall sulfur content is relatively higher at near surface region than in the bulk. Meanwhile, different sulfur species were observed in the case of ZDDP tribofilms compared to FFO only as well as

P\_DEHP FFO, P\_DEHP+SB1 and P\_DEHP+SB2 tribofilms. S L-edge spectra of FFO only blend exhibits several peaks which are labeled as peak **a'**, **b'**, **c'**, **d'** and **e'**. The S L-edge spectra of P\_DEHP, P\_DEHP+SB1 and P\_DEHP+SB2 also exhibit peaks **a'**, **b'**, **c'**, **d'** and **e'** similar FFO only blend. By fingerprint match analysis with model compounds spectra, peak **a'** and **b'** can be assigned to sulfide (-2 oxidation state) species primarily iron sulfides. Peak **e'** is commonly present in all the sulfate structures which confirms that sulfur in these tribofilms is also present as sulfates (+6 oxidation state). In addition to that, presence of peaks **c'** and **d'** suggests the sulfates are primarily of iron sulfates since peak **c'** originates from iron sulfates absorption edge as pre-edge shoulder before peak **d'**. Since Zn is not present in these tribofilms, we can eliminate the possibility of ZnSO<sub>4</sub> however we cannot completely eliminate the possibility for the formation of CaSO<sub>4</sub> in these tribofilms. On the other hand, ZDDP FFO tribofilms exhibit peaks a, b, c, d and e which aligns well with the ZnS spectra. ZDDP FFO tribofilms primarily exhibit that sulfur is primarily present as sulfide (-2 oxidation state).

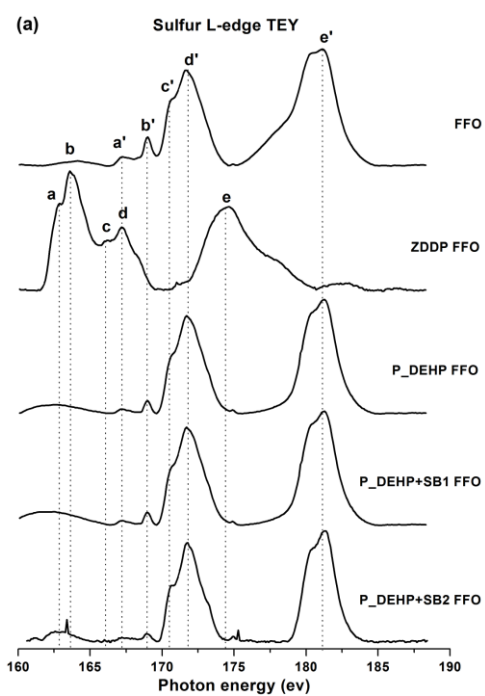


Figure 51a: S L<sub>2,3</sub>-edge TEY spectra of tribofilms derived from FFO (no Zn, no P), ZDDP FFO, P\_DEHP FFO, P\_DEHP+SB1 FFO and P\_DEHP+SB2 FFO blends (plotted in black lines).

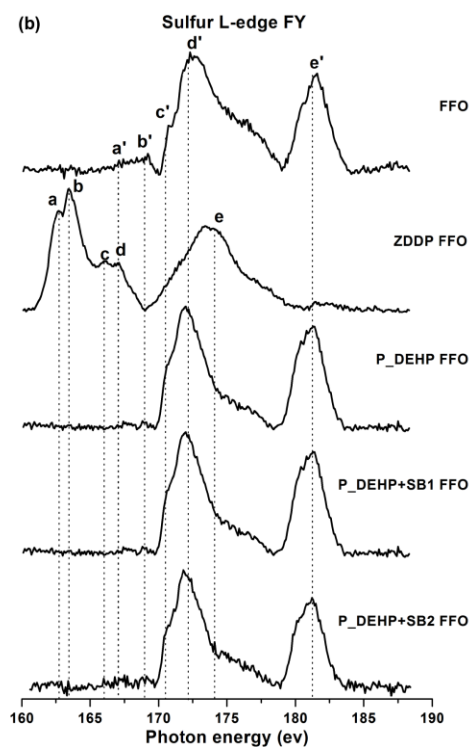


Figure 51b: S L<sub>2,3</sub>-edge FY spectra of tribofilms derived from FFO (no Zn, no P), ZDDP FFO, P\_DEHP FFO, P\_DEHP+SB1 FFO and P\_DEHP+SB2 FFO blends (plotted in black lines).

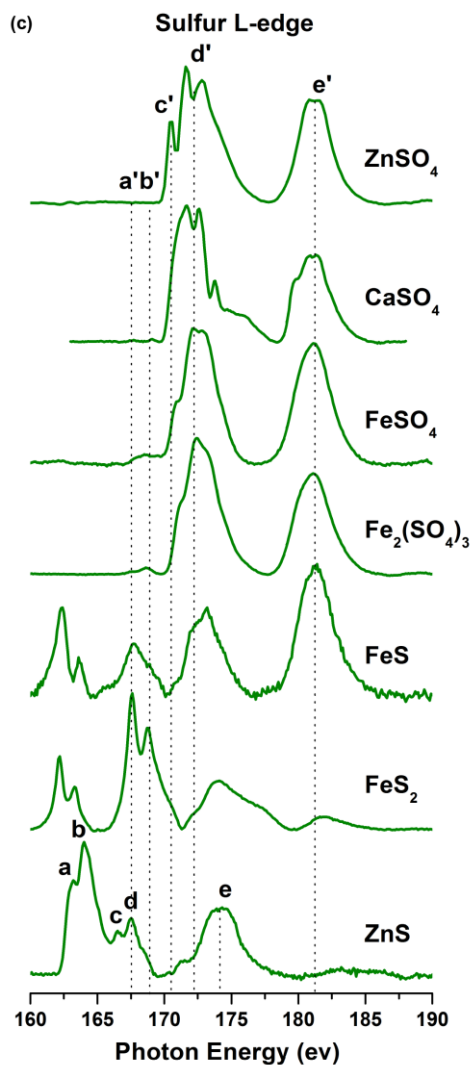


Figure 51c: S L<sub>2,3</sub>-edge FY spectra of model compounds.

#### 8.3.3.4 Calcium Characterization (Ca K-edge)

Calcium K-edge spectra were also acquired to compliment the results observed from P L<sub>2,3</sub>-edge and S L<sub>2,3</sub>-edges. Ca K-edge TEY and FY spectra of tribofilms are plotted in Figure 52a and 52b and are compared with model compounds in Figure 53c. Three peaks are identified and are labeled as peak **a**, **b** and **c**. By fingerprint matching

with model compounds, the presence of either or both calcium phosphate and sulfate is determined. These results compliment the earlier findings of P and S spectra.

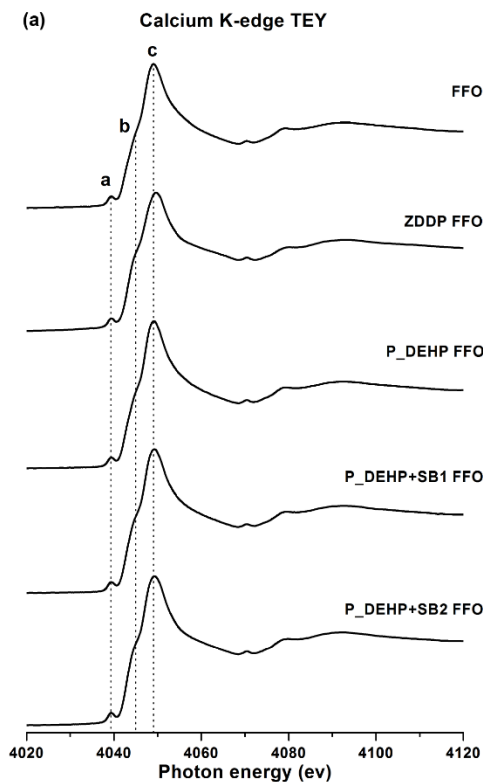


Figure 52a: Ca K-edge TEY spectra of tribofilms derived from FFO (no Zn, no P), ZDDP FFO, P\_DEHP FFO, P\_DEHP+SB1 FFO and P\_DEHP+SB2 FFO blends (plotted in black lines).

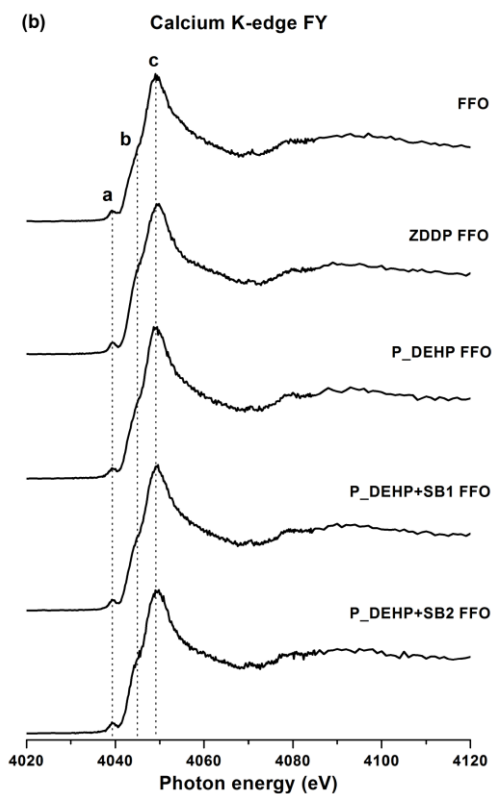


Figure 52b: Ca K-edge FY spectra of tribofilms derived from FFO (no Zn, no P), ZDDP FFO, P\_DEHP FFO, P\_DEHP+SB1 FFO and P\_DEHP+SB2 FFO blends (plotted in black lines).



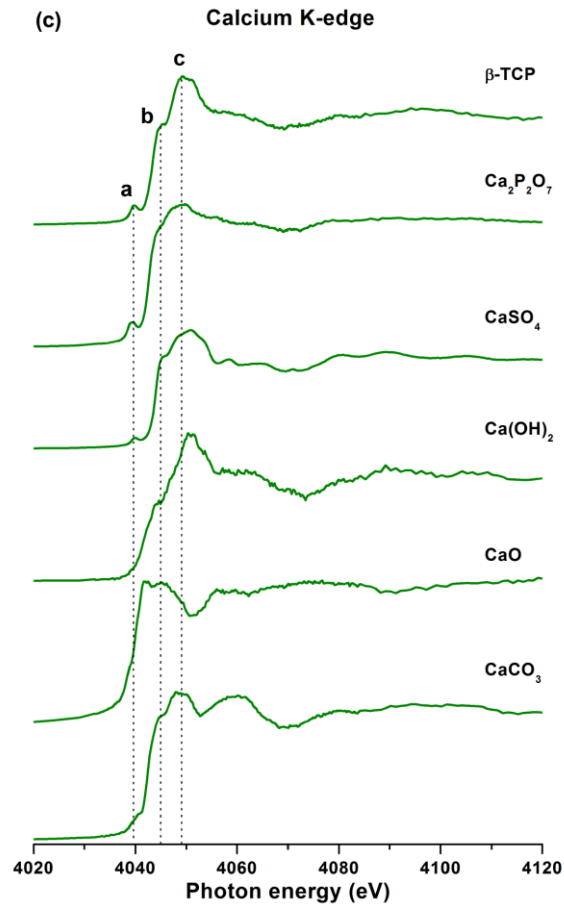


Figure 52c: Ca K-edge FY spectra of model compounds.

#### 8.4 Conclusions

No improvement observed in friction response by the addition of P\_DEHP and P\_DEHP+SB to the FFO (no P, no Zn). Interestingly, addition of ZDDP resulted into relatively higher coefficient of friction.

P\_DEHP and binary additive mixture of P\_DEHP+SB show significant improvement in wear protection in comparison with ZDDP in FFO blends.

XANES analysis of tribofilms indicates that phosphorous is primarily present in the form of calcium phosphates.

Sulfur L<sub>2,3</sub>-edge spectra show that ZDDP tribofilms are primarily composed of zinc sulfides and FFO only, P\_DEHP FFO, P\_DEHP+SB1 FFO and P\_DEHP+SB2 FFO tribofilms are composed of iron sulfates and iron sulfides and to some extent calcium sulfates.

Boron is primarily present in the form of boric acid/boron oxide and boron phosphate to some extent.

## Copyrights and permission

Copyrights and permission to reuse the published data and figures in dissertation has been granted from the publisher.

## References

- [1] Spikes HA. The history and mechanisms of ZDDP. *Trib Lett* 2004;17:469-489.
- [2] Minami I. Ionic liquids in tribology. *Molecules* 2009;14:2286-305.
- [3] Federal Emission Standards Reference Guide.
- [4] 2017 and Later Model Year Light-Duty Vehicle Greenhouse Gas Emissions and Corporate Average Fuel Economy Standards, Final Rule. In: Anonymous Federal Register, National Archive and Records Administration: Environmental Protection Agency and Department of Transportation National Highway Traffic Safety Administration; 2012, p. 62623.
- [5] Ferrick Kevin. Technical Bulletin 1 API 1509, Engine Oil Licensing and Certification System. ;2010.
- [6] Holmberg K, Andersson P, Erdemir A. Global energy consumption due to friction in passenger cars. *Tribol Int* 2012;47:221-34.
- [7] Holmberg K, Andersson P, Nylund N, Mäkelä K, Erdemir A. Global energy consumption due to friction in trucks and buses. *Tribol Int* 2014;78:94-114.
- [8] Qu J, Barnhill WC, Luo H, Meyer HM, Leonard DN, Landauer AK et al. Synergistic Effects Between Phosphonium-Alkylphosphate Ionic Liquids and Zinc Dialkyldithiophosphate (ZDDP) as Lubricant Additives. *Adv Mater* 2015.
- [9] Qu J, Luo H, Chi M, Ma C, Blau PJ, Dai S et al. Comparison of an oil-miscible ionic liquid and ZDDP as a lubricant anti-wear additive. *Tribol Int* 2014;71:88-97.
- [10] Totolin V, Minami I, Gabler C, Dörr N. Halogen-free borate ionic liquids as novel lubricants for tribological applications. *Tribol Int* 2013;67:191-8.

- [11] Sharma V, Gabler C, Doerr N, Aswath PB. Mechanism of tribofilm formation with P and S containing ionic liquids. *Tribol Int* 2015;92:353-64.
- [12] Qu J, Blau PJ, Dai S, Luo H, Meyer III HM. Ionic liquids as novel lubricants and additives for diesel engine applications. *Tribology letters* 2009;35:181-9.
- [13] Chen X, Elsenbaumer RL, Aswath PB. Synthesis and Tribological Behavior of Ashless Alkylphosphorofluoridothioates. *Tribol Int* 2013;69:114-24.
- [14] Chen X, Kim B, Elsenbaumer R, Aswath PB, Aswath PB. Synthesis and Antiwear Behavior of Alkylthioperoxydiphosphates. *Tribology - Materials, Surfaces and Interfaces* 2012;6(3):121-33.
- [15] Kim B. Tribological Performance of Ashless Antiwear Additives Under Extreme Pressure Conditions. Ph D Dissertation 2009;University of Texas at Arlington.
- [16] Kim B, Mourhatch R, Aswath PB. Properties of tribofilms formed with ashless dithiophosphate and zinc dialkyl dithiophosphate under extreme pressure conditions. *Wear* 2010;268:579-91.
- [17] Erdemir A, Eryilmaz O. Achieving superlubricity in DLC films by controlling bulk, surface, and tribochemistry. *Friction* 2014;2:140-55.
- [18] Ala'A A, Eryilmaz O, Erdemir A, Kim SH. Nano-texture for a wear-resistant and near-frictionless diamond-like carbon. *Carbon* 2014;73:403-12.
- [19] Macián V, Tormos B, Bermúdez V, Ramírez L. Assessment of the effect of low viscosity oils usage on a light duty diesel engine fuel consumption in stationary and transient conditions. *Tribol Int* 2014;79:132-9.

- [20] Somers AE, Khemchandani B, Howlett PC, Sun J, MacFarlane DR, Forsyth M. Ionic Liquids as Antiwear Additives in Base Oils: Influence of Structure on Miscibility and Antiwear Performance for Steel on Aluminum. *ACS applied materials & interfaces* 2013;5:11544-53.
- [21] Anand M, Hadfield M, Viesca J, Thomas B, Battez AH, Austen S. Ionic liquids as tribological performance improving additive for in-service and used fully-formulated diesel engine lubricants. *Wear* 2015;334:67-74.
- [22] Barnhill WC, Qu J, Luo H, Meyer III HM, Ma C, Chi M et al. Phosphonium-Organophosphate Ionic Liquids as Lubricant Additives: Effects of Cation Structure on Physicochemical and Tribological Characteristics. *ACS applied materials & interfaces* 2014;6:22585-93.
- [23] Pisarova L, Gabler C, Dörr N, Pittenauer E, Allmaier G. Thermo-oxidative stability and corrosion properties of ammonium based ionic liquids. *Tribol Int* 2012;46:73-83.
- [24] Cai M, Liang Y, Yao M, Xia Y, Zhou F, Liu W. Imidazolium ionic liquids as antiwear and antioxidant additive in poly (ethylene glycol) for steel/steel contacts. *ACS applied materials & interfaces* 2010;2:870-6.
- [25] Yu B, Bansal DG, Qu J, Sun X, Luo H, Dai S et al. Oil-miscible and non-corrosive phosphonium-based ionic liquids as candidate lubricant additives. *Wear* 2012;289:58-64.
- [26] Gusain R, Gupta P, Saran S, Khatri OP. Halogen-Free Bis (imidazolium)/Bis (ammonium)-Di [bis (salicylato) borate] Ionic Liquids As Energy Efficient and

- Environment-Friendly Lubricant Additives. ACS applied materials & interfaces 2014;6 (17):15318-28.
- [27] Totolin V, Minami I, Gabler C, Brenner J, Dörr N. Lubrication Mechanism of Phosphonium Phosphate Ionic Liquid Additive in Alkylborane–Imidazole Complexes. Tribology Letters 2014;53:421-32.
- [28] Jiménez AE, Bermúdez M. Ionic liquids as lubricants of titanium–steel contact. Tribology letters 2009;33:111-26.
- [29] Jimenez A, Bermudez M. Ionic liquids as lubricants of titanium–steel contact. Part 2: friction, wear and surface interactions at high temperature. Tribology letters 2010;37:431-43.
- [30] Bermúdez M, Jiménez A, Sanes J, Carrión F. Ionic liquids as advanced lubricant fluids. Molecules 2009;14:2888-908.
- [31] Keskin S, Kayrak-Talay D, Akman U, Hortaçsu Ö. A review of ionic liquids towards supercritical fluid applications. The Journal of Supercritical Fluids 2007;43:150-80.
- [32] Wilkes JS. Properties of ionic liquid solvents for catalysis. Journal of Molecular Catalysis A: Chemical 2004;214:11-7.
- [33] Zhao H. Innovative applications of ionic liquids as “green” engineering liquids. Chem Eng Commun 2006;193:1660-77.
- [34] Hough WL, Rogers RD. Ionic liquids then and now: from solvents to materials to active pharmaceutical ingredients. Bull Chem Soc Jpn 2007;80:2262-9.

- [35] Torimoto T, Tsuda T, Okazaki K, Kuwabata S. New frontiers in materials science opened by ionic liquids. *Adv Mater* 2010;22:1196-221.
- [36] Ye C, Liu W, Chen Y, Yu L. Room-temperature ionic liquids: a novel versatile lubricant. *Chemical Communications* 2001:2244-5.
- [37] Hsu SM. Molecular basis of lubrication. *Tribology International*, 2004; 7;37:553-9.
- [38] Castro W, Weller DE, Cheenkachorn K, Perez JM. The effect of chemical structure of basefluids on antiwear effectiveness of additives. *Tribol Int* 2005;38:321-6.
- [39] Barnes AM, Bartle KD, Thibon VRA. A review of zinc dialkyldithiophosphates (ZDDPS): characterisation and role in the lubricating oil. *Tribol Int* 2001;34:389-95.
- [40] Willermet PA, Dailey DP, Carter RO,III, Schmitz PJ, Zhu W. Mechanism of formation of antiwear films from zinc dialkyldithiophosphates. *Tribology International* 1995;28:177-87.
- [41] Watkins RC. The antiwear mechanism of zddp's. Part II. *Tribol Int* 1982;15:13-5.
- [42] Spedding H, Watkins RC. Antiwear Mechanisms of ZDDP's - 1. *Tribol Int* 1982;15:9-12.
- [43] Somayaji A, Aswath PB. Antiwear perforce of ZDDP and fluorinated ZDDP in the presence of antioxidants. *Tribology Transactions Under Review* (2006).
- [44] Mourhatch R, Aswath PB. Mechanism of Boundary Lubrication with Zinc Dialkyl Dithiophosphate. *Proceedings of the STLE/ASME International Joint Tribology Conference 2006;San Antonio, TX, USA:IJTC-12054.*



- [45] Jones RB, Coy RC. Chemistry of the Thermal Degradation of Zinc Dialkyldithiophosphate Additives. ASLE Trans 1981;24:91-97.
- [46] Taylor L, Dratva A, Spikes HA. Friction and wear behavior of zinc dialkyldithiophosphate additive. 2000;43:469-79.
- [47] Parekh K, Chen X, Aswath PB. Synthesis of Fluorinated ZDDP Compounds. Tribol Lett 2009;34:141-53.
- [48] Mourhatch R, Aswath PB. Tribological behavior and nature of tribofilms generated from fluorinated ZDDP in comparison to ZDDP under extreme pressure conditions---Part 1: Structure and chemistry of tribofilms. Tribol Int 2011;44:187-200.
- [49] Warren OL, Graham JF, Norton PR, Houston JE, Michalske TA. Nanomechanical properties of films derived from zinc dialkyldithiophosphate. Tribology Letters 1998;4:189-98.
- [50] Mourhatch R, Aswath PB. Tribological behavior and nature of tribofilms generated from fluorinated ZDDP in comparison to ZDDP under extreme pressure conditions—Part II: Morphology and nanoscale properties of tribofilms. Tribol Int 2011;44:201-10.
- [51] Najman MN, Kasrai M, Bancroft GM, Frazer BH, DeStatio G. The correlation of microchemical properties to antiwear (AW) performance in ashless thiophosphate oil additives. Tribol Lett 2004;17(4):811-22.

- [52] Kim BH, Jiang J, Aswath PB. Mechanism of Wear at Extreme Loads and Boundary Conditions with Ashless Anti-wear Additives: Analysis of Wear Surfaces and Wear Debris. *Wear* 2011;270(3-4):181-94.
- [53] Sarin R, Gupta AK, Tuli DK, Verma AS, Rai MM, Bhatnagar AK. Synthesis and performance evaluation of O, O-dialkylphosphorodithioic disulphides as potential antiwear, extreme-pressure and antioxidant additives. *Tribol Int* 1993;26:389-94.
- [54] Nicholls M, Najman MN, Zhang Z, Kasrai M, Norton PR, Gilbert PUPA. The contribution of XANES spectroscopy to tribology. *Canadian Journal of Chemistry* 2007;85:816-30.
- [55] Swami KK, Prakash S, Mondal PK, Dohhen KC, Sarin R, Tuli DK et al. Additive-additive interactions: The search for synergistic antioxidant-antiwear phosphorodithioate compositions. *Lubr Sci* 2002;14:385-92.
- [56] Sharma V, Erdemir A, Aswath PB. An analytical study of tribofilms generated by the interaction of ashless antiwear additives with ZDDP using XANES and nano-indentation. *Tribol Int* 2015;82:43-57.
- [57] Sharma V, Dörr N, Aswath P. Chemical-Mechanical Properties of Tribofilms and its Relation to Ionic Liquid Chemistry. *RSC Adv* 2016;6:22341-56.
- [58] González R, Bartolomé M, Blanco D, Viesca J, Fernández-González A, Battez AH. Effectiveness of phosphonium cation-based ionic liquids as lubricant additive. *Tribol Int* 2016;98:82-93.

- [59] Chen X, Kim B, Elsenbaumer RL, Aswath PB. Alkylphosphorofluoridothioates Having Low Wear Volume and Methods for Synthesizing Same. U S Patent Application 2011;US20110319303.
- [60] Zhang J, Liu W, Xue Q. The friction and wear behaviors of S-[2-S-(2-hydroxypropyl)benthiazole]dioctyldithiocarbamic acid ester as additive in liquid paraffin. *Wear* 1999;224:50-5.
- [61] Walters DK, Thomas AS. Transition-metal free lubricants. European Patent Application 1995;EP19900314188.
- [62] Hua W, Jing L, Hongling Y, Xiangqiong Z, Lingbo L, Tianhui R. The tribological behavior of diester-containing polysulfides as additives in mineral oil. *Tribol Int* 2007;40:1246-52.
- [63] Phillips WD. Ashless phosphorous-containing lubricating oil additives. In: Rudnick LR, editor. *Lubricant Additives-Chemistry and Applications*, 2nd Edition, Chemical Industries 124, Danvers, MA, U.S.A.: CRC Press; 2009, p. 63-121.
- [64] Najman MN, Kasrai M, Bancroft GM. Chemistry of anti-wear films from ashless thiophosphate oil additives. *Tribology Letters* 2004;17(2):217-29.
- [65] Vipper AB, Lashkhi VL, Belov PS, Parfenova VA, Blokhina IV. Antifriction and antiwear efficiency of ashless thiophosphates and dithiophosphates. *Chemistry and Technology of Fuels and Oils* 1983;19:136-9.
- [66] Ribeaud M. Volatility of phosphorus-containing anti-wear agents for motor oils. *Lubr Sci* 2006;18:231-41.

- [67] Camenzind H, Clark D, Dratva A, Fletschinger M, Ribeaud M, Rohrbach P et al. New Ashless, Hydrolytically Stable and FZG Active Antiwear Agent. *Tribol Trans* 2002;45:223-31.
- [68] Bhushan B, Palacio M, Kinzig B. AFM-based nanotribological and electrical characterization of ultrathin wear-resistant ionic liquid films. *J Colloid Interface Sci* 2008;317:275-87.
- [69] Palacio M, Bhushan B. A review of ionic liquids for green molecular lubrication in nanotechnology. *Tribology letters* 2010;40:247-68.
- [70] Lu Q, Wang H, Ye C, Liu W, Xue Q. Room temperature ionic liquid 1-ethyl-3-hexylimidazolium-bis(trifluoromethylsulfonyl)-imide as lubricant for steel–steel contact. *Tribol Int* 2004;37:547-52.
- [71] Liu W, Ye C, Gong Q, Wang H, Wang P. Tribological performance of room-temperature ionic liquids as lubricant. *Tribology Letters* 2002;13:81-5.
- [72] Wang H, Lu Q, Ye C, Liu W, Cui Z. Friction and wear behaviors of ionic liquid of alkylimidazolium hexafluorophosphates as lubricants for steel/steel contact. *Wear* 2004;256:44-8.
- [73] Phillips B, Zabinski J. Ionic liquid lubrication effects on ceramics in a water environment. *Tribology Letters* 2004;17:533-41.
- [74] Cai Z, Meyer III HM, Ma C, Chi M, Luo H, Qu J. Comparison of the tribological behavior of steel–steel and Si<sub>3</sub>N<sub>4</sub>–steel contacts in lubricants with ZDDP or ionic liquid. *Wear* 2014;319:172-83.

- [75] Xiao H, Guo D, Liu S, Pan G, Lu X. Film thickness of ionic liquids under high contact pressures as a function of alkyl chain length. *Tribology letters* 2011;41:471-7.
- [76] Otero I, López ER, Reichelt M, Fernández J. Friction and anti-wear properties of two tris(pentafluoroethyl)trifluorophosphate ionic liquids as neat lubricants. *Tribol Int* 2014;70:104-11.
- [77] Liu X, Zhou F, Liang Y, Liu W. Tribological performance of phosphonium based ionic liquids for an aluminum-on-steel system and opinions on lubrication mechanism. *Wear* 2006;261:1174-9.
- [78] Saurín N, Minami I, Sanes J, Bermúdez M. Study of the effect of tribo-materials and surface finish on the lubricant performance of new halogen-free room temperature ionic liquids. *Appl Surf Sci* 2016.
- [79] Minami I, Inada T, Sasaki R, Nanao H. Tribo-chemistry of phosphonium-derived ionic liquids. *Tribology letters* 2010;40:225-35.
- [80] Zhang C, Zhang S, Yu L, Zhang P, Zhang Z, Wu Z. Tribological behavior of 1-methyl-3-hexadecylimidazolium tetrafluoroborate ionic liquid crystal as a neat lubricant and as an additive of liquid paraffin. *Tribology Letters* 2012;46:49-54.
- [81] Gabler C, Dörr N, Allmaier G. Influence of cationic moieties on the tribolayer constitution shown for bis(trifluoromethylsulfonyl)imide based ionic liquids studied by X-ray photoelectron spectroscopy. *Tribol Int* 2014;80:90-7.
- [82] Pisarova L, Totolin V, Gabler C, Dörr N, Pittenauer E, Allmaier G et al. Insight into degradation of ammonium-based ionic liquids and comparison of tribological

- performance between selected intact and altered ionic liquid. *Tribol Int* 2013;65:13-27.
- [83] Jiménez AE, Bermúdez MD, Iglesias P, Carrión FJ, Martínez-Nicolás G. 1-N-alkyl - 3-methylimidazolium ionic liquids as neat lubricants and lubricant additives in steel–aluminium contacts. *Wear* 2006;260:766-82.
- [84] Somers AE, Biddulph SM, Howlett PC, Sun J, MacFarlane DR, Forsyth M. A comparison of phosphorus and fluorine containing IL lubricants for steel on aluminium. *Physical Chemistry Chemical Physics* 2012;14:8224-31.
- [85] Yao M, Fan M, Liang Y, Zhou F, Xia Y. Imidazolium hexafluorophosphate ionic liquids as high temperature lubricants for steel–steel contacts. *Wear* 2010;268:67-71.
- [86] Battez AH, González R, Viesca J, Blanco D, Asedegbega E, Osorio A. Tribological behaviour of two imidazolium ionic liquids as lubricant additives for steel/steel contacts. *Wear* 2009;266:1224-8.
- [87] Jimenez A, Bermúdez M. Ionic liquids as lubricants for steel–aluminum contacts at low and elevated temperatures. *Tribology Letters* 2007;26:53-60.
- [88] Qu J, Bansal DG, Yu B, Howe JY, Luo H, Dai S et al. Antiwear performance and mechanism of an oil-miscible ionic liquid as a lubricant additive. *ACS applied materials & interfaces* 2012;4:997-1002.
- [89] Kamimura H, Kubo T, Minami I, Mori S. Effect and mechanism of additives for ionic liquids as new lubricants. *Tribol Int* 2007;40:620-5.

- [90] Qu J, Chi M, Meyer III HM, Blau PJ, Dai S, Luo H. Nanostructure and composition of tribo-boundary films formed in ionic liquid lubrication. *Tribology Letters* 2011;43:205-11.
- [91] Parekh K. Interactions between antiwear agent and novel additive in engine oils. 2007.
- [92] Mourhatch R. Tribological and Antiwear Mechanisms of Fluorinated Zinc Dialkyl Dithiophosphate in Comparison to Zinc Dialkyl Dithiophosphate in Engine Oils. 2008:161.
- [93] Mourhatch R, Aswath PB. Nanoscale properties of tribofilms formed with zinc dialkyl dithiophosphate (ZDDP) under extreme pressure condition. *Journal of nanoscience and nanotechnology* 2009;9:2682-91.
- [94] Grubin AN. Fundamentals of the hydrodynamic theory of lubrication of heavily loaded cylindrical surfaces. Translation of Russian Book No. 30 ed. Moscow,USSR: Central Scientific Research Institute for Technology and Mechanical Engineering, 1949.
- [95] Dowson D, Higginson GR. *Elastohydrodynamic Lubrication*. London, UK: Pergamon Press, 1966.
- [96] Archard JF, Cowking EW. Elastohydrodynamic lubrication at point contacts. *Proc Inst Mech Eng* 1965-1966;180:47-56.
- [97] Hamrock BJ, Dowson D. ISOTHERMAL ELASTOHYDRODYNAMIC LUBRICATION OF POINT CONTACTS. *Journal of Lubrication Technology, Transactions ASME* 1977;99 Ser F:15-23.

- [98] Lu X, Khonsari MM, Gelinck ERM. The Stribeck Curve: Experimental Results and Theoretical Prediction. *J Tribol* 2006;128:789,789-794.
- [99] Khorramian BA, Iyer GR, Kodali S, Natarajan P, Tupil R. Review of antiwear additives for crankcase oils. *Wear* 1993;169:87-95.
- [100] Bhushan B. *Modern Tribology Handbook, Volume 2*. 2000;2:1760.
- [101] Dowson D. Developments in lubrication - the thinning film. *J Phys D* 1992;25:334,334-339.
- [102] Miyoshi K. *Solid lubrication fundamentals and applications*. NASA 1998.
- [103] Kapadia R, Glyde R, Wu Y. In situ observation of phosphorous and non-phosphorous antiwear films using a mini traction machine with spacer layer image mapping. *Tribol Int* 2007;40:1667-79.
- [104] Topolovec-Miklozic K, Forbus TR, Spikes HA. Film thickness and roughness of ZDDP antiwear films. *Tribology Letters* 2007;26:161-71.
- [105] Fujita H, Spikes HA. The formation of zinc dithiophosphate antiwear films. *Proc Inst Mech Eng Part J* 2004;218:265-77.
- [106] Martin JM, Grossiord C, Le Mogne T, Bec S, Tonck A. The two-layer structure of Zndtp tribofilms: Part I: AES, XPS and XANES analyses. *Tribology International* 2001;34:523-30.
- [107] Minfray C, Martin JM, Esnouf C, Le Mogne T, Kersting R, Hagenhoff B. A multi-technique approach of tribofilm characterisation. 2004;447-448:272-7.



- [108] Fuller MS, Fernandez LR, Massoumi G, Lennard W, Kasrai M, Bancroft G. The use of X-ray absorption spectroscopy for monitoring the thickness of antiwear films from ZDDP. *Tribology Letters* 2000;8:187-92.
- [109] Somayaji A, Mourhatch R, Aswath PB. Nanoscale Properties of Tribofilms from ZDDP and Fluorinated ZDDP in the Presence and Absence of Antioxidants. *Journal of Nanoscience and Nanotechnology* 2007;7:4378-4390.
- [110] Ito K, Martin J, Minfray C, Kato K. Low-friction tribofilm formed by the reaction of ZDDP on iron oxide. *Tribology International* 2006;39:1538-44.
- [111] Nehme G, Mourhatch R, Aswath PB. Effect of contact load and lubricant volume on the properties of tribofilms formed under boundary lubrication in a fully formulated oil under extreme load conditions. *Wear* 2010;268 (9-10):1129-47.
- [112] Zhang Z, Yamaguchi ES, Kasrai M, Bancroft GM. Tribofilms generated from ZDDP and DDP on steel surfaces: Part 1. Growth, wear and morphology. *Proc World Tribol Cong* 2005:617-8.
- [113] Yin Z, Kasrai M, Bancroft GM, Laycock KF, Tan KH. Chemical characterization of antiwear films generated on steel by zinc dialkyl dithiophosphate using X-ray absorption spectroscopy. *Tribol Int* 1993;26:383-8.
- [114] Martin JM, Mansot JL, Berbezier I, Dexpert H. The nature and origin of wear particles from boundary lubrication with a zinc dialkyl dithiophosphate. *Wear* 1984; 16;93:117-26.

- [115] Cao LL, Sun YM, Zheng LQ. Chemical structure characterization of the boundary lubrication film using X-ray photoelectron spectroscopy and scanning Auger microprobe techniques. *Wear* 1990;140:345-357.
- [116] Morina A, Neville A. Understanding the composition and low friction tribofilm formation/removal in boundary lubrication. *Tribol Int* 2007;40:1696-704.
- [117] Erdemir A. Genesis of superlow friction and wear in diamondlike carbon films. *Tribol Int* 2004;37:1005-12.
- [118] Martin JM, Le Mogne T, Boehm M, Grossiord C. Tribochemistry in the analytical UHV tribometer. *Tribol Int* 1999;32:617-26.
- [119] Fuller M, Yin Z, Kasrai M, Bancroft GM, Yamaguchi ES, Ryason PR et al. Chemical characterization of tribochemical and thermal films generated from neutral and basic ZDDPs using X-ray absorption spectroscopy. *Tribology International* 1997;30:305-15.
- [120] Jean Michel Martin. Antiwear mechanisms of zinc dithiophosphate: a chemical hardness approach. *Tribology Letters* 1999;6:1,1-8.
- [121] Yin Z, Kasrai M, Fuller M, Bancroft GM, Fyfe K, Tan KH. Application of soft X-ray absorption spectroscopy in chemical characterization of antiwear films generated by ZDDP Part I: the effects of physical parameters. *Wear* 1997;202:172-91.
- [122] Yin Z, Kasrai M, Bancroft GM, Fyfe K, Colaianni ML, Tan KH. Application of soft x-ray absorption spectroscopy in chemical characterization of antiwear films

- generated by ZDDP Part II: the effect of detergents and dispersants. *Wear* 1997;202:192-201.
- [123] Fuller MLS, Kasrai M, Bancroft GM, Fyfe K, Tan KH. Solution decomposition of zinc dialkyl dithiophosphate and its effect on antiwear and thermal film formation studied by X-ray absorption spectroscopy. *Tribol Int* 1998;31:627-44.
- [124] Zhang Z, Yamaguchi E, Kasrai M, Bancroft G, Liu X, Fleet M. Tribofilms generated from ZDDP and DDP on steel surfaces: Part 2, chemistry. *Tribology Letters* 2005;19:221-9.
- [125] Pereira G, Lachenwitzer A, Kasrai M, Bancroft GM, Norton PR, Abrecht M et al. Chemical and mechanical analysis of tribofilms from fully formulated oils Part 1 – Films on 52100 steel. *Tribology* 2007;1:48-61.
- [126] Pereira G, Munoz-Paniagua D, Lachenwitzer A, Kasrai M, Norton PR, Capehart TW et al. A variable temperature mechanical analysis of ZDDP-derived antiwear films formed on 52100 steel. *Wear* 2007;262:461-70.
- [127] Najman M, Kasrai M, Michael Bancroft G, Davidson R. Combination of ashless antiwear additives with metallic detergents: Interactions with neutral and overbased calcium sulfonates. *Tribology International* 2006;39:342-55.
- [128] Mourhatch R, Parekh K, Aswath PB. A multi technique study of the tribological behavior and the tribofilms generated from fluorinated thiophosphate compounds in comparison to normal ZDDP. 2006;2006:12.

- [129] Ji H, Nicholls MA, Norton PR, Kasrai M, Capehart TW, Perry TA et al. Zinc-dialkyl-dithiophosphate antiwear films: Dependence on contact pressure and sliding speed. *Wear* 2005;258:789-99.
- [130] :- 797-809.
- [131] Li Y, Pereira G, Lachenwitzer A, Kasrai M, Norton PR. X-ray absorption spectroscopy and morphology study on antiwear films derived from ZDDP under different sliding frequencies. *Tribology Letters* 2007;27:245-53.
- [132] Li Y, Pereira G, Kasrai M, Norton PR. Studies on ZDDP anti-wear films formed under different conditions by XANES spectroscopy, atomic force microscopy and <sup>31</sup>P NMR. *Tribology Letters* 2007;28:319-28.
- [133] Nicholls MA, Do T, Bancroft GM, Norton PR, Kasrai M, Capehart TW et al. Chemical and mechanical properties of ZDDP antiwear films on steel and thermal spray coatings studied by XANES spectroscopy and nanoindentation techniques. *Tribology Letters* 2003;15(3):241-8.
- [134] Kasrai M, Lennard WN, Brunner RW, Bancroft GM, Bardwell JA, Tan KH. Sampling depth of total electron and fluorescence measurements in Si L- and K-edge absorption spectroscopy. *Appl Surf Sci* 1996;99:303-12.
- [135] Sutherland DGJ, Kasrai M, Bancroft GM, Liu ZF, Tan KH. Si L- and K-edge x-ray-absorption near-edge spectroscopy of gas-phase  $\text{Si}(\text{CH}_3)_x(\text{OCH}_3)_{4-x}$ : Models for solid-state analogs. *Phys Rev B* 1993;48:14989-5001.

- [136] Yin Z, Kasrai M, Bancroft GM, Tan KH, Feng X. X-ray-absorption spectroscopic studies of sodium polyphosphate glasses. *Phys Rev B* 1995;51:742-50.
- [137] Costello MT, Kasrai M. Study of surface films of overbased sulfonates and sulfurized olefins by X-Ray Absorption Near Edge Structure (XANES) spectroscopy. *Tribology Letters* 2006;24:163-9.
- [138] Bakunin VN, Kasrai M, Kuzmina GN, Bancroft GM, Parenago OP. Influence of temperature and ZDDP concentration on tribochemistry of surface-capped molybdenum sulfide nanoparticles studied by XANES spectroscopy. *Tribology Letters* 2007;26:33-43.
- [139] Patel M, Aswath PB. Morphology, structure and chemistry of extracted diesel soot: Part II: X-ray absorption near edge structure (XANES) spectroscopy and high resolution transmission electron microscopy. *Tribol Int* 2012;52:17-28.
- [140] Bianconi A, Koningsberger D, Prins R. X-ray absorption: principles, applications, techniques of EXAFS, SEXAFS and XANES. *XANES Spectroscopy* (DC Koningsberger & R.Prins, eds.). John Wiley & Sons, Inc., New York, NY (573-662) 1988.
- [141] Meisel A, Leonhardt G, Szargan R, Källne E. X-ray spectra and chemical binding. : Springer, 1989.
- [142] Behrens P. X-ray absorption spectroscopy in chemistry: II. X-ray absorption near edge structure. *TrAC Trends in Analytical Chemistry* 1992;11:237-44.
- [143] Behrens P. X-ray absorption spectroscopy in chemistry: I. Extended X-ray absorption fine structure. *TrAC Trends in Analytical Chemistry* 1992;11:218-22.

- [144] Kruse J, Leinweber P, Eckhardt K, Godlinski F, Hu Y, Zuin L. Phosphorous L<sub>2,3</sub>-edge XANES: Overview of Reference Compounds. *Journal of Synchrotron Radiation* 2009;16:247-59.
- [145] Kasrai M, Puller M, Scaini M, Yin Z, Brunner RW, Bancroft GM et al. Study of tribochemical film formation using x-ray absorption and photoelectron spectroscopies. In: D. Dowson, C.M. Taylor, T.H.C. Childs and G. Dalmaz, editor. *Tribology Series*: Elsevier; 1995, p. 659-669.
- [146] Nicholls MA, Norton PR, Bancroft GM, Do BH. Nanometer Scale Chemomechanical Characterization of Antiwear Films. *Tribol Lett* 2004;17:205-16.
- [147] Harp G, Han Z, Tonner B. X-ray absorption near edge structures of intermediate oxidation states of silicon in silicon oxides during thermal desorption. *Journal of Vacuum Science & Technology A* 1990;8:2566-9.
- [148] Li D, Bancroft GM, Kasrai M, Fleet ME, Feng XH, Tan KH. High-resolution Si and P K- and L-edge XANES spectra of crystalline SiP<sub>2</sub>O<sub>7</sub> and amorphous SiO<sub>2</sub>-P<sub>2</sub>O<sub>5</sub>. *Am Mineral* 1994;79:785-8.
- [149] Bec S, Tonck A, Georges JM, Coy RC, Bell JC, Roper GW. Relationship between mechanical properties and structures of zinc dithiophosphate anti-wear films. *Proc R Soc London* 1999;Volume 455:4181,4181 - 4203.
- [150] Mosey N, Woo T, Kasrai M, Norton P, Bancroft G, Müser M. Interpretation of experiments on ZDDP anti-wear films through pressure-induced cross-linking. *Tribology Letters* 2006;24:105-14.

- [151] Yu LG, Yamaguchi ES, Kasrai M, Bancroft GM. The chemical characterization of tribofilms using XANES - Interaction of nanosize calciumcontaining detergents with zinc dialkyldithiophosphate. *Canadian Journal of Chemistry* 2007;85:675-84.
- [152] Patel M, Aswath PB. Structure and chemistry of crankcase and cylinder soot and tribofilms on piston rings from a Mack T-12 dynamometer engine test. *Tribol Int* 2014;77:111-21.
- [153] Nicholas J. Mosey, Martin H. Müser, Tom K. Woo. Molecular mechanisms of anti-wear pad formation and functionality of lubricant additives. *Science* 2005;307:1612,1612-1615.
- [154] Mosey NJ, Woo TK, Müser MH. Mechanism of wear inhibition by ZDDP lubricant additives - Insights from molecular scale simulations. *American Chemical Society, Division of Petroleum Chemistry, Preprints* 2005;50:332-5.
- [155] Bancroft GM, Kasrai M, Fuller M, Yin Z, Fyfe K, Tan KH. Mechanisms of tribochemical film formation: stability of tribo- and thermally-generated ZDDP films. *Trib Lett* 1997;3:47,47-51.
- [156] Dodd JC. GAS ENGINE LUBRICATING OIL COMPOSITION. 2015.
- [157] Gosvami NN, Bares JA, Mangolini F, Konicek AR, Yablon DG, Carpick RW. Tribology. Mechanisms of antiwear tribofilm growth revealed in situ by single-asperity sliding contacts. *Science* 2015;348:102-6.
- [158] Kasrai M, Fleet ME, Muthupari S, Li D, Bancroft G. Surface modification study of borate materials from B K-edge X-ray absorption spectroscopy. *Physics and chemistry of minerals* 1998;25:268-72.

- [159] Zhang Z, Yamaguchi ES, Kasrai M, Bancroft GM. Interaction of ZDDP with borated dispersant using XANES and XPS. *Tribol Trans* 2004;47:527-36.
- [160] Erdemir A, Fenske G, Erck R. A study of the formation and self-lubrication mechanisms of boric acid films on boric oxide coatings. *Surface and coatings technology* 1990;43:588-96.
- [161] Chase M. NIST—JANAF Thermochemical Tables (Journal of Physical and Chemical Reference Data Monograph No. 9). American Institute of Physics 1998:1-1951.
- [162] Willermet PA, Dailey DP, Carter III RO, Schmitz PJ, Zhu W, Bell JC et al. The composition of lubricant-derived surface layers formed in a lubricated cam/tappet contact, II. Effects of adding overbased detergent and dispersant to a simple ZDTP solution. *Tribology International* 1995;28(3):163-75.
- [163] Wan Y, Suominen Fuller ML, Kasrai M, Bancroft GM, Fyfe K, Torkelson JR et al. Effects of detergent on the chemistry of tribofilms from ZDDP: studied by X-ray absorption spectroscopy and XPS. In: D. Dowson, M. Priest, G. Dalmaz and A.A. Lubrecht, editor. *Tribology Series*: Elsevier; 2002, p. 155-166.
- [164] Kasrai M, Fuller MS, Bancroft GM, Ryason PR. X-ray absorption study of the effect of calcium sulfonate on antiwear film formation generated from neutral and basic ZDDPs: Part 1—phosphorus species. *Tribol Trans* 2003;46:534-42.



